Politecnico di Torino

ScuDo
Scuola di Dottorato ~ Doctoral School
WHAT YOU ARE, TAKES YOU FAR

Doctoral Dissertation
Doctoral Program in Civil and Environmental Engineering (35^{th}cycle)

Geographically-based approaches to the statistical analysis of rainfall extremes

By

Paola Mazzoglio

******

Supervisors:
Prof. Pierluigi Claps, Supervisor
Prof. Ilaria Butera, Co-Supervisor

Doctoral Examination Committee:
Prof. Gabriele Villarini, Referee, University of Iowa
Prof. Giuseppe Formetta, Referee, Università di Trento
Prof. Attilio Castellarin, Università di Bologna
Prof. Alberto Viglione, Politecnico di Torino
Prof. Daniele Ganora, Politecnico di Torino

Politecnico di Torino
2022

Declaration

I hereby declare that the contents and organization of this dissertation constitute my own original work and does not compromise in any way the rights of third parties, including those relating to the security of personal data.

Paola Mazzoglio
2022

* This dissertation is presented in partial fulfillment of the requirements for **Ph.D. degree** in the Graduate School of Politecnico di Torino (ScuDo).

Acknowledgements

First, I want to thank my PhD supervisors, Pierluigi Claps and Ilaria Butera, for contributing to my personal and professional growth, for the support received in these years and for the opportunities that they offered to me.

Thanks to Demetris Koutsoyiannis, Theano (Any) Iliopoulou and Panayiotis Dimitriadis for advising me during my research period in Athens. The work described in Section 7.6 was performed with their supervision and help.

Thanks for the scientific support offered by Daniele Ganora in Chapter 5, by Massimiliano Alvioli in Section 6.5 and by Roberto Deidda in Section 7.4.2. Thanks also to Jost von Hardenberg and Paolo Dabove for some useful suggestions received during the yearly evaluations of my PhD path.

I would like to express my gratitude to Gabriele Villarini and Giuseppe Formetta for their suggestions to improve and strengthen this work. Thanks also to the other members of the doctoral examination committee, Attilio Castellarin, Alberto Viglione and Daniele Ganora.

Thanks to Giulia Evangelista, Irene Monforte, Martina Brunetto and Giuseppe Volpini for having shared with me some working experiences and lots of lunch breaks in these three years. Thanks to the old and new room mates of Ufficio 6 for their support and their friendship.

Thanks to Simone Balbo for having believed in me since the beginning and for making me understand that doing research is funny and that this is the job I would like to do "when I grow up". Thanks also to Guido Di Carlo for being one of the best friends I could ever wish to have by my side over these years spent on a roller coaster.

Thanks to my family.

Last but not least, I acknowledge the regional agencies involved in the management of the rain gauge networks that provided the rainfall measurements included in the Improved Italian – Rainfall Extreme Dataset (I^2-RED) and the LEXIS (Large-scale EXecution for Industry & Society) H2020 project (grant agreement 825532) for the provision of the surface rainfall intensity data of the Italian weather radar mosaic used in Section 7.3.

Abstract

Extreme rainfall is one of the most critical hazards worldwide, and Italy makes no exception: the vulnerability is particularly high due to a high population density associated with complex topography, extended coastlines, and high climate variability. The statistical investigation of short-duration rainfall extremes is thus a challenging and evolving topic.

In this work, the first national-scale quality-controlled dataset of rainfall extremes is presented, together with simple but effective methods for the detection of errors and inconsistencies. The so-called Improved Italian - Rainfall Extreme Dataset (I^2-RED) is a collection of short-duration (1, 3, 6, 12 and 24 hours) annual maximum rainfall depths measured by more than 5200 rain gauges from 1916 to the present. An exploratory statistical analysis carried out to identify extremes that could be considered "critical" in relation to the local climatology is here reported. This work highlighted that particularly intense rainfall events (in relation to the mean annual rainfall depth) are generally concentrated near the coastline. However, the work also shows a uniform spatial distribution of time series that contains a maximum value twice as large as the second highest one, suggesting that these “Super-Extremes” can be recorded almost everywhere. The analysis was then further expanded by investigating the possible presence of temporal trends in the time series. The results confirmed that rainfall extremes of different durations are not increasing uniformly over Italy and that separate tendencies emerge in different sectors, even at close distances.

A second dataset was thus created: it represents a collection of daily maxima recorded over a domain that coincides with the Po river basin and Liguria region. This second dataset was used to compute the Hershfield factor, that is a coefficient used to retrieved 24 h sliding maxima starting from fixed daily maxima, allowing to

take advantage of the relevant amount of information included in historical records of daily extremes.

The investigation of the influence of elevation and other geomorphological and climatological parameters on the index rainfall (computed using the data of I^2-RED) was also performed. The results of the national-scale regression analysis did not confirm the assumption of elevation being the sole driver of the variability of the index rainfall. However, when comparing the results of the best multivariate regression models with univariate regressions applied to small areas, it clearly emerged that "local" rainfall–topography relationships outperform the country-wide multiple regressions, offer a uniform error spatial distribution and allow the effect of morphology on rainfall extremes to be better reproduced.

Finally, a sequential application of interpolation to the annual maxima (patched kriging) is performed to provide reconstructed time series that are consistent with the measured values. Different configurations of the patched kriging incorporating the main results achieved in the overall work are applied and discussed. A first application over an area (Piedmont, Aosta Valley and Liguria) that is both bigger and more complex than the one used in the original methodology (Piedmont) is here presented and an improved methodology that handles the local-scale influence of elevation on the extremes is proposed. The application serves also to highlight the possible influence of a record-breaking event in the rainfall frequency analysis. Then, a comparison with other established approaches is performed over Sardinia and Thessaly (Greece).

The results summarized in this dissertation provide quantitative information for improving the rainfall frequency analysis for a future provision of maps of design rainfall for different return periods at the national scale, with potential impacts also in the flood risk assessment and reduction field.

Contents

List of Figures

List of Tables

Chapter 1

Introduction

1.1 Rationale of the Work

The investigation of the spatial variability of precipitation is the object of considerable research efforts and is still an evolving topic. The complexity linked to precipitation is induced by an unpredictable space-time variability and discontinuities both in space and time. Moreover, the time scale is a relevant variable: different behaviours and thus different problems emerge with increasing time windows.

Despite these shortcomings, the mechanisms that led to the genesis and development of rainfall events are quite well described in the literature (see e.g., Dayan et al. (2015)). Also the influence of reliefs on the spatial variability of rainfall depths, mainly in terms of variation of rainfall depth with increasing elevation, is relatively well understood (Smith (1979)). However, this is particularly true when dealing with multi-daily, monthly or annual precipitations. Extremes are instead more complex, and the number of studies performed to understand this complexity is lower.

The dependence of rainfall on elevation may be relevant in Italy (Avanzi et al. (2015)), that is the area investigated in this dissertation, due to the high degree of geographical and morphological heterogeneity of the country. However, a detailed analysis of the spatial variability of short-duration annual maximum rainfall depths and their connection to the landforms do not exist. Detailed studies are often complicated by the lack of dense and evenly distributed measuring networks and continuous time series (Libertino et al. (2018b)), posing major problems especially when dealing with the understanding of unpredictable events like convective storms. Possible

improvements in terms of spatial coverage could be secured by including remote precipitation measurements performed by satellites or weather radars. However, these sensors do not provide a direct measure of the rainfall intensity and are affected by errors and high uncertainty. Considering all these drawbacks, we can still consider the rain gauge measurements as the source of information with the highest accuracy.

Further complexity is introduced by the rare occurrence of "Extraordinary Extreme Events" (EEEs) (Pelosi et al. (2020)) or "Super-Extremes" (Libertino et al. (2016)) or "Black Swans" (Taleb (2007)), that are weather phenomena that can persist for hours over a small area producing rainfall amounts in the same orders of magnitude of the mean annual precipitation of that site. These high-impact events can often be easily explained once they occurred but could not have been predicted a priori. The rarity of these events can undermine the robustness of statistical approaches used for rainfall frequency analysis (see e.g. Laio et al. (2010)) and the assessment of the probability of occurrence of similar events (see e.g. Viglione et al. (2013)).

When writing this thesis, a major rainfall event affected the Marche region. This very intense quasi-stationary convective event developed since the afternoon of 15th September 2022 and, in about 8 hours, more than 300 mm of rainfall was recorded by a few rain gauges. Among all, the Cantiano rain gauge measured the highest values in the entire region (101.4 mm in 1 hour, 256.6 mm in 3 hours, 384 mm in 6 hours, 419 mm in 12 hours and 419 mm in 24 hours). Thanks to the data collected by the Regional Functional Center of Civil Protection of the Marche region it was possible to obtain some information about the rarity of the event.

To quantify the "extremeness" of this event, we can somehow compare these values with the climatology of the location. It is worth recognizing that the impact of the same amount of rainfall can produce significantly different damages depending on the area. As an example, we can consider a 170 mm rainfall falling in 24 hours over the city of Catania (Sicily). Here, the mean annual precipitation is about 650 mm (Braca et al. (2021)) and thus this extreme event that corresponds to the 26% of the expected yearly rainfall would certainly produce significant damages. The same amounts would instead be less problematic in other areas, such as the city of Verbania (Piedmont), located in an area characterized by 1800 mm mean annual rainfall (Braca et al. (2021)), thanks to infrastructures more prepared and designed to face similar extremes.

For the Marche region case study, the mean annual precipitation is about 1300 mm (Braca et al. (2021)) and, thus, the ratio is about 30%. Is this a particularly significant value? From a quick check of some of the main websites about historical meteorological records, it is possible to affirm that significantly higher historical values in relation to the mean annual precipitation have occurred in the past. So, which indicators effectively represent the rarity of the event?

We can start with the computation of the observed Severity Index (SI) of a rainfall event. Having established a reference duration, for example 3 hours, this index is computed as the ratio between the maximum rainfall depth observed in 3 hours during the event and the average of the maximum annual values historically observed in 3 hours. In the case of the event observed in Cantiano, this ratio is equal to 256.6 mm / 37.7 mm = 6.81.

How can we estimate the denominator of this equation? It is extracted from the historical series of the measurements of the Cantiano rain gauge, a series that has a length of more than 70 years, therefore very long and reliable in the Italian context. Repeating this operation for all the durations, the results that were obtain are:

- for the duration of 1 hour, SI = 3.82;
- for the duration of 3 hours, SI = 6.81;
- for the duration of 6 hours, SI = 7.87;
- for the duration of 12 hours, SI = 6.29;
- for the duration of 24 hours, SI = 4.72.

Are these indexes exceptionally high? To get an idea of the entity of these values, the same operation have to be repeated for the all-time Italian rainfall records, retrieved from https://www.arpal.liguria.it/files/HOME/massimiliguria20211004.jpeg (accessed on 27th September 2022).

For the 1 h duration, the record rainfall (181 mm) occurred in Vicomorasso in 2011. The average 1 hour extreme of that location, computed from the historical records, is 52.8 mm, corresponding to SI = 3.43.

For the 3 h duration we have to refer to the 377.8 mm fallen in Urbe - Vara Superiore in 2021, an area characterized by a mean rainfall depth of 144 mm, that allows to estimate a SI equal to 3.31.

Finally, the 6 h record of 496 mm of Montenotte Inferiore (year 2021) occurred in an area of 93.4 mm average rainfall, allowing to estimate a SI of 5.3.

From a quick look at Figure 1.1, which compares the Severity Indexes of the Cantiano event with those of the three Italian records of 1, 3 and 6 hours, the rarity of the characteristics of the Marche event clearly emerge.

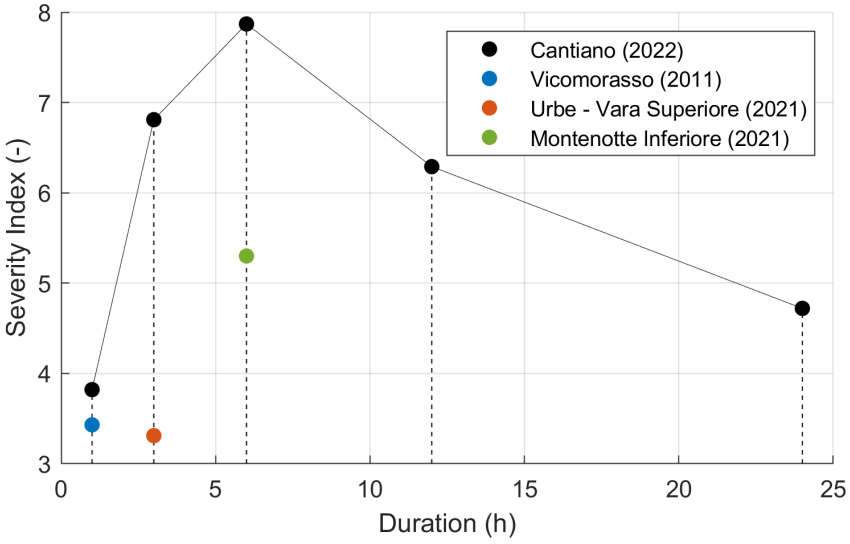

Fig. 1.1 Severity Index of the Cantiano, Vicomorasso, Urbe - Vara Superiore and Montenotte Inferiore case studies.

However, some open questions still remain. Should we expect another event of a similar entity in the near future in the same area? And what about other areas close by? Did this event happen in a place where such a large amount of rainfall would never have been expected? Did the geography and the morphology of that area contributed to enhance the rainfall quantity? Can we systematically map the spatial distribution of these Super-Extremes? Is the frequency of these Super-Extremes increasing over time? If yes, is this increase uniform over Italy? How can we cope with these records when performing a statistical investigation of these time series?

A considerable amount of meteorological measurements are potentially available in Italy for the investigation of these Super-Extremes but an easy and straightforward use of all of these information is not possible due to the very complex historical evolution of the national monitoring networks, that is managed by 21 different regional hydrological agencies since late '80 (Libertino et al. (2018b)). Each shift was often accompanied by changes in the network configuration and instrument

upgrade, which were not always properly documented. Moreover, the changes were not performed simultaneously in all the Italian regions, posing major problems when dealing with instruments located along the borders, often included in the databases of both regions with different values induced by different validation procedures. More details about the complexity of the Italian rain gauge network is provided in this dissertation. This work can be viewed as a first, massive effort to recover all the available information about extreme events that occurred starting from early '900 and transform them into a digital quality-controlled database that can be used to address the open points previously highlighted.

Independently from the problems related to data availability, considerable research is still needed to transform the established knowledge into concrete and robust tools for the assessment and management of the risk associated with extreme rainfall events, especially in a territory with a complex morphology and climate such as Italy.

1.2 Thesis Outline

The aims of this dissertation stem from the considerations mentioned above. Here, the meteorological aspects that lead to such extreme phenomena are only briefly mentioned. Instead, the main focus is the data-driven investigation of pieces of evidence and the development of operational tools for improving the prediction of extreme rainfalls over large areas, even in the case of extraordinary rainfall amounts.

The thesis is structured as follows.

Chapter 2 introduces the main concepts behind the regional rainfall frequency analysis approach, highlighting problems in the availability of complete and homogeneous data for the whole Italian country. The pros and cons of the approaches mentioned in this chapter are discussed.

In Chapter 3, the methodological approach adopted to build an improved and quality-controlled version of a database of annual maxima (in terms of both the rainfall depth values and the position of the rain gauges) is presented. The new database can be used as a more reliable research support for the frequency analysis of the rainfall extremes. A descriptive analysis of the maximum values of the stations, which provides an additional quality check and reveals different intriguing spatial features of Super-Extreme rainfall events, is also presented.

Chapter 4 deals with the reconstruction of a database of daily annual maximum rainfall depths, which is the time scale at which the majority of rainfall measurements in the world is available, especially in early '900. These records have been used for the computation of the Hershfield factor, a well-established index equal to the ratio between the 24 h and the daily extremes, widely used to recover the equivalent 24 h extremes from the historical daily records.

Chapter 5 investigates the spatio-temporal trends of sub-daily extremes in Italy. The investigation is performed both at the national and at the regional level using time series of at least 30 years using the record-breaking analysis, the Mann-Kendall test, the Regional Kendall test and the Sen's slope estimates.

Chapter 6 presents a systematic study of the relationship between geomorphological parameters and the average annual maxima (index rainfall) across the whole of Italy, with a specific focus on the influence of elevation.

Chapter 7 deals with the geographically-based analysis of rainfall quantiles, starting from the implementation of the patched kriging methodology over two areas that are more complex (from a geomorphological and climatological point of view) than the one used for the first application. Then, the concept of regional ombrian model is introduced, and a first comparison with the patched kriging is performed.

Chapter 8 concludes the dissertation. The main results achieved and the open points are here discussed.

Chapter 2

Regional Rainfall Frequency Analysis

The work described in this chapter has been partially derived from Claps et al. (2022b).

2.1 Introduction

Environmental engineers, hydrogeologists and, more generally, practitioners need a high number of field observations to answer engineering questions and design water management infrastructures. The collection of such information is often expensive and challenging, and its management and integration with historical data are complicated by the lack of homogeneous databases of measurements over large areas.

Suppose a long and complete rainfall depth time series is available at the site of interest. In this case, the application of standard frequency analysis techniques allows to build reliable intensity – duration – frequency (IDF) relationships for the estimation of the design rainfall for a given return period (Claps et al. (2022b); Koutsoyiannis and Iliopoulou (2022)). This application, which dates back decades (Sherman (1931); Bernard (1932)), generally requires annual maximum rainfall depths computed over time intervals from 1 to 24 hours. However, in some cases, annual maxima of sub-hourly or daily durations are also considered, especially when dealing with very small (in the first case) or large (in the second case) river basins.

Unfortunately, long and complete time series are available only for a limited part of Earth's surface (Kidd et al. (2017); Libertino et al. (2018a)). The increasing number of rain gauges installed annually by the various monitoring agencies allows an increase in the spatial details but further exacerbates the problem of working with records that are too short compared to historical ones. Thus, in ungauged locations and data-scarce regions, the design rainfall estimation is performed using techniques based on the concept of hydrologic similarity (Hosking and Wallis (1997)) that transfer the information of other gauged sites with similar characteristics. In other words, regionalization techniques rely on the "space-for-time substitution": the missing time series of the ungauged location is reconstructed by filling the gap with measurements coming from "spatially close" gauged sites (Blöschl (2011); Grimaldi et al. (2011)). The same approach can be applied in gauged locations with short time series compared to the return period under investigation (Faulkner (1999); Naghettini and Pinto (2017)).

Most of the regionalization methods rely on the "index flood approach" (Dalrymple (1960)) for the estimation of the design rainfall: the rainfall quantile $h_{d,T}$ related to duration d and return period T can be computed by multiplying the index variable h_d (that is generally computed as the mean or the median of the measurements distribution) with a dimensionless frequency quantile $K_{d,T}$ named "growth factor" (Equation 2.1):

$$h_{d,T} = h_d \cdot K_{d,T} \tag{2.1}$$

The index variable h_d is usually modelled with an average depth-duration curve which follows the power law

$$h_d = a \cdot d^n \tag{2.2}$$

where a is the scale factor (representing the best unbiased linear estimation of mean 1 h rainfall annual extreme) and n is the scaling exponent.

The estimation of rainfall quantiles is usually performed following the "simple-scaling approach" (Burlando and Rosso (1996)): the growth curve is considered as extracted from the same probability distribution for all the durations. Thus, a single growth factor is computed for the entire region, independently from the duration, leading to a compacted fan of IDF curves that follow the equation

$$h_{d,T} = h_d \cdot K_T \tag{2.3}$$

Limitations and exceptions to this approach, such as those highlighted e.g. in Marani (2003), are not discussed here because Svensson and Jones (2010) pointed out that this hypothesis is widely used in regional analyses adopted in various countries.

Traditional regional frequency analyses (RFA) are based on three steps:

- the data availability check;
- the definition of a homogeneous region and its growth curve K_T;
- the computation of the index rainfall curve h_d for the ungauged site using locally-available direct measure or through various spatial interpolation approaches.

In the last decades, statistical techniques that fall under the umbrella of "regional frequency analysis" have been developed to cope with data scarcity and fragmentation. This chapter explains the regional rainfall frequency analysis concept and summarizes the main techniques that can be used to address this problem. The three steps mentioned above will form the structure of this chapter, which represents an updated version of Claps et al. (2022b).

2.2 Variables to be Regionalized, Data Preparation, and Data Scarcity

2.2.1 Regionalized Variables

The selection of the proper variable to be regionalized represents a key point of the rainfall frequency analysis approach. Suppose that continuous rainfall measurements at high resolution (1-2 minutes for electronic, modern devices, or a continuous line for analogic, historical devices) are available. In this case, the "complete duration series" (CDS) can be computed using a moving average window of width d to process the series. The so-computed CDS includes all the rainfall measurements of a specific year aggregated using different durations and can be used to extract the peak values.

Partial duration series or peak-over-threshold (POT) series can be computed by extracting only those values that exceed a fixed threshold. Block maxima series are

instead computed by extracting only the highest values that occur within a fixed interval: if the period coincides with a calendar year, the extraction allows obtaining the annual maximum series (AMS).

Both approaches have their pros and cons, but the latter is the most common one, following the suggestion of Gumbel (1954). Moreover, one must consider that only AMS records are available for older time series, limiting the possibility of applying a POT-based method. POT is mainly preferred when it is necessary to increase the length of the time series for the estimation of critical high-return period and can provide valuable results when dealing with heavy-tailed distribution (Madsen et al. (1997); Marani and Zanetti (2015)). However, it should be noted that Claps and Laio (2003) pointed out that this approach is highly sensitive to the identification of the threshold.

The following step is related to the definition of the variable needed to compute the growth factor. Different alternatives are reported in the literature. Possible options are the regionalization of rainfall quantiles (Svensson and Jones (2010)) for a specific duration considering the simple scaling assumption (Soltani et al. (2017)) or for multiple durations considering the multiscaling approach (i.e., using a growth factor that varies both with the duration and with the return period; Burlando and Rosso (1996)). Other authors, instead, suggest that the regionalization of other variables must be preferred, such as the parameters of the probability distribution (see Svensson and Jones (2010) and reference therein) or the sample ordinary moments, or the L-moments (Smithers and Schulze (2001); Modarres and Sarhadi (2011); Ngongondo et al. (2011)).

The proper selection of the variable to be regionalized and the dependence of the variance of the regionalized parameters on the record length requires a deep understanding of the spatio-temporal variability for a proper estimation of high return period quantiles. An average practitioner can thus encounter some problems in distinguishing and understanding the different outcomes obtained when different variables are chosen. The production of precise regional guidelines is thus recommended to avoid severe inconsistencies during “critical application”, e.g. in areas with few data and high hydroclimatic or geomorphological variability (Libertino et al. (2018a)).

2.2.2 Data Preparation and Data Scarcity

Recent approaches tend to focus on the correct estimation of the return period of new record-breaking rainfall events that sometimes are recorded by rain gauges recently installed and thus with short time series. These measurements are often included in databases of other time series that are affected by sensor replacements, station relocations and gaps.

Two different approaches can be used to deal with data fragmentation.

The first one is based on the definition of a record length threshold: in this approach only time series longer than the threshold are considered in the RFA. Even if this approach can be considered precautionary, it also discards essential information included in short records and thus can affect the reliability of the overall RFA (Ouali et al. (2016); Libertino et al. (2018a)).

The second approach tries to conserve all the available information in relation to its influence on each parameter that must be estimated (Laio et al. (2011)): despite short records cannot be considered for the computation of the higher-order moments, they can still be relevant to improve the first order parameter estimation. In this case, robust assumptions are needed to avoid errors (Teegavarapu and Nayak (2017)). Numerous data augmentation techniques based on interpolation, data reconstruction or ancillary data have been developed recently to solve this problem. Pappas et al. (2014) used the correlation of the time series to deal with the gaps, highlighting that low autocorrelation or frequent/systematic missing data can undermine the methodology. Libertino et al. (2018a) developed the patched kriging to reconstruct missing information through a sequential application of the ordinary kriging to the measured annual maxima. Uboldi et al. (2014) suggested a bootstrap procedure that accounts for all the measurements in nearby gauged sites to obtain homogeneous annual maxima time series. However, this application is susceptible to outliers and can provide quantiles that significantly deviate from the ones computed using only the measured series. Finally, Ouali et al. (2016) proposed a conditional quantile regression to cope with data fragmentation. Ancillary data such as rainfall estimates provided by weather radars (Goudenhoofdt et al. (2017); Ochoa-Rodriguez et al. (2019); Kašpar et al. (2021)) and by satellite missions (Qamar et al. (2017)) can also be used in areas affected by data scarcity for data augmentation. However, considerable efforts have still to be spent on this topic to take advantage of such

information due to the low spatio-temporal resolution of satellite data (Zorzetto and Marani (2020)).

2.3 Regional Methods

2.3.1 Fixed Region and Region-Of-Influence Methods

In the RFA context, a homogeneous region is a domain where the statistical properties of the investigated variable can be considered constant. These regions are used to pool together all the data that fall inside them for the computation of a unique growth factor curve. The so-computed growth factor is kept constant for every point of the region.

A nondimensional sample can be obtained by normalizing all the time series that fall inside the region with the index value. If the curve is computed directly from the nondimensional sample, the method is named "station-year". The definition of a unique growth factor on the basis of this methodology is practical. Still, it does not allow us to properly take into account the different uncertainty that derives from the different lengths of the pooled series. A weighted average can be used to address this problem.

Moments of different order can be devised from different pooled sample using a hierarchical scheme, when a specific probability distribution is selected (e.g., the TCEV; Rossi and Villani (1994a)). More in general, regional L-moments of different order (Hosking and Wallis (1997)) coming from the same or from different samples can be regionalized (Alila (1999)).

The delineation of such homogeneous region is based on procedures that evolved over time (Reed et al. (1999)). The first approaches were based on fixed and non-overlapping geographical regions defined by splitting the study area into smaller regions that can be considered as similar in the geographic space from a climatological or morphological point of view (Cole (1966); see Figure 2.1). In the following years, some authors (e.g., Acreman and Wiltshire (1989)) suggested new methods for the delineation of fixed homogeneous region in the non-geographic spaces to minimize the usage of subjective delineation criteria. Relevant examples are regions defined in the space of the geomorphological descriptors, such as latitude, longitude,

elevation or distance from the sea (Le Gall et al. (2022)). Operational difficulties can emerge when the estimation point is in proximity of the boundaries of two adjacent regions. In this case, different delineation algorithms or subjective choices would potentially cause the point to fall in different regions that could be characterized by significantly different parameters, leading thus to different estimates, and hampering the overall robustness of the approach.

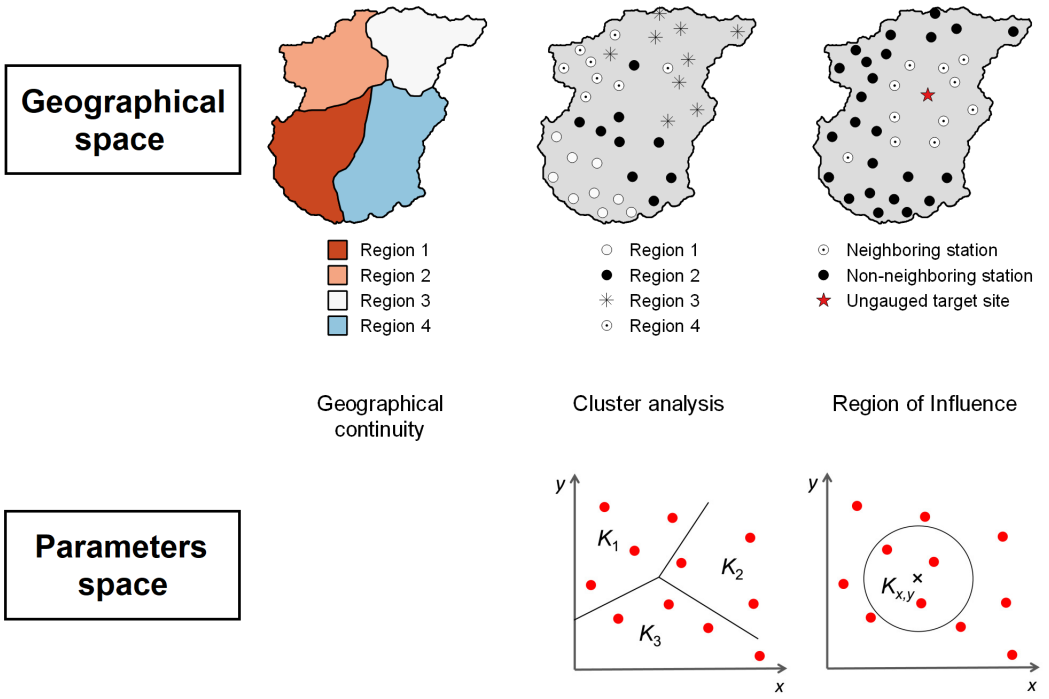

Fig. 2.1 Visual representation of the main differences among the geographical contiguity (fixed and non-overlapping regions), cluster analysis and region of influence approaches. Source: Claps et al. (2022b). Copyright holder: Elsevier.

Cluster analysis was then introduced to classify groups with similar behaviour within large collection of measurements or parameters (Satyanarayana and Srinivas (2008); Modarres and Sarhadi (2011); Ngongondo et al. (2011); Naghettini and Pinto (2017), Le Gall et al. (2022)). All these methods organize measurements into fixed and non-overlapping clusters (into the parameter space) with high internal similarity and with evident dissimilarities with all the others (Figure 2.1). However, Ganora and Laio (2016) suggested that, after the delineation, further adjustment may be required to ensure the internal homogeneity of all the regions.

To solve the shortcomings of these two approaches, the region-of-influence (ROI) approach (Burn (1990)) was proposed. This method has been progressively refined over the past years and represents the base of several national-scale applications, as highlighted by Svensson and Jones (2010). Into the ROI approach, the regions are no longer fixed (in whatever space) because a specific and individual region is defined for each ungauged sites of the study area (Figure 2.1). This method grants a good level of continuity of the estimates while moving in all the ungauged sites.

For all the three methods summarized before, the regionalized curve can be extended to ungauged sites only if the pooled sample is statistically homogeneous. Specific tests, as those mentioned in Hosking and Wallis (1997), can verify the statistical homogeneity (or the heterogeneity and thus outliers and discordant data) by comparing the sample L-moment ratios (dimensionless L-variance, L-skewness and L-kurtosis) of the different stations. Samples with statistical characteristics that are too different from those of the whole group are identified using discordancy measures (Hosking and Wallis (1997); Naghettini and Pinto (2017)). This approach requires the continuous application of these tests: large regions generally produce large samples that are less homogeneous, while small regions pool a little amount of data that generally cannot satisfy a minimum data requirement (see the UK FORGEX method reviewed in Svensson and Jones (2010)). The main drawback of this interactive process is that it converges to different but equally likely solutions.

Delineation processes aided by ancillary climatological information have been successfully suggested to limit such subjectivity, and possibly underline that the rainfall extremes are produced by similar weather mechanisms (Persiano et al. (2020)). Relevant examples of the definition of homogeneous regions performed using the mean annual precipitation are reported in Schaefer (1990), Alila (1999) and Gaál et al. (2008).

2.3.2 Regionless Methods

The name “regional frequency analysis” suggests that the definition of a region is necessary to pool a “critical mass” of data. However, if the return period that we want to investigate is small or if we want to estimate only lower order moments, the number of pooled information can significantly decrease (Rossi and Villani (1994a)). Similarly, if we want to investigate a highly variable quantity as the

index rainfall, the definition of homogeneous regions loses its significance. For this reason, interpolation and geostatistical methods (or, equivalently, non-geostatistical and geostatistical methods) have been suggested to estimate the index rainfall in ungauged sites (Trefry et al. (2005); Faulkner and Prudhomme (1998)). In recent years, recent advances in GIS techniques led to increased interest in these methods, not only for the index rainfall but also for higher order parameters.

The simplest interpolation techniques that can be used is based on Thiessen polygons: in essence, in every ungauged location, the record of the closest rain gauge is assigned (Goovaerts (2000)). This methodology, mostly used for the estimation of the areal rainfall, has been applied in several case studies, such as in the south of France (Creutin and Obled (1982)), in the central Continental United States (Tabios III and Salas (1985)) and in the south of Portugal (Goovaerts (2000)).

The spatial variability of low order moments can be assessed using regression methods than include geographical, geomorphological, and climatological covariates, especially in areas with complex topography that can play a significant role (Prudhomme and Reed (1998); Prudhomme and Reed (1999); Beguería and Vicente-Serrano (2006); Van de Vyver (2012); Carreau et al. (2013)). In all the cited work, however, a geographic-based investigation and explanation of possible model inadequacies are lacking.

Other possible approaches are those based on splines, thin plate splines (Carey-Smith et al. (2018)) or bilinear surface smoothings (Malamos and Koutsoyiannis (2016a); Malamos and Koutsoyiannis (2016b); Iliopoulou et al. (2022)).

By applying the inverse distance weighting (IDW) method, in each ungauged site it is possible to compute an estimate using a weighted average of the measurements collected in nearby gauged locations (Tabios III and Salas (1985); Goovaerts (2000)). This method considers the distance as the only relevant prediction criterion: in other words, the influence of each measurement on the site of interest decreases quadratically with its distance. The main drawback of this methods is the “bull’s eye effect”, an artifact that consists in an overweight of the measurements around the gauged locations. This artifact can be softened using geostatistical approaches like kriging. Considered the high recent interest in using geostatistical techniques into regionless methods, a separate section will be dedicated to this topic.

2.3.3 Geostatistical Techniques

A good estimate of the unknown variable, possibly free of artifact, and a measure of the estimation error is needed in most applications. Several geostatistical techniques, also referred to as kriging interpolations, were developed to fill these gaps in the past years.

The kriging technique was initially developed by Krige and Matheron (Matheron (1963)) and its application is becoming widely used in hydrology because of the characteristics of the rainfall fields. The spatial variability of rainfall is not a random process: given two measures in two different positions, the closer they are, the more similar they will be. Geostatistics takes advantage of the spatial correlation between neighboring stations to perform an estimate in an ungauged position (Goovaerts (1999)). Thus, the spatial dependence of rainfall measurements, which was usually considered a problem in the past approaches, can now be an advantage. In these past RFA methods, the target is the definition of homogeneous regions. The intersite dependence, that is quantifiable with the spatial correlation, acts like a reduction of the number of independent values available in such region because correlated time series merely duplicates the information content, reducing the added value of the inclusion of new stations (Svensson and Jones (2010)).

In kriging, the variogram defines the spatial variability of the estimates. It can be defined as the half of the spatial variance of the variable Z in two points spaced h, using the equation

$$\gamma(h) = \frac{1}{2}E\{[Z(x+h) - Z(x)]^2\} \tag{2.4}$$

where x is the location and E is the expected value (Blöschl (2011)). The kriging technique is a best linear unbiased estimator (BLUE). The estimator is called "best" when it leads to the minimum variance and "unbiased" when the expected value of the estimation error is zero (Kitanidis (1997)). The linear condition allows the evaluation of the unknown value $\hat{z}_0$ in position x_0 as a weighted average of nearby measurements, using the equation

$$\hat{z}(x_0) = \sum_{i=1}^{n} \lambda_i z(x_i) \tag{2.5}$$

where λ_i is the interpolation weight in position x_i and n is the number of measurements used in the interpolation.

The application of the ordinary kriging (OK) is based on the assumption that the mean values is constant but unknown. The spatio-temporal complexity of rainfall fields as a result of orographic effects can lead to heterogeneity and anisotropy that are not adequately handled by applying the ordinary kriging (Prudhomme and Reed (1999)). The local mean may not be representative of the local value in the presence of strong trends and thus, the ordinary kriging should not be applied over the entire domain. A possible solution consists in restricting the analysis using smaller moving windows around the estimation location to apply an ordinary kriging using only the data within the windows. The window size should be small enough to consider the sub-areas as stationary and large enough to include enough measurements (Grimes and Pardo-Igúzquiza (2010); Fouedjio (2017)).

The presence of significant trends can be adequately handled by using other approaches. As an example, the trend can be removed for a safer application of the ordinary kriging on the detrended values (Prudhomme and Reed (1999)). This methodology is named detrended kriging or regression kriging (RK) and can be successfully applied if the correlation coefficient of the trend is high and if the variables have a significant number of common data point to build the regression model (Ahmed and De Marsily (1987)). Consequently, regression kriging might perform poorly if the sample is small and non-representative, if the points do not represent the entire domain or if they are concentrated only in the central part and if a non-linear relation links the target variable and predictors (Hengl (2007)). Moreover, bad performances can also be achieved if the data come from different sources and if the data have been sampled with a biased design (Hengl (2007)).

The correlation between the observed variable and an additional information, also named “drift” or “external drift”, can be handled using kriging with external drift (KED) (Varentsov et al. (2020)). The drift is not likely to be constant in all the directions (Hudson and Wackernagel (1994)). When dealing with rainfall measurements, the elevation is often considered as the drift. Only in recent years, weather radar data have been used as well (Berndt et al. (2014)). While in regression kriging the deterministic (i.e., the regression model) and the stochastic (i.e., the kriging) prediction are performed separately, in KED both components are predicted simultaneously, i.e. the drift is modelled together with the variable (Hengl (2007)). Measurements of the second variable should be available at many locations and should be able to represent the underlying structure of the first, low-sampled variable (Ahmed and De Marsily (1987)). Moreover, the two variables should be highly

correlated (Ahmed and De Marsily (1987)). If this correlation is high, the RK and KED prediction error will be lower than OK error (Hengl et al. (2003)).

The cokriging has been developed to improve the estimation of a variable by using another spatially correlated variable with better spatio-temporal availability (Ahmed and De Marsily (1987)). It represents an extension of the classical kriging approach that handles multivariate data and a multivariate variogram or a covariance model (Wackernagel (1998)). With this approach, measurements may not cover all the sample locations: the data can be available either at the same or at different points for each variable, leading to isotopic (in the first case) or heterotopic (in the second case) datasets (Ahmed and De Marsily (1987); Wackernagel (1998)). More specifically, if the variables are available at different points and have no sample location in common, we can refer to heterotopic data, while if variables share some locations, we can refer to partial heterotopic data. If data of all variables are available at all sample point, an isotopic condition occurs. Cokriging should be used to improve the prediction if the number of secondary variables is low and if they are not available at all sample locations (Hengl et al. (2003)). If the secondary variables are available in all the locations and are correlated with the main variable, KED should be used (Hudson and Wackernagel (1994); Hengl et al. (2003)). A strong correlation between the primary and the secondary variables is fundamental to obtaining a stable cross-variogram (Prudhomme and Reed (1999); Grimes and Pardo-Igúzquiza (2010)). If the data have spatially correlated residuals and the correlation coefficient is high (> 0.7), cokriging is, in general, a better estimation compared to other techniques (Ahmed and De Marsily (1987)). Conversely, cokriging provides results like those obtained with kriging with external drift or regression kriging. In the case of spatially uncorrelated residual of the estimation, cokriging introduces less bias but does not give the best estimates: in this case, regression kriging is a better estimator for all values of the correlation coefficient, but with a slightly higher bias compared to KED (Ahmed and De Marsily (1987)).

Independently from the techniques, kriging is used to interpolate the distribution parameters or the rainfall quantiles (Das (2019)). Ordinary kriging is a quick and reasonably accurate predictor if the spatial interpolation is the only desired result. However, the presence of noise induced by measurement or sampling errors can affect the optimal nature of the ordinary kriging. As a consequence, when the data to be interpolated are statistical values (e.g. the parameters of a distribution), the results can be affected by the noise of the data. The kriging for uncertain data (KUD)

has been proposed to provide an answer (De Marsily (1986); Furcolo et al. (1995); Deidda et al. (2021)). Considering that measurements are assumed to be known with an uncertainty, in KUD the interpolation is less sensitive to the local sample, compared to the ordinary kriging. Consequently, values obtained from considerable record lengths are typically characterized by less variance and, thus, the sample values are confirmed by the kriging.

Geostatistical techniques generally outperform all the other interpolation methods described in Section 2.3.2 (Tabios III and Salas (1985); Goovaerts (2000); Das (2019)). The improvement became relevant when dealing with a low or uneven data density. This positive behavior is particularly important when dealing with rainfall measurements because the agencies in charge of the maintenance of the rain gauge network usually install new devices mainly considering the spatial variability of the rainfall phenomena and the accessibility of the observation sites, instead of guaranteeing a uniform data density. However, even sophisticated techniques such as the kriging can suffer from the lack of data, uneven density, or low data representativity in a complex environment as the mountainous regions, especially considering that the spatial structure of rainfall is highly influenced by the accumulation time of the rainfall amount (Prudhomme and Reed (1999); Grimes and Pardo-Igúzquiza (2010)).

2.4 Methods Adopted in the Practice: the Italian Example

A detailed review of the RFA approaches used in Canada, United States, Sweden, France, Germany, United Kingdom, South Africa, New Zealand, and Australia is reported in Svensson and Jones (2010) and references therein. In several nations, rainfall or hydrological atlases support the practitioners, that can take advantage of already computed precipitation estimates for different durations and return periods. It is interesting to notice that in many nations, more established methods developed in the past are still preferred to new ones. The Italian case is not mentioned in such revision. This section describes the main techniques currently in use in Italy, reviewing them in an international context.

The methodology developed in the Valutazione delle Piene (VAPI) project represents the main national method. The VAPI methodology (Rossi and Villani (1994a))

is based on a hierarchical approach in selecting homogeneous regions, where higher-order parameters are considered uniform in areas larger than the homogeneous regions of mid and low-order parameters. It is also one of the few methods based on a four-parameter distribution, the two-component extreme value (TCEV) distribution, and the parameter combinations allow three levels of fixed and non-overlapping regions (Rossi and Villani (1994a)).

During this project, the Italian territory was divided into macro-regions (named "compartments"): for each compartment, a detailed analysis was performed, and the recommended RFA methodology is described in a series of publications referred to each region. The full list of reports and relevant maps are available on http://www.idrologia.polito.it/gndci/Vapi.htm (accessed on 25th August 2022). The different compartments (also visible in Figure 2.2) are:

- North-West Italy, including the areas of Torino, Milano and Genova (corresponding to Aosta Valley, Liguria, Piedmont, Lombardy and some areas of Emilia-Romagna and Trento province);
- Triveneto, including the areas of Bolzano and Venezia (mainly Trentino-Alto Adige, Veneto and Friuli Venezia Giulia regions);
- compartment of Bologna, Pisa, Rome and Emilian areas of the Po river basins (corresponding to the regions of Tuscany, Emilia-Romagna and Marche);
- compartment of Rome and Pescara (mainly Lazio, Umbria, Abruzzo and Marche regions);
- compartment of Napoli (Campania region);
- Basilicata;
- compartment of Catanzaro (corresponding to Calabria region);
- Palermo (corresponding to Sicily region);
- Cagliari (corresponding to Sardinia region).

Fig. 2.2 Screenshot of the http://www.idrologia.polito.it/gndci/Vapi.htm website (accessed on 18th November 2022).

An evolution of the VAPI procedure has been developed for Piedmont (Furcolo et al. (1995)): a TCEV distribution is applied within a regionless approach based on kriging for uncertain data (KUD). Similarly, a dedicated regionalization was developed for Aosta Valley (Centro Funzionale Regione Autonoma Valle d'Aosta and Fondazione CIMA (2009)).

One of the main limitations of the VAPI is the lack of computer tools that can be used for its application: the mathematical formulation is described inside several regional reports. The second main limitation of this methodology is the lack of updates: the database used for its development has never been updated; thus, the procedure does not consider recent record-breaking events. To overcome this problem, new methods have been developed in smaller areas.

As an example, in Sardinia a geostatical methods based on KUD has recently been released (Deidda et al. (2021)). An application of this methodology is reported in this dissertation (Chapter 7 and Appendix D). In recent years, the patched kriging (PK) methodology (Claps et al. (2015); Libertino (2017); Libertino et al. (2018a)) has been developed as a data augmentation technique that can properly manage fragmented annual maxima time series of different lengths. The technique has been applied in Piedmont (North-West of Italy) and represents the operational regionalization technique recommended by ARPA Piemonte (i.e., the Regional Agency for Environmental Protection). The PK is one of the few RFA approaches developed to take advantage of all the available measurements, regardless of the length of the time series and the station relocation. Moreover, it is one of the few methodologies that considers the possible influence of elevation on the spatial variability of rainfall extremes (i.e., the orographic effect). Several studies proved that better predictions could be obtained when considering the relations between rainfall depth and elevation and explicitly include adjustment factors for specific topographic conditions (Svensson and Jones (2010)). As an example, in Canada adjustment factors depending on the type of relief are applied in mountainous regions (Svensson and Jones (2010)); in Germany, the KOSTRA model used for the spatial interpolation considers the gradient and the orientation of the slope of the terrain (Svensson and Jones (2010)); in the United States, the PRISM model includes several coefficients that depend on the geomorphology and allows the reconstruction of missing data (Daly et al. (2002)).

However, the availability of different regionalization methods for the same areas can pose a problem to non-expert users that need to choose among different probability distributions and different regionalization methods (Svensson and Jones (2010)). Model selection criteria, like the Akaike information criterion, the Anderson-Darling criterion and the Bayesian information criterion can support the evaluation of the model performances, even if the identification of the "best model" is a difficult task (Di Baldassarre et al. (2009); Velázquez et al. (2011)). Conversely, a model-averaging approach can reduce the uncertainties in the estimation of large return period quantiles. The possibility of having simple GIS-based softwares for a multi-model RFA can facilitate their applicability. A recent example is the MultiRain tool that has been developed for Piedmont region (Grasso et al. (2020)).

2.5 Conclusions

The state of the art of rainfall regional frequency analysis, developed to estimate the design rainfall in ungauged sites, has been reviewed in this chapter. While for many years the definition of homogeneous regions has been highly debated, now the attention is focused on regionless methods. However, it is worth highlighting that most of the national approaches are still based on the definition of homogeneous regions, while most advanced techniques as those based on geostatistics are still not used, even if widely documented into the literature.

Every approach mentioned in this chapter has its pros and cons, thus not allowing to define the "best" way to perform a regionalization (Svensson and Jones (2010); Blöschl (2011)). The following parts of this thesis will address the main shortcomings previously mentioned, suggesting new possible improvements applicable to established methodologies.

Chapter 3

Sub-daily Rainfall Extremes: the Improved Italian – Rainfall Extreme Dataset (I^2-RED)

The work described in this chapter has been partially derived from Mazzoglio et al. (2020).

3.1 Introduction

The frequent recurrence of intense rainfall events that trigger catastrophic flash floods is a climatic signature of Italy, and is one of the causes of the high vulnerability of the Italian territory, where a high population density is associated with a complex topography, extended coastlines and high climate variability. According to the Istituto Superiore per la Protezione e la Ricerca Ambientale (ISPRA), 4.1% of the Italian territory is characterized by a high probability of inundation scenario (return period of 20–50 years), 8.4% by a medium-probability scenario (return period of 100–200 years) and 10.9% by a low-probability scenario (Trigila et al. (2018)). An accurate estimation of extreme rainfall (in terms of magnitude, duration and frequency) is urgently needed for such a complex and vulnerable territory for planning, design and management purposes. The need to build a uniform dataset of rainfall extremes for Italy is evident, due to its position in the middle of the Mediterranean Sea, to integrate meteorological and climate data from the past, and to better discriminate the hazard

of rainfall deriving from Synoptic Systems, Convective Systems or Mediterranean Hurricanes ("Medicanes") (Cavicchia et al. (2014); Libertino et al. (2018b); Greco et al. (2020); Pelosi et al. (2020); Zhang et al. (2021)).

Rainfall frequency and large-scale trend analyses require a complete, updated and quality-controlled dataset of extreme rainfall depths, which are usually available in the form of annual maxima records. Unfortunately, this type of information still requires efforts to increase the uniformity of the data: such information is fragmented in Italy (each Italian Region collects a subset of this information) and processed/stored in different formats (Libertino et al. (2018b)). The most recent effort made to complete a uniform Italian database of rainfall extremes is the Italian–Rainfall Extreme Dataset (I-RED; Libertino et al. (2018b)), which is an upgrade of the first database, created as part of the Characterisation of Ungauged Basins by Integrated uSe of hydrological Techniques (CUBIST) project (Claps et al. (2008)). The latter was mainly based on the digitalization of the Hydrological Yearbooks of the National Hydrological and Mareographic Service (SIMN) and on some additions resulting from the Valutazione delle Piene (VAPI) project (Rossi and Villani (1994b)). Among other databases, it is worth mentioning the one available for extreme daily rainfall (Pelosi et al. (2020)) and the one created by the Italian National Research Council (CNR) Research Institute of the Geo-Hydrological Protection (IRPI), which made reference to approximately 800 rain gauges in north-eastern Italy, in Trentino-Alto Adige, Veneto and Friuli Venezia Giulia regions (data available in digital format on https://www.irpi.cnr.it/en/product-service/dati-sulle-piogge-massime-annuali-nellitalia-nord-orientale/ (accessed on 18th November 2022)). As far as daily observational precipitation datasets are concerned, the ARchivio Climatologico per l'Italia centro-Settentrionale (ARCIS) database (Pavan et al. (2019)) is also interesting, as it was created using 1762 stations in north and central Italy, and interpolated them to produce a high-resolution (5×5 km) daily gridded dataset from 1961 to 2015. Other datasets that cover the Italian domain are reanalysis datasets, such as ERA5-Land (1950–present, 0.1° spatial resolution) (Muñoz Sabater (2019)), NOAA 20th-century reanalysis V3 (1836–2015, 1° spatial resolution) (Slivinski et al. (2019)) and MERIDA (1990-present, 7 km spatial resolution) (Bonanno et al. (2019)). The advantages of working with a rain-gauges-based dataset, like I-RED, emerge both as regards to the greater spatial resolution and in consideration that its annual maxima reflect the actual highest

rainfall in moving windows with length from 1 to 24 h. This is not the case for the reanalysis datasets.

The original I-RED database has been already used in a few investigations (see, e.g., Libertino et al. (2019)), but its coverage is limited to 2010, which does not allow, e.g., answering technical questions about recent and very severe weather events in Italy (e.g., the 2018 "Vaia Storm", Davolio et al. (2020)). It was therefore decided to update the available sources of data and to proceed with an advanced data quality control, in terms of consistency, redundancy, gap-filling of records and systematic geographical checks, to ensure that the corrected position and elevation of the stations could be of help in investigations on the spatial distribution of extreme statistics. The elevation of the Italian territory is quite variable, and it is therefore very important to deal with correct data about the geographic positions of the rain gauges in view of, for example, a geostatistical analysis, where the elevation provides additional information as a secondary variable (Goovaerts (1999); Prudhomme and Reed (1998)).

Such an effort has led to the production of a newly compiled first version of the Improved I-RED (I^2-RED) database, which includes, in the first release, the annual maximum rainfall depths for 1, 3, 6, 12 and 24 consecutive hours from 5265 weather stations across Italy, recorded between 1916 and 2019. Further inclusions were performed in subsequent steps: each chapter of this dissertation is therefore related to the most recent and updated version of the database at the time of the analysis. Details about the quality-control procedures applied to correct inconsistencies and errors are presented in the following sections, as well as details about the automatic and non-automatic quality checks applied by the agencies involved in the data collection before the data can be released.

The database shows a high level of uniformity: all the rainfall measurements are expressed in mm, while the positions of all the rain gauges are converted into a single, uniform reference system. Metadata are included in the database in pdf file format. The final version of the I^2-RED database is available on Zenodo, albeit with restricted access, due to the data policies of the regional hydrological agencies. Information about the data policies is reported at the end of this manuscript. A Digital Object Identifier (https://doi.org/10.5281/zenodo.4065266) and relevant keywords have also been assigned. Data are stored in both mat and in csv format (to make it accessible to all open-source programs). No specific code is required to access or work with the

data. The volume of the final database is less than 10 MB, thus making the database easily transferable and storable.

This chapter is structured as follows: Section 3.2 deals with the details of the data collection; the data updating and gap filling are described in Section 3.3, while the applied quality control procedures, e.g., to recover station elevations, are described in Section 3.4. A description of the quality-controlled database is given in Section 3.5, together with climatological information. An extreme value analysis and an additional error detection procedure are reported in Section 3.6. The discussion and conclusions are reported in Section 3.7, while the data policy is reported in Appendix A.

3.2 Data Collection and Data Policy

The historical data (i.e., data acquired before the dismantlement of SIMN) included in I-RED are freely available in the SIMN Hydrological Yearbooks. The dismantlement of SIMN, which was planned with Legislation Decree 112/1998, resulted in the data collection and management tasks being transferred to a regional level, that is, to 19 Regions and 2 Autonomous Provinces. Once the regional services had been set-up, the local authorities adopted different data distribution policies, even though, according to the Italian law, an Open Data policy should be applied to public data for research and no-profit purposes. The most important laws regarding Open Data in Italy are Legislative Decree 82/2005, Legislative Decree 36/2006, Law 221/2012, Legislative Decree 179/2012 and Law 114/2014 (Libertino et al. (2018b)).

As of 2022, some agencies have not published the data (raw or validated) on their website, and only make them available upon request, to track data usage and prevent them from being used for commercial purpose. Access to the data is granted after either sending a request or filling a request form that users can find on the agency's website. Those who have received authorization are then granted access to a database, the delivery of digitized tables or, on occasion, the delivery of pdf files. Information about the validation criteria applied by the regional agencies and measurement accuracy are, unfortunately, not provided together with the data. In early 1900, most of the instruments were mechanical ones. Starting from about 1980, all old mechanical stations were replaced with mechanical and digital ones. This led to data with different accuracies within the same dataset.

A list of the hydrological agencies that conduct the data collection and management after the dismantlement of SIMN are reported in Appendix A. The Provinces of Trento and Bolzano are located in the same Region, but are handled separately, because they have different data providers. To include them in the list, we generically refer to Italian "regions". Figure 3.1 summarizes the data policies of the original data, as reported in Appendix A. Information about the data policies and how raw data can be accessed is also included. In the new database, I^2-RED, each Italian "region" has a specific progressive number that ranges from 1 to 21, and this number is reported in the rainfall station ID assigned to I^2-RED.

Fig. 3.1 Data policy of the data reported in I^2-RED for the 21 Italian "regions". The provinces of Trento and Bolzano, despite being located in the same Region, are shown separately in the map as the data providers and the policies are different. Modified figure from Mazzoglio et al. (2020).

Because of the complexity of the data-merging operations, most of the work requested to build the new I^2-RED database was performed manually, by visually inspecting the data. Data merging was of fundamental importance, particularly as some "regions" did not have an editable, easily accessible and complete version of the database (most of them store the data in pdf files, on a yearly basis). Only some "regions" have carried out activities to merge historical and new data in an easily accessible format. Different geographic coordinate systems are used by the regional agencies. In some cases, historical and new data are even geo-referenced within the same "region" using different systems. In the I^2-RED database, all the station coordinates were made available in the Universal Transverse Mercator coordinate system (that is, WGS 84 UTM 32 N, EPSG 32632) to guarantee uniformity at the national level.

Like the I-RED database, which was created following four different procedures, depending on the data availability (Libertino et al. (2018b)), the creation of I^2-RED required the application of different methods that would be able to allow a rigorous quality check to be made, as described in detail in Section 3.3. Other quality checks are also described in Section 3.4 and Section 3.6. The entire workflow is summarized in Figure 3.2.

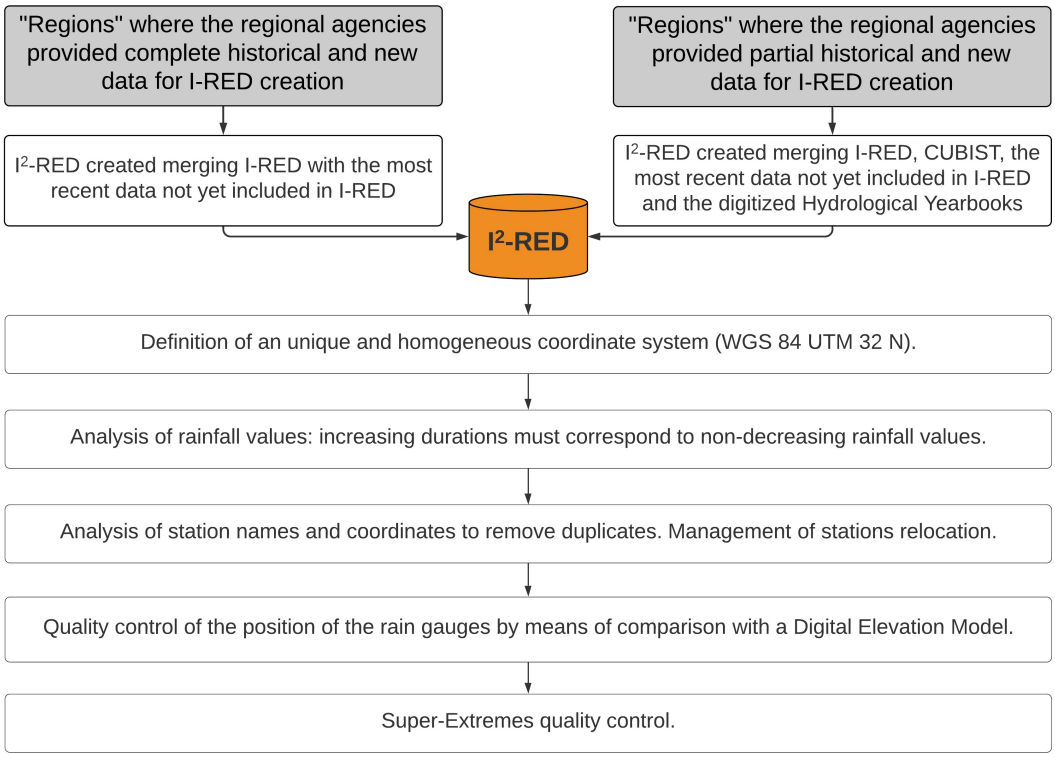

Fig. 3.2 Quality control workflow applied during the creation of I^2-RED. Modified figure from Mazzoglio et al. (2020).

The newly compiled first version of the I^2-RED database consists of 5265 stations, and the data covers the 1916–2019 period (the number of available stations can be seen in Figure 3.3). The lack of a considerable number of measurements between 1940 and 1950 is due to the Second World War, while the apparent reduction in the number of rain gauges between 1996 and 2000 was mainly induced by the effect of the dismissing of SIMN: in those years, some “regions” decided not to upgrade or repair the old rainfall stations, and most of the old mechanical tipping-bucket rain gauges were progressively substituted by automatic ones. Finally, the decreasing number of stations that emerges in recent years is due to the fact that, for the most recent years, validated data were not yet available in some “regions” at the time of the data collection.

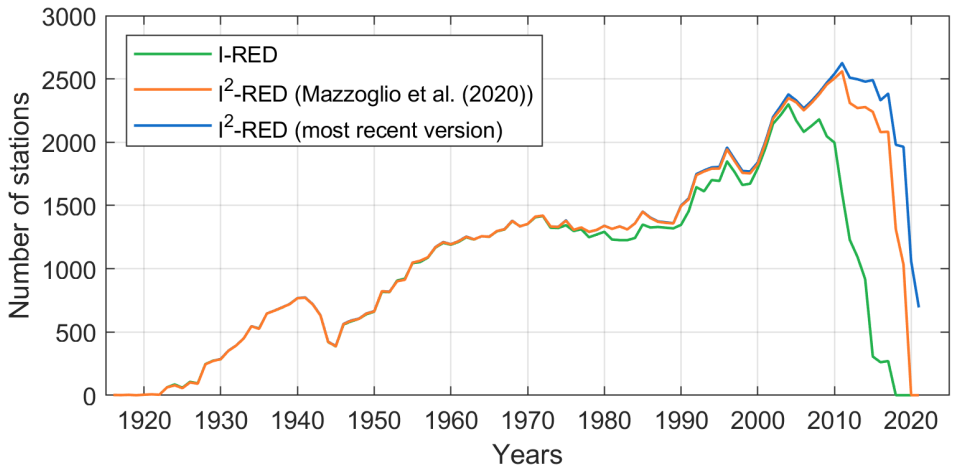

Fig. 3.3 Number of stations included in the two I-RED databases year by year. The green line refers to I-RED, while the red line refers to the version of I^2-RED used in Mazzoglio et al. (2020) and in this chapter. The blue line refers to the most recent and updated version of I^2-RED.

3.3 Data Update and Quality Control

As reported in Section 3.2, the data updating was accompanied by a robust and ad-hoc quality check that has taken into account how I-RED was originally created. In particular, in "regions" where the data provider had already digitized their part of the SIMN database, the CUBIST database was not used. In this case, the data updating performed in I^2-RED involved updating I-RED with the most recent data. In the other cases (i.e., in "regions" where the agencies only had partial coverage of historical data), the remaining historical measurements were extracted from the CUBIST database, and the data updating performed in I^2-RED was carried out manually in three steps, to maximize the available data and avoid duplicates. First, the I^2-RED database was updated to include the data for the most recent years that was not included in I-RED. Second, any data that were missing were extracted from CUBIST and then included. Third, because of the low number of digitized data for some years, a manual data input from the Hydrological Yearbooks proved to be necessary to fill the gaps in both the CUBIST database and in the digitized versions of the historical data received from the local authorities. To do so, the Hydrological Yearbooks (available as a scanned copy in pdf format) were digitized using optical

Table 3.1 Missing transcription in I-RED and I^2-RED for the different durations. The percentages were evaluated by comparing the total number of records related to each duration (i.e., 105,940 for I-RED and 122,217 for I^2-RED). Source: Mazzoglio et al. (2020).

Database	1 h	3 h	6 h	12 h	24 h
I-RED	0.98%	1.23%	1.12%	1.19%	0.88%
I^2-RED	0.87%	1.06%	1.01%	1.06%	0.78%

character recognition (OCR) software and compared with the already available data to detect values that had not been included.

Thanks to the previously mentioned gap-filling procedures in I^2-RED, it was possible to reduce the percentage of missing transcriptions. However, some inconsistencies in the series still persisted, e.g., cases in which a rainfall measurement was not available for a specific duration but was available for others. This could be due to transcription mistakes in the Hydrological Yearbooks. Table 3.1 shows the percentage of these missing transcription within both databases, and also highlights the greater completeness reached with I^2-RED.

A first algorithm-based analysis was performed to verify that rainfall values corresponding to increasing durations were consistent (i.e., the annual maxima related to a 1 h interval had to be lower or at least equal to the 3 h one). Several errors emerged within the database, thus highlighting the necessity of checking the value of the raw data to substitute it with the correct one or with a "Not a Number".

For a complete description of the first raw data quality improvement achieved in I^2-RED, it is important to highlight that almost every hydrological agency also has rainfall stations in nearby "regions", as a result of the joint management of interregional basins. The values reported in the I^2-RED database were therefore checked by comparing the time series of each rain gauge with all the other ones: this check allowed us to identify some stations located along the regional boundaries that had been included twice (sometimes with the same station name, sometimes not) with similar positions and the same rainfall values. As some "regions" shared their data with other agencies before applying a validation procedure, the visual data check was of fundamental importance to avoid data duplication. Stations with the same name, similar coordinates and with a time overlap were merged if the rainfall measurements were the same, otherwise they were considered as different stations in the presence of geographic or record length discrepancies. A few cases

of station-overlapping were also found in the case of stations with almost the same latitude/longitude (i.e., at a distance of less than 200 m).

A brief mention should also be made of the thorny problem of station relocation. Unfortunately, some "regions" did not track the relocation of some stations by changing the name, the position, or the instrument code in their databases. When it was possible to recognize that new and historical data had been collected by different weather stations (e.g., thanks to some years of missing data or to the information collected by regional authorities, reports), the data were handled separately, and two different stations were reported in I^2-RED. When it was not possible to obtain such information, the time series were merged and only one rain gauge was considered.

3.4 Quality Control on the Station Elevation

As mentioned in Section 3.1, one of the main innovations of the I^2-RED database, with respect to I-RED, is the extensive application of quality controls, both through manual and automated methods. We used the European Digital Elevation Model (EU—DEM), version 1.1 (European Environment Agency (2016)), a Digital Surface Model (DSM) with European coverage, a 25 m resolution and a relatively unbiased (-0.56 meters) overall vertical accuracy of 2.9 meters RMSE to check the reliability of each station elevation.

The planimetric position of each rain gauge was used to extract the corresponding elevation values from EU-DEM. After a comparison between the elevations obtained from EU-DEM and those reported in I-RED, several errors emerged in the original database. The relative difference between these two measurements was evaluated, and a threshold value equal to 150 m was used to identify rain gauges that needed to be checked and corrected before using the data for further analyses. As reported in Figure 3.4a, 790 stations out of a total of 5265 were affected by significant elevation errors, which varied from 150 to more than 2000 m.

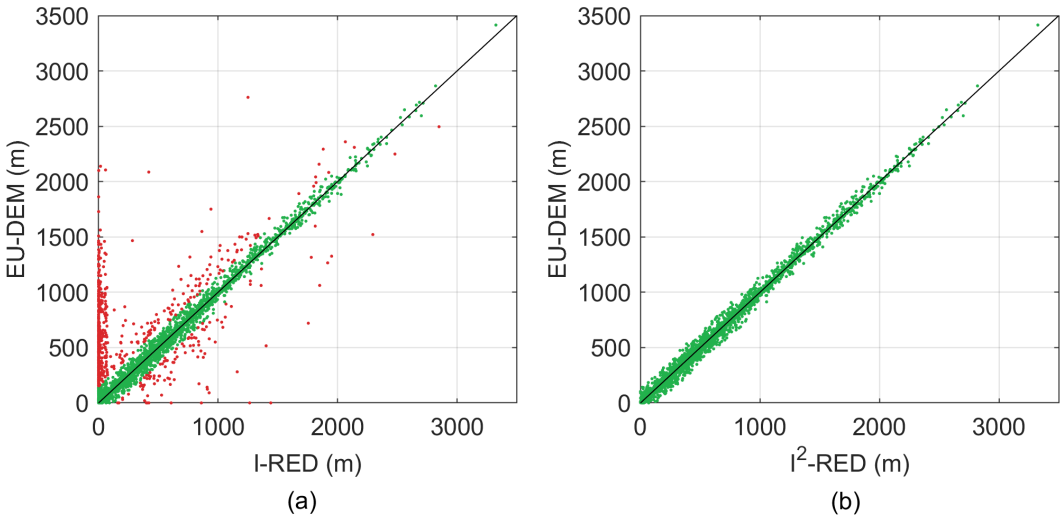

Fig. 3.4 Comparison between the elevation values before (a) and after (b) the quality control. The red dots in (a) identify the rain gauges included in I-RED that are characterized by an elevation discrepancy greater than 150 m, while the green ones identify rain gauges with a discrepancy lower than 150 m. Panel (b) refers to the same information for the I^2-RED database. Modified figure from Mazzoglio et al. (2020).

During this geographic analysis, it emerged that there were three types of elevation errors: (i) only an incorrect elevation, (ii) an incorrect position but correct elevation, (iii) both an incorrect position and an incorrect elevation. To understand the reasons for this variety of errors, it is important to note that the accuracy of the coordinates is not uniform in either the I-RED database or in the I^2-RED one. The coordinates of the rain gauges installed in recent years are characterized by metric or sub-metric precision, while the old ones have kilometric precision (i.e., in the Hydrological Yearbooks, they are expressed in degrees and in minutes, and no information is reported about seconds). Such a low positional accuracy explains why considerable errors could arise in the position and, more importantly, in the elevation, especially in mountainous areas.

A manual correction was applied to each of the points highlighted with a red dot in Figure 3.4a. In particular, information about the correct position was collected from other sources available online (e.g., reports, scientific publications). In some cases, the agencies involved in the data collection were contacted directly to discuss the issue. In the case of the Autonomous Province of Bolzano-Alto Adige, it was possible to partially substitute the positions derived from the Hydrological Yearbooks with more accurate ones, thanks to detailed information received from the competent

Table 3.2 Distribution of the rain gauges included in I^2-RED over different elevations. Source: Mazzoglio et al. (2020).

Elevation (m)	Number of station	Percentage
≤ 200 m	1782	34%
200 m < x $\leq$ 500 m	1499	28%
500 m < x $\leq$ 1000 m	1314	25%
1000 m < x $\leq$ 1500 m	401	8%
>1500 m	269	5%

regional agency. When possible (i.e., for the most recent stations), Google Earth was used to visually check whether a rain gauge was present in the position reported in the database, taking advantage of the Street View mode. In a few cases, when it was not possible to obtain further information about the position (e.g., for stations that were active in the early 1900s), a rain gauge was not relocated, and the elevation extracted for EU-DEM was confirmed. The results of the elevation quality control are shown in Figure 3.4b, which shows that all the rain gauges previously affected by an elevation error greater than 150 m have now been corrected in the I^2-RED database.

The distribution of the rain gauges over the different elevations in Italy is reported in Table 3.2. As can be seen, 34% of the rain gauges are located in sites with a lower elevation than 200 m a.s.l., while 62% of the rain gauges are located in sites with a lower elevation than 500 m a.s.l. Only 5% of the rain gauges are located in areas with a high elevation (i.e., > 1500 m a.s.l.).

3.5 Time and Space Uniformity of the Database

After the operations described in the previous sections, a new and reliable data source was compiled for the extreme rainfall in Italy. The main features of the data collection and of the update are presented in this section.

I-RED (Libertino et al. (2018b) was made up of 105,940 different records for every duration. The new I^2-RED database presents 122,217 records. By dividing the number of records by the number of stations (5265), it is possible to obtain the average length of the time series: 22.5 years for I-RED and 23.2 years for I^2-RED.

Some features of the rainfall stations are mapped in Figure 3.5. Figure 3.5a, in particular, maps the length of the time series of each rain gauge included in I^2-RED. Out of a total of 5265 rain gauges, only 3782 rain gauges have a time series equal to or longer than 10 years, 2283 rain gauges have a time series equal to or longer than 20 years, 1436 rain gauges have a time series equal to or longer than 30 years, 693 rain gauges have a time series equal to or longer than 50 years and 52 rain gauges have a time series equal to or longer than 80 years.

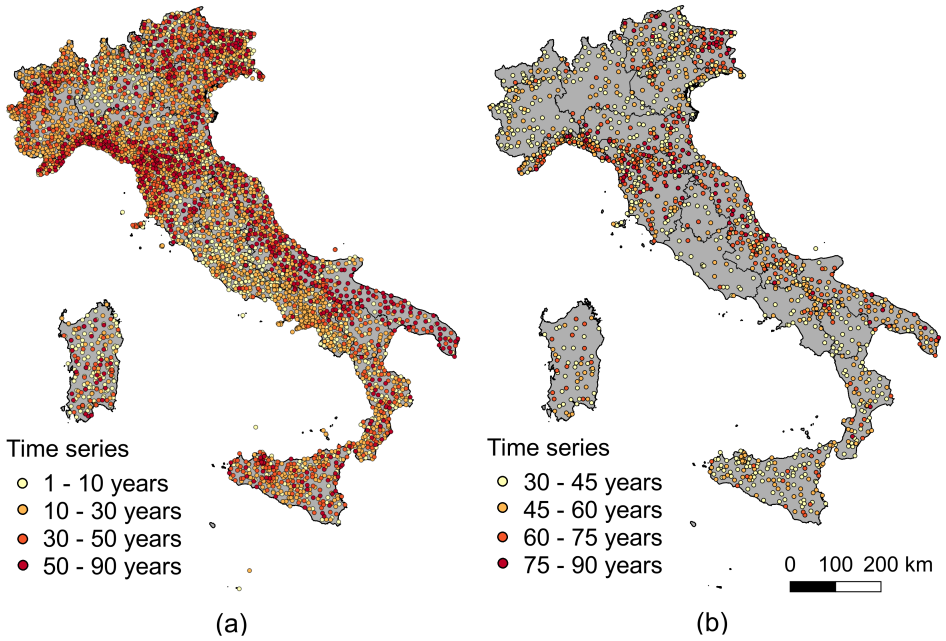

Fig. 3.5 (a) Position of the rain gauges in I^2-RED. The color refers to the length of the time series. (b) Spatial distribution of the rain gauges with a time series longer than 30 years. Modified figure from Mazzoglio et al. (2020).

The evolution in the management of the rain gauge network is one of the main factors that has led to a short and fragmented dataset in Italy. It is important to highlight that, although the database consists of 5265 rain gauges, only 1436 of these are characterized by a time series of at least 30 years, which is the standard length for climatological analyses (Li et al. (2018)) (Figure 3.5b). Although the most recent stations were installed to locally increase the network density, they unfortunately still provide little suitable information for these types of analysis. The inhomogeneity of the record length is also influenced by the different degrees of accuracy adopted by each regional agency. In fact, some agencies recorded small relocations of the station position, which do not break the series, while others did not (as already pointed

out in Section 3.3). To become aware of the spatial and temporal evolution of the Italian rain gauge network, it may be useful to watch a stop-motion video that shows a map of the active rainfall stations for each year of the whole observation period (https://www.mdpi.com/2073-4441/12/12/3308/s1 (accessed on 26th August 2022)).

The geographical uniformity and density of the stations throughout Italy are also worth considering. Observing the map in Figure 3.5b, it is possible to observe that Umbria, Lazio, Sardinia, Campania and Lombardy are characterized by the lowest densities (for named "regions" see Figure 3.1). In particular, the coastal area of Campania shows a very low number of rain gauges, even though it is known to be an area that is affected by a high number of extreme events. A general picture of the network density in the different "regions" in Italy is reported in Table 3.3.

However, more detailed information about the station density is still needed, due to the particular form of the Italian peninsula, and to an apparent proliferation of stations in highly urbanized areas. A clear variation in station density can, in fact, affect the spatial analyses of extreme rainfall quantiles, or evaluations related to the areal persistence of trends, as pointed out by Libertino et al. (2019). Figure 3.6 shows two density maps built with the I^2-RED database, using a spatial grid of 2×2 km. The number of rain gauges available within a 10 km radius, centered in the cell, was computed for each pixel of the grid (Figure 3.6a). Dense spots may be observed in correspondence to the cities of Rome, Turin, Bologna, etc. The sum of all the observations pertaining to the stations contained in the circle was systematically computed to take into account the density of observations (Figure 3.6b), thereby allowing any evident non-uniformity in the data density to emerge. High-density values can be observed for Northern Italy, especially over Liguria, southern areas of Piedmont, Tuscany and Friuli Venezia Giulia.

Table 3.3 Number of rain gauges with at least 30 years of measurements. The areas of the 21 "regions" were derived from ISTAT data (https://www.istat.it/it/files//2013/02/Superfici-dei-comuni.pdf (accessed on 26th August 2022)). Modified table from Mazzoglio et al. (2020).

"Region"	Number of rain gauges	Area (km^2)	Average contributing area (km^2/rain gauge)
Abruzzo	69	10,832	157
Basilicata	37	10,073	272
Calabria	69	15,222	221
Campania	36	13,671	380
Emilia-Romagna	125	22,453	180
Friuli Venezia Giulia	64	7,862	123
Lazio	28	17,232	615
Liguria	94	5,416	58
Lombardy	64	23,864	373
Marche	47	9,401	200
Molise	26	4,461	172
Piedmont	106	25,387	240
Apulia	98	19,541	199
Sardinia	58	24,100	416
Sicily	143	25,832	181
Tuscany	152	22,987	151
Autonomous Prov. of Trento	39	6,207	159
Autonomous Prov. of Bolzano	46	7,398	161
Umbria	13	8,464	651
Aosta Valley	14	3,261	233
Veneto	108	18,407	170

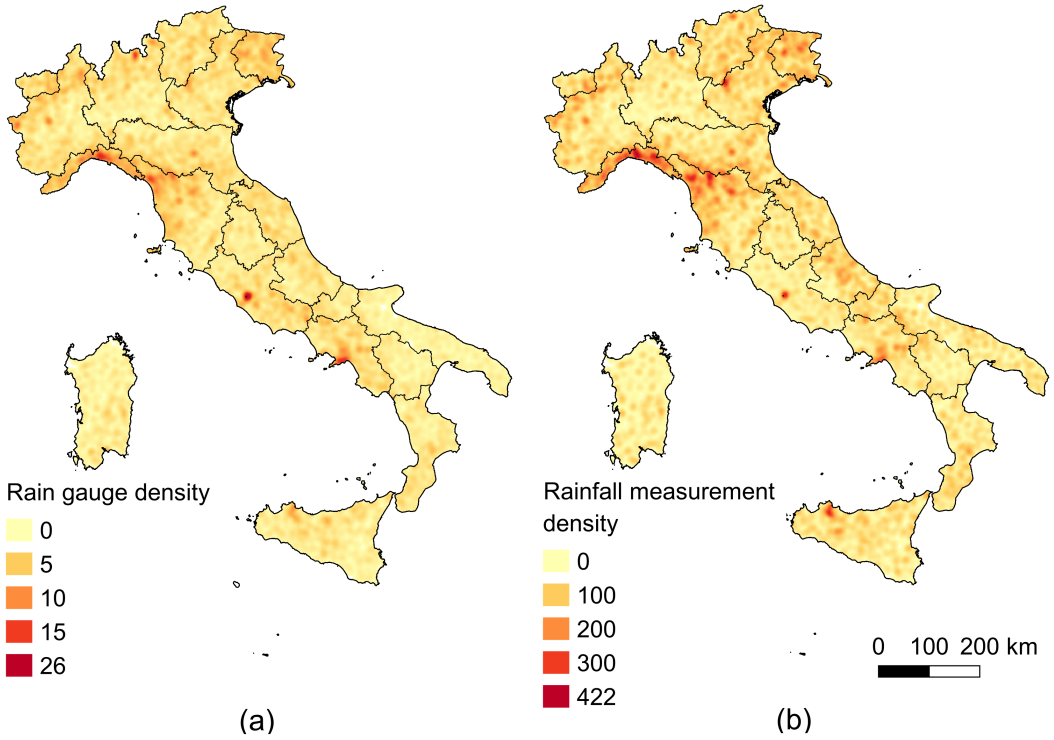

Fig. 3.6 (a) Kernel density map (obtained using QGIS Heatmap Plugin) with a spatial resolution of 2 × 2 km. The colors refer to the number of rain gauges available within a 10 km radius centered in each cell. (b) Kernel density map obtained with a distance equal to 10 km, spatial resolution of 2 × 2 km, and weighted with the length of the time series. The colors refer to the number of measurements (i.e., the sum of the lengths of all the time series available within a 10 km radius centered in each cell). Modified figure from Mazzoglio et al. (2020).

To explore the potential of the database to map the climatology of extreme rainfall at the national scale, a first preliminary analysis was conducted over the entire domain, starting with the representation of the parameters of the intensity–duration–frequency curves (IDF). As introduced in Chapter 2, the mean depth–duration curve is often expressed in the form of a power law relationship (Burlando and Rosso (1996))

$$h_d = a \cdot d^n \tag{3.1}$$

where h_d is the average of the annual maximum precipitation depth for the duration d, and a and n are site parameters estimated by means of linear regression between d and the available values of h_d. If a rainfall quantile h_d is required for a given return

period T, the above expression can be multiplied with a growth factor K_T, according to the index value approach (Svensson and Jones (2010)).

Rain gauges with at least 10 years of data were used to estimate both a and n for all the gauge sites. Kriged maps were then produced by applying an ordinary kriging with a spherical variogram and variable windows (a maximum value of 30 km was set to find at least five rain gauges). To avoid the smoothing effect of kriging induced by the fact that a station grid may not have coincided with the interpolation grid, pixels that contained one or more rain gauges were forced to have the IDF parameters equal to the maximum ones obtained within the pixel. The mapped values for a and n are shown in Figure 3.7a-b.

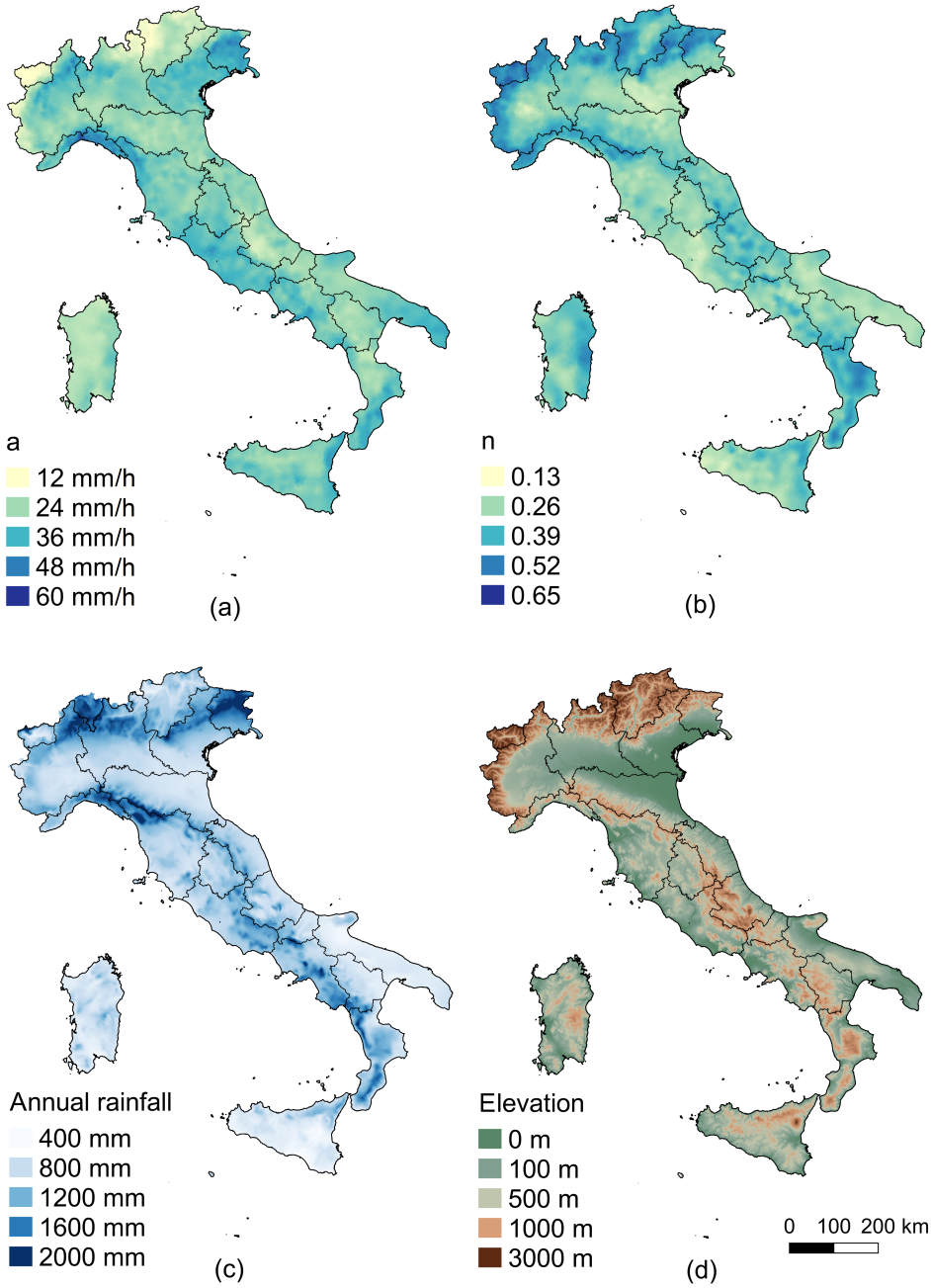

Fig. 3.7 Parameters a (a) and n (b) of the IDF curves evaluated on the basis of the data contained in I^2-RED. The maps are characterized by a 1 × 1 km spatial resolution. (c) Mean annual precipitation as mapped by Crespi et al. (2018). (d) Elevation data, Shuttle Radar Topography Mission (SRTM) digital elevation model. Modified figure from Mazzoglio et al. (2020).

The parameter a is approximately the average maximum rainfall recorded for a 1 h interval, and it shows higher values in Liguria, Friuli Venezia Giulia and in the northern part of Piedmont (Figure 3.7a). This parameter shows some similarities with the spatial distribution of the mean annual rainfall (Figure 3.7c) that is used here for climatic comparisons. This last map was compiled by Crespi et al. (2018) at a 30-arc-second resolution using rainfall measurements related to the 1961–1990 period. The parameter n (Figure 3.7b) shows higher values for high-altitude areas, such as in the alpine region.

To show to which extent the spatial distribution of these parameters can agree with known phenomena, a Digital Elevation Model of Italy was reported in Figure 3.7d. Local factors, such as the steepness of the terrain, slope orientation, aerosol content and stability of the atmosphere, can influence the orographic enhancement of precipitation, especially for long aggregation intervals (Napoli et al. (2019)). This can be recognized in the map of the exponent n (Figure 3.7b) as the higher n, the higher the increase in h_{24} with respect to the corresponding value h_1 (parameter a). On the other hand, short aggregation intervals (e.g., 1 h) show a different behavior, which leads to decreasing rainfall amounts as the altitude increases, especially over Northern Italy, as already shown in Allamano et al. (2009) and in Avanzi et al. (2015).

Similar results in terms of IDF parameters were obtained in regional-scale studies over Piedmont (Libertino et al. (2018a)), the Trento province (Borga et al. (2005)) and Sicily (Forestieri et al. (2018)), thus confirming the importance of working with a complete and updated dataset to avoid problems along the regional boundaries. The maps presented here can help showing the influence of the terrain morphology on the spatial variability of the averages of the rainfall extremes and point out the importance of having reliable information for the plano-altimetric position of stations.

3.6 Super-Extreme Quality Control

The highest values measured in each station, which were defined as "Super-Extremes" (Libertino et al. (2016)), have a particular importance in relation to the occurrence of the highest rainstorms in the Mediterranean area, and are worth emphasizing. These “station maxima”, computed for all the stations and all the durations, were analyzed to possibly identify further errors in the data, which had not been detected in the data

digitization and in the record upgrade process. By examining these values, it was indeed possible to detect unrealistically high annual extremes, after dividing them by the local mean annual precipitation depth (shown in Figure 3.7c).

This ratio, called "Normalized" Maximum Value (*NMV*), has helped to detect very high rainfall amounts relative to the climatology of the site. The *NMV* index was built as

$$NMV = \frac{X_n}{MAP} \tag{3.2}$$

where X_n is the station maximum value, while the mean annual precipitation (*MAP*) comes from an existing digital map (Crespi et al. (2018)). This index was introduced to highlight truly "extreme" events, that is, to distinguish them from other events, albeit very intense, which occurred in locations characterized by high annual rainfall amounts. Using various thresholds for *NMV* and considering the related frequency of occurrence, the aim was to provide an empirical, yet objective, representation of the spatial distribution of the highest relative extreme rainfall events in Italy, and to obtain clues about any local anomalies. In this regard, Figure 3.8 shows, as an example, the positions where *NMV* exceeds 0.5 for the 24 h aggregation interval. In comparison to Pelosi et al. (2020), and to some other well-known hydrometeorological disasters that had happened in Italy, the presence of some clusters was predictable, e.g., in Sicily, in Sardinia and in the Calabria Regions.

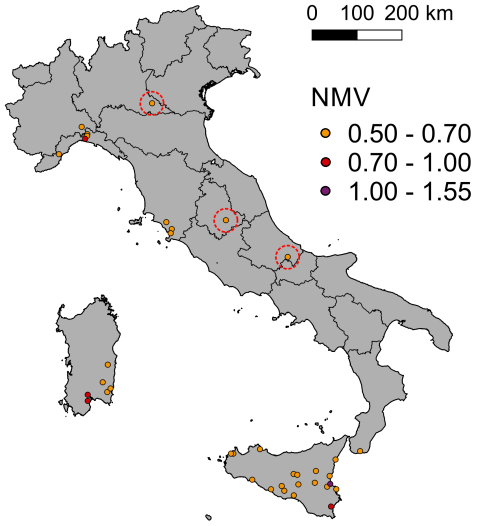

Fig. 3.8 Rain gauges characterized by greater "Normalized" Maximum Values (*NMV*) than 0.5 for the 24 h interval. The red circles indicate anomalous values. Modified figure from Mazzoglio et al. (2020).

However, some anomalies emerged for some very isolated values (circled dots in Figure 3.8). These values were checked by verifying the hourly or daily rainfall measurements acquired by the same and by nearby stations (when available) and by looking for evidence of a relevant heavy rainfall event in the news, in scientific articles and/or in disaster reports. After all these controls, all of these exceptional values proved to be the results of errors, and in all cases were attributable to a misplaced decimal separator in the original printed figures; the corresponding data were therefore adjusted in the dataset.

Figure 3.9a shows the highest *NMV* values of the corrected dataset for the 24 h aggregation interval, after lowering the threshold to 0.35. The map shows that most of the values are concentrated in areas with low mean annual precipitation (see Figure 3.7c as a reference). This may imply that the flooding impact in those areas may be higher, as infrastructures and the populations are not accustomed to frequent and intensive rainfall events in a dry climate.

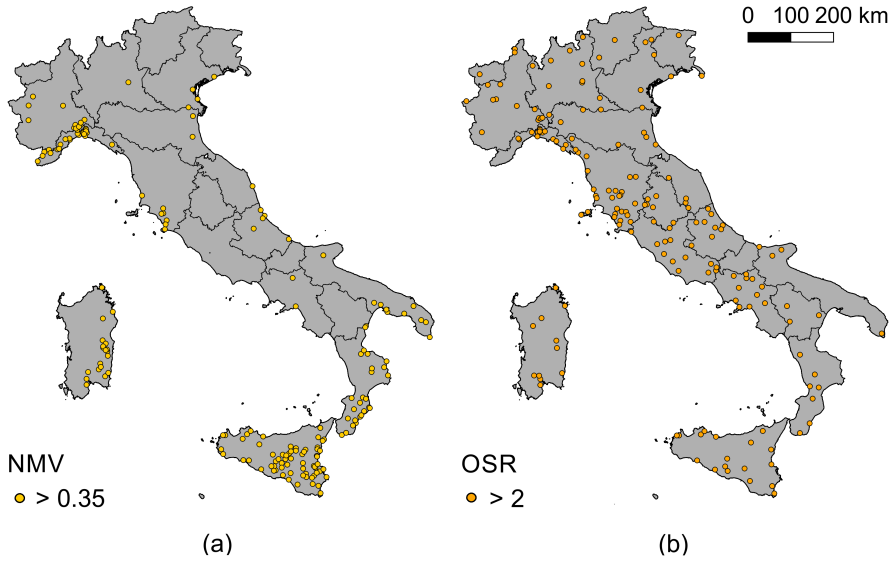

Fig. 3.9 (a) *NMV* of the corrected 24 h dataset. Values lower than 0.35 were removed from the figure to highlight the localities where the most extreme rainfall events occurred. (b) Rain gauges characterized by greater *OSR* than 2 for the 24 h interval. Modified figure from Mazzoglio et al. (2020).

A different empirical index was applied to station maxima considering the highest *k*th sample values. In a record of size *n*, the *n*th order statistic is the maximum value of the record (X_n), while the *n*-1th order statistic is the second-highest value (X_{n-1})

and so on (Kottegoda and Rosso (2008)). By extracting the nth and the n-1th order statistics of the annual maxima for each rain gauge, a non-dimensional index, named the "Order Statistic Ratio", was computed as

$$OSR = \frac{X_n}{X_{n-1}} \tag{3.3}$$

In Adler (2015), one can find some results on the distribution of the ratio of two smallest order statistics from an exponential variate. Even though no available results were found in the literature about finite-sample distribution of the ratio of the two highest-order statistics from extreme-value distributions, we assume that can be of interest to observe its spatial variability. This empirical ratio can be considered as an "outlier index" and has the advantage of being independent of preliminary assumptions about the probability distribution of the various samples.

The spatial distribution of the higher *OSR* values, computed for the 24 h maxima, can be observed in Figure 3.9b, where only rain gauges characterized by a greater *OSR* than 2 are reported. Counter-intuitively to the outcomes of previous analyses, the spatial distribution of these points is rather uniform, thus showing that high *OSR* values occur (and may occur in the future) at almost every site: even the areas with the lowest data density show these events. However, the Liguria Region is an exception, as it presents a significant concentration of high *OSR* values.

An attempt was made to find *NMV* and *OSR* threshold values that would allow a few but significant extreme events to be identified. In this regard, applying greater *NMV* thresholds than 0.35 and *OSR* ones greater than 2 allowed us to identify almost the same number of "Super-Extremes" (176 in the first case, 172 in the second one). These maps show that, with almost the same number of points, different selection criteria produce significantly different spatial distributions of these "severity" indexes. In both cases, the applied normalizations make the relevance of the selected events somewhat "relative", while absolute criteria (i.e., a threshold value of 250 mm/day) are applied in other cases, such as Pelosi et al. (2020).

3.7 Conclusions

Despite the high rain gauge network density throughout the Italian territory, an updated and quality-controlled dataset of annual maxima rainfall events over the entire Italian territory was not available before this work. The availability of only short and fragmented series of rainfall measurements, combined with the reduced spatial domains covered by each regional agency, had led to a somewhat limited representativeness of the results used to represent the climatology of extreme events in Italy, as shown, e.g., by Libertino et al. (2019).

In the present study, a new, updated and quality-controlled dataset of the annual maxima rainfall events was proposed, together with a representation of descriptive statistics that may be used to highlight the areas that are more vulnerable to extreme rainfall. More than 2000 different errors (in terms of incorrect planimetric/altimetric positions of the rain gauge or rainfall values) were detected in the original data and subsequently adjusted to improve the accuracy of a previous version of the database (I-RED), and this in turn led the release of I^2-RED.

The study shows simple but effective methods for the detection of errors in both the rainfall records and in the station positions. These methods are mainly based on the use of a digital elevation model to identify any position/elevation errors, and on the analysis of the severity of the most relevant extreme rainfall events.

Finally, analyses of the 24 h maxima of the stations were performed to preliminarily exploit the potential of the proposed database and to fine-tune the selection of the possible data errors. The maps of these Super-Extremes indices suggested that a high spatial persistence of particularly extreme rainfall events is concentrated in the coastal areas of the Italian territory, possibly due to the effects induced by a steep and complex orography near the sea (Fiori et al. (2014)). Further studies, based on the new database presented here, can suggest methods that can be used to objectively identify a coherent selection of Super-Extreme events, with the aim of contributing to the knowledge on the spatial distribution of this particular hazard.

Chapter 4

Spatial Variability of Empirical Indices: The Hershfield Factor

The work described in this chapter has been submitted and is currently under review.

4.1 Introduction

For decades, several hydrological variables as the rainfall depths were measured on a calendar day basis, usually at 9 a.m. local time (Morbidelli et al. (2021)). In Italy, those daily measurements are published in the Hydrological Yearbooks, a collection of data usually available only in printed format. The availability of shorter duration records as those described in the previous chapter was limited by the requirement of continuous monitoring rainfall gauges. After the replacement of the mechanical rain gauges with the automatic ones in the last decades of the 20th century, the reference time for the calendar day rainfall measure was shifted to 00 a.m. However, the daily measurement approach was never ended, even if it is widely known that such discretization in time leads to bias when dealing with extreme events (Papalexiou et al. (2016)). Considering the vast heritage of measurements and its simplicity, the majority of annual maximum rainfall depths in the world are at the daily scale, i.e. expressed over fixed 24 h (F-maxima).

It is clear, however, that sliding 24 h maxima obtained from continuous measurements (S-maxima) are more useful values. They refer to 24 h periods starting at any

instant and cannot be less than the F-maxima (Figure 4.1). An analysis conducted over the United States proved that the S-maxima statistics like the median, the mean and the standard deviation are higher than those of F-maxima and have a greater dispersion; the difference between the F- and S-maxima statistics increases as the time interval increases and appears to become constant for time scales larger than 36 hours (Papalexiou et al. (2016)).

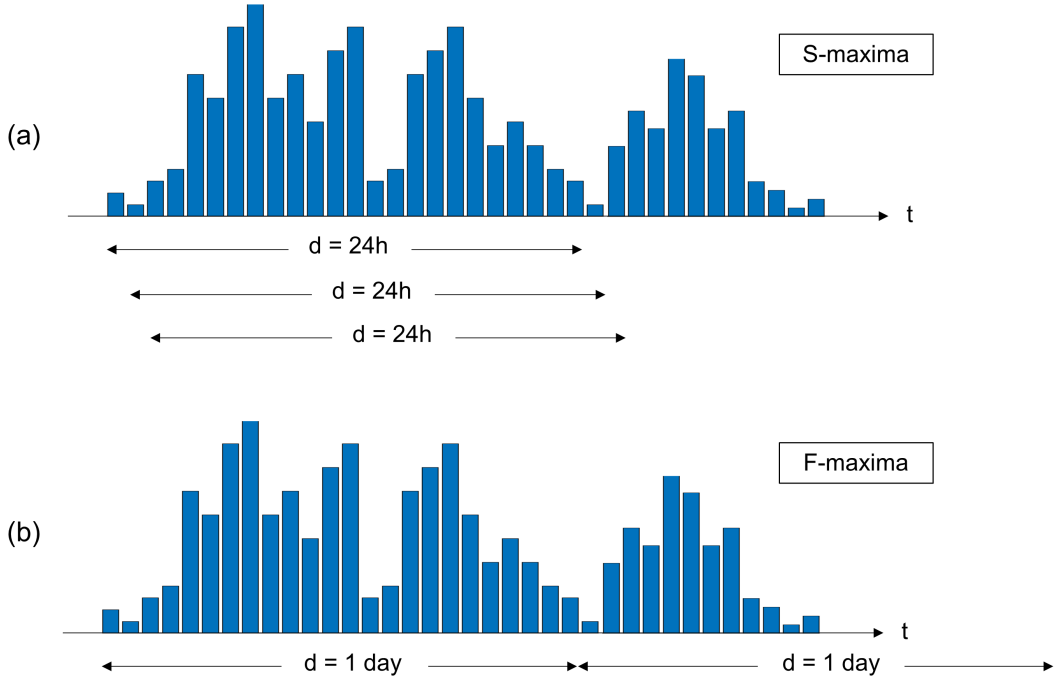

Fig. 4.1 Moving windows used to compute S-maxima (a) and F-maxima (b).

The ratio between F- and S-maxima, named Hershfield factor (H), has been suggested to correct the incongruences induced by the different time discretization, allowing to take advantage of the relevant amount of information included in historical records of F-maxima (Hershfield (1961); Harihara Ayyar and Tripathi (1973); van Montfort (1990); Dwyer and Reed (1995); van Montfort (1997); Papalexiou et al. (2016); Llabrés-Brustenga et al. (2020)).

H acts as a multiplier that aims at correcting the underestimation caused by the daily time sampling. Hershfield himself suggested to use a value equal to 1.13 after an analysis carried out using data covering the United States (Hershfield (1961)). In a recent analysis in the United States, Papalexiou et al. (2016) obtained a value equal to 1.14. An application over India suggested a value equal to 1.15 (Harihara Ayyar and

Tripathi (1973)). Over China, van Montfort (1997) obtained values in the range 1.04 – 1.17. Dwyer and Reed (1995) suggested a mean value of 1.16, while proposing differences according to different regimes: a correction factor of 1.15 for rainfall regimes with more frequent short-duration concentrated events, and 1.17 for sites with rainfall regimes with more frequent longer events, such as those produced by large frontal systems. Llabrés-Brustenga et al. (2020) obtained a mean value of 1.125 over Catalonia (Spain) and highlighted considerable variations within the year: summer is the season in which lower H (1.093) was obtained, justified by the fact that rainfall is often raised by the influence of the diurnal cycle and the S-maxima are not usually split by daily measuring in the morning; in spring, a higher H (1.161) was obtained, possibly determined by the fact that rainfall events are more often split when F-maxima measurements are taken at 8 a.m.

All these studies (except Papalexiou et al. (2016) and Llabrés-Brustenga et al. (2020)) are based on short and mostly obsolete records. In our study, we investigated the possibility of using $\approx$ 1000 stations with at least 10 years of both F- and S-maxima for the same years, covering the period from early 1900 until today, to enrich the availability of S-maxima rainfall measurements, by selecting the data-rich Po river basin and the Liguria region (North of Italy) as a case study. The objective is to obtain mean values of H for the stations where both F- and S-maxima data are available and make these value available, through spatial interpolation, to F-maxima stations where S-maxima data are unavailable.

4.2 Data Management and Quality-control

In this study, an area of about 90,000 km^2 extent located in the North of Italy that coincides with the Po river basin and the Liguria region was analyzed. The different administrative regions included in this area and the elevation data are represented in Figure 4.2.

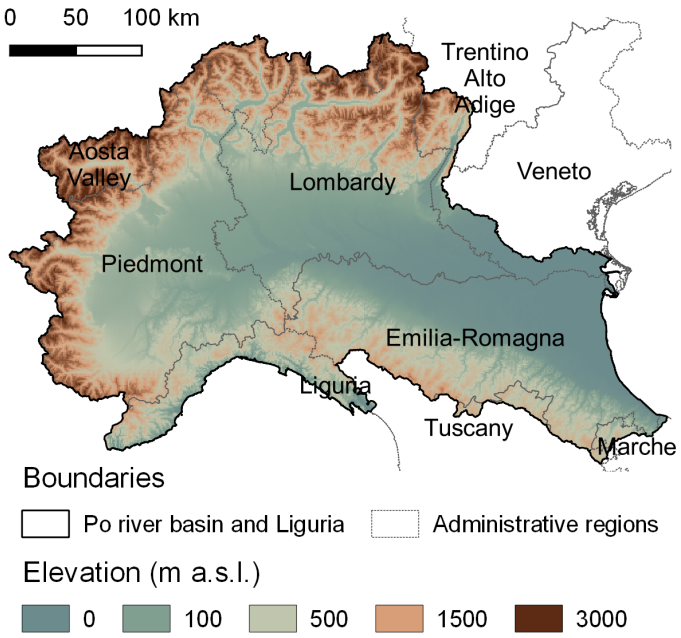

Fig. 4.2 Elevation data with borders and names of the administrative regions. Source: Shuttle Radar Topography Mission (Farr et al. (2007)).

Annual maximum rainfall depths related to a 24 h time interval (i.e., the S-maxima) are derived from the Improved Italian – Rainfall Extreme Dataset (I^2-RED; Mazzoglio et al. (2020)), a collection of rainfall extremes recorded since 1916 by more than 5200 rain gauges installed all over Italy. In this analysis only the time series of the 1713 rain gauges installed in the study area were used.

A set of validated F-maxima (i.e., quality-controlled daily annual maxima published in a dedicated table of annual maxima) is available in digital format on the websites of some regional hydrological agencies, such as ARPA Piemonte for the years 1988 – 2018 (http://www.arpa.piemonte.it/rischinaturali/accesso-ai-dati/annali_meteoidrologici/annali-meteo-idro/banca-dati-meteorologica.html, accessed on 1st October 2022), the Functional Center of the Autonomous Aosta Valley Region for the years 1994 – 2016 (https://presidi2.regione.vda.it/str_dataview_download, accessed on 1st October 2022), the VAPI Piemonte project for the years 1913 – 1986 (Villani (2003)), Meteotrentino for the years 1921 – 2009 (https://www.meteotrentino.it/#!/content?menuItemDesktop=111, accessed on 1st October 2022) and ARPA Veneto for the years 1984 – 2021 (https://www.arpa.veneto.it/bollettini/storico/precmax/, accessed on 1st October 2022). The spatio-temporal coverage of these datasets (Figure 4.3) is indeed very limited with respect to the printed version

of the Hydrological Yearbooks. The digitization of the Yearbooks tables containing validated F-maxima would require a massive effort, out of the scope of this work. To fill the spatio-temporal gaps caused by missing validated data, we resorted to available historical continuous daily rainfall time series, available in digital format, that are partially uncontrolled. The main data source that we used is the SCIA database (http://www.scia.isprambiente.it/wwwrootscia/Home_new.html, accessed on 1st October 2022). It has been integrated with few daily time series, coming from: ARPA Piemonte for 1988 onwards (http://www.arpa.piemonte.it/rischinaturali/accesso-ai-dati/annali_meteoidrologici/annali-meteo-idro/banca-dati-meteorologica.html, accessed on 1st October 2022), the "Banca dati meteoclimatica" of Liguria region (https://www.regione.liguria.it/servizi/item/14279-banca-dati-meteoclimatica.html, accessed on 1st October 2022), the "Atlante climatico della Liguria" for the years 1960 – 2010 (Agrillo and Bonati (2013)) and the Dext3r webapp (https://simc.arpae.it/dext3r/, accessed on 1st October 2022).

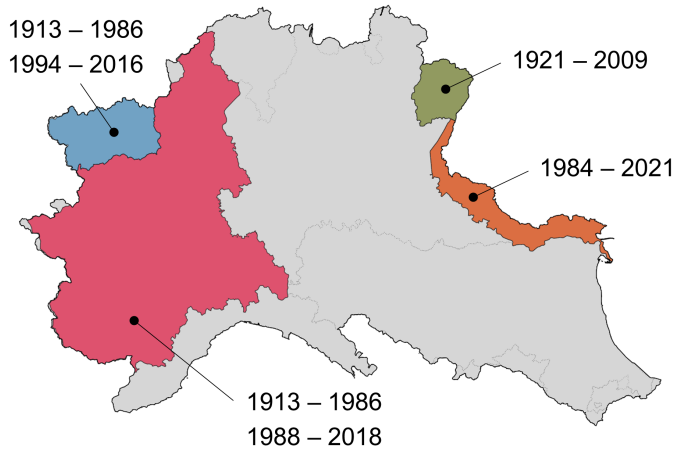

Fig. 4.3 Spatio-temporal availability of the validated F-maxima. Grey colour indicates areas where a database of daily annual maxima in digital format is not available.

In this study the influence of the change of the time of the daily measurements was not considered, because precise and extensive information on the years in which the hydrological agencies started to record the daily measurement at 00 a.m. is not available. However, it should be noted that Llabrés-Brustenga et al. (2020) pointed out that very high H is obtained only in the case of F-maxima taken with starting time in the afternoon. They also argue that F-maxima is usually more precise if sampled at 0 a.m., even though 8 a.m. can be considered as a good sampling time.

All the continuous daily time series of the datasets mentioned before were merged into a unique dataset. The SCIA database was found lacking some of the most relevant F-maxima recorded in recent years in the Liguria region: a manual gap-filling procedure was thus performed through comparison with the printed version of the Hydrological Yearbooks. Afterwards, to verify the correctness of the continuous daily data, high precipitation values (greater than 500 mm) were manually controlled, to verify if they were realistic. In a few cases, these high values were removed, because caused by a mistake with decimals in the table.

After this merging and control operations, only continuous time series with at least 330 out of 365 daily measurements were used to compute the annual F-maxima. These were integrated with the already validated F-maxima.

The data merging procedure allowed us to reach a total of about 1000 stations with at least 10 years of both F- and S-maxima for the same years. Nevertheless, the total number of F-stations is significantly higher: in this region, 2149 stations with F-maxima are available, allowing to have a data density of 1 rain gauge every 42 km^2 (the data density of the sub-daily time series is of 1 rain gauge every 53 km^2). In Figure 4.4 it is possible to observe the spatial distribution of the F- and S-maxima. From this figure one can realize that the data density is not uniform: even including the F-maxima, several locations in the lowlands or at high elevations are still poorly sampled.

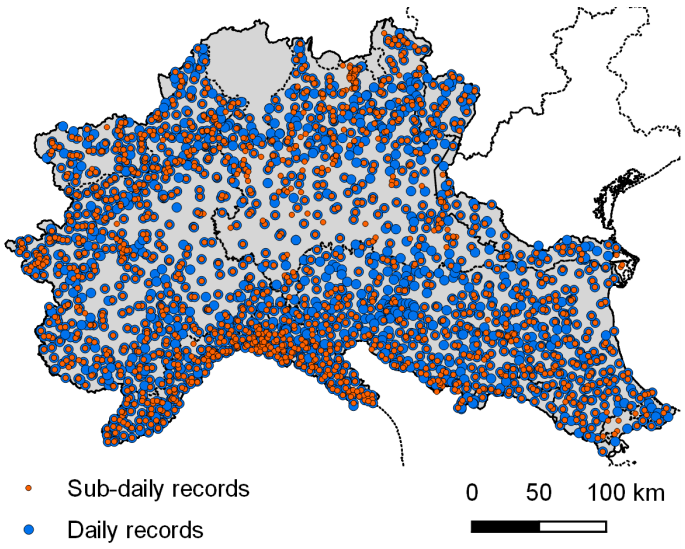

Fig. 4.4 Spatial distribution of the sub-daily and daily records.

In Figure 4.5 it is possible to see the time history of the available stations. From this figure it clearly emerges that, for instance, before 1980 only a subset (< 50%) of the rain gauges was equipped with a continuous recording device.

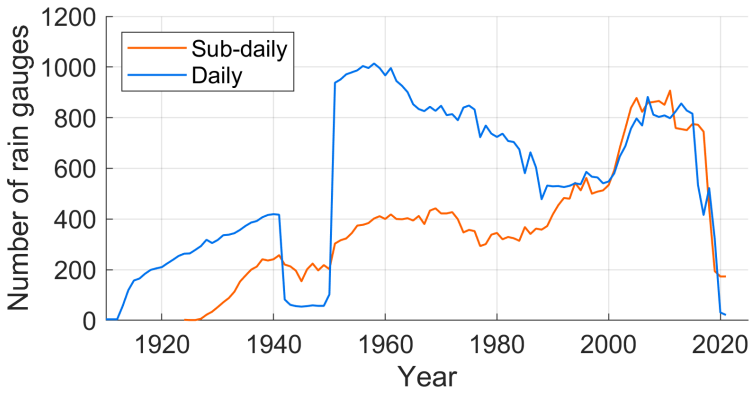

Fig. 4.5 Time history of the number of active rain gauges.

4.3 Evaluation of the Hershfield Factor

For all the stations and all the years where both the F-maxima and S-maxima are available, the Hershfield factor was computed according to its definition:

$$H = \frac{h_{24}}{h_g} \tag{4.1}$$

where h_{24} is the 24 h annual maximum and h_g is the daily maximum in a given year.

As a general rule, $1 \leq H \leq 2$ (van Montfort (1997)). It can be equal to 1 if the S-maxima occurred inside the same calendar day, while it can be equal to 2 if the extreme event is equally divided into two days.

In a first step, we analysed H using only the validated data, whatever the record length, to obtain reliable results that would be compared to those obtained using the entire dataset.

Even in validated data we found cases in which F-maxima were higher than S-maxima. This inconsistency is not unusual, and can be attributed to errors in the digitization, due to the manual daily recording. These occurrences, and the others in which we found $H > 2$, were manually corrected. Figure 4.6a shows the box plot of

the individual H values obtained year by year: the overall median H is 1.112, while the whiskers ends are, respectively, 1 and 1.585. The overall mean value obtained for H is 1.170, somewhat higher than those in the literature.

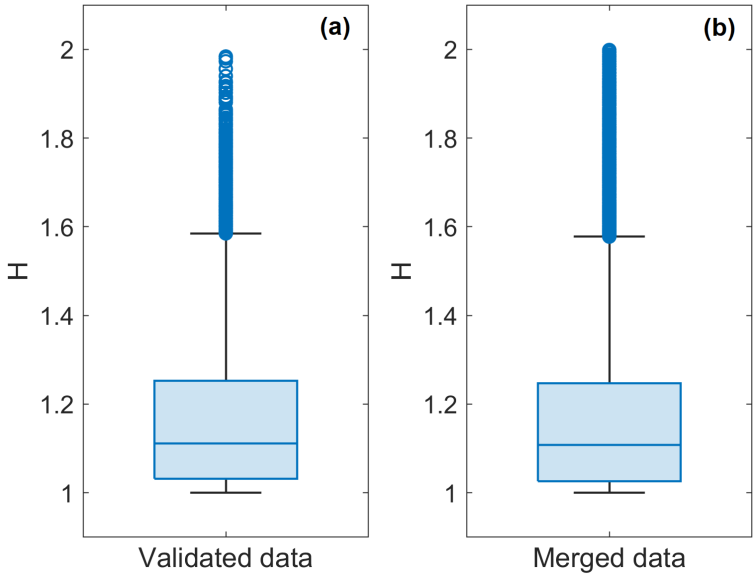

Fig. 4.6 Box plot of the yearly Hershfield factors computed using the validated data (a) and from the merged dataset (b). Each box plot displays the following information: the median, the lower and upper quartiles (blue box), any outliers (computed using the interquartile range, depicted as a blue dot), and the minimum and maximum values that are not outliers (black whiskers).

Having removed only the undeniable anomalies does not exclude the possibility that other anomalies may have occurred. The limits of the box plot were used to filter out possible outliers in the process of extending the computation to the entire dataset. Therefore, when computing the H values for all the stations using the entire dataset, made of validated and not validated data, we used series with at least 10 years of data and we used the whiskers ends of the validated data (1 and 1.585) as thresholds to remove the outliers. After this computation, the median H resulted of 1.144 and the mean resulted equal to 1.146, which are in line with the values reported in the literature. By increasing the minimum record length to 20 years we obtained an average of H equal to 1.142, and a median equal to 1.141, suggesting that even a time series of only 10 years could provide reliable estimates.

Examinig the box plots in Figure 4.6 one can recognize that the variability of the H computed from the entire dataset turns out to be similar to the one of the validated

data, despite a higher number of outliers. This evidence confirms the suitability of using also non-validated data to guarantee an higher spatio-temporal coverage of F-maxima.

After the computation and validation of the H values in the so-reached ≈ 1000 stations, a spatial interpolation at 1 km resolution of the mean H was performed. This procedure was realized using the ordinary kriging (Figure 4.7). By analyzing the spatial distribution of the interpolated Hershfield factor within the study area, we found variability patterns similar to those available in the literature, i.e. the mean (at station) H values turn out to be non uniform over the space. They seem influenced by the geographic position of the stations, and the patterns entail the possibility to identify some distinct areas with a positive or negative anomaly with respect to the spatial average. More specifically, higher values emerge in the Northern part of the examined region, mainly in Piedmont and Lombardy. The Aosta Valley, despite its location in the northern parts, shows different anomalies. This difference could probably be attributed to different prevailing rainfall mechanisms occurring in the Aosta Valley, possibly due to the presence of high peaks at the borders between Piedmont and the Aosta Valley, which act as a barrier. An influence of the geographic position was also pointed out over Catalonia (Spain) by Llabrés-Brustenga et al. (2020), and over China, where van Montfort (1997) analyzed monthly H values in relation to the location of the station, the autocorrelation within its daily measurements and the fraction of wet days.

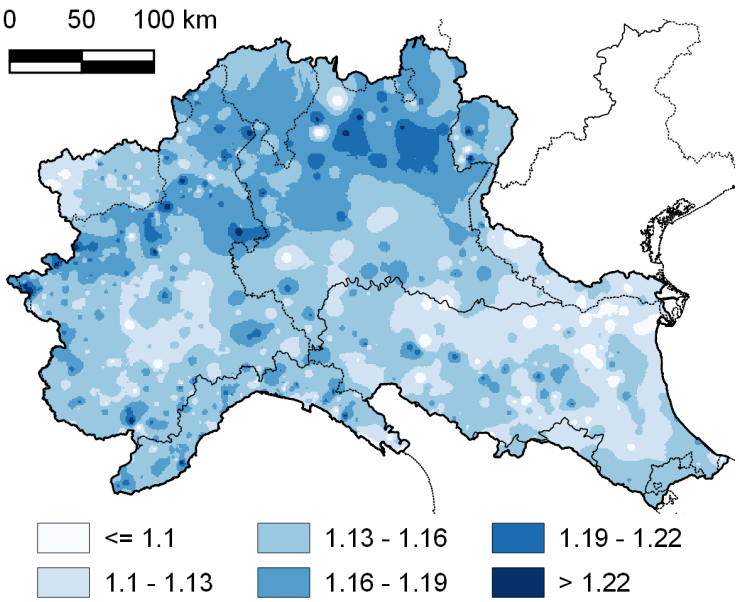

Fig. 4.7 Spatial distribution of the Hershfield factor obtained by applying and ordinary kriging with spherical variogram.

The exam of the spatial distribution of H has suggested the necessity to perform an additional data control, as some suspicious isolated anomalies clearly emerged (Figure 4.8a). This happened especially in areas where official and quality-controlled annual maxima were not available, so that F-maxima were computed from continuous daily records. For these isolated "peaks" of H, the time series of the rain gauges have been checked and the incorrect data have been replaced using the values reported in the printed version of the Hydrological Yearbooks, as depicted in Figure 4.8b. Note that Figure 4.7 already report the fully corrected version of the map.

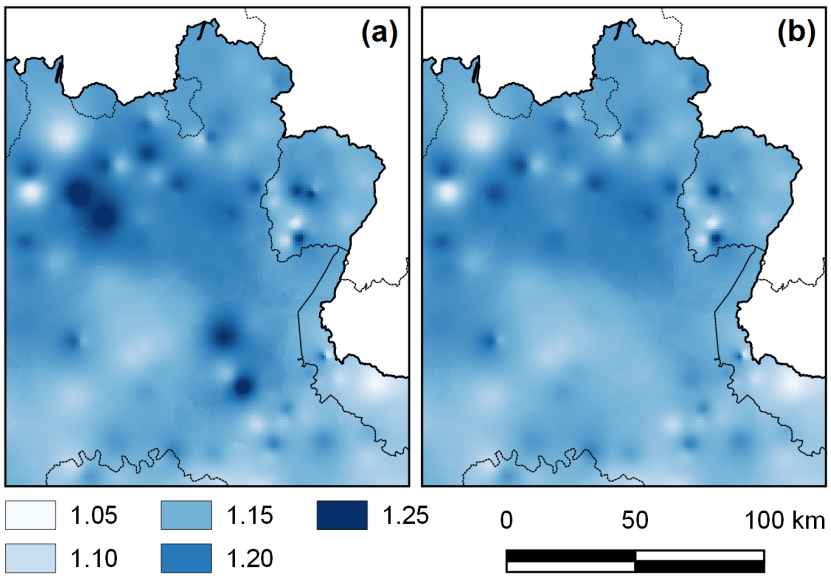

Fig. 4.8 Spatial distribution of the Hershfield factor before (a) and after (b) the site-specific data-cleaning operation. Focus over the Eastern part of Lombardy region.

4.4 Discussion

To increase the spatial detail of the extremes of precipitation over the North of Italy, a consistent database including daily precipitation (F-maxima) can be used. The analysis of ratio between 24 h and daily extremes (Hershfield factor) throughout the investigated area can allow to estimate annual S-maxima (i.e. over 24 h) in the stations that lack this information. In some areas (mountain regions and the lowlands between Piedmont and Lombardy) the increase in detail is noteworthy, and can provide important improvement over the spatial analysis of 24 h extremes.

Before proceeding with the use of these reconstructed data, some care must be exerted about the reliability of these newly-computed maxima. In these terms, it is worth mentioning that Koutsoyiannis and Iliopoulou (2022) pointed out that there is no theoretical basis behind the "inflation" through the Hershfield factor, even though it can represent an acceptable estimate from an engineering point of view. The authors pointed out that all realizations are stochastically equivalent and there is no theoretical basis for their correction. By correcting the series, its stochastic properties can be distorted.

In terms of series properties, indeed, Papalexiou et al. (2016) had previously noted that the ratios between the mean values of F- and S-maxima deviate from the standard deviation ratios: this implies that the application of the H factor cannot appropriately preserve the standard deviation of the F-maxima. These authors have then introduced an approach that simultaneously corrects both the mean and the standard deviation errors.

Despite the caveats, however, we cannot ignore that the possibility to include data recorded in decades at the beginning of the past century (see Figure 4.5) can produce relevant benefit in the spatial detail of the process. This suggests to us to proceed with the application of the H factor to include the F-maxima in the existing 24 h records.

On the other hand, when looking for trends in the data, to protect the reconstructed data from the distortion mentioned by Koutsoyiannis and Iliopoulou (2022) robust methods can be used, as Sen's method, the non-parametric Mann-Kendall test and the Spearman rank correlation test that all exhibit negligible sensitivity to data distortion (Morbidelli et al. (2021)).

4.5 Conclusions

In this study a complex data merging operation was performed to recover all the F-maxima recorded starting from the 20th century by 2149 stations. This dataset was then used to evaluate the Hershfield factor, that is a coefficient computed as the ratio between the S-maxima and the F-maxima that can be relevant for the reconstruction of missing sub-daily annual maxima. The interpolation realized, reported with a map in Figure 4.7, allows to reconstruct the missing S-maxima in stations with only F-maxima, and improves the knowledge of the spatial variability of sub-daily rainfall extremes.

In view of the extension of this data-recovering procedure to the entire Italy, further investigations are to be directed to the correction of distortion effects noted in the statistical properties of the reconstructed series. In that sense, it is important to consider the trade-off between the increase of uncertainty on the 24 h series properties and the increase in the spatial detail of S maxima in data-scarce regions.

Chapter 5

Spatial Issues of Trend Analysis of Rainfall Extremes in Italy

The work described in this chapter has been partially derived from Mazzoglio et al. (2022c).

5.1 Introduction

The impact of climate change on extreme rainfall regimes is a debated topic: recent works do not seem to support the perception of an increase in rainfall frequency and severity over the entire globe (IPCC (2021), Fowler et al. (2021a)). The different time scales used in such studies complicate the comparison. While most of them are performed at a daily scale, a limited number are focused on sub-daily durations. The lack of studies at sub-daily scales is exacerbated by less available, more fragmented and unevenly distributed short-duration (1 to 24 h) rainfall records.

Thanks to the recently released Improved Italian – Rainfall Extreme Dataset (I^2-RED) (Mazzoglio et al. (2020)) we performed both national and regional-scale analyses of short duration (1, 3, 6, 12 and 24 h) rainfall depth trends, covering the period from early 1900 to the present. The inclusion of more than 10 years of recent data in most of the Italian regions as compared to Libertino et al. (2018b) allowed us to obtain an up-to-date picture of changes compared with Libertino et al. (2019) and to propose a comparison with analyses published in the past years.

Similar to Libertino et al. (2019), the frequency of occurrences of the "extremes of the extremes" was analyzed using a record-breaking (RB) test, while the possible trend in intensity has been investigated using Mann-Kendall test and Sen's slope estimator. The comparison of results can provide new elements of assessment regarding the "speed" of change of some rainfall characteristics over Italy.

5.2 Data and Methods

5.2.1 Rainfall Data

The rainfall data used in this paper come from the Improved Italian – Rainfall Extreme Dataset (I^2-RED). It represents an updated and quality-controlled version of the dataset used in Libertino et al. (2019). The increase in the number of stations is reported in Figure 5.1: the new database presents a significant improvement in terms of data availability, especially from 2005 onward. Like Libertino et al. (2019), in this work only time series with at least 30 years of data (either continuous or discontinuous) were considered, regardless of the year in which the time series start.

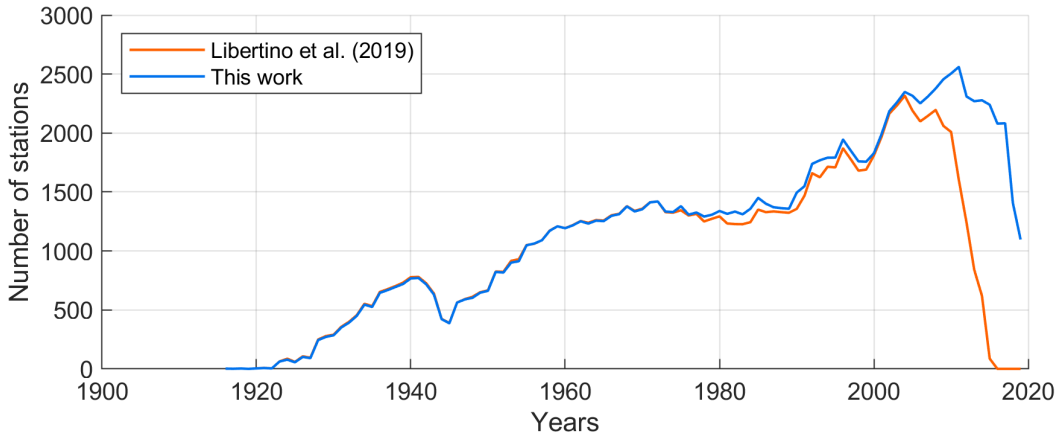

Fig. 5.1 Number of stations active in each year used in Libertino et al. (2019) and in this work. Modified figure from Mazzoglio et al. (2022c).

The area under investigation corresponds to the whole of Italy, where the complex shape, marked mountainous characteristics (Figure 5.2a) and peculiarly varied climatic conditions determine significant variability of the spatial context analyzed. The methods described below are applied both at the national scale and over limited-area

regions, selected as pilot cases (Figure 5.2b). These are: the upper Po basin (UP-PO), the Dolomites (DOL), the coastal areas between Liguria and Tuscany (LIG), the Calabria region (CAL) and the Sardinia region (SAR). These areas are hot-spots emerging from the previous analysis of Libertino et al. (2019).

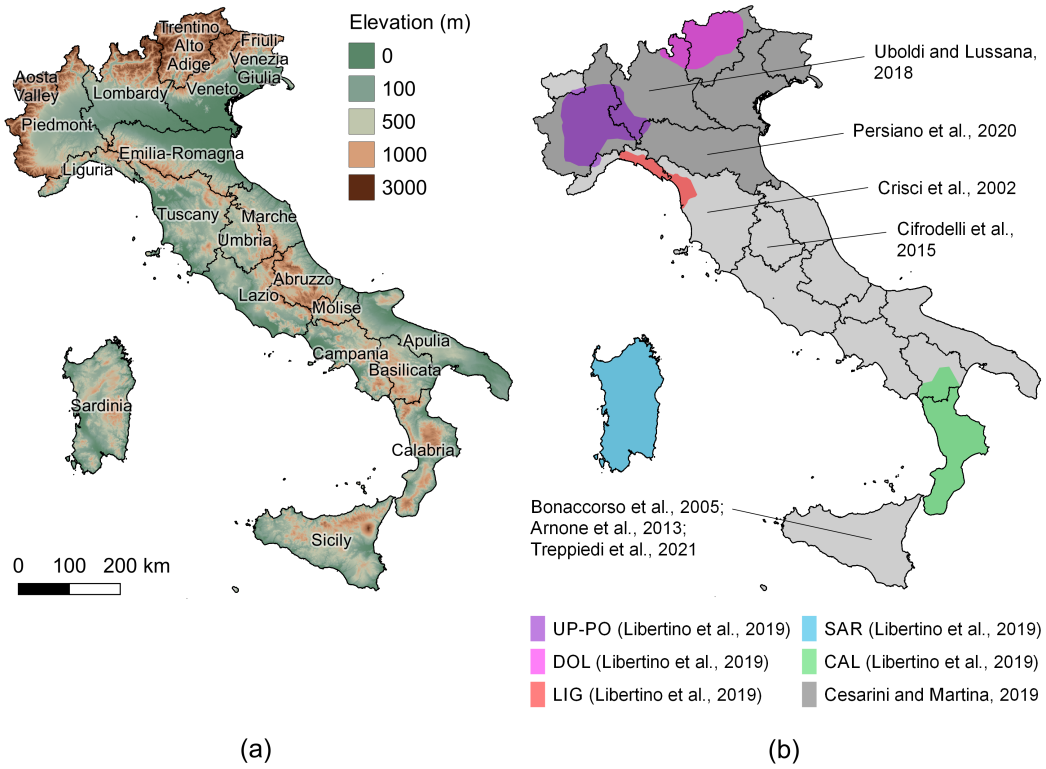

Fig. 5.2 Elevation data from NASA Shuttle Radar Topography Mission (SRTM) Digital Elevation Model (DEM) of Italy with the boundaries of the 20 administrative Italian regions (a). Geographic extent of the 5 pilot cases used in Libertino et al. (2019) and indication of the regions covered by the literature studies mentioned in Section 5.3 (b). Modified figure from Mazzoglio et al. (2022c).

5.2.2 Record-breaking (RB) Analysis

A rainfall measurement is considered as RB if it is higher than all the previous values in the time series (Lehmann et al. (2015)). The aim of the RB analysis (Glick (1978)) is thus the investigation of a possible increase or decrease in time of the frequency of occurrence of RB values.

Following what has been done in Libertino et al. (2019) and in Lehmann et al. (2015), annual maxima for each duration were used to create a matrix M_g with size n_g x Y (where n_g is the number of rain gauges and Y is the number of years). For each row of the M_g matrix, if the annual maximum is a RB value we set to 1 the corresponding value in the M_{RB} matrix; otherwise, we set it to 0. The vector of the observed annual RBs (V_{obs}) was obtained by summing along the columns of M_{RB} and then compared with the number of expected RBs in a stationary climate (V_{exp}). The vector V_{exp} was obtained by summing the values along the columns of M_{exp}, which is defined by assigning to each non-null value of each time series the expected RB probability under independent and identically distributed (*iid*) conditions. The annual RB anomaly (Lehmann et al. (2015)) is then evaluated at each time step by computing the normalized difference between V_{obs} and V_{exp} using

$$V_{anom} = \frac{V_{obs} - V_{exp}}{V_{exp}} \cdot 100 \tag{5.1}$$

The entire workflow is summarized in Figure 5.3.

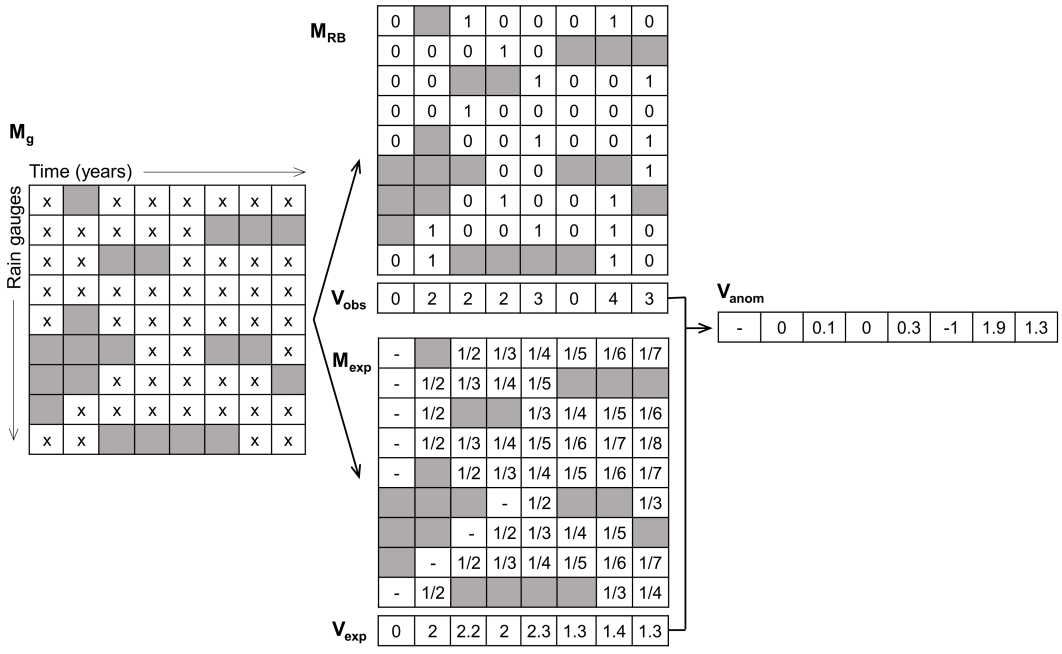

Fig. 5.3 Workflow of the RB analysis, applied separately for each duration (1 to 24 h) and for each region (ITA, UP-PO, LIG, DOL, CAL and SAR).

We tested the significance of the observed trends using a "field significance" bootstrap-based procedure (Libertino et al. (2019)). We estimated the test statistics (in our case, the regional normalized annual RB anomaly) considering both the observed time series and 1000 replicates that we obtained by bootstrapping along the time axis. If the observed statistic falls inside the 95% confidence bound of the bootstrapped distribution, we can consider it compatible with the *iid* hypothesis.

5.2.3 Mann-Kendall Test, Regional Kendall Test and Sen's Slope Estimator

The Mann-Kendall (MK) test (Mann (1945)) and the computation of the Sen's slope estimator have been first applied to each individual station to investigate at-site statistically-significant trends.

The MK test assesses if there is a monotonic upward or downward trend of the variable of interest over time and is based on the ranking of observations, and not on their absolute values; being nonparametric it does not require assumptions on the distribution of observations. However, when the interest is on a region, the spatial correlation of the series of neighbor stations can be relevant. For this reason, the Regional Kendall test (RKT) is adopted to correct the site-specific MK results within a region by accounting for the cross-correlation between the series (Helsel and Frans (2006)). The RKT provides one test statistic for each region (UP-PO, DOL, LIG, SAR, CAL and ITA) and for each time interval (1 to 24 h durations) that we considered. Then, the van Bell and Hughes test (van Belle and Hughes (1984)) was applied to quantify the reliability of the RKT results by assessing the homogeneity among the different trends of the stations included in a specific region. If the stations of the same region have different trend directions, the regional trend is not meaningful. In this case, while the single-station MK results can still be considered for a local trend analysis, their values are not representative of any large-scale spatial behavior.

The Sen's slope estimator was instead included as a method that can be robustly fit a linear trend to a sample without being sensitive to outliers. This approach is thus preferred to more classical simple linear regression.

5.3 National and Regional Trend Analyses

Most of the results that were obtained with the updated record-breaking analysis (Figure 5.4) and the RKT test (Table 5.1) are similar to the ones presented in Libertino et al. (2019), despite the inclusion of data in the most recent years (about +10% of new data for each duration).

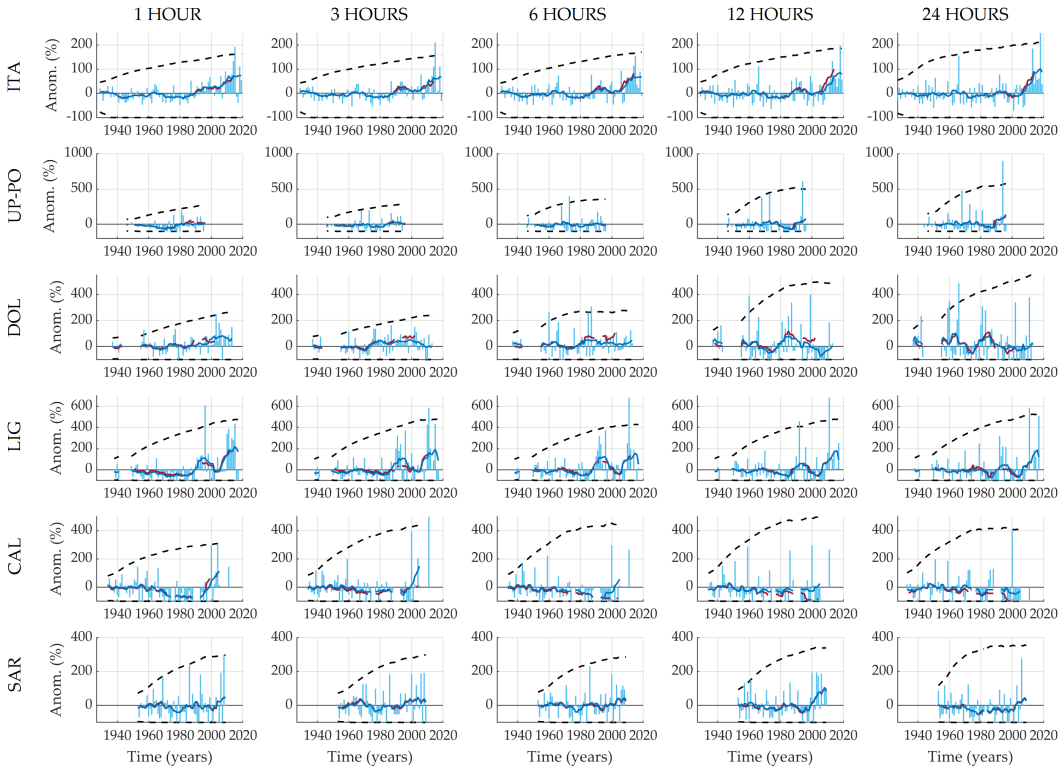

Fig. 5.4 Record-breaking analysis. Each row refers to a different region (ITA, UP-PO, DOL, LIG, CAL and SAR) while each column presents a different duration (1, 3, 6, 12 and 24 hours). Light blue bars represent the annual RB anomalies and the blue line represents the long-term RB anomalies (obtained by smoothing using a 10-year moving average filter the annual RB anomalies). For comparison purposes, the long-term RB anomalies obtained in Libertino et al. (2019) were inserted in red. The 95% confidence interval for the *iid* model are also included (black dashed lines). Modified figure from Mazzoglio et al. (2022c).

For the whole of Italy (first row of Table 5.1) the results that we obtained by applying the RKT are very similar to the ones reported in Libertino et al. (2019): positive Sen's slopes were obtained for all the durations but the regional trend is neither homogeneous nor statistically significant. Moving from a national to a limited-area analysis, we can mention also that in the Upper Po basin (second row

Table 5.1 RKT analysis. The sign of the values indicates increasing/decreasing Sen's slopes provided by the RKT. The values reported in bold represent a significant trend under a 5% significance level while the * indicates that the trend in the region is not homogeneous according to the van Belle and Hughes test (van Belle and Hughes (1984)). Source: Mazzoglio et al. (2022c).

Region	1 h	3 h	6 h	12 h	24 h
ITA	0.014 *	0.024 *	0.029 *	0.033 *	0.024 *
UP-PO	**-0.093**	-0.042	-0.033	-0.024 *	0.010
DOL	**0.053 ***	**0.069 ***	**0.080**	**0.115 ***	**0.152**
LIG	0.017 *	0.043	0.071 *	0.106 *	0.113
CAL	-0.028 *	-0.035	-0.050*	-0.083 *	-0.200 *
SAR	0 *	-0.021	-0.036	-0.050 *	-0.058

of Table 5.1) the situation is quite similar to Libertino et al. (2019): negative slopes characterize the 1 to 12 h durations, while the 24 h slope is positive. However, in our case, only the 1 h trend is statistically significant, even if the trend is homogeneous for all durations (except for the 12 h duration). The massive inclusion of new data also in the DOL region (about +45% of new data) allowed us to cover a longer period. Like in Libertino et al. (2019), all the durations show a positive homogeneous statistically-significant trend, but the new analysis shows higher slope coefficients (third row of Table 5.1). Results comparable with Libertino et al. (2019) were obtained also for the LIG, CAL and SAR regions (fourth, fifth and sixth rows of Table 5.1). It is worth mentioning that the inclusion of the most recent data in the LIG region allowed us to significantly expand the period that we covered with the RB analysis.

In Figure 5.4 the results obtained with the at-site Mann-Kendall test are reported while Figure 5.6 shows the Sen's slope estimates.

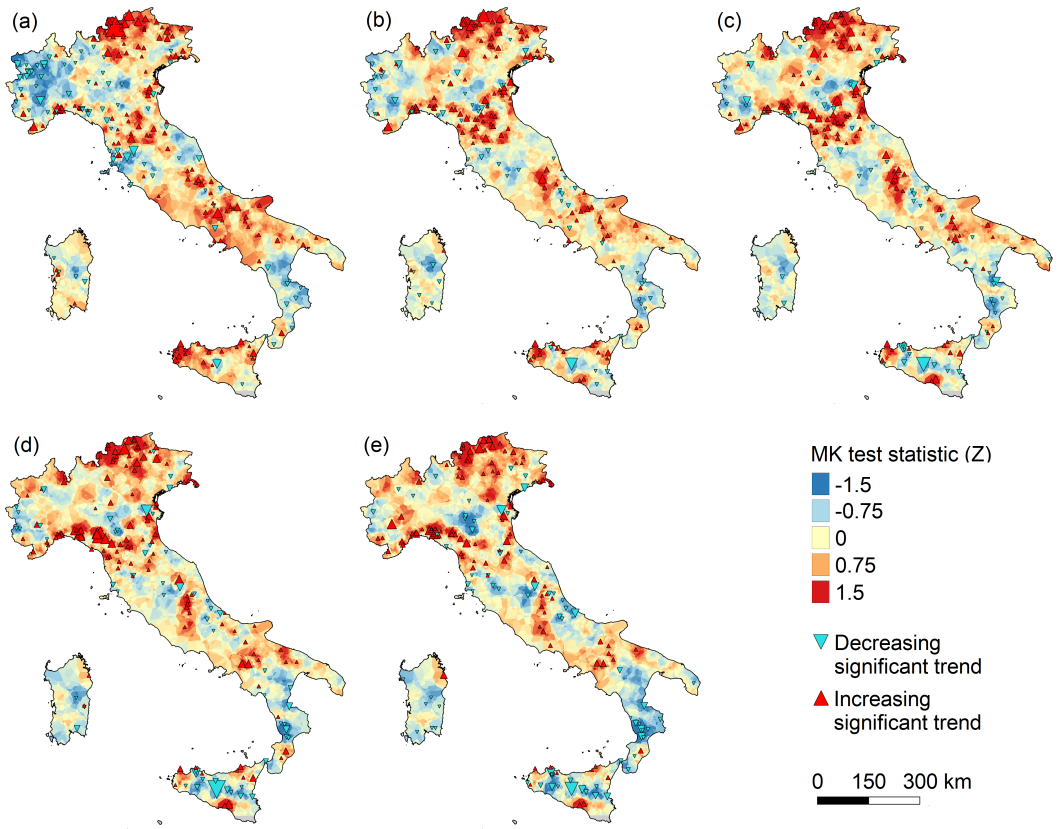

Fig. 5.5 Position of the rain gauges that present a significant trend at a 5% significance level in the case of (a) 1, (b) 3, (c) 6, (d) 12 and (e) 24 h durations. The size of the triangle is inversely proportional to the significance level. The background maps are obtained with a spatial interpolation of the Mann-Kendall test statistics performed using ordinary kriging. Modified figure from Mazzoglio et al. (2022c).

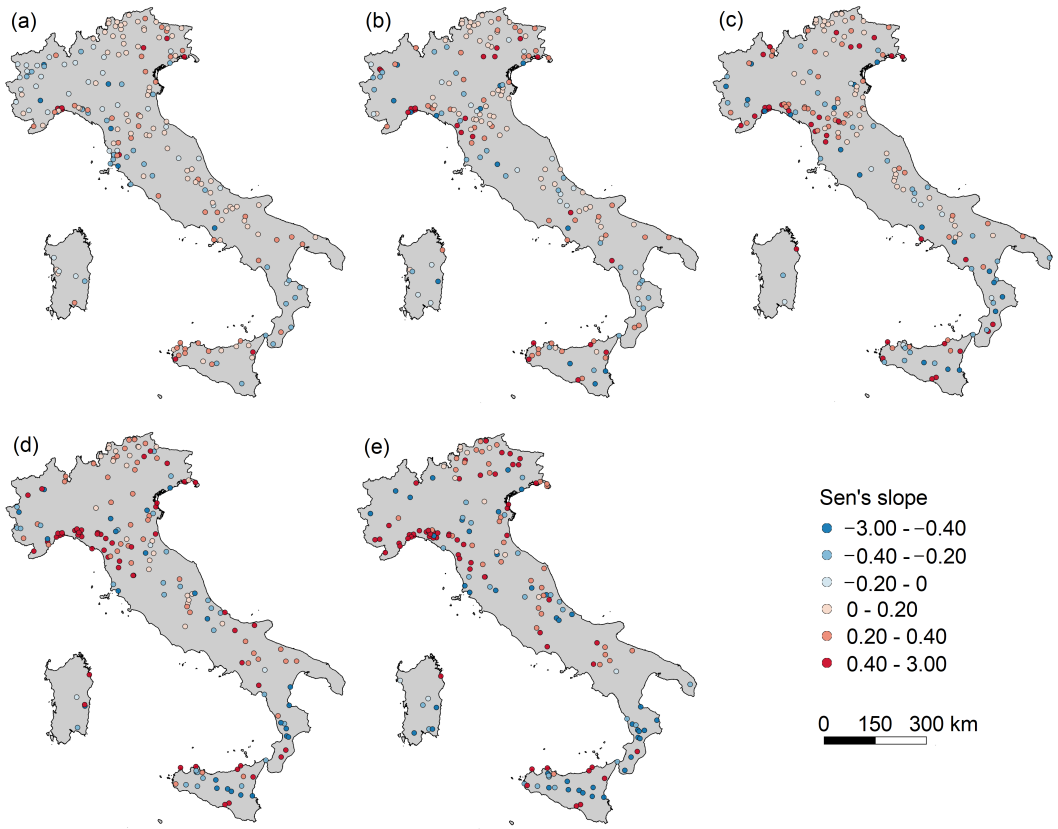

Fig. 5.6 Position of the rain gauges that present a significant trend at a 5% significance level in the case of (a) 1, (b) 3, (c) 6, (d) 12 and (e) 24 h durations. The color indicates the Sen's slope. Modified figure from Mazzoglio et al. (2022c).

Over the North of Italy (Piedmont, Lombardy, Trentino Alto Adige, Veneto, Friuli Venezia Giulia and Emilia-Romagna) an overall large presence of stations with increasing trends were detected by Cesarini and Martina (2019), especially in the North-East. Cesarini and Martina (2019) also highlighted that the difference between the number of increasing and decreasing statistically significant trends grows with the duration. In this work we obtained similar results: for the 1 h duration, we obtained a cluster of decreasing trends in the North-West and a cluster of positive trends in the North-East. The number of positive trends in the North-West decreases with increasing durations. The inclusion of a considerable amount of data over Libertino et al. (2019) allowed us to detect a more pronounced positive rainfall trend in the North-East.

Over Lombardy, Uboldi and Lussana (2018) found a general decrease of 1 h rainfall and an increase of longer duration events. The results are confirmed by our

study. The only exception is the Alta Valtellina (North-East of Lombardy), where an increasing trend for all the durations is pointed out in Uboldi and Lussana (2018), in Libertino et al. (2019) and in this study.

In the Emilia-Romagna region, most of the statistically-significant trends are located in the Apennines, along the borders with Liguria and Tuscany, and in the North-Eastern area near Veneto. Quite similar results were also obtained by Persiano et al. (2020). The inclusion of new data, compared with Libertino et al. (2019), allowed us to detect reinforced positive trends for 3 to 24 h durations.

Over Tuscany, the situation is more complex. In this analysis, we observed a general increase in the Northern part and a general decrease in the Southern part for all the durations. The only exception is for the 1 h data, where decreasing trends emerge in the North-West area near Liguria. Compared with Libertino et al. (2019) we obtained reinforced increasing trends in North Tuscany. Crisci et al. (2002) observed a prevalence of decreasing trends in the analysis of all the data acquired in the XX century and a large number of positive trends in the analysis of the 1970 - 1994 period.

Over the Umbria region, only four rain gauges show a statistically significant trend (positive in the Northern part, negative in the Southern), even if only for some durations. The analysis carried out by Cifrodelli et al. (2015) suggests that there is not a common trend in the area: the analysis of time series of a rain gauge in the North of the region suggests that variations are reduced, while the analysis of two rain gauges located in the Central part provided contrasting results: in one location the averages of the annual maxima generally increase in the recent years, while in the other a significant reduction is observed.

In Sicily, Bonaccorso et al. (2005), Arnone et al. (2013) and Treppiedi et al. (2021) saw an increasing trend for short durations (the higher number of positive statistically-significant trends emerged when analyzing the 1 h duration). Bonaccorso et al. (2005) and Arnone et al. (2013) obtained a decreasing trend for longer durations. Arnone et al. (2013) also observed an increasing trend in stations near the coastline, but they were not able to detect a defined spatial pattern. Our results confirmed marked increasing trends for the 1 h duration, especially along the North and North-West coast. For durations longer than 6 h we detected a large number of locations with negative trends, especially in the central parts of the Island, far from the coastline.

In contrast with Arnone et al. (2013), thanks to the massive inclusion of new data, the presence of spatial clusters clearly emerges.

For all the other regions, a comparison is not possible due to the lack of similar studies.

A comparison with the Sen's slopes obtained all over Italy shows the need to further investigate the spatial coherence of trends and the trend type (linear, parabolic, exponential, etc.). Further work could be addressed to investigate such local trends and to reconcile the results reported in Figures 5.5 and 5.6, being the Sen's slope estimator used to investigate linear variations while the MK test is tailored to assess something more general than a linear trend.

5.4 Conclusions

In this work we conducted an improved spatio-temporal trend investigation of short-duration annual maximum rainfall depths, using the most complete collection of short-duration annual maximum rainfall depths available in Italy. The record-breaking analysis, the Mann-Kendall test (both at station-level and at a regional level) and the Sen's slope estimator are used to investigate if statistically significant trends are present over Italy.

The results confirmed that the presence of long-term trends cannot be evaluated by merging all the data collected over Italy and that the segmentation of the territory is mandatory. Further studies can be conducted to evaluate new possible segmentation of the Italian territory for the evaluation of the Regional Kendall test.

Chapter 6

Geographically-based Analysis of Rainfall Statistics in Italy

The work described in this chapter has been partially derived from Mazzoglio et al. (2022a). Part of this chapter will be submitted to a scientific journal in the upcoming months.

6.1 The Rationale of Spatial Mapping of Rainfall Statistics

Datasets of rainfall features with large coverage in space and time can be relevant in a vast range of applications, like hydraulic design, water resources management and climate change impact assessment. Not many of these datasets refer to the features of the extremes of precipitation, which are of increasing interest for both scientists and practitioners because of the evolution of the hydrologic hazard in the recent years (Fowler et al. (2021a); Fowler et al. (2021b)).

Dataset related to large areas are generally created by spatial interpolation of irregularly spaced rain gauge data into a regular grid (Daly et al. (1994); Daly et al. (2002); Crespi et al. (2018); Thornton et al. (2021)). To control the quality of the interpolation it is necessary to understand the spatial distribution of the rainfall features, particularly by investigating some geographic factors that can be considered responsible for the spatial variability of the rainfall amounts.

In regions with almost flat orography, rainfall variability can be handled with interpolation techniques (e.g. inverse distance weighting and ordinary kriging)that do not require to consider other spatial covariates. On the other hand, in regions with significant elevation variability, the spatial patterns of rainfall depth statistics are known to be affected by the geomorphological setting (Smith (1979); Basist et al. (1994); Prudhomme and Reed (1998); Prudhomme and Reed (1999); Faulkner and Prudhomme (1998)) and the interpolation requires methods that can explicitly account for the elevation effect (e.g., Prudhomme and Reed (1999); Daly (2006); Claps et al. (2022b)). Several of the approaches available in the literature consider the elevation as an explanatory variable, such as: simple and multiple regression models (Basist et al. (1994); Prudhomme and Reed (1998); Prudhomme and Reed (1999); Allamano et al. (2009)), local regressions or georegressions (Daly et al. (1994)), geographically-weighted regressions (Thornton et al. (1997); Brunsdon et al. (2001); Daly et al. (2002); Di Piazza et al. (2011); Crespi et al. (2018); Thornton et al. (2021)), residual or regression kriging (Prudhomme and Reed (1999); Di Piazza et al. (2011); Crespi et al. (2018)), kriging with external drift (Goovaerts (1999); Pellicone et al. (2018)) and cokriging (Diodato and Ceccarelli (2005); Pellicone et al. (2018)).

The impact of orography on daily, multi-daily and annual precipitation events can generally be attributed to the so-called “orographic enhancement of precipitation” or "orographic effect", i.e., an increase in rainfall depth along the windward slope of a relief and a decrease on the lee side, due to the lifting and the consequent drying of the air mass (Smith (1979); Daly et al. (1994); Frei and Schär (1998); Napoli et al. (2019)). In a complex landscape, this effect can also entail significant precipitation values on the lee side, due to landforms that cause a delay in the hydrometeorological formation of precipitation and falling raindrops (Smith (1979)).

Some differences emerge when dealing with rainfall extremes. The impact of the orography on extreme rainfall depths and the complicated atmosphere–orography interactions for large areas are still not sufficiently understood for sub-daily rainfall events. In a country like Italy, characterized by a high degree of morphological heterogeneity (Figure 6.1), these relations assume an evident importance, considering the significant exposure to Mediterranean storms (Claps and Siccardi (1999)). The focus of this study is thus the entire Italian territory ($\approx$ 300,000 km^2), considered as a representative case, both in terms of variety of landforms and in terms of variability of the rainfall extremes, as will be seen in the following.

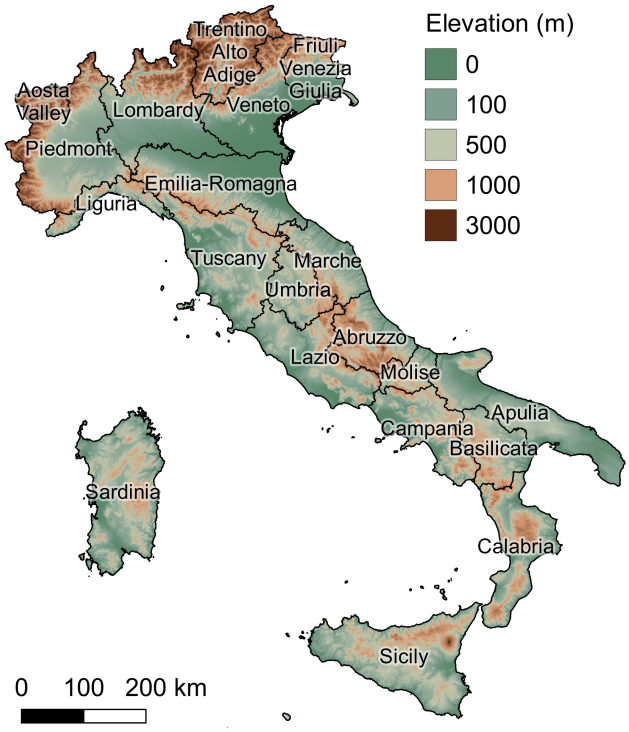

Fig. 6.1 Elevation data (Shuttle Radar Topography Mission; Farr et al. (2007)) with the boundaries of the 20 Italian administrative regions.

Most of the existing studies in Italy have focused on limited areas (Allamano et al. (2009); Caracciolo et al. (2012); Pelosi and Furcolo (2015); Furcolo et al. (2016); Furcolo and Pelosi (2018); Libertino et al. (2018a); Formetta et al. (2022)), and the only attempt to deal with sub-daily data covering the entire nation was made by Avanzi et al. (2015).

These studies suffered from a lack of a comprehensive and quality-assessed national database for sub-daily extremes. Several of them analyzed the Italian Alpine area. For instance, Frei and Schär (1998) focused on the entire European Alps region and showed that the foothills enhance monthly and seasonal precipitation, while inner valleys produce an orographic shielding effect on rainfall. Nevertheless, they did not find a unique precipitation depth–elevation relationship that could be considered valid for the entire Alps and attributed the observed variability to the effects of slope and shielding. Allamano et al. (2009) investigated the dependence of sub-daily annual maximum rainfall depths on elevation over the Italian Alpine region. They found a significant decreasing trend for increasing elevations and a nonuniform slope coefficient over the longitude range. The slope of the rainfall depth–elevation

regression was shown to decrease for event durations that increased from 1 to 24 h. Libertino et al. (2018a) showed that in the western sector of the Italian Alps (Figure 6.1) shorter durations (1–3 h) are characterized by a negative slope coefficient as a function of elevation (statistically significant at a 5% level), while longer durations (12–24 h) show a positive slope and also a significant correlation, and the trend of the extremes over 6 h loses significance with elevation. Over Trento province, Formetta et al. (2022) identified a reverse orographic effect for hourly and sub-hourly durations and an orographic enhancement for a duration of about 8 h (or longer).

Other regional works that attempted to identify orographic effects in the Mediterranean part of Italy are available for Campania and Sicily. Pelosi and Furcolo (2015) and Furcolo et al. (2016) analyzed the daily annual maximum rainfall depths over Campania (see Figure 6.1 for the geographical location) and attempted to explain systematic variations as being the result of the presence of orographic barriers, identified through the application of an automatic geomorphological procedure (Cuomo et al. (2011)). Their results showed a link between orographic elements and a local increase in rainfall depths and allowed orographic elements that produced enhanced variability of extreme rainfall to be identified. The same group later worked on sub-daily annual maximum rainfall depths (Furcolo and Pelosi (2018)) and proposed a power law amplification factor of rainfall over three mountainous systems.

Caracciolo et al. (2012) found that the longitude, latitude, distance from the sea and a concavity index are the variables that govern the spatial variability of rainfall depths in Sicily. However, these authors found that no linear relationship between sub-daily annual maximum rainfall depths and elevation was significant at a 5% level over the entire island of Sicily.

All of the previously mentioned analyses refer to an analytic relationship that connects annual maximum rainfall depths of various durations, i.e., the average depth–duration (ADD) curve of the simple-scaling approach, which is usually represented by a power law

$$h_d = a \cdot d^n \tag{6.1}$$

where h_d is the average of the annual maximum rainfall depths of duration d, a is a scale factor and n is a scaling exponent.

Avanzi et al. (2015) analyzed the spatial variability of the ADD curve parameters, a and n, at a national scale, as obtained from measurements of 1494 stations

distributed throughout Italy. They referred to the so-called "reverse orographic effect", i.e., the relationship found between parameter a and elevation, which shows a decreasing trend. On the other hand, the scaling exponent n appears to increase nonlinearly with elevation. More details are provided in the following section.

On the basis of the described background and the significant improvements offered by a new, up-to-date rainfall dataset, i.e., the Improved Italian-Rainfall Dataset, I^2-RED (Mazzoglio et al. (2020)), the present work has considered more than 3700 stations with at least 10 years of data to relate the average rainfall depths in all the durations (index rainfall) to several morphological variables and investigate their dependency on elevation and on other geomorphological and climatological parameters.

Searching for models that allow the index rainfall to be estimated for various durations in any location in Italy is the first, important, necessary step toward addressing the building of depth–duration–frequency curves over the entire country. For this purpose, simple (Section 6.2) and multiple (Section 6.3) national-scale regression models were first investigated. Four geomorphological classifications (Section 6.4) were then introduced to perform local-scale regression analysis to tackle the evident spatial clustering of the regression residuals (Section 6.5). The comparisons made between the results obtained from the wide-area and the local regressions allowed the role of the morphology in rainfall variability to be discussed, as shown in Section 6.6. Section 6.7 reviews the main studies based on local analyses of the precipitation vs elevation relationship. Section 6.8 contains a description of the data and of the methodology, with emphasis on the available options for the parameter identification and the management of local inconsistencies that can arise, for instance, where excessive extrapolation is allowed. Section 6.9 shows the application, over the whole of Italy, of the revised cell-based regression approach. In the same section, the choice of the parameters and the model constraints are widely discussed, to provide an understanding of the performances that different variants of the proposed model configuration can produce. A cross-validation approach and an accurate check of residual spatial distribution are then used to select the best model in Section 6.10. The results are shown in terms of maps at 1-km resolution. In the same section, a discussion of the results, that include maps at 1-km resolution and the evidence of some orographic effects, complete the analysis. Section 6.11 contains the main conclusions.

6.2 Simple Linear Regression Analysis

6.2.1 Methods

As the first step of the analysis, the influence of elevation on the spatial distribution of the average of short-duration (1 to 24 h) annual maximum rainfall depths was investigated. The ADD curve parameters were calculated for all the stations of the I^2-RED dataset to compare them with previous studies (mainly Avanzi et al. (2015)). Parameters a and n (see Equation 6.1) were initially obtained by means of a linear regression of the logarithm of the average of all the available extremes over the 1 to 24 h durations. The median values of these parameters were computed across Italy to compare them with those of Avanzi et al. (2015), who grouped the stations into elevation ranges of 50 up to 1000 m a.s.l. and into intervals of 100 m for higher elevations. Both series of medians (a and n) were then plotted against the median elevation of each interval (to account for the fact that the distribution of the rain gauges in each elevation interval was skewed) and fitted regression models. The differences between the measured and estimated rainfall statistics were studied to assess the effectiveness of the regression models, considering the observed averages of the extremes over 1, 3, 6, 12 and 24 h. Performance indices for each station were obtained using the estimation errors Δ_d

$$\Delta_d = h_{avg}(d) - \hat{a} \cdot d^{\hat{n}} \tag{6.2}$$

where $h_{avg}(d)$ is the sample average of the extreme rainfall depth for duration d, while $\hat{a}$ and $\hat{n}$ are the estimates of parameters a and n.

In this chapter, only the results related to the shortest and the longest of the five durations (1 and 24 h) are shown and discussed, as they can be considered the most representative of the different classes of rainfall events (convective and stratiform, respectively). The corresponding dependent variables are called $\overline{h}_1$ and $\overline{h}_{24}$ in the following.

The error statistics that were computed are the bias, the mean absolute error (MAE), the root mean square error (RMSE) and the Nash–Sutcliffe model efficiency (NSE) coefficient (Nash and Sutcliffe (1970); Wasserman (2004)). Among all the statistics, particular attention was dedicated to spatial bias, i.e., the bias evaluated as

the difference between the spatial mean of the observations over a generic area, and the corresponding values predicted by the model.

6.2.2 Results

By applying the procedure described in Section 6.2.1, results that are in agreement with those of Avanzi et al. (2015) were obtained. Parameter a decreases linearly with elevation (R^2 = 0.89), through the equation

$$a = 30.61 - 0.0060 \cdot z \tag{6.3}$$

which is comparable with the equation obtained in Avanzi et al. (2015)

$$a = 29.17 - 0.0062 \cdot z \tag{6.4}$$

while parameter n increases nonlinearly with elevation, through the following equation:

$$n = 0.54 - exp[-0.000077 \cdot (z + 1650)] \tag{6.5}$$

For comparison purposes, Avanzi et al. (2015) obtained

$$n = 0.54 - exp[-0.00086 \cdot (z + 1452)] \tag{6.6}$$

for the latter parameter. The variable z of Equations 6.3, 6.4, 6.5 and 6.6 is the station elevation retrieved from I^2-RED data. The fitting of the four models is reported in Figure 6.2.

Table 6.1 Comparison of national-scale error statistics related to the estimates performed in Mazzoglio et al. (2022a) with Equations 6.3 and 6.5 and in Avanzi et al. (2015) with Equations 6.4 and 6.6. Source: Mazzoglio et al. (2022a).

Error statistic	$\overline{h}_1$ (Eqs. 6.4, 6.6)	$\overline{h}_1$ (Eqs. 6.3, 6.5)	$\overline{h}_{24}$ (Eqs. 6.4, 6.6)	$\overline{h}_{24}$ (Eqs. 6.3, 6.5)
Bias (mm)	2.65	1.07	9.64	6.05
MAE (mm)	5.48	5.29	22.22	22.27
RMSE (mm)	7.39	6.98	32.81	31.99
NSE (-)	-0.01	0.10	-0.02	0.03

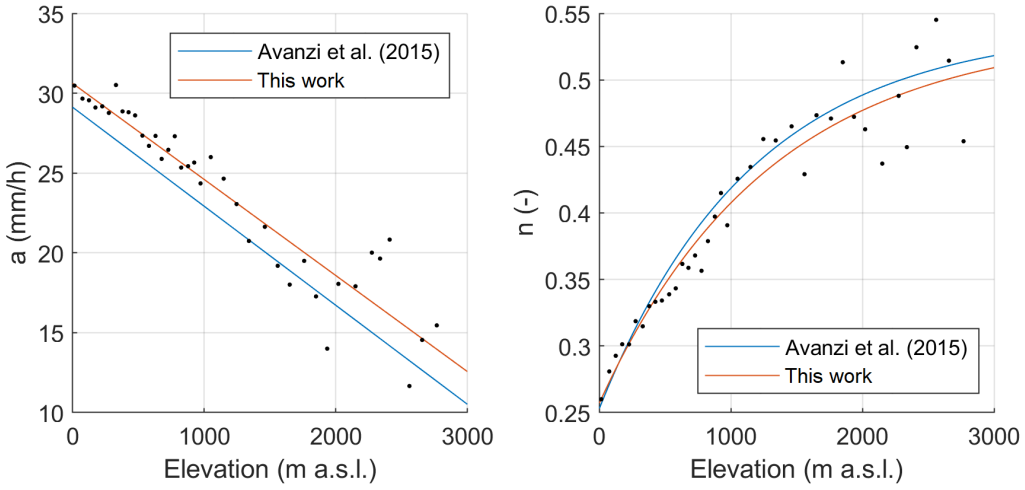

Fig. 6.2 Fitting of the national-scale simple regression models of Avanzi et al. (2015) (blue line) and the one proposed in this work (red line) on I^2-RED data. Modified figure from Mazzoglio et al. (2022a).

As already mentioned, parameter a is roughly equivalent to $\overline{h}_1$. Its overall inverse dependence on elevation is somewhat counterintuitive, even though other authors have confirmed this dependence (e.g., Allamano et al. (2009); Marra et al. (2021)).

The error statistics computed on the two sets of residuals (i.e., in this work and in Avanzi et al. (2015)) are listed in Table 6.1. The results show that the increase in the number of stations and the recording length achieved in I^2-RED have led to an improvement compared to the results of Avanzi et al. (2015). This result is not surprising, but more insights can be derived from the observation of the spatial distribution of the residuals, which were not discussed explicitly in the previous literature.

In this regard, we mapped differences Δ_1 and Δ_{24} to investigate where the under- and overestimations show spatial coherence. The maps, reported in Figure 6.3, clearly show that clusters of residuals with high residuals of the same sign emerge in various areas of the country: for instance, many coherent errors larger than 3 times the MAE are present in the Liguria region (see Figure 6.1 for the geographic position) for both durations. Therefore, despite the high R^2 values, significant spatially correlated errors can undermine the practical validity of these general relationships.

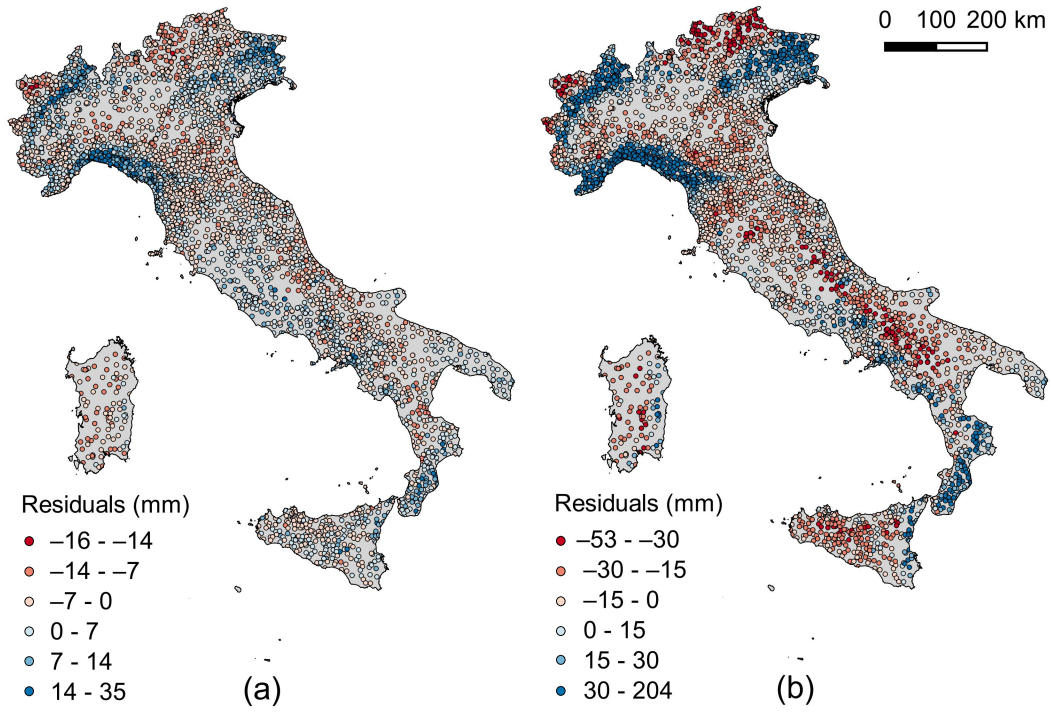

Fig. 6.3 Residuals of the estimations of the 1 h (a) and 24 h (b) durations performed using Equations 6.3 and 6.5. Modified figure from Mazzoglio et al. (2022a).

On the basis of these results, the need for a more detailed spatial analysis of these variables became evident. A set of new analyses, aimed at reducing the local bias and increasing the reliability of the results, was therefore introduced.

6.3 National-scale Multiple Linear Regression Analysis

6.3.1 Methods

In an attempt to improve the evaluation of the relationships between rainfall and topography, an analysis of the relationships between rainfall and several geomorphological (and climatological) parameters, which may complement the explanatory power of elevation, was undertaken. Unlike what was done in Avanzi et al. (2015), multivariate models were used in the literature to relate rainfall statistics and various morphological variables, both of which were evaluated at the same location. In these approaches, no aggregated or median spatial statistics of rainfall were considered. Prudhomme and Reed (1998) and Prudhomme and Reed (1999), for instance, identified meaningful geographic and morphological attributes of each location as good explanatory variables of the daily rainfall maxima in Scotland. They showed that obstruction indices, derived from the orography, and the distance from the coastline are able to define how morphological barriers influence the characteristics of the extremes. These appear to work better than the EXPO variable used by Basist et al. (1994) and Konrad II (1996).

Basist et al. (1994) defined EXPO as the distance between a rain gauge and an upwind barrier whose elevation is at least 500 m higher than the station. Konrad II (1996) suggested an elevation of the barrier at least 150 m higher than the station. Prudhomme and Reed (1998) also tried to use this variable, setting the elevation difference at 200 m, but concluded that the definition of EXPO has several drawbacks, as it is based on arbitrary thresholds and is defined assuming a specific and subjective direction.

Introducing new variables with omnidirectional meaning, as the distance from the sea, the obstruction and the barrier, which are evaluated in the eight main directions, Prudhomme and Reed (1998) were able to explain a much larger percentage of variability in the annual maximum daily rainfall than that explained by the EXPO variable.

Caracciolo et al. (2012) applied this latter approach on the island of Sicily (south of Italy): they found that the longitude, elevation, a barrier obstruction index and the distance from the coastline are able to represent the spatial variability of parameter a

for the whole island, while the longitude, elevation, a concavity index and the slope are able to satisfactorily describe the variability of exponent n. They also noticed that different descriptors became significant when analyzing smaller portions of the island.

Based on the above considerations, in this work the approach suggested by Prudhomme and Reed (1998) and Prudhomme and Reed (1999) was followed, considering two groups of variables computed for each station location:

1. *Geographic and climatic variables*. These do not require computation and do not depend on the landscape forms, that is, longitude (*LONG*, expressed in the WGS84 UTM32N reference system, in m), latitude (*LAT*, expressed in the WGS84 UTM32N reference system, in m), elevation above sea level (z, in m), minimum distance from the coastline (C, in km) and mean annual rainfall (*MAR*, taken from Braca et al. (2021), in mm); the latter represents a very robust climatological variable, which is seldom used as ancillary information but easily available throughout the world thanks to the presence of various rainfall databases (Schneider et al. (2011); Fick and Hijmans (2017); Muñoz Sabater (2019)).

2. *Morphological variables or descriptors.* These are based on a digital elevation model (DEM), computed for each cell in a square grid. These variables are as follows:

    - slope (S, in degrees), defined as the angle of the inclination of the terrain to the horizontal, which is evaluated using the eight closest DEM cells;
    - obstruction (*OBS*, in degrees), defined as the maximum angle needed to overcome the highest orographic obstacles in the eight main cardinal directions (i.e., the maximum of the angles subtended by the line that connects the rain gauge with the highest orographic peak within a 15 km radius in the eight main directions; see Figure 6.4);
    - barrier (*BAR*, in m), defined as the distance between the rain gauge and the highest orographic obstacle defined in *OBS* (Prudhomme and Reed (1998) and Prudhomme and Reed (1999); see Figure 6.4);
    - maximum slope angle (*MSA*, in degrees), i.e., the angle with the greatest slope needed to overcome obstacles within a 15 km radius in the eight main directions (see Figure 6.4);

- maximum slope angle distance (*MSAD*, in m), defined as the equivalent of *BAR* but computed with respect to *MSA* (see Figure 6.4);
- openness (*OP*, in radians), defined as a mean angular measurement of the relationships between the surface of the relief and the horizontal distances, in the eight main directions (Yokoyama et al. (2002)).

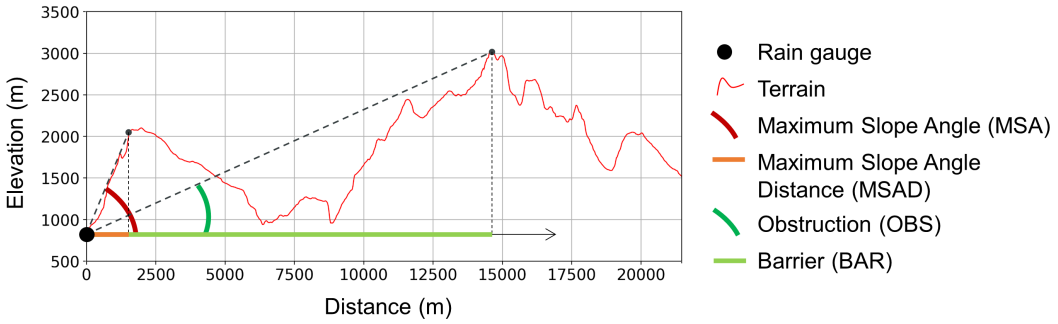

Fig. 6.4 Representation of the *MSA*, *MSAD*, *OBS* and *BAR* morphological variables. Modified figure from Mazzoglio et al. (2022a).

The values of all of these variables depend on the landscape forms and can vary according to the resolution of the used DEM. In this case, after thorough consideration, the Shuttle Radar Topography Mission (SRTM) DEM, which has a resolution of 30 m (Farr et al. (2007)), was adopted. However, the openness required to be evaluated on the SRTM DEM resampled at a resolution of 500 m due to computational limitations. This computation was conducted with the SAGA "Topographic openness" module, using a radial limit of 5 km. This value was obtained after testing different radial limits and selecting the one that presents the best correlation with the mean rainfall depth.

Multiple linear regression models were built, based on the following relationship:

$$Y = X \cdot \beta + \delta = \sum_{i=1}^{N} \beta_i X_i + \delta \tag{6.7}$$

where the dependent variable Y is related to the matrix of the independent variables X or covariates. The vector β in Equation 6.7 contains the regression model coefficients, and δ is the vector of the residuals.

To select the best model equation, the number i of covariates can be increased as necessary, according to the criteria of statistical significance of the estimated param-

eters. Caracciolo et al. (2012), for instance, used a stepwise regression approach. In this work, a generalized multiple regression approach is preferred, whereby increasing the number of covariates to $i + 1$ does not necessarily preserve the descriptors that were the most significant at step i. This approach entails always considering all the possible combinations of two, three or four covariates until the "best" model is found. Other tests made using five or more variables did not lead to significantly higher R^2_{adj} values.

The best regression model was selected on the basis of an analysis of the regression residuals, favoring models with the highest adjusted coefficient of determination, R^2_{adj}. Student's t test was used to quantify the significance of the independent variables. The possible presence of multicollinearity was checked for each model in which all the covariates passed Student's t test, as this could lead to the formulation of an unstable model. Multicollinearity was measured using the variance inflation factor (VIF), which is determined by placing the jth independent variable as the dependent variable and calculating the coefficient of determination R^2_{adj} of the multiple regression performed on the remaining p-1 in dependent variables (Equation 6.8).

$$VIF_j = \frac{1}{1 - R^2_j} \tag{6.8}$$

Values of VIF greater than 5 were associated with an unacceptable level of multicollinearity, and the corresponding model was discarded (Montgomery et al. (2012)).

6.3.2 Results

The equations of the best regression models (built using two to four variables) are reported in Equations 6.9 to 6.11 for $\overline{h}_1$ and in Equations 6.12 to 6.14 for $\overline{h}_{24}$. The R^2_{adj} values in Equations 6.9 to 6.11 are 0.46, 0.52 and 0.54, respectively. The coefficients of determination are higher for $\overline{h}_{24}$, i.e., 0.66, 0.67 and 0.68 (Equations 6.12 to 6.14, respectively).

$$\overline{h}_1 = 20.3163 - 0.0080 \cdot z + 0.0117 \cdot MAR \tag{6.9}$$

$$\overline{h}_1 = -21.6293 - 0.0061 \cdot z + 0.0134 \cdot MAR + 26.2682 \cdot OP \tag{6.10}$$

$$\overline{h}_1 = -10.6928 - 0.0051 \cdot z - 0.0273 \cdot C + 0.0131 \cdot MAR + 19.8449 \cdot OP \quad (6.11)$$

$$\overline{h}_{24} = 16.1392 - 0.0937 \cdot C + 0.0712 \cdot MAR \quad (6.12)$$

$$\overline{h}_{24} = 33.1529 - 1.8574 \cdot 10^{-5} \cdot LONG - 0.1319 \cdot C + 0.0701 \cdot MAR \quad (6.13)$$

$$\overline{h}_{24} = 127.2773 - 2.9498 \cdot 10^{-5} \cdot LONG - 1.9130 \cdot 10^{-5} \cdot LAT + \\ -0.0971 \cdot C + 0.0735 \cdot MAR \quad (6.14)$$

Considering the three $\overline{h}_1$ models (Equations 6.9 to 6.11), it is possible to notice the negative slope coefficient associated with elevation. This confirms what was discussed in the previous section. On the other hand, it is remarkable that the best models found for $\overline{h}_{24}$ do not include the elevation: this outcome can be explained by considering the fact that MAR is always significant, regardless of the number of variables. Models in which *MAR* was excluded actually present z as a significant covariate but with less relevance than the regression models for $\overline{h}_1$.

Regardless of the number of the variables considered, and despite the marked increase in the corresponding value of R^2_{adj}, compared to the simple regression, the residuals of the multivariate regressions appeared to be still characterized by spatial clustering and high local errors, basically all in the same areas in Figure 6.3. In other words, resorting to additional variables but keeping a uniform relationship between each variable and precipitation across Italy does not produce a decisive reduction in the bias for large areas of the country. Thus, it was decided to deconstruct the modeling approach and to look for clues of distinct generating mechanisms in distinct areas of Italy.

6.4 Sub-national-scale Multiple Linear Regression Analysis

6.4.1 Methods

In this section, an additional paradigm is introduced into the models for the spatial variability of precipitation to reduce the spatial bias, namely the selection of limited areas to build sub-national regression models, as an alternative to using data for the whole of Italy. Such an attempt was already made by Caracciolo et al. (2012), who

Table 6.2 Error statistics of the multiple regression models at a national scale and for the four macro-regions described in Section 6.4.1, for $\overline{h}_1$ and $\overline{h}_{24}$. Source: Mazzoglio et al. (2022a).

Error statistic	$\overline{h}_1$ Nation	$\overline{h}_1$ Four regions	$\overline{h}_{24}$ Nation	$\overline{h}_{24}$ Four regions
Bias (mm)	0	0	0	0
MAE (mm)	3.83	3.65	13.14	11.71
RMSE (mm)	4.98	4.77	18.43	16.53
NSE (–)	0.54	0.58	0.68	0.74

borrowed the subdivision criterion from previous regional frequency analyses. In this work, we have focused on the role of geography and morphology in the spatial variability of annual maximum rainfall depths.

To better understand how to move from national-scale relationships to relationships valid for smaller areas, we started by considering the Alpine area separately from the Apennine region along the entire peninsula, and from the two main islands (Sicily and Sardinia; see Figure 6.1 for the geographic positions), as a first approximation. We then built four different multivariate models: (1) the Alpine region (i.e., from Piedmont, including the western part of Liguria, eastward up to Friuli Venezia Giulia, delineated using the SOIUSA classification, as suggested by Accorsi (2016)); (2) the Apennine region, including peninsular Italy; (3) Sicily; and (4) Sardinia. The best regression models for these four regions was evaluated using up to four covariates, as described in Section 6.3.1.

6.4.2 Results

The new set of models built for the four regions were tested by computing the error statistics over the entire country. The obtained results indicated that they provided higher R^2_{adj} than for the national case and better error statistics (see Table 6.2 for a comparison with the previous multivariate approach). The better results achieved in terms of RMSE, MAE and NSE at the national scale are due to the improvements obtained for the two main islands (Sicily and Sardinia). More insights are provided in Section 6.6.

It is interesting to compare the results obtained for the individual Alpine region with those of Allamano et al. (2009), who analyzed almost the same area. In that

case, the ADD curve parameters appeared to be related to elevation and longitude. For the different durations Allamano et al. (2009) also estimated a regression model by linear regression between rainfall depth, elevation and longitude. The dependence of short-duration rainfall on elevation and longitude was found to be statistically significant for all the time intervals, except for the 1 h duration: in this case, the longitude was not statistically significant. In our application, the best relationships found for $\overline{h}_1$ and $\overline{h}_{24}$ are those of Equations 6.15 and 6.16 (characterized by R^2_{adj} = 0.75 and 0.76, respectively):

$$\overline{h}_1 = 60.9365 - 1.6664 \cdot 10^{-5} \cdot LAT - 0.0046 \cdot z + 0.0148 \cdot MAR + 25.1825 \cdot OP \tag{6.15}$$

$$\overline{h}_{24} = 59.0632 - 7.2955 \cdot 10^{-5} \cdot LONG - 0.2223 \cdot C + 0.4306 \cdot OBS + 0.0822 \cdot MAR \tag{6.16}$$

As expected, the $\overline{h}_1$ - z relationship has a negative slope, and the Equation 6.15 does not include the longitude as covariate, in agreement with Allamano et al. (2009). The same negative relationship is found in a 24 h equation that includes z (which produces an R^2_{adj} = 0.74, that is, lower than that of Equation 6.16). These findings confirm the results of Allamano et al. (2009), who found a general decrease in rainfall depth for increases in elevation for all the durations (up to 24 h). Equation 6.16 also confirms that, although $\overline{h}_1$ decreases systematically with elevation over the whole alpine region, the dependence of $\overline{h}_{24}$ on z decreases as the longitude increases, i.e., moving westward.

The full set of equations used for the four regions is provided in Appendix B, together with the R^2_{adj}.

Although the improvements achieved with multivariate models over the simple regressions are evident, they were not decisive in providing a homogeneous spatial distribution of the errors. Even with the best model, it was not possible to reduce the clustering effect shown in Figure 6.3 for the peninsular region (see Figure 6.5). We believe that a model capable of describing the observed spatial variability of the index rainfall simultaneously at a national and a local level requires additional insights, which can be obtained using a finer spatial segmentation of Italy into geographical zones.

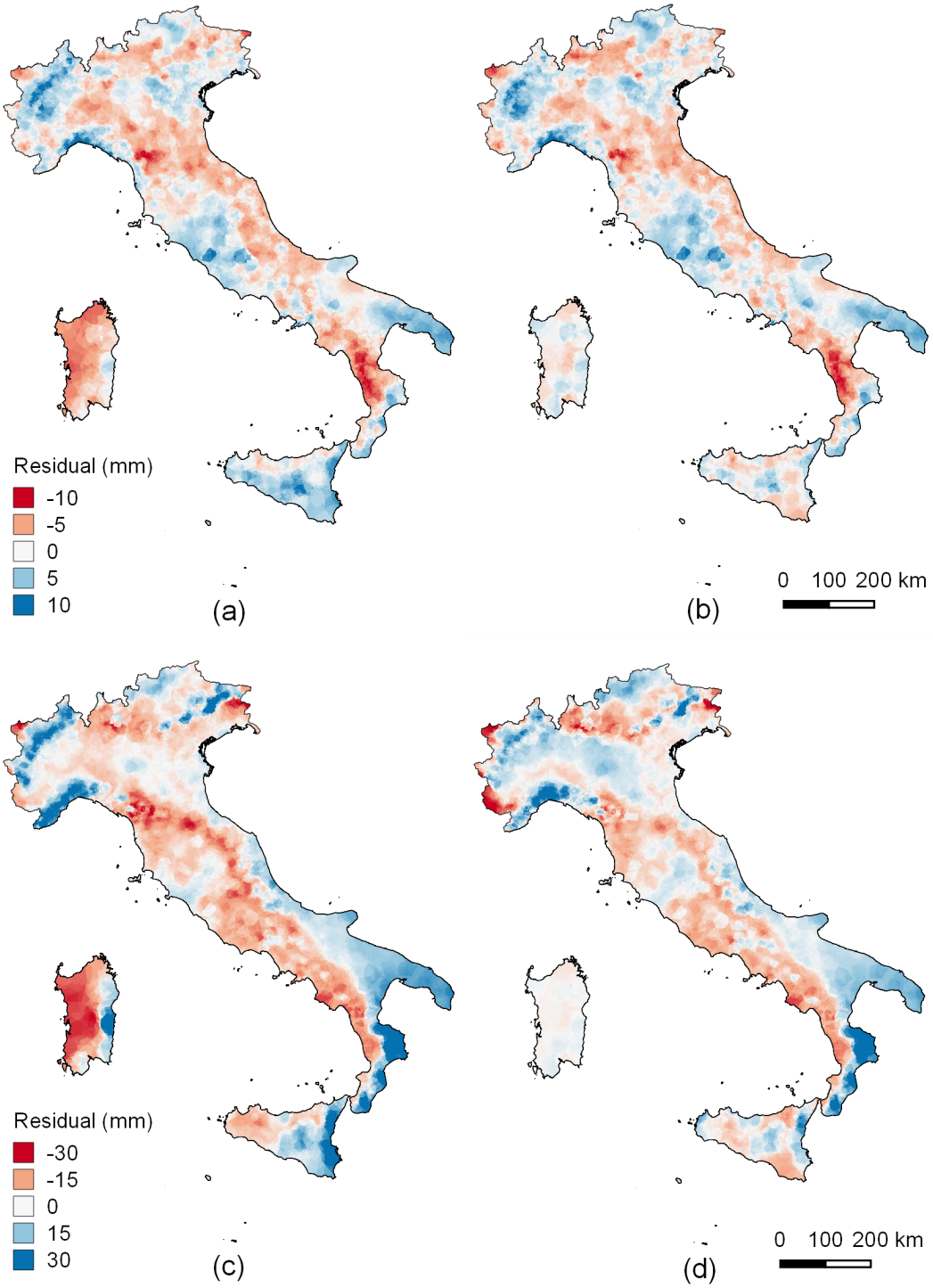

Fig. 6.5 Maps of the residual for the 1 h national-scale multiple linear regression model (a), 1 h four-region multiple linear regression model (b), 24 h national-scale multiple linear regression model (c) and 24 h four-region multiple linear regression model (d). Marked improvements can now be achieved in some areas adopting a sub-national approach, especially for Sardinia. However, these models are not able to reduce the clustering effect in the peninsular region. Source: Mazzoglio et al. (2022a).

6.5 Zonal-scale Simple Linear Regression Over Geomorphological Regions

6.5.1 Methods

On the basis of the considerations presented above pertaining to the spatial clustering of residuals, the possibility of obtaining a meaningful segmentation of large areas in subdomains that could be used to obtain "zonal" relationships between annual maximum rainfall depths and terrain properties was examamined. The main reasoning behind the segmentation is that some macroscopic morphological differences can determine markedly different behaviors of the relationships between rainfall and elevation (or other local variables). One example concerns what happens in the windward and leeward sides of mountain ridges, which represent transversal obstacles to the humid masses coming from the sea. Accordingly, some general geomorphological classifications of the landscape that delineate homogeneous areas based on the homogeneity of the macroscopic land properties, such as convexity and texture, were considered.

Four geomorphological classifications (GCs), named here as GC1 to GC4, were considered according to their diversity and success in the geomorphological literature.

The first classification, called GC1, was proposed by Iwahashi and Pike (2007); they classified the Earth's surface into 16 topographic types, at a 1 km resolution, based on slope gradient, local convexity and surface texture. The raster map, which is available on the European Soil Data Centre website (https://esdac.jrc.ec.europa.eu/content/global-landform-classification, accessed on 7th September 2022), was here vectorized and then, to reduce the presence of small areas, which could have an extent of just a few square kilometers, all the areas covered by fewer than 10 pixels (10 km^2) were merged with the adjacent class. Among the four different classifications that were used, this is the only one that has a worldwide coverage, as all the other classifications are available at a national scale. A detailed description of the methodologies used by the authors is available in the related references, thus allowing all the classifications to be reproduced over other nations.

The second classification – GC2 – is the Carta delle Unità Fisiografiche dei Paesaggi italiani ("Map of the physiographic units of Italian landscapes") and is included in the Carta della Natura ("Map of nature"; Amadei et al. (2003)). A vector

map, which was obtained by means of a visual interpretation of satellite images, aided by the analysis of further land cover maps and morphological–lithological characteristics, was available at a 1:250,000 scale.

The third classification – GC3 – was proposed by Guzzetti and Reichenbach (1994). It was obtained, in vector format, by combining an unsupervised three-class cluster analysis of four properties of altitude (altitude itself, slope curvature, frequency of slope reversal and elevation–relief ratio) with a visual interpretation of morphometric maps and an inspection of geological and structural maps.

The fourth classification – GC4 – is the one that delineates zones with the greatest detail, as it is based on local morphometric properties of the landscape. It was proposed by Alvioli et al. (2020), who considered a set of 439 watersheds, covering the whole of Italy, grouped into seven clusters on the basis of the various properties of the slope units within each basin, e.g., a distribution of slope unit sizes and aspects. In this work, adjacent watersheds of the same class were collapsed (GIS Dissolve), thus producing a total of 178 areas. Geomorphologically homogeneous terrain partitions were defined as "slope units" that were delimited by drainage and divide lines and delineated with a method that was first introduced by Alvioli et al. (2016) and which is widely used in the literature for geomorphological zonation purposes.

An additional geomorphological classification, which was proposed by Meybeck et al. (2001) and which has a worldwide coverage, was also considered. It is based on a combination of a relief roughness index and elevation and in principle could have been a good fifth candidate. However, it was not included in this analysis because, except for a very large geographical zones, the resulting delineated areas often contained very few rain gauges, which would have made it impossible to perform the desired statistical analyses.

Coherently with the aim of addressing connections between terrain properties and rainfall at a more zonal level, a set of linear regression models between elevation and index rainfall was built for all the classifications, considering an individual model for each outlined geomorphological zone. Only the internal rain gauges in each of these homogeneous zones with a minimum of five available stations that had to ensure at least 100 m of difference in elevation were considered for the regressions. There were four possible outcomes of the applications: (a) a positive and significant correlation (at the 5% level), (b) a negative and significant correlation; (c) a nonsignificant

correlation and (d) an insufficient number of stations or an insufficient difference in elevation.

6.5.2 Results

The four geomorphological classifications previously described were used to pool the data needed to fit the regression models. The slope coefficients obtained for each geomorphological zone are mapped in Figures 6.6a–d for the 1 h duration and in Figures 6.7a–d for the 24 h duration.

A comparison of the maps included in Figures 6.6a–d and 6.7a–d clarifies that the more detailed the geomorphological zonation is, the less likely it is to satisfy the requirements necessary to build a significant regression. On the other hand, if one applies regression models to finer geomorphological classifications, it is possible to see that the regression sign is not uniform over the entire country. For example, with regard to 1 h data, it is possible to clearly recognize the presence of zones with a positive rainfall depth versus elevation trend for pre-hill/plain morphology in both GC3 (Figure 6.6c) and GC4 (Figure 6.6d).

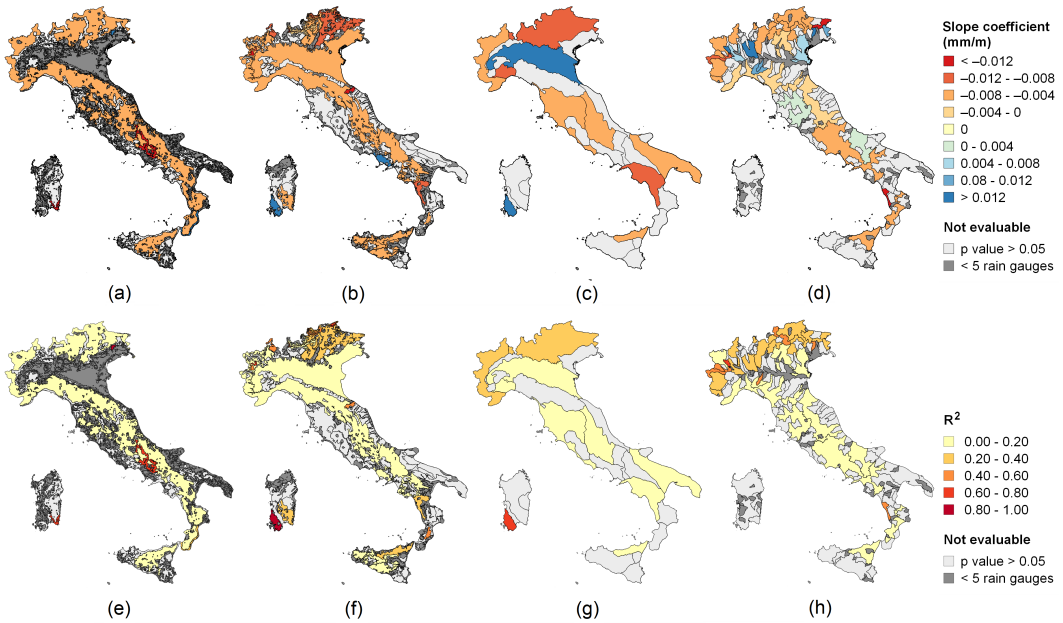

Fig. 6.6 Slope coefficients of the regression between the mean 1 h rainfall depth and elevation for GC1 (a), GC2 (b), GC3 (c) and GC4 (d) and the R^2 of the regression between the mean 1 h rainfall depth and elevation for GC1 (e), GC2 (f), GC3 (g) and GC4 (h). In the first row, blue areas denote geographical zones, where $\overline{h}_1$ or $\overline{h}_{24}$ increase together with elevation, while the red palette applies to zones where rainfall decreases with elevation. The color intensity is proportional to the respective slopes. In the second row, the color intensity is proportional to the R^2. In both rows, the light gray color denotes zones in which the linear regression is not statistically significant (at a 5% level), while dark gray denotes insufficient data (case d). Modified figure from Mazzoglio et al. (2022a).

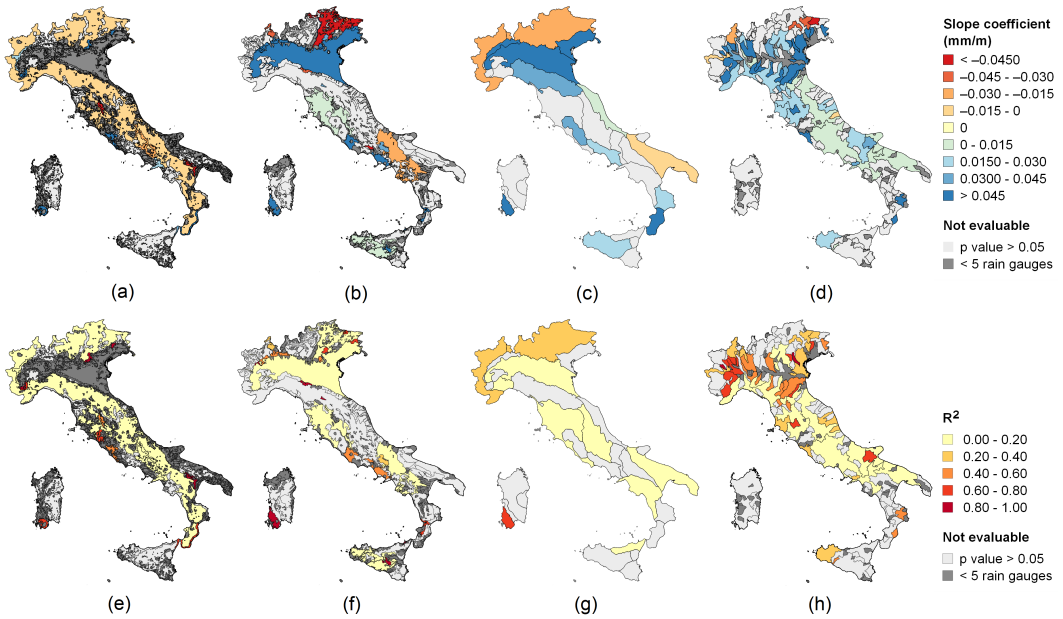

Fig. 6.7 Slope coefficients of the regression between the mean 24 h rainfall depth and elevation for GC1 (a), GC2 (b), GC3 (c) and GC4 (d) and the R^2 of the regression between the mean 24 h rainfall depth and elevation for GC1 (e), GC2 (f), GC3 (g) and GC4 (h). In the first row, blue areas denote geographical zones, where $\overline{h}_1$ or $\overline{h}_{24}$ increase together with elevation, while the red palette applies to zones where rainfall decreases with elevation. The color intensity is proportional to the respective slopes. In the second row, the color intensity is proportional to the R^2. In both rows, the light gray color denotes zones in which the linear regression is not statistically significant (at a 5% level), while dark gray denotes insufficient data (case d). Modified figure from Mazzoglio et al. (2022a).

The spatial distribution of the light gray zones is an important piece of information: no trend can be assumed over these areas because the p-value is greater than 0.05. Consequently, $\overline{h}_1$ can be considered constant over these areas. Finally, the occurrence of the dark gray zones is directly connected to the kind of classification: the smaller the areas delineated by the classification are, the more likely it is that the requirement of having at least five rain gauges with at least 100 m difference in elevation is not satisfied. In this regard, it can be observed that the above requirements are not met for the elevation difference, i.e., in plain areas, and it is necessary to assume a constant $\overline{h}_1$ in the area as being the most reasonable value.

The maps in Figures 6.6a–d show that the availability of more detail in the spatial analysis of the relationship between rainfall depth and elevation has a remarkable effect on both the sign of the regression and the slope of the regression line in several areas. In addition, even the quality of the relationship can improve, as can be seen

Table 6.3 National-scale error statistics for the 1 h interval. Statistics for GC1, GC2 and GC3 were only evaluated over areas where the regression was statistically significant at a 5% level, while GC4 was tested on both statistically significant areas and over the entire nation, using the mean rainfall, where there was a p-value > 0.05 or where the requirement of at least five rain gauges with at least 100 m difference in elevation was not satisfied. Source: Mazzoglio et al. (2022a).

Regression model	Bias (mm)	MAE (mm)	RMSE (mm)	NSE (-)
GC1	0	5.94	7.67	0.10
GC2	0	5.65	7.18	0.15
GC3	0	5.15	6.77	0.27
GC4 over statistically significant areas	0	4.53	5.84	0.50
GC4 over the entire nation	0	3.87	5.12	0.52

from a comparison of Figures 6.6e–h: far more areas with high R^2 can be seen in Figure 6.6h than in Figure 6.6e. This allows us to conclude that lower values of R^2 are obtained in wider areas.

The same analysis was conducted on $\overline{h}_{24}$, where all of the above outcomes were confirmed, except for the sign of the precipitation vs elevation relationship (Figure 6.7).

To test the reliability of the regression models built over the GCs, the linear equations found in each geomorphological zone were applied to all the rain gauge positions, to obtain errors that could be examined at the country scale. The global indices computed for the GC areas in which the regressions were statistically significant are reported in Table 6.3 for $\overline{h}_1$ and in Table 6.4 for $\overline{h}_{24}$. These results clearly show a lower performance of the GC1 than the national-scale regression model. On the other hand, the error statistics in Tables 6.3 and 6.4 show that GC4 produces the smallest errors, and this geomorphological subdivision therefore presents the best performances. It is possible to understand this result by considering that GC4 uses watershed units, while the other classifications are based on the automatic processing of digital terrain data.

Table 6.4 National-scale error statistics for the 24 h interval. Statistics for GC1, GC2 and GC3 were only evaluated over areas where the regression was statistically significant at a 5% level, while GC4 was tested on both statistically significant areas and over the entire nation, using the mean rainfall, where there was a p-value > 0.05 or where the requirement of at least five rain gauges with at least 100 m difference in elevation was not satisfied. Source: Mazzoglio et al. (2022a).

Regression model	Bias (mm)	MAE (mm)	RMSE (mm)	NSE (-)
GC1	0	30.44	39.49	-0.11
GC2	0	20.30	31.29	0.11
GC3	0	20.03	28.84	0.32
GC4 over statistically significant areas	0	14.84	21.12	0.61
GC4 over the entire nation	0	14.36	20.73	0.60

6.6 Discussion about National vs Zonal Approach

The different regression models used in this work to investigate the role of morphology in the spatial distribution of sub-daily annual maximum rainfall depths produced results deserving some comments. First of all, it must be mentioned that a nationwide multiple regression model that includes morpho-climatic attributes represents a significant step forward with respect to the simple regression model, as the error statistics show. In this approach, working at a national scale and given the elongated shape of the Italian peninsula, geographic location was expected to play a major role in the spatial distribution of extremes, even though this evidence was not mentioned in similar national-scale analyses (see, e.g., Faulkner and Prudhomme (1998) for the UK, and Avanzi et al. (2015) for Italy). The role of geography progressively weakened while seeking further improvements, in terms of MAE and RMSE, through the application of distinct multiple regressions to four macro-regions, i.e., the Alps, peninsular Italy and the main islands (Figures 6.8 and 6.9).

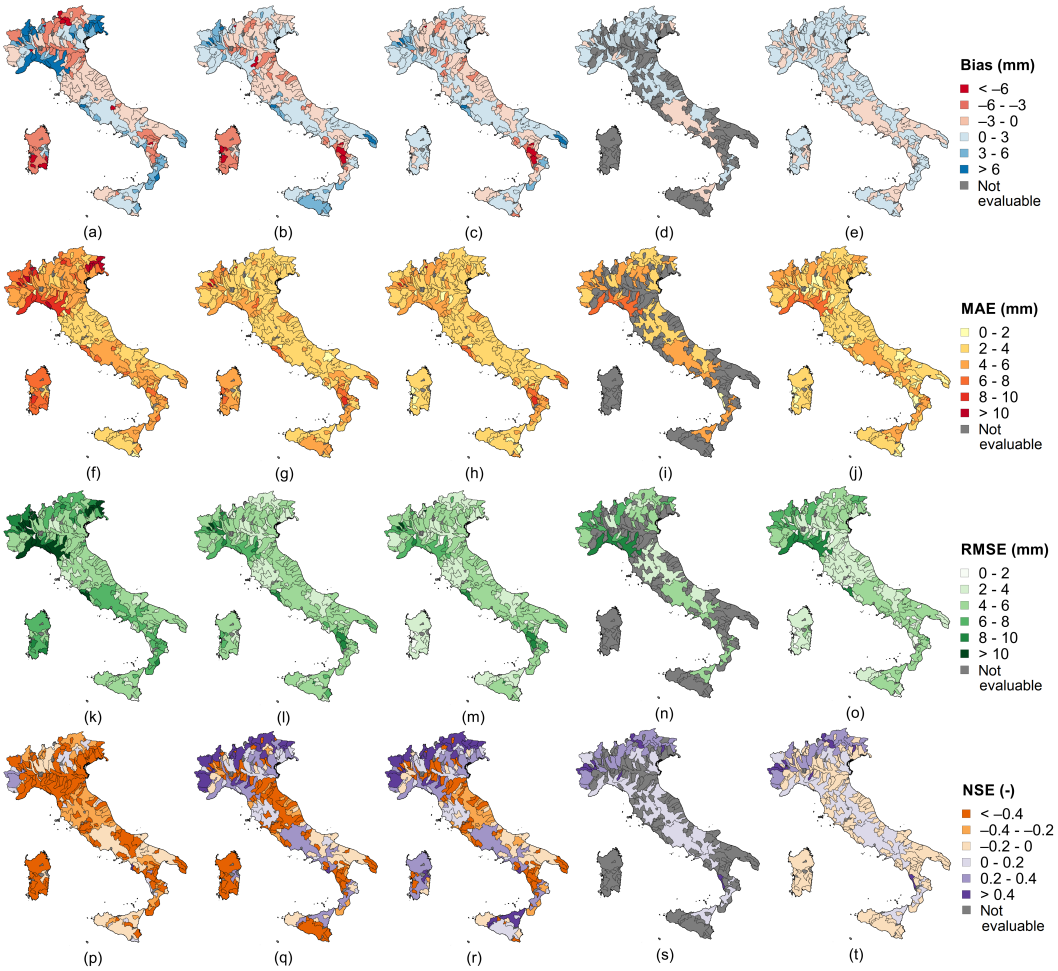

Fig. 6.8 Error statistics for the 1 h duration in the case of the national-scale regression model (a, f, k, p), the national-scale multiple linear regression model (b, g, l, q), the four-region multiple regression model (c, h, m, r) and GC4 simple linear regression model over statistically significant areas (d, i, n, s) and over the entire nation (e, j, o, t). Modified figure from Mazzoglio et al. (2022a).

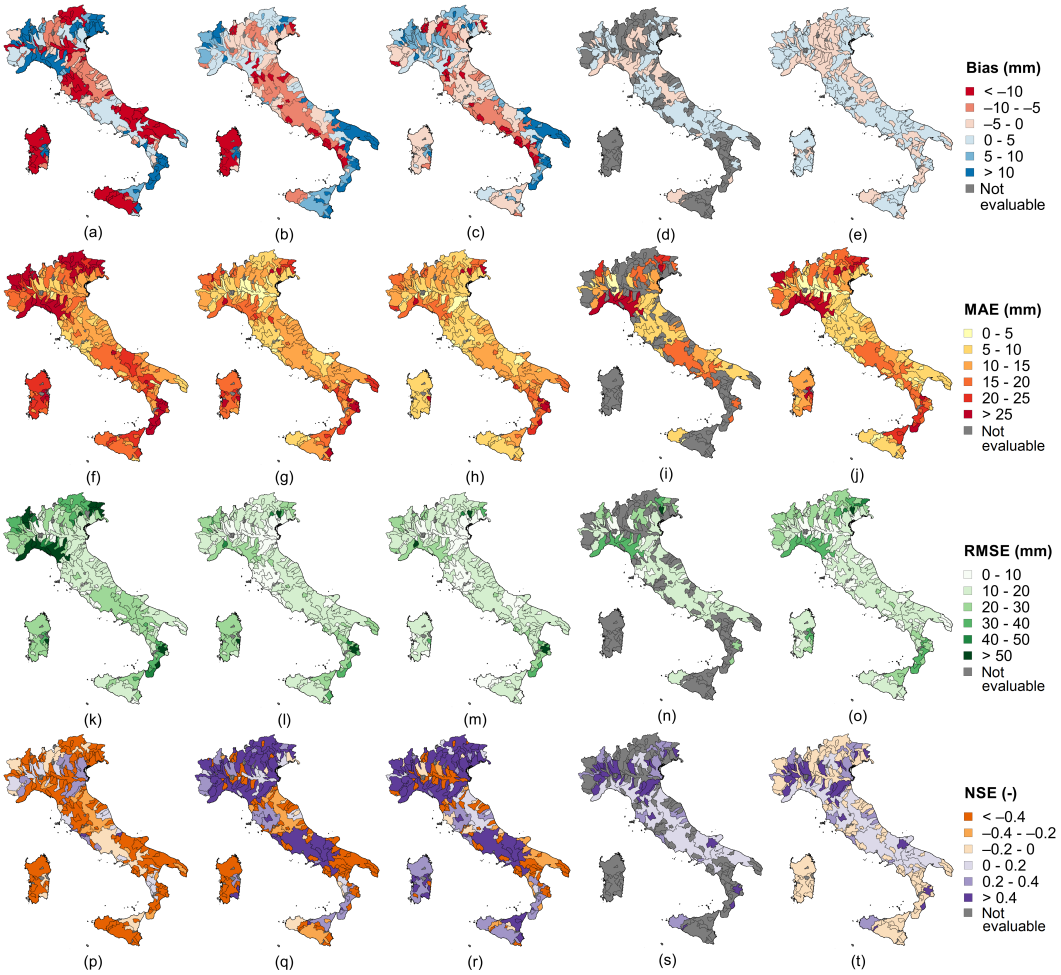

Fig. 6.9 Error statistics for the 24 h duration in the case of the national-scale regression model (a, f, k, p), the national-scale multiple linear regression model (b, g, l, q), the four-region multiple regression model (c, h, m, r) and GC4 simple linear regression model over statistically significant areas (d, i, n, s) and over the entire nation (e, j, o, t). Modified figure from Mazzoglio et al. (2022a).

Our findings show that, while the 24 h index rainfall exhibits a clear overall dependence on the geographic location at a full national scale (Equation 6.14), the same does not apply to 1 h extremes (Equation 6.11). In an area with a lesser span in latitude (the Italian Alps), instead, the 1 h extremes curiously show some dependence on latitude (Equation 6.15). Formetta et al. (2022) followed a similar reasoning, recognizing the role of geography and elevation as they partitioned by longitude and elevation even a small area (the province of Trento) before applying their statistical analyses.

While the multivariate regression can be a good tool to express geographic dependence, and on 24 h extremes the national scale helps in drawing some general findings, the residual errors in large clustered areas are still very significant. Therefore, geographic attributes seem not to drive uniformly the variability of rainfall extremes across Italy, as the high residuals of the multiple regression over these areas do not apparently follow any latitudinal/longitudinal gradient.

The better suitability of the application of multiple regressions on four regions is confirmed by the increase of the adjusted coefficient of determination (R^2_{adj}), as reported in Section 6.3.2 and in Appendix B. Moreover, while the national-scale multiple regression model provides high negative residuals over Sardinia and high positive residuals over Sicily, the four-region multiple regression model significantly improves this result (see Figures 6.5, 6.7, 6.8 and 6.9 for more details). However, similar improvements were not achieved in the peninsular and alpine areas of the country.

The subsequent investigations undertaken in Section 6.5 descend from the above considerations; i.e., the building of regressions in morphological zones that are a fraction of the whole area is an attempt to overcome the highlighted lack of regularity in the dependence between rainfall and geography. Among all the considered geomorphological classifications, the selection of rain gauges for the model application is more effective in the case of GC4 (Alvioli et al. (2020)), which also embeds hydrographic information. The GC4 model behaves reasonably well for both the 1 and 24 h durations, compared to the multiple regression models, as far as the national scale is considered. Table 6.5 summarizes all the previously mentioned statistics.

Analyzing the error statistics computed globally at the national scale, it seems that the four-region multiple regression approach is the most precise. However, this is not necessarily true at a local scale. To clarify the drawbacks that large-scale regression models can produce, for the 1 h case, we compared the residuals obtained from the four-region multiple regression model (Figure 6.10a) in the areas identified by GC4 with the residuals of the GC4 regression model by selecting: (1) the GC4 areas that were statistically significant (Figure 6.10b) and (2) the entire nation (Figure 6.10c). The mean rainfall depths were considered over nonstatistically significant areas (i.e., the gray zones visible in Figure 6.10b). The GC4 regression models were statistically significant for $\overline{h}_1$ for 45% of the Italian area, for a total of 31 different zones, while the GC4 model for $\overline{h}_{24}$ were statistically significant in 49% of the area,

Table 6.5 Error statistics for the 1 and 24 h intervals at a national scale. Average spatial values are used for the gray areas in Figure 6.6d. The bias of the national simple regression is different from zero, being evaluated as $bias_d = \frac{1}{n} \cdot \sum h_{avg}(d) - \hat{a} \cdot d^{\hat{n}}$. Source: Mazzoglio et al. (2022a).

Regression model	Bias (mm)	MAE (mm)	RMSE (mm)	NSE (-)
1 h National simple regression	1.07	5.29	6.98	0.10
1 h National multiple regression	0	3.83	4.98	0.54
1 h Four-region multiple regression	0	3.65	4.77	0.58
1 h GC4 regression	0	3.87	5.12	0.52
24 h National simple regression	6.05	22.27	31.99	0.03
24 h National multiple regression	0	13.14	18.43	0.68
24 h Four-region multiple regression	0	11.71	16.53	0.74
24 h GC4 regression	0	14.36	20.73	0.60

for a total of 47 different zones. From a comparison of the maps in Figure 6.10, it is possible to note that the multiple regression model has a spatially nonuniform bias while the average bias obtained from the individual models in the zones selected by GC4 is zero all over Italy. Maps of all the other statistics are reported in Figure 6.8. This outcome is also evident for the 24 h case (see, for example, the maps of the bias, that is Figure 6.9a–e).

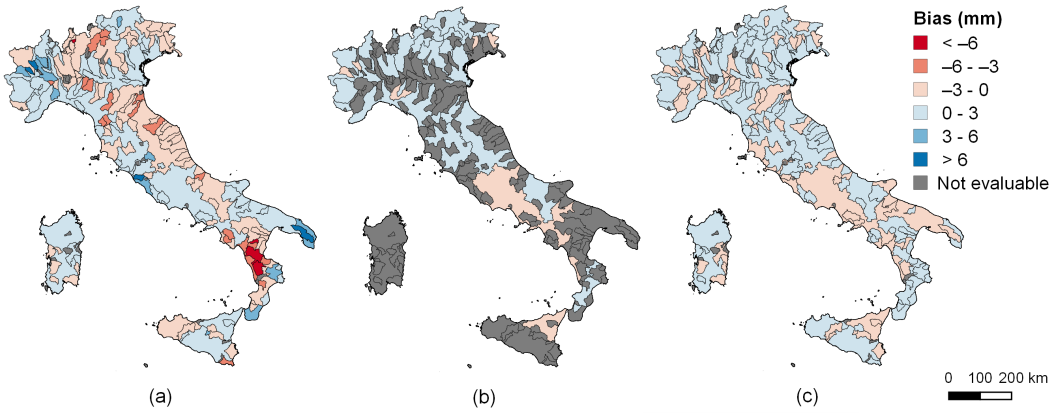

Fig. 6.10 The 1 h case. Local bias for the four-region multiple regression model (a), the GC4 simple linear regression model over statistically significant areas (b) and the GC4 simple linear regression model over all the areas (c). Modified figure from Mazzoglio et al. (2022a).

An additional comparison was undertaken to investigate the local bias. In this case, the bias was computed for each GC4 zone. The bias values obtained using

the four conditions were compared in the cases of: (1) the national-scale simple regression model (Equations 6.3 and 6.5), (2) the national-scale multiple linear regression model (Equations 6.11 and 6.14), (3) the four-region multiple regression model (Equations B.3, B.6, B.9, B.12, B.15, B.18, B.21 and B.24, in Appendix B) and (4) the GC4 simple regression model (Section 6.5).

The results are illustrated in the maps of Figure 6.11, which show the best regression model for each area in different colors. Figure 6.11a and b are related to $\overline{h}_1$, while Figure 6.11c and d refer to $\overline{h}_{24}$; Figure 6.11a and c only highlight the situations where significant regressions were found. The results in Figure 6.11b and d include the bias calculated in nonstatistically significant areas with respect to the spatial average of the rainfall depths. The good results obtained in the areas where the spatial mean values are adopted can be seen by comparing the borders of the GC4 areas with the clusters of the residuals of the multiple regression model (see Figure 6.5). A dedicated multiple regression model was built for the island of Sardinia: nevertheless, the bias all over the GC4 zones is smaller when the local spatial average is used. A good correspondence between the residual clusters and the GC4 borders is evident.

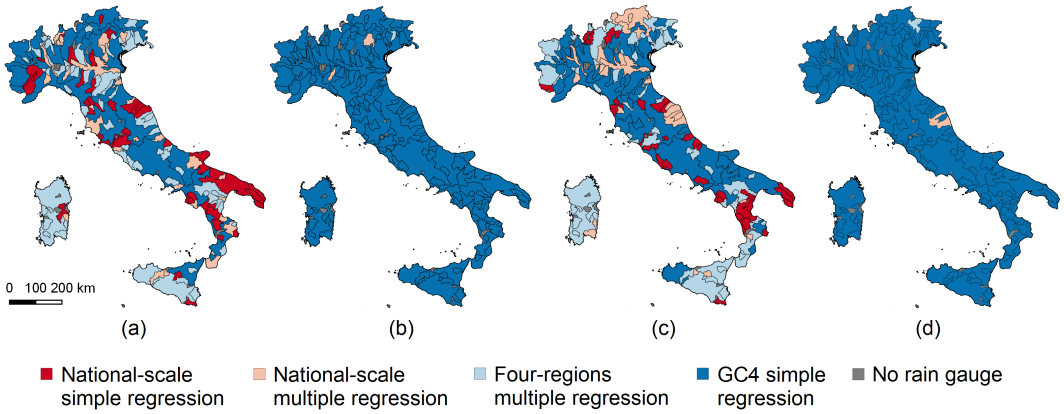

Fig. 6.11 Absolute bias assessment for all the regression models used for the 1 h case (a, b) and 24 h case (c, d). The color refers to the model that provides the lowest absolute value of the bias. The GC4 model bias in cases (a) and (c) was only evaluated for statistically significant areas, while it was evaluated over every area in (b) and (d) Modified figure from Mazzoglio et al. (2022a).

From Figure 6.11, it is possible to conclude that the morphological subdivisions allow building a set of simple linear regression models that can perform better almost everywhere than the other wide-area models in terms of local bias. However, finer

analysis could be performed to further investigate the spatial variability of rainfall extremes and how they are influenced by elevation.

6.7 From a Zonal to a Local Approach: The Georegression Approach

Among the methods listed in Section 6.1, univariate and multivariate linear regression models have the advantage of producing results that are statistically stable with respect to small errors in the observations; they also explain a large portion of the rainfall variability (Daly (2006)). Nevertheless, when applied to large areas with complex terrain features, the use of a unique regression model can lead to evident clustering of the residuals. This is why simple or multiple linear regressions usually provide better results if applied over small regions, as pointed out in Daly (2006)) and in the previous sections (see also Mazzoglio et al. (2022a)).

Geographically-weighted regression techniques have been developed to deal with local relationships between rainfall and geography. For instance, in the first version of PRISM, i.e. the Parameter-elevation Regressions on Independent Slopes Model (Daly et al. (1994)), the precipitation-elevation relationship is investigated with reference to any individual grid cell. The approach uses a local regression model that selects rain gauges located within a specific radius on topographic facets having an orientation similar to the one of the estimation cell. An improved version of PRISM (Daly et al. (2002)) uses a complex geographically-weighted regression model based on weighting functions that account, for every station, for the effects of elevation, terrain orientation, coastal proximity and a two-layer atmosphere introduced to handle non-monotonic variations with the elevation (Daly et al. (2002); Daly (2006)). In both the PRISM versions, the optimal search radius is identified through cross-validation and ranges from 30 to 100 km, in an attempt to adapt to the station density. Other works (Brunsdon et al. (2001); Fotheringham et al. (2003)) implemented a geographically-weighted regression with fixed or adaptive spatial kernels (using a Gaussian or exponential decay function). These latter approaches avoid the a priori selection of the radius used to select the points in the analysis of the spatially varying precipitation vs elevation relationships. A mixed approach is used in the Daymet model (Thornton et al. (1997); Thornton et al. (2021)): a Gaussian spatial kernel is applied only

to stations located within a specific search radius defined using a data density evaluation algorithm (a truncated Gaussian spatial kernel is the model used). In all these applications, each rain gauge included in the regression function is weighted by its distance from the grid cell where rainfall is to be estimated. This approach makes data measured far from the target cell irrelevant. It is interesting to note that all the above models consider only linear precipitation-elevation relationships.

Due to the lack of a complete national rainfall database, until recently, analyses based on geo-regression models were not extensively conducted over Italy. The only study available for the entire country (Crespi et al. (2018)) considers monthly and annual precipitations. Some studies are available for selected regions of Italy: Di Piazza et al. (2011) focused on monthly rainfall in Sicily, Golzio et al. (2018) and Crespi et al. (2021) analyzed monthly rainfall in the Central Alps region, while Frei and Schär (1998) and Isotta et al. (2014) addressed daily rainfall in Northern Italy. None of them, whatever the spatial coverage, has considered the rainfall extremes of sub-daily durations.

In addressing the goal of accurately reconstructing sub-daily extreme rainfall indices at a national scale, we can take advantage of a complete database of sub-daily annual maximum rainfall depths (Mazzoglio et al. (2020)). Within the framework of the spatial analysis of rainfall extremes, and based on the above considerations, the aims of this research are to: i) investigate the relationships between orography and sub-daily precipitation extremes in Italy and ii) build maps of sub-daily average rainfall extremes, that can be used for describing the spatial variability of the extremes over Italy. The approach undertaken is based on an improved local regression approach, that is able to preserve local features and to prevent the spatial clustering of the residuals.

The main novelties introduced in this work are: i) a definition of the optimal search radius on the basis of the station density (this is something that has been already attempted in Daymet (Thornton et al. (2021)) using a georegression model that includes a truncated Gaussian kernel and that is further expanded here; ii) a methodology that, contrary to PRISM, allows also negative rainfall-elevation relationships, following recent investigations conducted by Allamano et al. (2009), Avanzi et al. (2015) and Mazzoglio et al. (2022a) to investigate the presence of negative orographic gradients for shorter durations; iii) the inclusion of constraints regarding the minimum elevation difference among the rain gauges pooled to form

the local sample and the maximum extrapolation allowed. This latter point allowed us to solve some well-known problems remarked in Daymet, such as the possibility of having negative estimated values (previously solved by forcing them to zero) or estimated values that are more than two time higher than the measured ones.

6.8 The Local Regression Approach: Methods

The nature of the approach proposed involve a strict relationship between data and methods. The reason is that the selection of the sample to be subjected to local regression is based itself on the quality of the results of the regression applied. In this section, the interactions between the two components is preliminary exposed.

6.8.1 Data catalog

As performed in the first sections of this chapter, in this study only time series with at least 10 years of data (from more than 3800 stations) are used. At-site average rainfall extremes for the 5 durations are computed and constitute our sample.

Elevation data of the rain gauges and of the surrounding terrain come from the Shuttle Radar Topography Mission (STRM) Digital Elevation Model (DEM) at 30 m resolution (Farr et al. (2007)) resampled at 1-km resolution using a cubic interpolation, as in Daymet (Thornton et al. (2021)). The elevation of the rain gauges was derived from the resampled DEM using the station coordinates, following the approach suggested in PRISM (Daly et al. (1994); Daly et al. (2002)) and also adopted in Daymet (Thornton et al. (1997); Thornton et al. (2021)). This step is not trivial and has methodological implications. In fact, the authors involved in the development of PRISM pointed out that the relationship between precipitation and elevation is more representative if local elevations are derived from a low-resolution DEM, that is able to describe better the scale of orographic processes and to filter out local elevation details.

More details will be provided in the application section, where the regression models are applied to each cell of the resampled DEM.

6.8.2 Linear Regression Model

To examine the relations between sub-daily rainfall depths and orography, local linear regression models have been built. The linear regression model that we use is

$$\overline{h}_d = a + b \cdot z + \varepsilon \tag{6.17}$$

where $\overline{h}_d$ is the mean rainfall extreme of an assigned duration d (with d = 1, 3, 6, 12 and 24 hours in our case), a is the intercept, b is the slope (that represents the rainfall gradient), z is the elevation and ε is the residual of the regression.

As mentioned in Section 6.7, approaches that use a unique linear regression model applied over vast areas are known to produce high residuals and high bias (see also Brunsdon et al. (2001) and the first sections of this chapter). For this reason, the parameters a and b are allowed to be space-dependent, i.e. Eq. 6.17 assumes the form

$$\overline{h}_d(x,y) = a(x,y) + b(x,y) \cdot z(x,y) + \varepsilon(x,y) \tag{6.18}$$

where $\overline{h}_d$, a, b, z and ε have the same meaning as in Eq. 6.17 but are related to a generic position with coordinates (x,y).

Similarly to the Daymet model (Thornton et al. (1997)), we consider linear rainfall-elevation relationships by using slope coefficients $b(x,y)$ dependent only on the planimetric coordinates. In most applications of the PRISM model, the minimum allowable slope coefficient $b(x,y)$ is set to zero, because Daly et al. (2002) argue that the rainfall depth can only increase with elevation. Considering that previous works conducted over Italy suggest that a reduction of rainfall depth with elevation is possible (e.g. Allamano et al. (2009), Avanzi et al. (2015), Libertino et al. (2018a), Formetta et al. (2022), Mazzoglio et al. (2022a)), in our work we do not disregard negative values obtained for the $b(x,y)$ parameter. Nevertheless, values of the $b(x,y)$ parameter need to be in a reasonable range, as will be explained in Section 6.9.3.

6.8.3 Local Sample Identification

To estimate the parameters of the local regression (Eq. 6.18) in every (x, y) position, a "local" reference sample must be identified with a number n of station included in an area adequate for a regression. Similarly to Daly et al. (2002), we proceed by

selecting n stations available in a circular area of radius r, whose center coincides with the centroid of the grid cell to which the regression is referred. The length of the radius and the minimum number of stations required for reaching a reasonable local estimate are parameters that have to be conveniently tuned.

If r is small, a low number of rain gauges would be selected (in some cases, the low data density can imply that no rain gauge can be selected). If r is large, the relationship ceases to be "local", and model performance can degrade. The definition of the number of stations necessary for the regression is strongly driven by the station density and its uniformity on the territory, being desirable that the regression model is applicable on a high percentage of the territory. To provide a baseline, we started to use local samples gathered in circles of varying radii, to perform a rain gauge density analysis. The search of the modal value of stations available in circles of different radius can be a first approach for defining n. As a reference, when the PRISM model considers all the stations (independently on the orientation of the topographic facet on which these stations are installed), the authors account for the availability of 10 to 30 stations within a radius of 30 to 100 km (Daly et al. (2002)).

To define the most appropriate radius of the area needed for selecting the local sample, in this work two approaches have been adopted:

- to use a unique, fixed radius $r = r_{fix}$;
- to use a radius interval, variable from r_{min} to r_{max}, that depends on data density.

In the first approach the regression parameters were evaluated using the data of rain gauges that are located inside a circular area of radius $r = r_{fix}$, whatever the statistical significance of the regression model. This approach is similar to the one used in the PRISM and in Daymet models. In the second approach, the radius increases from r_{min} to r_{max} in each cell, until a statistically-significant regression model is found (p-value < 0.05). The r_{max} is set to avoid regression models that gather data from areas that are too large. If, when reaching r_{max}, the model pools together at least n rain gauges, but the regression is not statistically significant, two alternatives can be considered: a) the model is applied without considering the p-value threshold; and b) the predicted value is set to the mean rainfall value evaluated using the n nearest stations. If n stations are not present even within a circle of radius r_{max}, the model is applied to the n nearest stations, regardless of their position.

It is worthwhile to observe that the evaluation of the mean rainfall depth, using the mean values of the n nearest stations, can be applied all over the territory. This approach, despite its simplicity, especially for areas with complex morphology, has the advantage of being very simple and can provide a valid starting point for additional comparisons with most complex methods. Notice that all the previously referenced works do not provide this comparison.

6.8.4 Artifacts and Model Corrections in High/Low Elevations

Application of systematic criteria for the selection of both the local sample and of the reference radius can involve the presence of artifacts in the final results. The analyses carried out in this research have shown that artifacts are mainly due to two causes: i) a non-consistent rainfall gradient; and ii) a level of extrapolation leading to unreasonable results.

As it concerns the first issue, an insufficient elevation range in the data sample was the reason for obtaining anomalously high (positive and negative) rainfall local gradient. To prevent the occurrence of this effect, we envisage to impose a minimum elevation range Δz (i.e. the difference between the highest and the lowest rain gauge) necessary to undertake the statistical estimation of the rainfall gradient.

Daly et al. (2002) addressed the same problem. In PRISM, the minimum valid rainfall gradient is set after normalization by the mean annual precipitation, and it is equal to 0 km^{-1} (it can be -0.5 km^{-1} only at high elevations) while a maximum slope of 3 km^{-1} is allowed. In the Italian context, characterized by a mean annual precipitation of about 1000 mm, applying a 3 km^{-1} threshold (i.e. a 3 mm/m value) would remove only a few of the outliers, appearing as too low for the 24 h maxima. Moreover, we could not find a physical explanation for excluding over-threshold gradient values. Using a selection criterion based on a minimum elevation range revealed indeed to be both efficient and straightforward to apply.

Considering the extrapolation aspects, it is well known that regression models applied in data scarce regions with a complex rainfall-elevation relationship can produce unrealistic results (Brunsdon et al. (2001); Crespi et al. (2018)). In Crespi et al. (2018) no constraint is assigned to grid cells with elevation higher than those of the rain gauges used in the local sample. Also in the first version of PRISM model (Daly et al. (1994)) extrapolation is allowed almost without constraints; nevertheless,

if the stations of the local sample have a lower elevation compared to the grid cell for which the estimation is performed, and the elevation range covered by the station elevation is small (less than 1000 m), a different slope coefficient is used in the precipitation-elevation function above the elevation of the highest station. In an improved version of PRISM (Daly et al. (2002)) the extrapolation is differently handled: the atmosphere is divided into two layers, and thus a different weight is assigned to each rain gauge depending on its elevation.

To decide how to handle the extrapolation in our work, we identified the situations in which extrapolation leads to inconsistent results. A model correction appears to be necessary both in mountainous and in very flat regions. Inconsistencies due to extrapolation can be encountered over the peaks or in narrow valleys, when all the rain gauges are located over the mountain sides. In this case, the local sample includes only rain gauges installed at location higher than the selected one. Another inconsistency can be encountered in grid cells of a plain area when the local sample of the model includes stations located over an isolated small hill. To face similar situations, different approaches have been tested, looking for more robust estimates at ungauged grid cells. Three alternative constraints are finally considered in the regression models:

- extrapolation is never allowed: in grid cells with an elevation z^* that is higher/lower than those of all the data of the local sample, the regression model is not applied and the predicted value is set as the value obtained by the model in correspondence of the elevation of the highest/lowest rain gauge used (see the ordinate $\overline{h}_d(z^*)$, i.e. the dashed line in Figure 6.12a);

- extrapolation is allowed to a limited extension, while elsewhere the regression limit value are used: in grid cells with an elevation z^* that is e_{max} higher/lower than those of the data of the local sample, the model is not applied and the predicted value is set as the value obtained by the model at an elevation that is e_{max} higher/lower than those of the highest/lowest rain gauge of the sample (see $\overline{h}_d(z^*)$, i.e. the dash-dot line in Figure 6.12b);

- extrapolation is allowed to a limited extension, while elsewhere the mean value is used: in grid cells with an elevation z^* that is higher/lower than those of the data of the local sample by an amount e_{max}, the model is not evaluated and the

predicted value is computed using the 5 nearest stations (see $\overline{h}_d(z^*)$, i.e. the dash-dot line in Figure 6.12c).

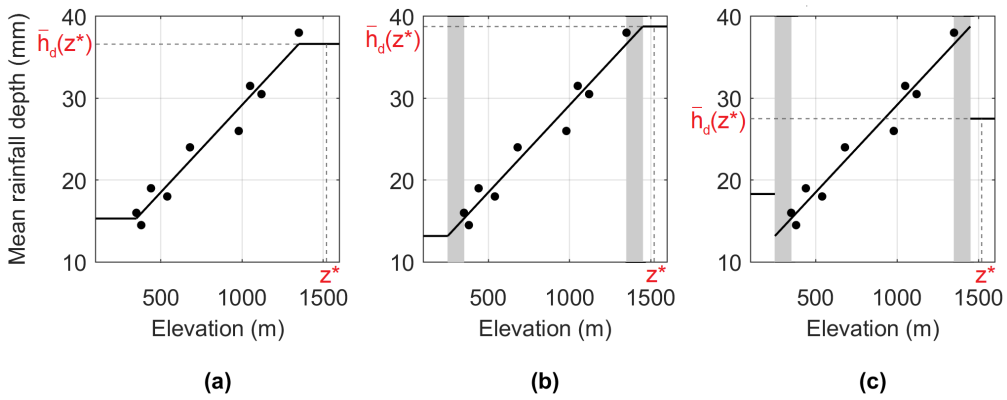

Fig. 6.12 Visual representation of the three approaches used to handle the extrapolation effect described in Section 6.8.4 for the estimation of the mean precipitation p at the elevation h^*. The black line represents the fit of the local sample; the vertical grey bars in case (b) and (c) represent the case of extrapolation e_{max} = 100 m allowed.

To summarize, in the last two cases (Figures 6.12b and 6.12c) an extrapolation is allowed up to a level e_{max}, while in the first one (Figure 6.12a) no extrapolation is allowed. In the third case (Figures 6.12c) marked discontinuities can appear when applying the constraint over a group of pixels, while in the first two cases (Figures 6.12a and 6.12b) discontinuities are not present. In all cases, extrapolation is not allowed when the elevation of the estimation cell is e_{max} higher than those of the rain gauges of the local sample.

In the subsequent sections, we present the results obtained applying the different alternative constraints mentioned above. The final value for e_{max} is also defined after proper testing.

6.9 The Local Regression Approach: Application

According to what defined above, we approach to the analysis of the spatial variability of precipitation extremes in Italy through a local regression framework. The definition of the model configuration passes through the setting of the model configuration parameters introduced in Section 6.8. In this section, the parameter values

are estimated for the Italian territory and a list of plausible model configurations is obtained.

6.9.1 Definition of the Local Sample

Italy has a $\approx$ 300,000 km^2 wide territory having marked mountainous characteristics (Figure 6.13a), that undermine the possibility of having a uniform rain gauge density. Even though an unprecedent rainfall data coverage is now available with the Improved Italian – Rainfall Extreme Dataset (Mazzoglio et al. (2020)), the search for algorithms that predict extreme rainfall indices based on local data will face a marked spatial data heterogeneity in station density, with changes up to half an order of magnitude in different areas of the country.

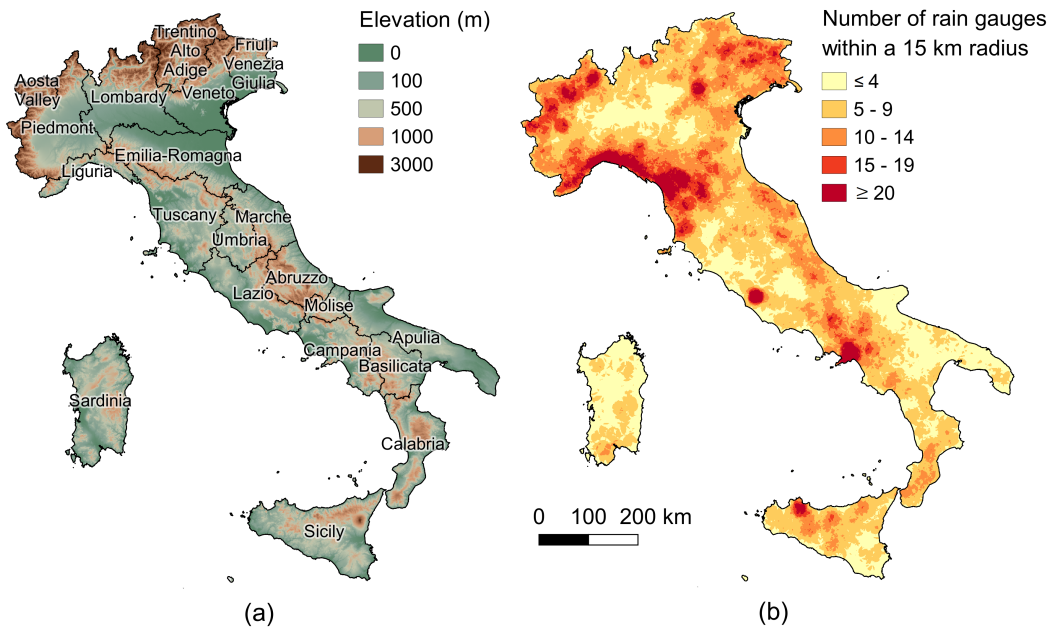

Fig. 6.13 Elevation data (a) and number of rain gauges available for each cell within a 15 km radius (b). Source: Shuttle Radar Topography Mission (Farr et al. (2007)).

For each grid cell all over Italy we evaluated the number of rain gauges (with a time series of at least 10 years of data) available within circles with radius of 10, 15, 20 and 25 km. The results are shown in Table 6.6 in terms of the mean, median, modal and standard deviation values found.

Table 6.6 Mean, median, modal and standard deviation values of the rain gauges falling in circles of variable radius.

Radius (km)	Mean (n°)	Median (n°)	Mode (n°)	Standard deviation (n°)
10	3.9	3	2	2.7
15	8.2	7	5	5.2
20	14.3	13	7	8.4
25	21.8	19	14	12.2

The values shown in Table 6.6 are useful both to understand what could be a reasonable minimum local sample size n and to the selection of r. We then evaluated that a local sample of 5 stations within a 15 km radius can provide a reference set similar to the one used in PRISM (1 station every 3 km of radius in average).

More specifically, using a fixed 15-km radius a local sample of at least 5 rain gauges is obtained in over 227,150 grid cells (Figure 6.13b), leading to an equal minimum density in about 75% of Italy. As we do not consider reliable a regression fitted using a local sample with less than 5 values, for the remaining 25% of the cells over Italy we computed the mean rainfall depth using the 5 nearest stations, independently on their distance from the reference cell. It is interesting to note that the spatial coverage of this 25% of under-threshold density cells (that can be recognized as the yellow areas of Figure 6.13b) is quite coherent, i.e. cells are spatially connected. These areas often coincide with flat regions, where we expect a limited influence of the orographic effect. We decided not to reduce the radius because, if we consider as an example the case of 10 km, only 93,735 grid cells ($\approx$ 31% of the Italian territory) can secure a local sample of at least 5 rain gauges.

Based on the results of Table 6.6, we considered model configurations with a fixed radius whose length is equal or greater than 15 km (r_{fix} = 15, 20 and 25 km), within which the criterion of pooling a minimum number of 5 stations was always kept valid.

For the variable radius approach, as described in Section 6.83, the radius length was allowed to vary between r_{min} = 1 km and r_{max} = 15 km to have a local regression. Some tests were performed using also larger r_{max} (up to 50 km) but we observed a marked decrease of the model performance, in terms of error statistics and residuals of the regressions, as the radius increases beyond 15 km. A quantitative estimation of the degradation of model performance is reported in Section 6.10.

6.9.2 Locally-averaged Rainfall Maps

As mentioned in Section 6.8.3, the estimation of the mean rainfall extremes using the average values of the n nearest stations can represent a strong reference for additional comparisons with all the other attempts based on more complex georegression models. In this case, no specific radius is used to put together a local sample whose spatial extension depends on the data density. This approach represents a step forward compared to the approach used in Section 6.2 to 6.6, where geographical and geomorphological classifications were used to pool the data before fitting the model.

Figure 6.14a shows the mean 1 h rainfall depth computed on the basis of the n = 5 nearest stations: it can be seen that this approach does not allow to model the orographic gradients (i.e., some of the spatial patterns that follow the orography are missing) and several artifacts are clearly visible. Moreover, Figure 6.14b shows clusters of high residuals in correspondence of orographically complex areas as the Prealps.

Figure 6.14c shows the comparison of the box plot of measured average values of the $\approx$ 3,800 time series with the reconstructed values of $\approx$ 300,000 pixels and confirms that a simple spatial averaging smooths the extremes: while the highest measured rainfall mean in 1 hour is 64 mm, the highest estimated value is 54 mm. The analysis of the spatial distribution of the extreme values shows a concentration of high values in Liguria, North of Piedmont and Friuli Venezia Giulia. The reconstructed map, instead, shows a cluster of values > 50 mm only in Liguria, that incidentally shows a high density of rain gauges. In all the other regions, the rain gauges characterized by high values are sparse, and this probably justifies that the reconstructed extremes are smoothed.

The results of Figure 6.14a suggests that, where possible, it is advisable to consider the links between rainfall and elevation with a georegression approach, using the bare local sample average as a baseline and as a surrogate of more accurate estimations when regressions are not possible.

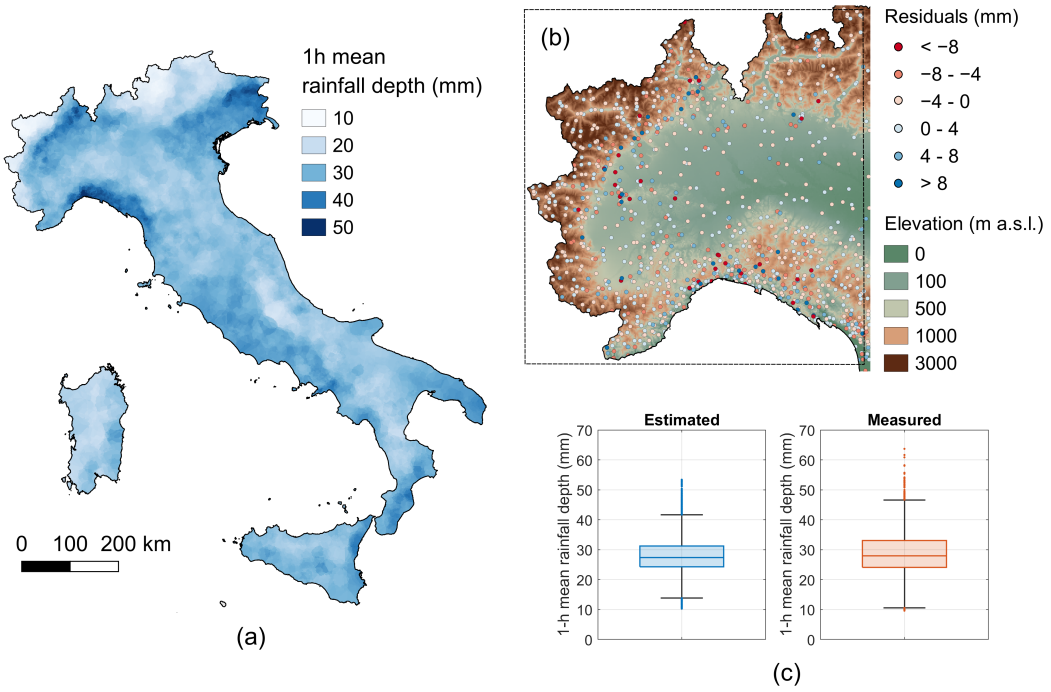

Fig. 6.14 Mean 1 h rainfall depth computed on the basis of the 5 nearest stations (a). Residuals of the 1 h model, with an indication of the elevation (b). Box plots of measured and estimated mean of 1 h values (c).

6.9.3 Effects of the Elevation Range in the Local Samples

To undertake the role of the elevation range of the sample we performed an analysis using the variable radius approach, without losing generality. For the analysis of this detail, moving from the results of Section 6.9.1, we referred to r_{min} = 15 km and r_{max} = 50 km and a minimum local sample size n = 5 to apply local regressions. We computed the precipitation gradient over elevation where possible, i.e. in the 75% of the Italian area and we checked the statistical significance and the spatial variability of the slope estimates. In terms of slope values, we noticed the presence of some consistent outliers in the box plots (see Figure 6.15). These very high values were mainly clustered in the flat areas, pointing to a data anomaly effect: we realized that an insufficient elevation range - Δz - in the data sample was the reason of obtaining anomalously high (positive and negative) rainfall local gradient. Based on the experience gained in Sections 6.2 to 6.6 and after some exploratory tests, we set the minimum Δz value to 100 m. Application of this constraint allowed us to

remove a considerable number of outliers, as shown in Figure 6.15 (lower row of each subplot).

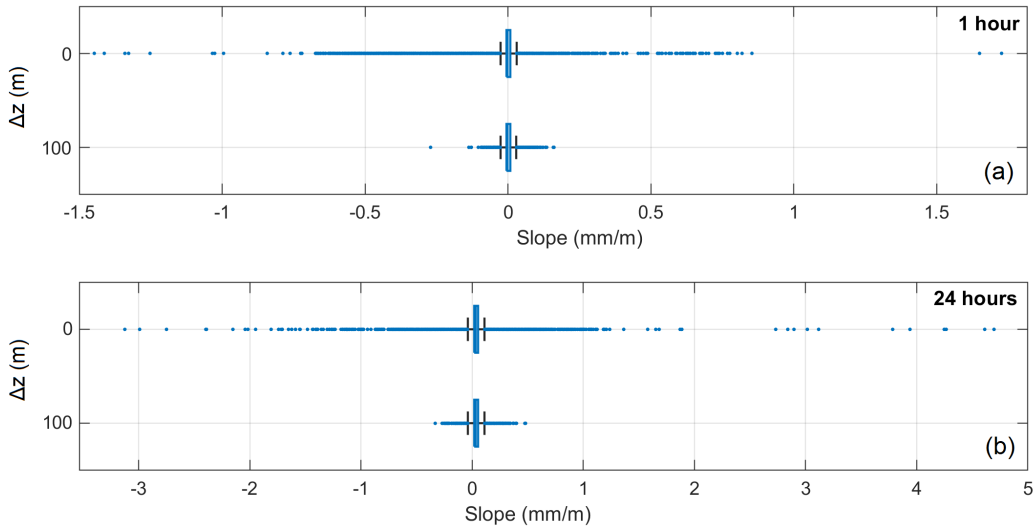

Fig. 6.15 Visual representation through box plots of the slope coefficients obtained with a regression model based on r = 15 to 50 km and Δh = 0 or 100 m in the case of 1 (a) and 24 h durations (b).

To support the assessment of the efficiency of the threshold criterion (Δz = 100 m), we tested its application comparing maps of estimated average rainfall extremes obtained without any constraint, to those built with the minimum range threshold Δz. Considering the average rainfall extremes in 24 hours, the maps in Figure 6.16 show that, when assuming no threshold, several artifacts appear (see e.g. the dark triangle in the left part of Figure 6.16c). For reference, elevation data are visible in Figure 6.16a. In that area, slopes are obtained by applying the local regression to rain gauges presenting very similar elevations (say, with a 5-10 m elevation range only). Incidentally, the mean rainfall depth presented moderate local variability (e.g., a 10 mm rainfall range). Applying, instead, the technique using the Δz = 100 m range threshold, we obtained more than reasonable improvements (Figures 6.16d and 6.16e) with removal of almost all artefacts. To verify the impact of using Δz = 100 m, among the proposed model configurations both cases with Δz = 100 m and Δz = 0 m are considered.

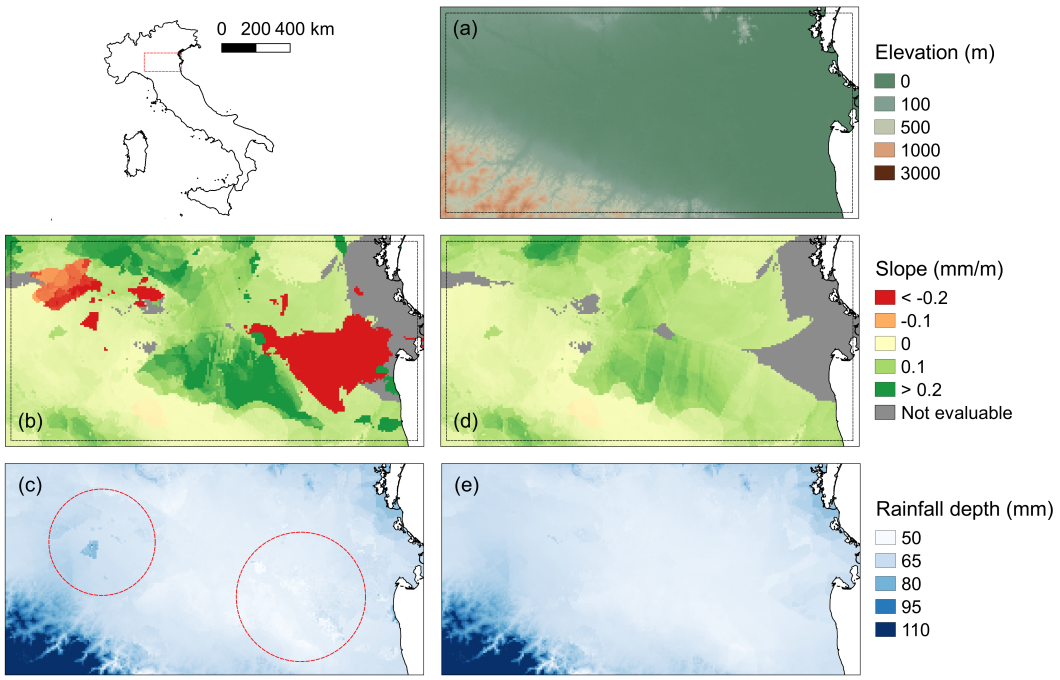

Fig. 6.16 Elevation map with the indication of the area investigated (a). 24 h mean rainfall depth estimated using radii variable from 15 to 50 km (simulation with an extrapolation of 100 m allowed and with mean rainfall depth evaluated using the 5 nearest rain gauges in uncovered cells) in the case of $\Delta z = 0$ m (c) and $\Delta z = 100$ m (e) and related slope coefficients (b and d). Red circles in (c) serve to highlight artifacts. Grey color defines areas where the local regression approach is not applicable e.g., due to the impossibility of pooling at least 5 rain gauges or to the lack of significance of the regression model.

6.9.4 Correction of Regression Application in Extrapolation

Preliminary tests made on selected mountain areas showed the importance of considering constraints in applying the regression equation well beyond the elevation ranges of the local sample, as pointed out in Section 6.8.4. Extrapolation showed to produce even negative values of rainfall estimates in areas with complex topography. After a preliminary sensitivity analysis that proved that higher values degraded the model performances, the threshold value of $e_{max} = 100$ m was selected for the alternative constraints outlined in Section 6.8.4.

To exemplify, we have reported in Figure 6.17 the estimated values of 24 h mean rainfall extremes in two mountainous areas of Italy: in Friuli Venezia Giulia (Figures 6.17a, 6.17c and 6.17e) and in Sicily, near the Etna volcano (Figures 6.17b, 6.17d and 6.17f). In Figures 6.17e and 6.17f the estimates are obtained by selecting a

maximum 100 m of extrapolation allowed. Figures 6.17c and 6.17d show the results obtained with the extrapolation allowed without limitations. Some cells with negative estimates appear in this latter case (the grid cells are highlighted in red in Figures 6.17c and 6.17d). The results in Figures 6.17e and 6.17f, obtained after correction, confirm that the extrapolation problem must be carefully handled. As mentioned in Section 6.8.4, we considered different limiting cases to tackle the problem. All three approaches to managing extrapolation presented in Section 6.8.4 are present in the model configurations examined to assess their impact.

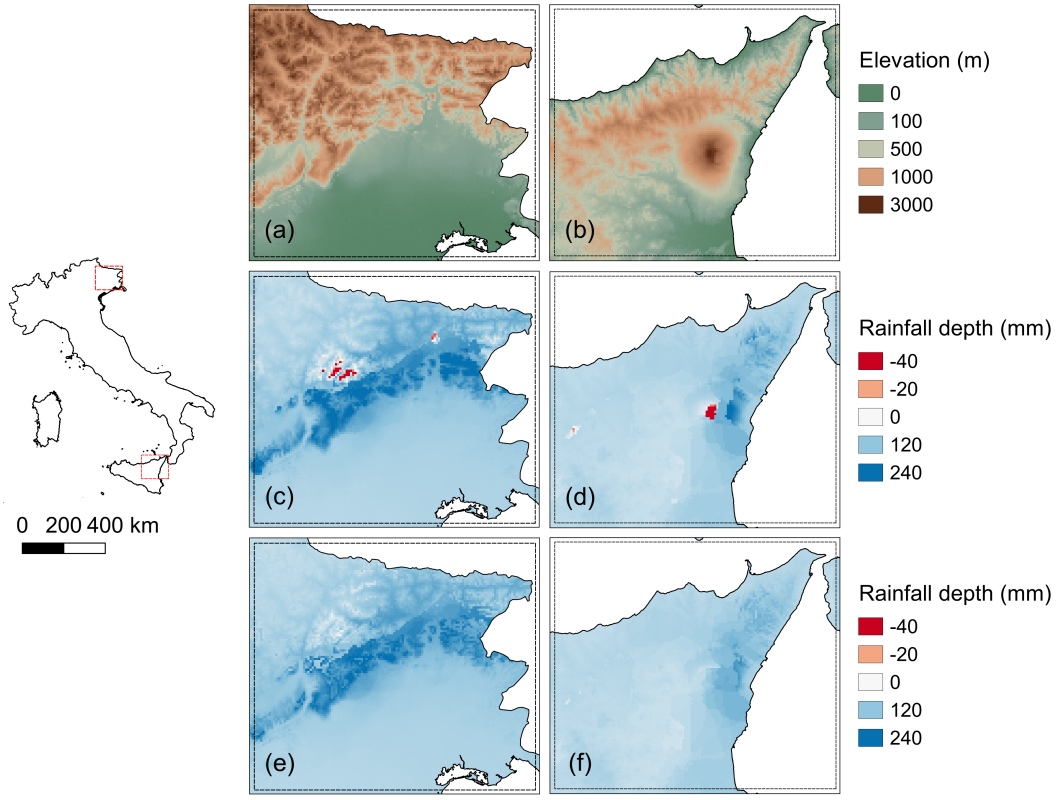

Fig. 6.17 Elevation data for Friuli Venezia Giulia (a) and Sicily (b). In (c, d) extrapolation is allowed without limits and red areas represent cells with negative estimated rainfall. In (e, f) extrapolation is limited to 100 m.

6.9.5 The Selected Model Configurations

As mentioned before, the geo-regression approach presented in this chapter, even if simple, involves the selection of different parameters, namely the number of rain gauges that forms the local sample n, the elevation difference among the rain

Table 6.7 Most relevant model configurations. Case 0 represents the case with mean values reconstructed using the 5 nearest stations, while all the other tests were performed using georegression models. The last column refers to the configuration described in Section 6.8.4: in configuration "a" extrapolation is not allowed while in "b" and "c" the extrapolation is allowed up to e_{max} (for the grid cells that would require extrapolation higher than e_{max}, in configuration "b" the predicted value is set equal to the value obtained by the model at an elevation that is e_{max} higher/lower than those of the highest/lowest rain gauge of the sample, while in configuration "c" the predicted value is computed using the 5 nearest stations).

Case	n (-)	Δz (m)	Radius configuration	r_{fix} (km)	r_{min} (km)	r_{max} (km)	e_{max} (m)	Extrapolation configuration
0	5	0	Variable	-	-	-	-	-
1	5	100	Variable (V1)	-	1	15	0	a
2	5	100	Variable (V1)	-	1	15	0	c
3	5	100	Variable (V2)	-	15	50	100	c
4	5	100	Fixed	15	-	-	100	b
5	5	100	Fixed	15	-	-	100	c
6	5	100	Fixed	20	-	-	100	c
7	5	100	Fixed	25	-	-	100	c

gauges of the local sample Δz, the area of support (r_{fix}, r_{min}, r_{max}) and the maximum extrapolation allowed e_{max}. On the basis of the analysis carried out in Section 6.9.1 to Section 6.9.4, meaningful combinations of the different parameters were applied and several techniques were jointly used to select the most valuable model. The most relevant model configurations considered in this study, in the following called "cases", are listed with their settings in Table 6.7.

As it can be seen, case 0 is the model configuration where the evaluation of the mean rainfall depth is performed using the mean values of the 5 nearest stations all over the territory. Cases 1, 2 and 3 consider the variable radius approach, but with a difference in the methodological approach if when reaching r_{max} the model pools together at least 5 rain gauges and the regression is not statistically significant: case 1 and case 2 applied the model without considering the p-value (Variable (V1)); case 3 used the mean rainfall value evaluated using the 5 nearest stations (Variable (V2)).

Cases 4, 5, 6 and 7 refer to the fixed radius approach, for two different extrapolations configurations and three radii: 15, 20 and 25 km.

6.10 The Local Regression Approach: Discussion

6.10.1 Residual Analysis and Model Selection

To evaluate the performance of the cases listed in Table 6.7, the residuals were carefully analyzed. For each case two sets of residuals were analyzed: i) the residuals obtained from a cross-validation (leave-one-out approach), that is "cross-validation configuration" and ii) the residuals obtained applying the regression on the whole data, that is "real model configuration".

As a first step, error statistical indexes were computed for each residual set: bias, mean absolute error (MAE), root mean square error (RMSE) and Nash-Sutcliffe model efficiency coefficient (NSE) (Nash and Sutcliffe (1970); Wasserman (2004)).

Results obtained for the 1 h duration are reported in Table 6.8 for the cross-validation configuration and in Table 6.9 for the real model configuration. Similarly, for the 24 h duration, the results of the cross-validation configuration are reported in Table 6.10 while the real model configuration is summarized in Table 6.11. The results shown in Tables 6.8 to 6.11 do not clearly indicate a model that is able to outperform all the others. Moreover, 1 and 24 h durations seem to perform differently. As expected, cases 3, 6 and 7 that consider a large radius do not perform well because the benefit of working with a local sample is lost. Focusing on short radii (cases 1, 2, 4 and 5), comparable performances of the models emerged. For the 1 h duration, as an example, the fixed radius case with r_{fix} = 15 km (case 5) performs slightly better in cross-validation mode (Table 6.8) but considering the performance of the real model (Table 6.9), the variable radius approach (cases 1 and 2) proved to be better, even if the improvement in terms of error statistics is limited.

For an accurate analysis of the residuals, we also analyzed the box plots of the reconstructed values for both the "real model configuration" and the "cross-validation configuration" (Figure 6.18), compared with the box plot of measured values. Figure 6.18 shows that models based on variable radii (with an upper threshold of 15 km, i.e. cases 1 and 2) proved to be able to cover almost the same measurement range of the measured values. Measured values have higher upper quartile and maximum whiskers, but the median values remain almost constant.

Table 6.8 Results of the cross-validation configurations for the 1 h duration. The values reported in bold represent the three models with better error statistics.

	Case 0	Case 1	Case 2	Case 3	Case 4	Case 5	Case 6	Case 7
BIAS (mm)	-0.110	**-0.004**	-0.021	**-0.011**	-0.019	-0.027	-0.019	**-0.011**
MAE (mm)	3.135	**3.120**	3.145	3.342	**3.113**	**3.105**	3.136	3.214
RMSE (mm)	4.151	**4.120**	4.172	4.429	**4.120**	**4.097**	4.151	4.259
NSE (-)	0.680	**0.685**	0.677	0.636	**0.685**	**0.688**	0.680	0.663
N_{RG} (-)	223	222	230	263	**221**	**214**	**216**	234

Table 6.9 Results of the real model configurations for the 1 h duration. The values reported in bold represent the three models with better error statistics.

	Case 0	Case 1	Case 2	Case 3	Case 4	Case 5	Case 6	Case 7
BIAS (mm)	-0.073	**-0.012**	**-0.024**	-0.031	-0.028	-0.028	-0.026	**-0.008**
MAE (mm)	**2.510**	**2.569**	**2.556**	2.945	2.603	2.603	2.779	2.957
RMSE (mm)	**3.351**	**3.440**	**3.433**	3.961	3.482	3.482	3.705	3.938
NSE (-)	**0.792**	**0.780**	**0.781**	0.709	0.775	0.775	0.745	0.712
N_{RG} (-)	**101**	**118**	**117**	189	122	122	151	184

Table 6.10 Results of the cross-validation configurations for the 24 h duration. The values reported in bold represent the three models with better error statistics.

	Case 0	Case 1	Case 2	Case 3	Case 4	Case 5	Case 6	Case 7
BIAS (mm)	-0.662	-0.144	-0.254	-0.255	-0.135	**-0.058**	**0.099**	**0.075**
MAE (mm)	**10.167**	**10.379**	10.512	11.042	10.450	**10.370**	10.836	11.464
RMSE (mm)	**14.873**	**15.403**	15.686	16.612	15.562	**15.404**	16.219	17.213
NSE (-)	**0.790**	**0.775**	0.767	0.738	0.771	**0.775**	0.751	0.719
N_{RG} (-)	**207**	**219**	236	275	225	**218**	250	280

Table 6.11 Results of the real model configurations for the 24 h duration. The values reported in bold represent the three models with better error statistics.

	Case 0	Case 1	Case 2	Case 3	Case 4	Case 5	Case 6	Case 7
BIAS (mm)	-0.475	-0.259	-0.214	-0.372	**-0.140**	**-0.140**	**-0.012**	**0.095**
MAE (mm)	**8.143**	**8.472**	**8.346**	9.643	8.684	8.684	9.637	10.607
RMSE (mm)	**12.024**	**12.759**	**12.528**	14.807	13.103	13.103	14.606	16.078
NSE (-)	**0.863**	**0.846**	**0.851**	0.792	0.837	0.837	0.798	0.755
N_{RG} (-)	**116**	**138**	**129**	193	142	142	192	240

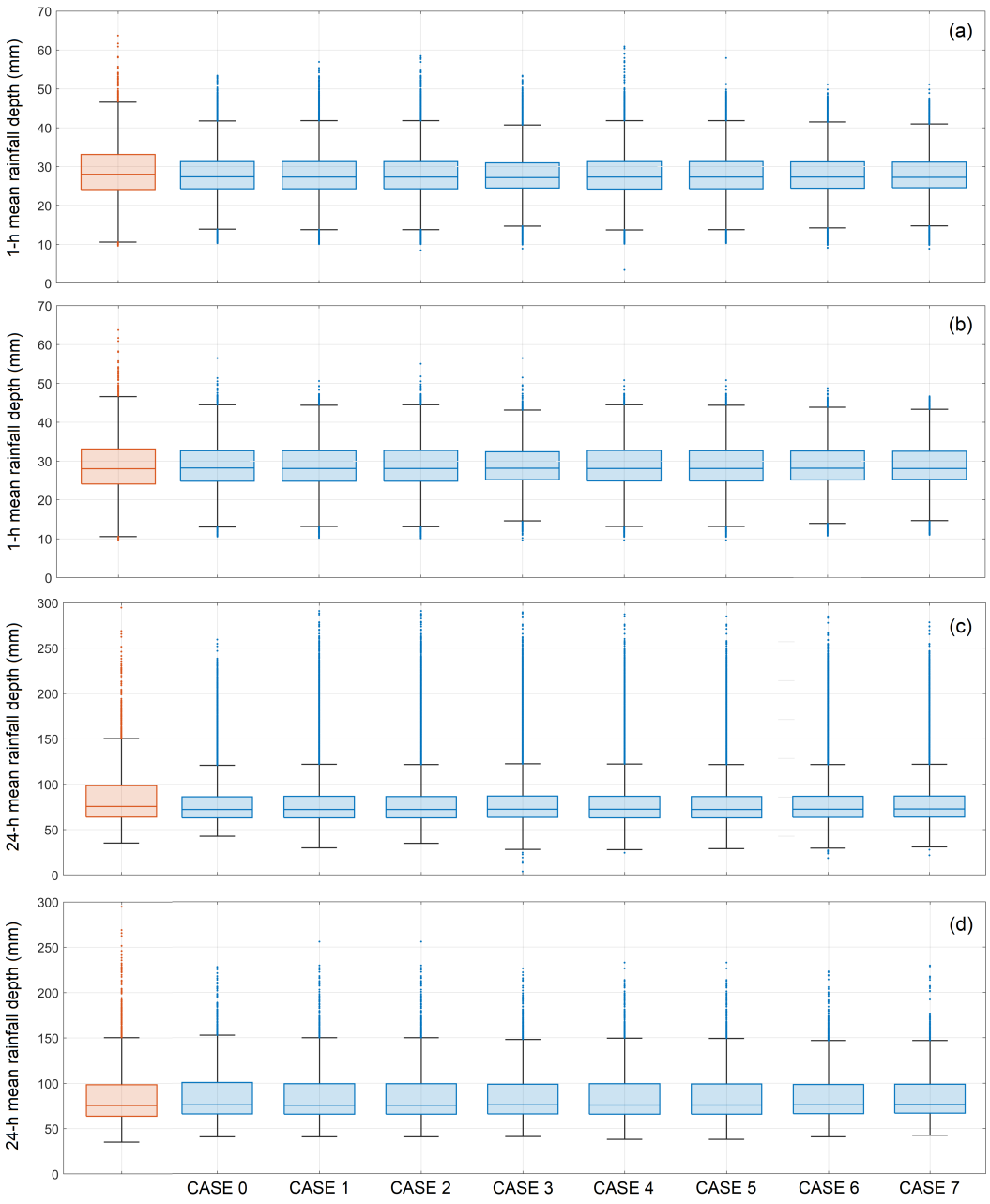

Fig. 6.18 Box plots of the real model configurations for the 1 (a) and 24 h (c) durations and box plots of the cross-validation configurations for the 1 (b) and 24 h (d) durations. The orange box plots refer to the measured values, while the blue box plots refer to the estimated value.

Thornton et al. (2021) pointed out that unrealistically high estimated rainfall values can be obtained using a local-regression approach. In their approach, if the estimated rainfall depth is more than twice the highest measured rainfall depth,

this anomalous value is reduced to twice the maximum measured rainfall depth. By applying constraints on the search radius and on the extrapolation, we never encountered this problem, independently on the duration that we considered.

A close inspection of the residuals and their spatial aggregation was also performed. The analysis of the spatial distribution of the residuals confirms what was outlined in Section 6.8.3: for the variable radius configuration, by increasing both r_{min} and r_{max} the benefit of using a local regression approach decreases. Case 3, with r_{min} = 15 km and r_{max} = 50 km, presents larger clusters, and significant residuals with opposite signs lying at close distances. By comparing the data density map (Figure 6.13) with the maps of the cross-validation residuals (not reported here for brevity) it emerges that the largest errors are in areas with complex topography. This fact suggests that, even with a high data density, some local behaviors were not correctly represented and managed when too large area were considered in the regression model. The higher spatial homogeneity of residuals in the case of smaller variable radii or fixed radius suggests that these models should be preferable. As an example, Figure 6.19 shows the residuals of the 1 h duration model (case 1).

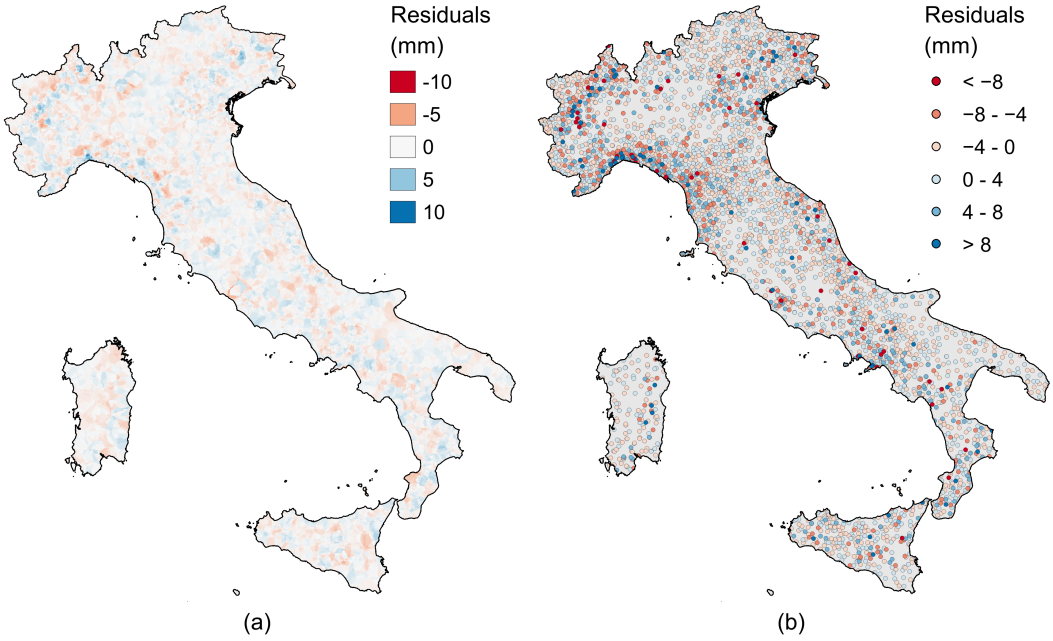

Fig. 6.19 Residuals of case 1, for duration = 1 h. Panel (a) shows the spatial interpolation of the residuals visible in (b) obtained by applying an ordinary kriging. By comparing (a) and (b) with Figures 6.3a, 6.5a and 6.5b, the improvements in terms of spatial modelling clearly emerge when moving from a national/sub-national to a local approach.

To have a complete picture of the model configurations of Table 6.7, we focused also on the estimation of the extreme values, following what emerged in Section 6.9.2. As an example, Figure 6.20a shows the location of the rain gauges with a 1 h mean rainfall depth of at least 50 mm while Figure 6.20(b to e) shows the location of the estimated values for case 0, case 1, case 2 and case 5. As it can be seen in Figure 6.20b a simple computation of the mean rainfall depth performed by using the 5 nearest rain gauges (case 0), even if providing good error metrics, cannot reconstruct the extremes in the northern part of the area. Conversely, a model based on a georegression, as cases 1 and 2, provides additional information, even if the area where we expect to reach high rainfall depths shows some underestimated values (Figures 6.20c and 6.20d). Model 5, despite good performance, is not able to reconstruct the extremes and, in addition, it overestimates the extremes in the North-East of the area (Figure 6.20e).

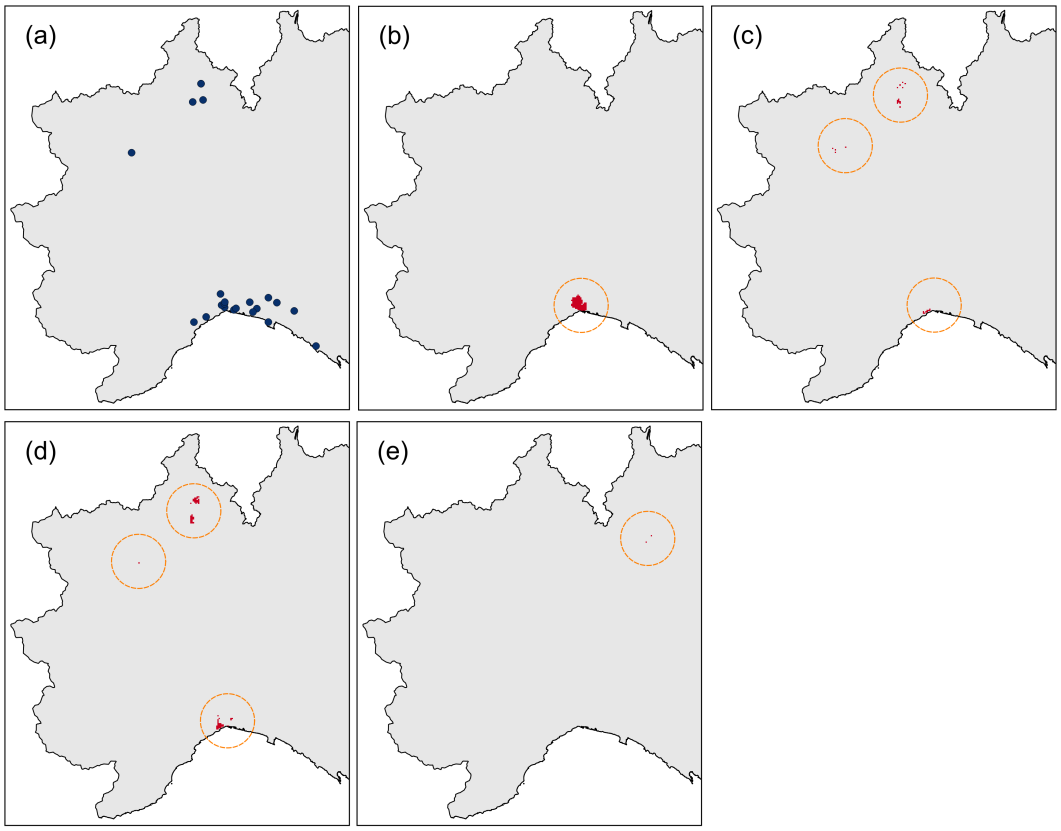

Fig. 6.20 Spatial distribution of the rain gauges with 1 h mean rainfall depth higher than 50 mm (a). Location of the estimated values higher than 50 mm for case 0 (b), case 1 (c), case 2 (d) and case 5 (e).

By integrating all the above features, we suggest that the model configuration of case 1 represents the best compromise and can be taken as the optimal model for all the durations.

6.10.2 Orographic Gradients and Rainfall Maps

For the best model configuration considered in Section 6.10.1 (case 1), it can be worth examining the spatial variability of the slope coefficients emerged by the regression models. These have been mapped in Figure 6.21 and represent an answer to the scientific question regarding the sign and the stability of the orographic effect on extreme rainfall.

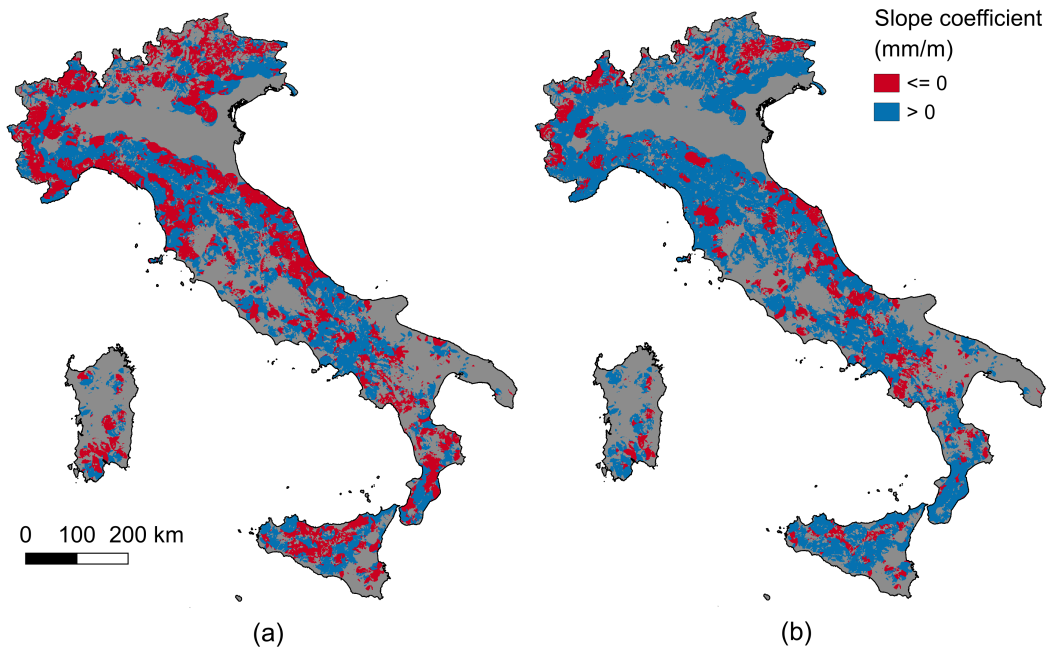

Fig. 6.21 Slope coefficients of the regression models for the 1 h (a) and 24 h (b) duration in the case of r = 1 to 15 km.

As introduced in the first part of this chapter, the orographic effect (rainfall gradient with elevation) appears to vary greatly with the duration of the extreme rainfall in Italy. In Figure 6.21a we show the gradient for the 1 h duration average rainfall extremes. The grey color is used for the areas where the regression model cannot be applied due to low data density or extrapolation constraints. Over most of the Alps, Liguria region and portions of the Apennines, a general decrease of the 1 h

mean rainfall depth with increasing elevation emerges (confirming thus the "reverse orographic effect" mentioned in Allamano et al. (2009), in Avanzi et al. (2015), in Formetta et al. (2022), and in Mazzoglio et al. (2022a)), while over most of the hills, pre-hills and flat areas, the mean rainfall depth increases with the elevation.

Figures 6.21b shows the slope coefficients for the 24 h duration, for the same model configurations. The maps confirm a general increase of the 24 h mean rainfall depth with increasing elevation over Italy, except for some hill/mountainous areas.

The optimal model configuration, case 1, is used to evaluate the mean rainfall depth of rainfall extremes over Italy, as reported in Figure 6.22. For short durations (e.g. for the 1 h interval, depicted in Figure 6.22a) the Northern areas of Aosta Valley and Bolzano province showed rainfall extremes smaller than in Southern Italy. For longer durations (e.g., for the 24 h interval, Figure 6.22e), these areas are affected by a mean rainfall depth comparable with the one recorded in Sicily and Sardinia Islands, in the Po Valley and in the Southern Apennines. The wetter areas are located in Friuli Venezia Giulia, in Liguria, in the northern areas of Piedmont and in Calabria. It is interesting to notice that the 1 and 24 h durations have different characteristics: as the duration increases, the highest values appears to be clustered in space and focused over limited areas.

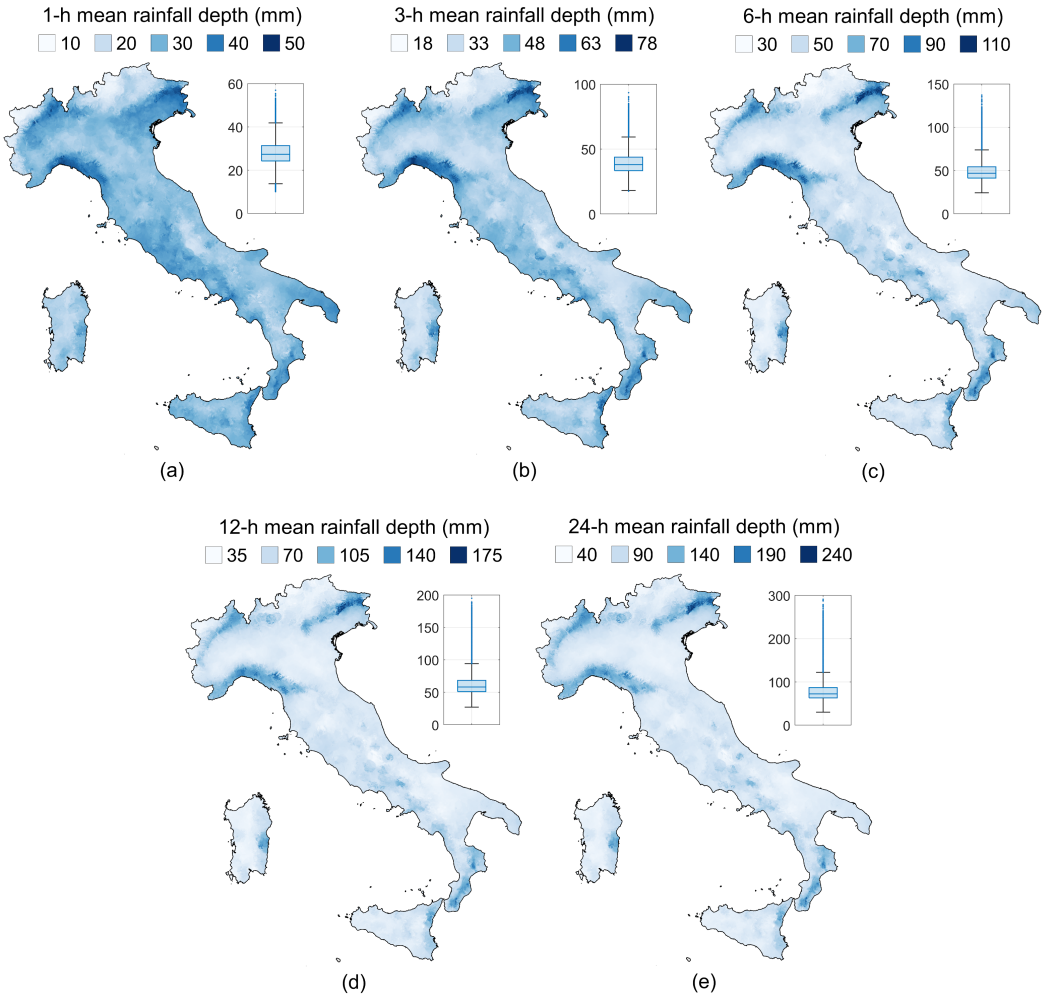

Fig. 6.22 Mean rainfall depth for 1 (a), 3 (b), 6 (c), 12 (d) and 24 (e) h intervals and related box plots.

6.11 Conclusions

In this chapter, the role of orography and morphology in short-duration annual maximum rainfall depths have been analyzed, taking advantage of a new and comprehensive database for Italy, I^2-RED (Mazzoglio et al. (2020)). The approach finds its relevance in the first use of the most complete and updated data collection of short-duration annual maxima available for the whole Italian territory. With respect to the previous knowledge on the topic, the analyses allowed us to better understand, confirm and extend previous results from the literature.

The results described here show that a national-scale simple regression model of precipitation vs elevation presents some weaknesses (high residual values, high local- and national-scale bias, and low NSE coefficient, etc.) and therefore needs to be improved.

The use of multiple regression models introduces some benefits, such as a reduction of MAE and RMSE at the national scale; nevertheless they were not successful in reducing the local bias.

Considering the necessity of working on smaller domains, several geomorphological classifications which are able to preserve the intrinsic value of the statistically significant landscape variables that emerge in regression models were analyzed. Four different geomorphological classifications available in literature were used to provide criteria for the identification of homogeneous zones. Simple linear regression models were applied over these homogeneous domains and the performances were compared at both a national and a zonal level. Among all the considered classifications, the selection of rain gauges for the model application was found to be more effective in the case of GC4 (Alvioli et al. (2020)), which embeds hydrographic information.

The best approach was selected by evaluating the error statistics for the bias at both a national and a zonal scale and at a national scale for MAE, RMSE and NSE. The obtained results have shown that using simple linear regression applied to the GC4 model produces better results than all the others, in the zones in which the GC4 model is statistically significant, in terms of bias. As far as national statistics are concerned, considering the mean rainfall depths in the gray zones in Figure 6.10b does not significantly affect the performance of GC4, in terms of MAE, RMSE and NSE, in particular for the 1 h duration. In short, it was propose using the GC4 model where possible and adopting the (spatial) mean value of the rainfall depths in case of a nonstatistically significant relationship.

The first part of this work has led to the following conclusions. The relationship between precipitation and elevation is not meaningful in all the areas in Italy, as already pointed out by Caracciolo et al. (2012) for the island of Sicily. In this chapter, this concept has systematically been extended to the whole country, and significant relationships have only been obtained for 45% of the area for $\overline{h}_1$ and 49% for $\overline{h}_{24}$. As far as the model that we suggest using is concerned, that is GC4, we are aware that improvements are possible, considering that no significant regressions were found over 55% ($\overline{h}_1$) and 51% ($\overline{h}_{24}$) of the territory. However, it should be pointed out that

the rainfall station density is not sufficient for the application of the method proposed here over 9% of the territory.

Then, a local approach was used. The proposed method optimizes the selection of the local sample based on the station density and allows to highlight the presence of several areas with negative orographic gradients in Italy. Moreover, the results show that a simple local regression approach that considers the elevation can be successfully applied to the mean values of the short-duration annual maximum rainfall depths. Different radii were used to select the local sample to be used in the regression model. Both the case of variable and fixed radius was considered. The optimal model configuration was selected by analyzing the regression residuals through cross-validations, visual inspection of their spatial distributions, and comparative analysis of their box plots. With regard to Italy, the results presented in Section 6.10 suggest that the estimation of the mean rainfall depth using a local regression calibrated for a limited spatial extent (circle with radius of 15 km at maximum) represents the best solution that preserves the local feature of the regressions and takes into account the different data densities over the entire country.

In the development of the regression model particular attention was paid to the presence of artifacts due mainly to a non-consistent rainfall gradient or to extrapolation issues. This work showed that the extrapolation must be carefully handled to avoid artifacts and, most importantly, negative values of the estimated mean rainfall depths. The presence of estimated rainfall depth with negative values is a widely-known problem. In the Daymet model (Thornton et al. (2021)) cell with negative values are truncated to zero. In our work, we preferred to investigate the causes that lead to anomalous values, being a null mean rainfall depth an unsuitable solution when dealing with annual maxima. In this work, negative gradients are not considered errors and are not equaled to zero, but their values are effectively controlled through appropriate constraints on data elevation range. By using a simple but effective constraint, we were able to mitigate extrapolation problems. This approach represents a step forward compared to previous studies on this topic, where these drawbacks are highlighted but no solutions are suggested. The results obtained with the cross-validation suggest that the extrapolation must not be allowed.

The maps and the methodological results presented in this work, regarding also orographic gradients, will help to investigate the different morphological/climatological

characteristics that lead to such variations and will support frequency analyses directed to estimate high return period rainfall quantiles.

Chapter 7

Geographically-based Analysis of Rainfall Quantiles

The work described in this chapter has been partially derived from Claps et al. (2022b), Mazzoglio et al. (2022b) and Mazzoglio et al. (2022d). Part of the results contained in this chapter will be submitted to a scientific journal in the upcoming months.

7.1 Background

As mentioned in Chapter 2, regionless methods based on interpolation and geostatistical techniques have recently been widely used to improve the rainfall regional frequency analysis. The main advantages come from the possibility of collecting information displaced over the entire region without the need to delineate regions and, thus, overcoming possible inconsistencies in areas located near the borders of each region. Moreover, geostatistical techniques allow the reconstruction of spatial information. This interesting feature solves the widely-known problems induced by missing data, fragmentation of the time series, non-uniform densities, and station relocation (Libertino et al. (2018b); Mazzoglio et al. (2020)).

Two different approaches can be used to overcome the data fragmentation problem: (a) a precautionary approach based on the exclusion of all the time series shorter than a specific length (usually 30 years) to obtain at-site parameters that will be, in

a second step, spatially interpolated; and (b) a conservative approach that tries to extract all the available information, even those included in short and fragmented time series. The first approach, even if it allows a more robust parameter estimation, can ignore important information hidden in short series and, thus, can lead to underestimating the risk associated with extreme events (mainly when long return periods are investigated) and must be appropriately managed. Instead, the second approach requires robust assumptions in the spatial model used for the reconstruction to obtain reliable estimates.

Independently from the approach, moving from a regional to a national application requires a step-by-step analysis of all the main drawbacks that could be encountered during the application. This chapter aims to investigate possible problems that may arise when increasing the area of interest, trying to solve them with the results obtained in the previous parts of this dissertation.

In this chapter, the focus is the patched kriging methodology, a regional frequency analysis approach developed to bypass some of these shortcomings, originally applied over Piedmont region (Claps et al. (2015); Libertino (2017); Libertino et al. (2018a)). The methodology will be briefly described here, but the reader is referred to Claps et al. (2015), Libertino (2017) and Libertino et al. (2018a) for a complete description of the original method. In the final part of the chapter, a comparison with the Regional Ombrian Model proposed by Iliopoulou et al. (2022) is performed.

7.2 The Patched Kriging Methodology

The patched kriging technique can be used to deal with a rainfall frequency analysis of annual maxima. According to the "index flood approach" (see Chapter 2 for more information), then extended also to rainfall, the rainfall quantile $h_{d,T}$ related to duration d and return period T can be evaluated by multiplying the index variable h_d (that, in most of the cases, is computed as the mean of the annual maxima of duration d) with a dimensionless frequency quantile $K_{d,T}$ also named as “growth factor” (see Equation 2.1). In that equation, both h_d and $K_{d,T}$ are computed from the rainfall measurements. The patched kriging has been developed to take advantage of all he available records for the computation of both h_d and $K_{d,T}$. It treats the various duration separately and consists of a year-by-year application of the ordinary kriging equations to all the available measurements. The application of the ordinary

kriging requires the verification of the second-order stationarity: this means that the covariance between two data points depends only on the distance and not on their location. Thus, the possible presence of trends is investigated. In the first application over Piedmont, the influence of elevation on rainfall extremes clearly emerged. Thus, a regional detrending with elevation was performed using the equation

$$h_d = m \cdot ln(z+1) + m_0 + \varepsilon_d \tag{7.1}$$

where m is the slope of the regression model, m_0 is the intercept and ε_d is the residual of the regression. The logarithm of the elevation z was here considered to limit the weight of the stations placed at a lower altitude. The model is built by considering all the measurements performed in all the years (i.e., it is based on the assumption that the precipitation vs elevation relationship is invariant over time). The trend significance is evaluated using the Student's t-test (significance level α = 0.05). The analysis of the relationship between rainfall depth and elevation also compensates and recovers the lack of information at the small scale, especially in data-scarce locations.

The de-trended values are then used to compute yearly variograms, which are weighted on the number of active rain gauges in each year to obtain a global sample variogram for each duration. The sample variogram is approximated using a theoretical variogram (an exponential one, in the case of Piedmont). The ordinary kriging is applied by using the 10 nearest stations for the estimation in each pixel. The latter value has been obtained after some preliminary tests and corresponds to the number that prevents the flattering of the estimates at a value almost equal to the global mean. Finally, the de-trended component is added.

The result is a "rainfall data cube", with a number of layers equal to the number of investigated years. Each pixel corresponds to a complete annual maxima time series of measured and estimated values. The kriging procedure also provides a "variance data cube", i.e., a pixel-by-pixel measurement of the estimate uncertainty. By coring the cubes along the time axis is thus possible to obtain n time series (with n equal to the number of grid cells investigated) with the associated uncertainty. The workflow described here is summarized in Figure 7.1.

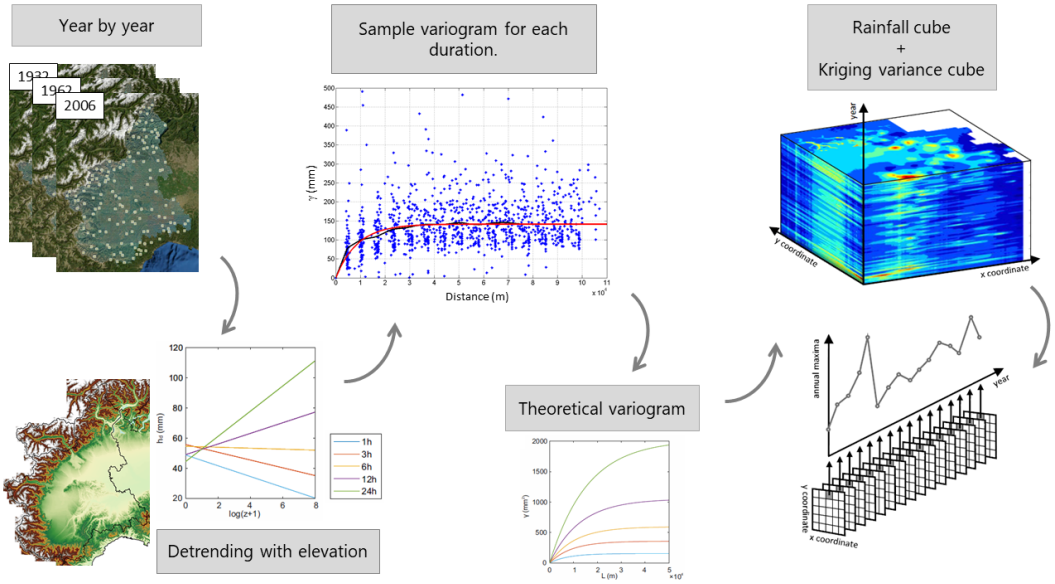

Fig. 7.1 The first steps of the patched kriging workflow. Source: Claps et al. (2022b). Copyright holder: Elsevier.

The main advantage of the patched kriging is the possibility of working with all the annual maxima, independently from the length of the time series they belong to, avoiding the need to discard the shortest one. The possibility of using all the available information is an essential requirement when dealing with large return periods.

The patched kriging technique merges the locally observed and interpolated values, which can have different statistical distributions. A weighted procedure was introduced to evaluate the sample L-moments of the reconstructed series to preserve the statistics of the original time series. This correction uses the kriging variance of each year to weight each contribution of each annual maxima in the estimation of the sample L-moments. The correction is based on the assumption that the kriging variance can be considered a measure of the estimation uncertainty because: (a) it is higher in cells far from the gauged grid cells, and (b) it increases when the number of data around the grid cell decreases. Thus, higher weights are assigned to measured values or years with a high number of available data. This correction allows us to preserve the spatial correlation of higher-order L-moments. More in detail, the weight

$$w_i = \frac{\sigma_{max}^2}{\sigma_i^2} \tag{7.2}$$

is assigned to the i-th value of the time series. In Equation 7.2, σ_i^2 is the kriging variance of the series and $\sigma_{max}^2 = max(\sigma_i^2)$.

When a rain gauge is installed in a previously ungauged grid cell, the kriging variance is expected to decrease drastically. This variation gives all the previous kriged values a weight almost equal to zero. Considering that L-moments computed on short time series are expected to lack reliability, this variation should be avoided because it would undermine the benefit of the patched kriging (i.e., the reconstruction of time series based on nearby measurements). Thus, a threshold w_{max} was set. If $w_i > w_{max}$, the value $w_i = w_{max}$ is considered. In the Piedmont case study, a w_{max} = 10 was defined after a sensitivity analysis aimed at assigning a larger weight to the measured values without completely discarding the contribution of the reconstructed values.

As mentioned before, the patched kriging merges observed and interpolated values, which can have different statistical distributions. This operation can potentially introduce bias and reduce the variability of the estimates and thus leads to a possible underestimation of the design rainfall. To correct this behaviour, a bias-correction procedure is applied to increase the variance of the cored series and to preserve the statistics of the original time series. The entire procedure is applied separately for each duration under investigation. This last step completes the process, making this method a complete RFA approach.

Suppose a situation when a series $x_i(t)$ is obtained with the patched kriging. The series has a temporal average equal to $\bar{x}_i$ and all the $x_i(t)$ values are thus underdispersed around $\bar{x}_i$. A simple approach that can be used to avoid underdispersion consists in inflating the distance from the mean through a multiplicative factor K_0 by using

$$\hat{x}_i(t) - \bar{x}_i = K_0 \cdot (x_i(t) - \overline{x_i}) \tag{7.3}$$

with $K_0 > 1$. Unfortunately, Equation 7.3 can produce not acceptable negative rainfall depths. To avoid this drawback, the logarithm of the variable is introduced in Equation 7.3, leading to

$$K = \frac{ln(\hat{x}_i(t)) - ln(\bar{x}_i)}{ln(x_i(t)) - ln(\overline{x_i})} \tag{7.4}$$

The attenuation of the variability is tackled by exploiting the wide availability of spatial information to develop a correction factor for each cell and each year of the domain. The spatial variability of the bias proved to be influenced by the distance of

the target grid cell from the closer gauged grid cells. As the distance between the target cell and the gauged grid cells decreases, the correction required by the grid cell becomes less relevant. It was therefore expected to have a correction factor K that is an increasing function of the distance from the gauged cells, following the equation

$$K = f(D_s) \tag{7.5}$$

where D_s is the distance and $f(D_s = 0) = 1$.

Due to the high annual variability of the network, which sees considerable variations in the number of active rain gauges, each grid cell is considered independently in each year. In addition, all the grid cells with a similar distance to the nearest gauged grid cells are supposed to have similar behaviour and thus are considered as belonging to the same sub-sample. The variance of the set of measurements is considered as the reference value for the calibration of the correction factor. To do so, several distance classes are computed, and each class's variance is corrected to be coherent with the reference value.

From an operational point of view, a D_s value is assigned to each cell for each year. D_s represents the inverse average distance of the target grid cell from the 10 nearest gauged grid cells and can be evaluated as

$$D_s = \frac{1}{\frac{1}{10} \cdot \sum_{j=1}^{10} (\frac{1}{\delta_j})} \tag{7.6}$$

with δ_j the number of cells that separate the target cell from the j-th closest gauged cell. In Equation 7.6 an inverse average distance is considered for the attribution of a D_s value almost equal to zero to the gauged grid cells that do not necessitate corrections (i.e., grid cells with measured values).

With the aim of estimating the dependence of K on D_s, the average of Equation 7.4 conditioned on D_s is considered. On the right side of Equation 7.4, the numerator is a variable that does not depend on D_s by definition. The average can therefore be written as

$$\frac{\Delta(D_s)}{a_0} = E\left[\frac{1}{ln(x_i(t)) - ln(\overline{x_i})}|_{D_s}\right] = f(D_s) \tag{7.7}$$

For each equally consistent D_s class, the value $\Delta(D_s)$ is evaluated, considering all the grid cells that belong to each class. The computation is performed for each year and each duration.

The $(\Delta(D_s), D_s)$ pairs evaluated for all the years are pooled together to compute the median value of each D_s class. For each duration, a correction function $K(D_s, d)$ is computed by interpolation (with a linear equation) of the previously computed median values with the aim of reducing the ratio between the variance of the measured data and the estimated ones for each D_s class. The so-computed correction factor $K(D_s, d)$ increases as the distance from the gauged grid cells increases, and then loses relevance. The coefficient can be therefore approximated with

$$K(D_s, d) = \begin{cases} 1 + \beta(d) \cdot D_s & D_s \leq l \\ 1 + \beta(d) \cdot l & D_s > l \end{cases} \tag{7.8}$$

For $D_s > l$ the behaviour appears to be less consistent. In the application over Piedmont, an l value equal to 25 km was used.

Once the correction factor is applied, each observation $\dot{x}_i(t)$ of the i cell for the generic year t is set using

$$\hat{x}_i(t) = \bar{x}_i \left(\frac{x_i(t)}{\bar{x}_i} \right)^K \tag{7.9}$$

where $\hat{x}_i(t)$ is the corrected value, $x_i(t)$ is the original value, $\bar{x}_i$ is the mean of the cored series and $K(D_s, d)$ is the correction factor. Equation 7.9 is in the form of a power law in order to avoid the estimation of negative rainfall depths.

The bias-corrected rainfall data cube can now be used to finalize the rainfall regional frequency analysis. The first step consists of the computation of the IDF curves. To evaluate the design rainfall for a set of different return periods and durations, a probability distribution that fits the data has to be identified. In the application over Piedmont, the L-moment ratio diagram suggested that the Gumbel is a good candidate for the representation of the extremes at the regional scale, even if the centroid of the cloud of points appears to be slightly shifted towards larger τ_3 values. Only in the case of series with larger skewness, a GEV distribution was suggested as the preferred one. Over Piedmont, a clear pattern (and a physical explanation) of grid cells where the GEV has to be preferred to the Gumbel can not be identified due to the different weather systems that produce the extremes (shorter duration annual maxima are usually extracted from convective events, while

longer durations are typically associated with stratiform events) and by the complex topography, that can influence the storm generation. In addition, boundary effects in the Northern part of the region can affect the results obtained at the edges.

7.3 Application of the Patched Kriging Methodology: Sensitivity Issues Over Piedmont, Aosta Valley and Liguria

7.3.1 Introduction

One of the main drawbacks of this approach is linked to the detrending procedure. In the Piedmont case study, a single regional detrending was performed by pooling together, for each duration, all the annual rainfall depth – elevation pairs. This approach can be reasonably applied over a small region such as the Piedmont one. However, a regional detrending can lose its applicability when larger areas are investigated, as highlighted in Chapter 6. In this case, a local-scale detrending could be a more appropriate approach.

The other major limitation of this methodology, already highlighted in Libertino (2017), is linked to the accuracy of the spatial reconstruction of the extent of the rainfall events. The actual spatial distribution of the rainfall pattern is not known because the only available information is located in correspondence of the rain gauges. The patched kriging tries to address this issue by using nearby information and ancillary variable (such as the elevation in the Piedmont case study) to reconstruct the phenomena. However, there is no evidence that a correct output is provided. To solve this problem, additional information can be retrieved from, as an example, weather radar data. This latter problem will not be addressed in this dissertation. However, weather radar data will be used to perform a spatial check of the extent of a severe rainfall event occorred in Liguria during 2021 and a comparison of the reconstructed 2021 annual maxima.

7.3.2 Application

To investigate the potentiality of the patched kriging over a larger area, the North-West of Italy (Aosta Valley, Piedmont and Liguria) was selected as a case study. This area can provide interesting insights into the pros and cons of the current methodology due to the complex morphology, climate and non-uniform rain gauge density. Moreover, Liguria was affected by the most severe rainfall events recorded in Italy since early '900 (i.e., since we have systematic rainfall monitoring performed with rain gauges). The last one, recorded in 2021, broke most of the all-time Italian records, by exceeding the previous 3, 6 and 12 h annual maximum records (Figure 7.2).

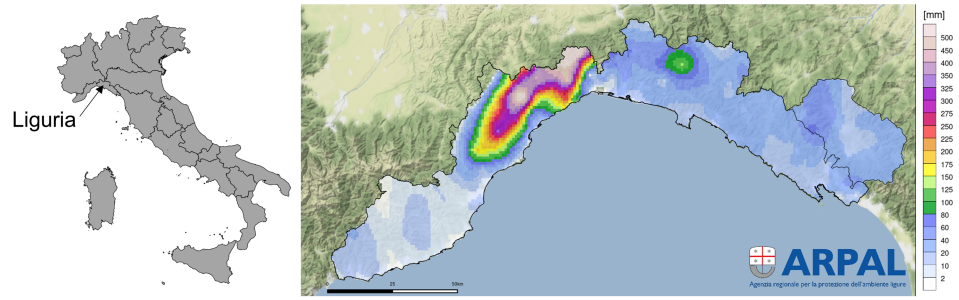

ALL-TIME ITALIAN RECORDS									
1 HOUR		3 HOURS		6 HOURS		12 HOURS		24 HOURS	
h (mm)	YEAR	h (mm)	YEAR	h (mm)	YEAR	h (mm)	YEAR	h (mm)	YEAR
181	2011 Vicomorasso	377.8	**2021** Urbe (Vara Sup.)	496	**2021** Montenotte Inf.	740.6	**2021** Rossiglione	948.4	1970 Genova Bolzaneto
178.2	**2021** Urbe (Vara Sup.)	363.6	2008 Capoterra	472	2011 Brugnato	717.8	1970 Genova Bolzaneto	932.6	1970 Valleregia
175.4	1996 Pomezzana	360.1	1959 Giffone	458.6	1954 Salerno	630	1970 Valleregia	883.8	**2021** Rossiglione
170.1	1964 San Luca	336.6	2011 Vicomorasso	446.4	1970 Genova Bolzaneto	563	**2021** Montenotte Inf.	749.2	1970 Genova Pontedecimo
162.1	1966 Stilo	328.4	2011 Brugnato	444.1	1959 Giffone	534.4	1935 Lavagnina	732	1970 Monte Cappellino

Fig. 7.2 Influence of the 2021 heavy rainfall events. Top: accumulated 24 h rainfall depths recorded by rain gauges until the 5th of October 2021 at 2 a.m. interpolated with a geostatistical method. Source: https://www.arpal.liguria.it/contenuti_statici/pubblicazioni/rapporti_eventi/2021/REM_20211002-05-rossaBD_vers20220203.pdf. Bottom: table containing the all-time Italian records (the 2021 records are reported in red). Source: Improved - Italian Rainfall Extreme Dataset (Mazzoglio et al. (2020)).

It was then decided to perform a new rainfall frequency analysis over this larger area by applying the patched kriging in four different configurations, using:

- the data of the entire NW Italy acquired from 1931 until 2020 within the original patched kriging workflow (configuration n°1);
- the data of the entire NW Italy acquired from 1931 until 2021 within the original patched kriging workflow (configuration n°2);
- the data of Liguria region acquired from 1931 until 2021 in an improved version of the patched kriging, that accounts for a regional detrending procedure (configuration n°3).
- the data of Liguria region acquired from 1931 until 2021 in a further improved version of the patched kriging, that accounts for a local detrending procedure (configuration n°4).

By comparing the results obtained only over the Liguria region with the first two configurations it is possible to investigate the influence of the 2021 records in the overall rainfall frequency analysis using the old methodology, while the comparison of the latter three will highlight the differences encountered when working with a smaller data sample, especially in terms of precipitation vs elevation relationship.

The new analysis is conducted using a 1 km grid size, despite in the original application developed by Libertino et al. (2018a) a 250 m resolution was selected. This choice was made on the basis of the results obtained in Chapter 6, following what has also been suggested by Daly et al. (1994) in terms of the representation of rainfall depth vs elevation with different spatial resolutions.

In the original application over Piedmont performed by Libertino et al. (2018a), the regional detrending described by Equation 7.1 was characterized by a statistically significant negative slope (m) for 1 and 3 h durations and by a positive slope for 12 and 24 h durations (Table 7.1). For the duration of 6 hours, no detrending was performed because of the lack of significance of the slope coefficient. In the new analysis, statistically-significant negative values for 1 to 12 h durations emerged from configurations n°1 and 2, while a statistically significant positive slope emerged for the 24 h duration (Table 7.1). This general behaviour completely changed when analyzing a smaller area as Liguria using only the data of its territory (configuration n°3): in this case, a statistically significant positive slope appeared for 3 until 24 h durations, while the 1 h duration lacks the significance of the hypothesis that m is different from 0 (Table 7.1). In configuration n°4, instead, the slope coefficient

Table 7.1 Slope m of the regression models used in the four configurations (* indicates a statistically significant trend at a 5% level).

Duration	Libertino et al. (2018a)	Conf. 1	Conf. 2	Conf. 3	Conf. 4
1 hour	-3.56*	-3.02*	-3.03*	0.10	Variable
3 hours	-2.57*	-3.54*	-3.53*	1.47*	Variable
6 hours	-0.32	-2.81*	-2.81*	3.38*	Variable
12 hours	3.52*	-0.85*	-0.85*	6.05*	Variable
24 hours	8.34*	2.52*	2.51*	9.96	Variable

varies from pixel to pixel, according to the methodology described in Sections 6.8 to 6.10 of Chapter 6. Modest differences between the configurations n°2, 3 and 4 are therefore expected to emerge in the following part of this section.

The following step of the patched kriging workflow, i.e. the bias correction, was performed in all the four configurations with D_s values until 15 km (see Equations 7.5 and 7.6 as a reference). Figure 7.3 shows the L-moment ratio diagrams obtained considering all the durations before (a) and after (b) the bias-correction for configuration n°2 (entire NW of Italy). Similarly, Figure 7.3(c, d) shows the same parameters for configuration n°3 (Liguria region, regional detrending) and (e) and (f) show the same parameters for configuration n°4 (Liguria region, local-scale detrending). Configuration n°1 is here not reported for brevity (results similar to configuration n°2 were obtained). In this figure it is possible to observe the variability of the coefficient of L-variation τ, defined as

$$\tau = L_{CV} = \frac{L_2}{L_1} \tag{7.10}$$

of the coefficient of L-skewness τ_3, defined as

$$\tau_3 = L_{CA} = \frac{L_3}{L_2} \tag{7.11}$$

and of the coefficient of L-kurtosis τ_4, defined as

$$\tau_4 = L_{KUR} = \frac{L_4}{L_2} \tag{7.12}$$

The distance between the centroid of the cloud of estimated values and the centroid of the cloud of measured values can be used as an indicator of the overall bias. The overlap of the two centroids after the bias-correction procedure suggests the effectiveness of the procedure from a visual point of view.

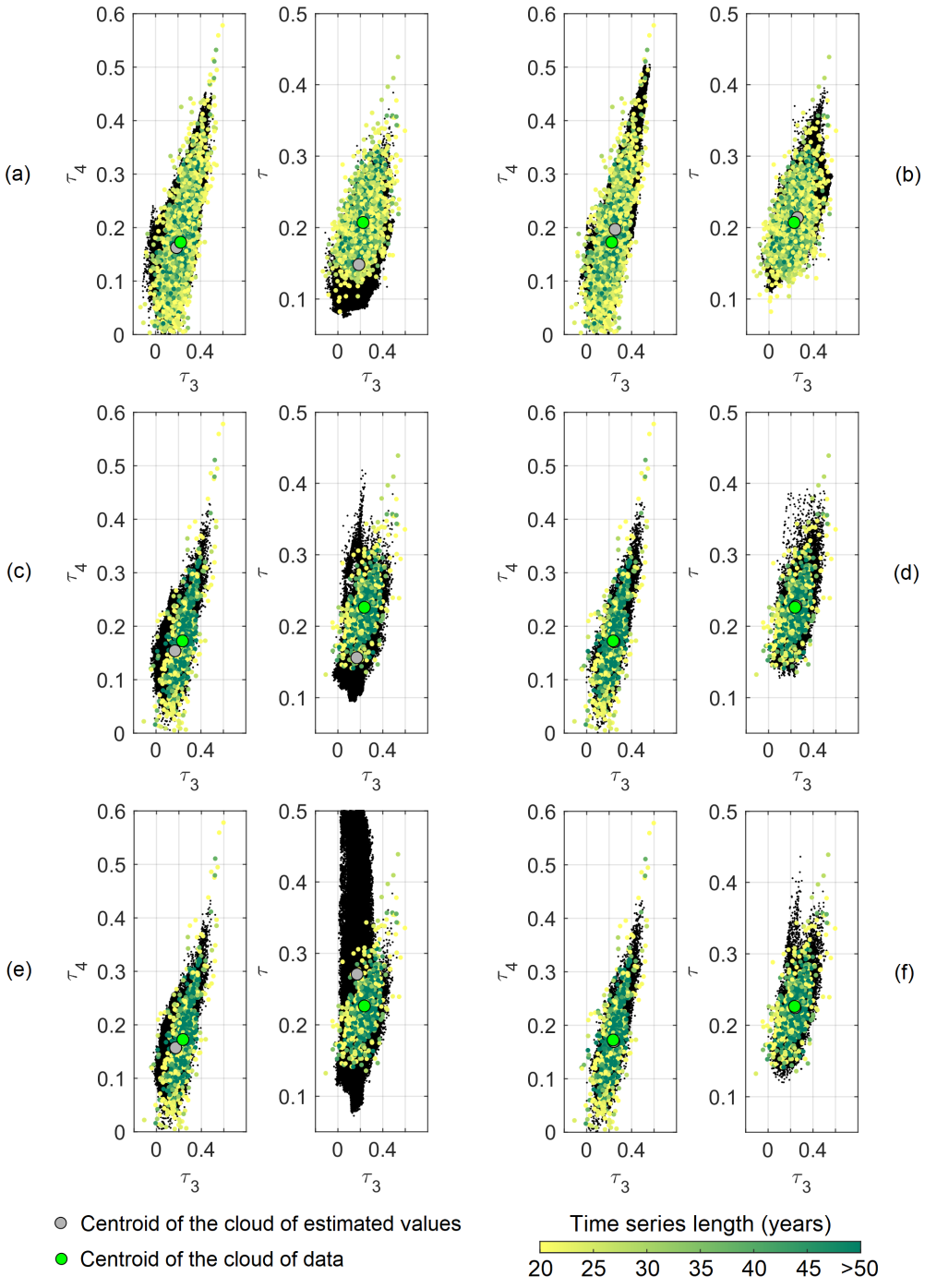

Fig. 7.3 L-moment ratio before (a, c, e) and after (b, d, f) the bias correction. τ, τ_3 and τ_4 are the coefficients of L-variation, L-skewness and L-kurtosis. Plots (a) and (b) refer to configuration n°2, plots (c) and (d) refer to configuration n°3 and plots (e) and (f) refer to configuration n°4. The black dots represent the L-moment ratios of all the cored series, made of measured and estimated values, while the coloured dots represent the L-moments of the measured series with a length of at least 20 years (of Piedmont, Aosta Valley and Liguria in configuration n°2, of Liguria in configurations n°3 and 4).

The bias-corrected rainfall datacubes obtained in the three configurations allowed us to perform a complete rainfall frequency analysis both with the Gumbel and the GEV distributions.

As a first comparison, the spatial variability over Liguria of the growth factor of a 200-year return period in the first two configurations was investigated by selecting the GEV distribution. Figure 7.4a shows the growth factor of configuration n°1 while Figure 7.4b is related to configuration n°2. Figure 7.4c shows the absolute difference among them: in this map, the influence of the 2021 records is clearly visible, especially in the Central-West part of the region. For comparison purposes, it is possible to compare this variation with:

- the 24 h annual maxima of the year 2021 spatially interpolated with the patched kriging (Figure 7.5a);
- the accumulated 24 h rainfall depths recorded by rain gauges until 5th of October 2021 at 2 a.m. (Figure 7.2);
- the accumulated rainfall of the 4th of October obtained from the adjusted surface rainfall intensity coming from the weather radar mosaic produced by the Italian Civil Protection Department (Figure 7.5b).

In the Central-West part of Liguria, the variation of the growth factor follows the same spatial patterns of these three maps. Some minor differences emerge in the eastern part of the region. The map produced by ARPA Liguria by means of a spatial interpolation of the rain gauge measurements (Figure 7.2) shows localized values up to 150 mm. The same rounded pattern is not visible in the radar data (Figure 7.5b). Few grid cells with rainfall depths up to 140 mm are visible, but with a different spatial configuration. By checking the hourly data available on the database of ARPA Liguria (https://ambientepub.regione.liguria.it/SiraQualMeteo/script/PubAccessoDatiMeteo.asp, accessed on 29th September 2022) it was possible to understand that a severe event occurred in late September 2021 (129.6 mm in 1 hour, 235.4 mm in 24 hours) induced such variation in the growth factor. Thus, the variations in the growth factor in the right side of the region are not caused by the same weather system.

When focusing on the data of Montenotte Inferiore station (that is the station that broke the all-time 6 h annual record), the influence of the 2021 records on the

Table 7.2 Local values (GEV distribution) of the Montenotte Inferiore station.

T (years)	2	10	50	100	200	500	1000
K(T) with 2021 non included	0.90	1.57	2.29	2.64	3.01	3.55	4.00
K(T) with 2021 included	0.80	1.66	3.02	3.86	4.93	6.78	8.62
$\Delta K(T)$	-0.10	0.09	0.73	1.22	1.92	3.23	4.62

increase of the growth factor clearly emerges (Table 7.2). For the same station, the IDF curves were computed for configurations n°1 (Figure 7.4d) and n°2 (Figure 7.4e). In both figures, black dots represent the 2021 annual maxima recorded by the Montenotte Inferiore rain gauges. The estimated return period of configuration n°1 is higher than 1000 years for all the durations, except for the 1 h one. In the second configuration, the return periods are in the range 80 - 280 years, depending on the duration.

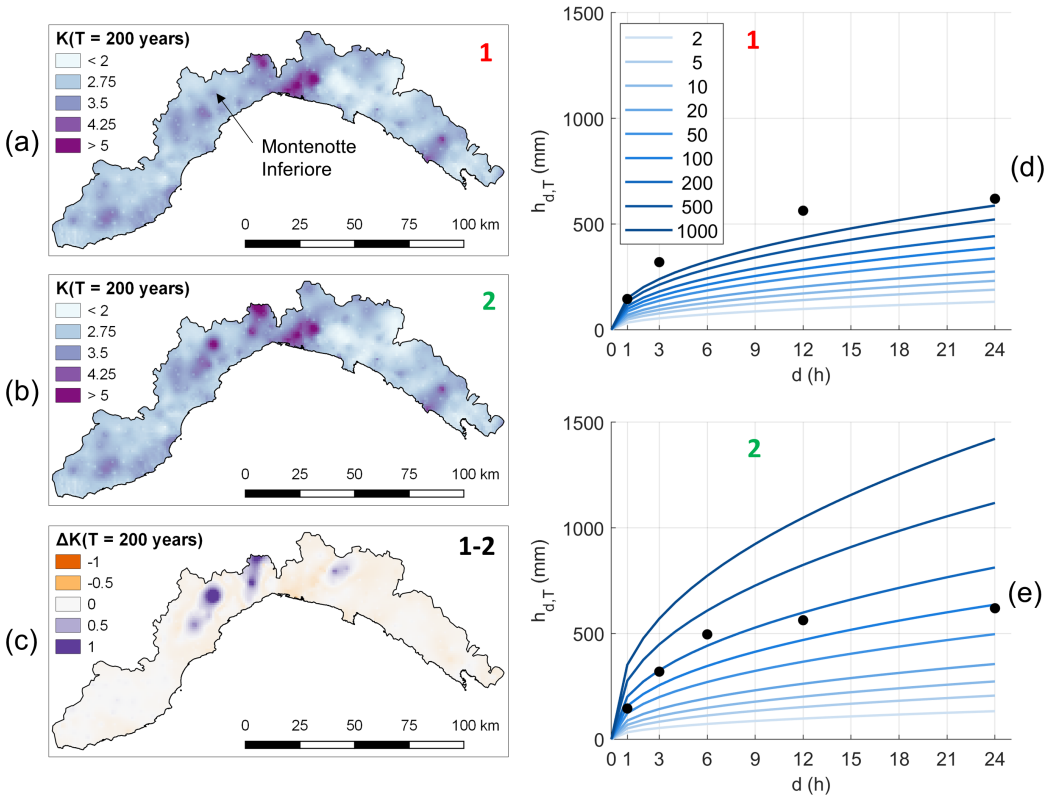

Fig. 7.4 Growth factor for return period of 200 years for configuration n°1 (a) and n°2 (b) and absolute difference (c). IDF curves for configuration n°1 (d) and n°2 (e).

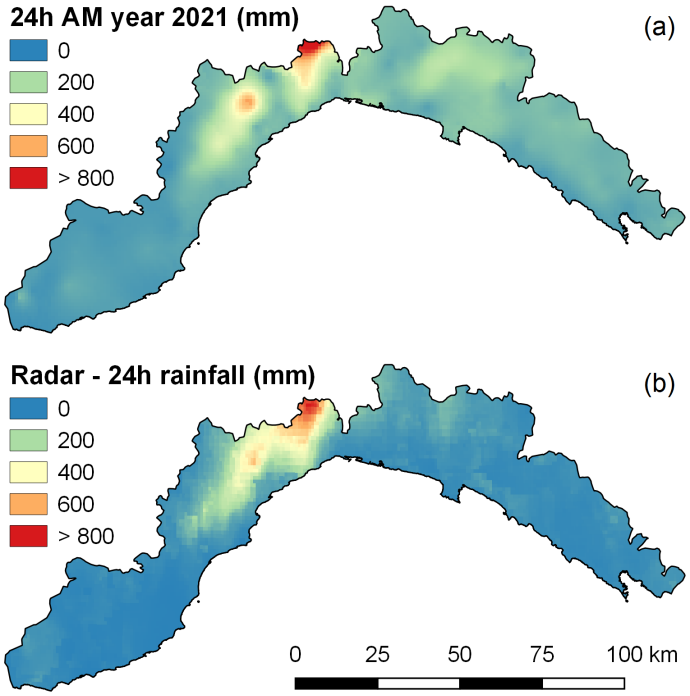

Fig. 7.5 Spatial interpolation of the 24 h annual maximum rainfall depths measured in 2021(a). Accumulated rainfall depth provided by weather radar. Source: weather radar mosaic produced by the Italian Civil Protection Department, made available within the framework of the LEXIS project.

The first results obtained with this analysis confirm the need to update the available information about rainfall quantiles as soon as a new severe event occurs.

One of the open points in the regionalization field is the investigation of the area influenced by a single, major event, its influence in the overall process and the possible extent of the variation of the distribution parameters and rainfall quantiles. This is something that has been already point out for example in Germany, where a major event happened near Münster (Shehu et al. (2022)) but that, up to now, still has to be understood. Providing a unique answer that can be relevant for all the nation could be challenging, especially considering the high topographic variability. However, in this thesis a first preliminary investigation is performed for the Liguria case study, and some preliminary comparisons with weather radar data are performed.

The comparison between configurations n°2 and n°3 allowed us to investigate the influence of working with a smaller sample within the actual version of the patched kriging. As shown in Table 7.1, for configuration n°2, which pools together the data of the entire region, a negative precipitation vs elevation relationship emerges for

Table 7.3 Comparison of the error statistics obtained from the cross-validation analyses of configurations n°2, n°3 and n°4.

Error statistic	h_1 Conf. 2	h_1 Conf. 3	h_1 Conf. 4	h_{24} Conf. 2	h_{24} Conf. 3	h_{24} Conf. 4
Bias (mm)	-0.31	-0.50	-0.14	-0.94	-1.46	-0.77
MAE (mm)	11.07	10.60	10.48	27.63	28.89	28.04
RMSE (mm)	15.13	14.44	14.29	41.83	42.78	41.22
NSE (-)	0.31	0.38	0.38	0.55	0.53	0.56

duration from 1 to 12 hours. The relationship between 24 h extremes and elevation is instead positive. Configuration n°3 pools together only the data of the Liguria region. A positive precipitation vs elevation relationship emerges in this case, but the relationship loses its significance when considering the 1 h duration. Even if surprising, this result is in line with Chapter 6 where we show significant variations in the orographic gradients over this specific interval for the 1 h duration.

A cross-validation procedure (leave-one-out approach) was implemented to evaluate the performance of these last three configurations in reconstructing the values of all the 144 time series with at least 20 years of data in the 1938 - 2021 period. For all the duration some improvements were obtained moving from configuration n°2 to n°4 (Table 7.3). If we consider the NSE coefficient, with configuration n°4 it was possible to obtain a +22.6% improvement compared to configuration n°2 for the 1 h duration, while for the 24 h duration the improvement is limited to + 1.8%. Similar variations emerge when analyzing the RMSE: in this case, a -5.6% reduction was achieved for the 1 h duration, while the variation is limited to -1.5% for the 24 h interval.

7.4 Application of the Patched Kriging Methodology: Sensitivity Issues Over Sardinia

7.4.1 Application

The patched kriging was then applied over Sardinia using the annual maxima of the I^2-RED database. The change of the region, compared to the previous section, is

based on two different motivations: the first one is the interest in investigating an area with different climatological and morphological characteristics compared to the North-West of Italy that in recent years was affected by a severe rainfall event, while the second one is related to the interest in performing further comparisons with other established methods, as will be described in the following parts of this section.

As mentioned in Section 7.2, the application of ordinary kriging requires to verify the hypothesis of stationarity of the second order: it is therefore necessary to remove from the measured values any dependencies on other variables through a detrending operation.

A multiple regression analysis at a regional scale (see Chapter 6 and Appendix B) showed that, contrary to what happens for Piedmont, where the extremes are particularly influenced by the elevation (Libertino et al. (2018a)), for Sardinia other variable are more relevant. After having discarded the variables that are both more complex to be computed and based on parameters that have to be fixed on the basis of a sensitivity analysis (as obstruction, barrier, maximum slope angle, maximum slope angle distance and openness), the geographical position and the mean annual rainfall proved to play a dominant role. The 1 h annual maxima were then detrended using longitude and latitude, while for the durations of 3 to 24 h longitude and mean annual rainfall were used.

The detrended values were then used for the next steps of the workflow, which include the application of the ordinary kriging for the construction of the rainfall data cube (and related kriging variance) and the bias correction. The results of the bias-correction performed in this specific case study are reported in Figure 7.6. Also in this application, the overlap of the two centroids after the bias-correction procedure suggests the effectiveness of the procedure.

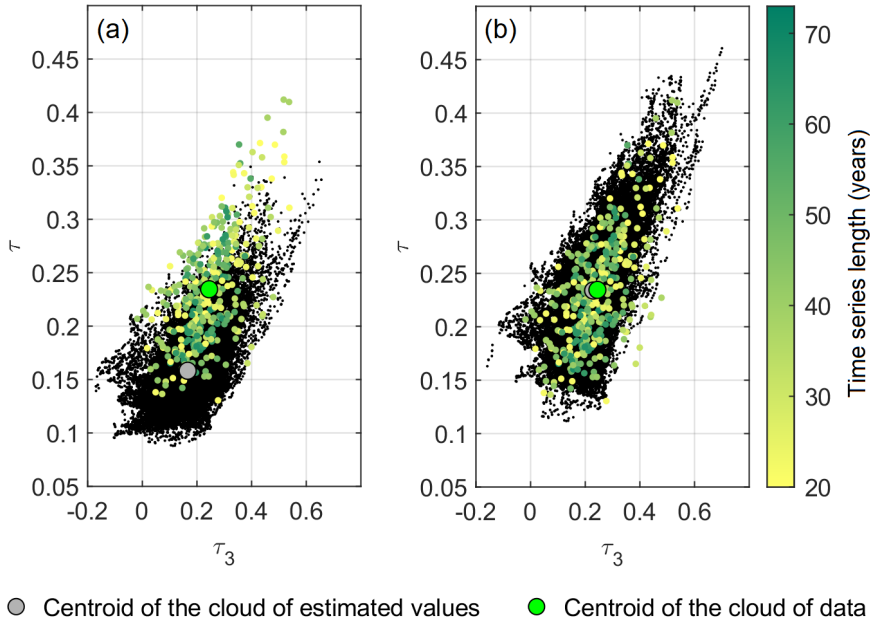

Fig. 7.6 Variability of the L-moment ratio before (a) and after (b) the bias-correction. The black dots represent the reconstructed data while the colored dots are the measured data coming from time series of at least 20 years. Modified figure from Mazzoglio et al. (2022d).

The mean regional values of τ, τ_3 and τ_4 computed on the basis of the reconstructed rainfall depths are, respectively, 0.234, 0.229 and 0.180. As a comparison, we can introduce the regional values obtained by Deidda et al. (2021) with a weighted averaging on the basis of the length of the time series, that are 0.225, 0.243 and 0.186. These values are quite similar to the ones obtained with the patched kriging, even if significant differences among the two datasets are present. In this study, sub-daily annual maxima were used, while Deidda et al. (2021) used daily annual maxima. These two datasets have also both a different temporal coverage (1929-2019 in this work, 1920-2008 in Deidda et al. (2021)) and a different data density (the time series with at least 30 years of data are 58 in this work and 256 in Deidda et al. (2021)).

The application of the patched kriging allowed us to obtain maps of interpolated values, as the index rainfall for different durations, the a and n parameters of the average depth - duration curves, the parameters of the GEV distribution and the growth factors for different return periods. Among all, it is interesting to focus on the map of the 24 h index rainfall evaluated on the basis of the bias-corrected maps of annual maxima (Figure 7.7b). As a comparison, the map of the daily index rainfall produced by Deidda et al. (2021) in a recent application was reported in Figure 7.7a

(more details about the methodology behind the study of Deidda et al. (2021) will be provided in the following part of this section). Figure 7.7 shows a good agreement between the two approaches in terms of spatial patterns. Figure 7.7b presents higher values being related to sliding 24 h maxima that are, as highlighted in Chapter 4, generally higher than the corresponding fixed daily maxima (Hershfield (1961) pointed out that sliding maxima are, at least for the United States of America, 1.13 times higher than the corresponding fixed maxima, while in Chapter 4 we obtained a mean value of 1.146).

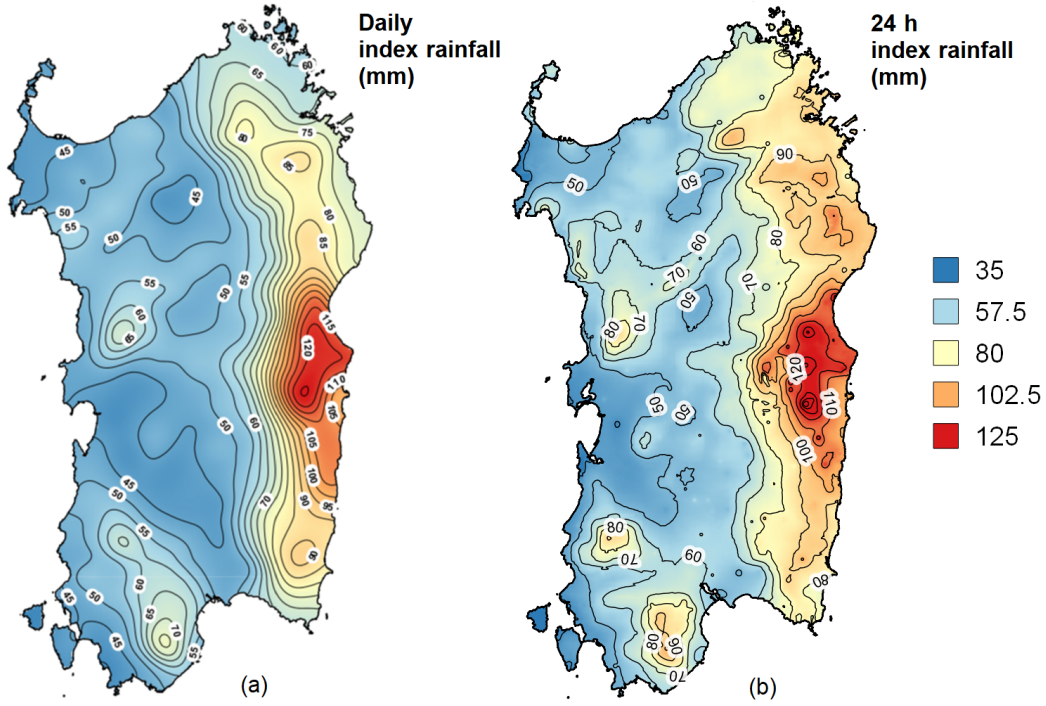

Fig. 7.7 Panel (a): daily index rainfall obtained by Deidda et al. (2021). Source: Deidda et al. (2021). Panel (b): 24 h index rainfall obtained with the patched kriging.

7.4.2 The Bitti case study

The heavy rainfall event that affected Sardinia on 28 November 2020, causing widespread damages in the Nuoro province and in the town of Bitti, produced high rainfall depths compared to historical values. The rainfall event began at about 00:30 a.m. of November 28 and continued without interruptions until 10:30 a.m. of the same day. The total rainfall depth reached about 330 mm but the greater intensities

were recorded in the final hours, from 07:15 a.m. until 09:15 a.m.. Figure 7.8 and Table 7.4 shows the maximum values reached in various durations.

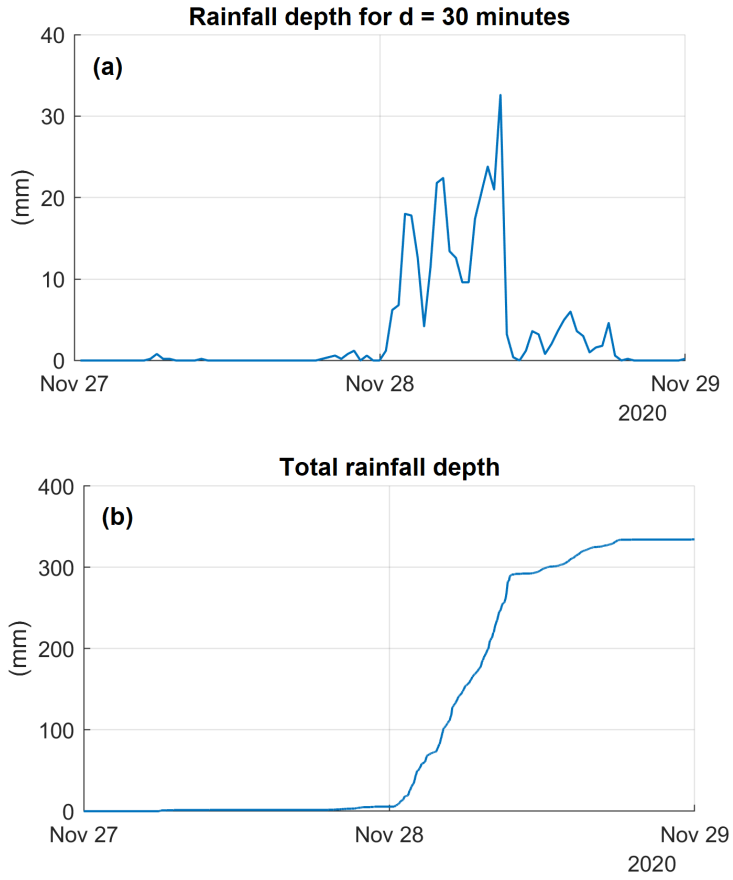

Fig. 7.8 Rainfall intensities recorded during 27 and 28 November 2020 by the San Giovanni - Bitti rain gauge. Rainfall depths over 30-minute intervals (a) and total rainfall depth (b).

Lacking hydrometric measurements, the examination of the severity of the event was performed thought the analysis of the rainfall depth, fortunately detected by the San Giovanni - Bitti station, which was put back into operation a few months before this severe event. However, the scarcity of observations of the station made it mandatory to resort to regional statistical methods to reconstruct the rarity of the event, methods that inevitably have a different reference dataset and which were therefore applied together, to provide elements for a multi-model estimate.

The estimate of the return period of a rainfall event is crucial for supporting the design of new hydraulic infrastructures. This need has led to the development of several regional rainfall frequency analysis methods, characterized by different

Table 7.4 Maximum accumulated rainfall depths for different durations recorded by the San Giovanni - Bitti station during the event of the 28th of November.

Duration (h)	Rainfall depth (mm)
0.25	23.8
0.5	33.6
0.75	42.0
1	54.0
3	125.4
6	218.0
9	283.2
12	293.4
24	327.2

levels of complexity. As highlighted in Chapter 2, the first methods were based on the identification of regions, suitable for selecting and merging data belonging to homogeneous areas. In recent years, on the other hand, greater importance has been given to methods that are continuous in space, without borders, based on geostatistical approaches.

The regional methods used in this application are:

- the VAPI Sardegna method (Deidda and Piga (1998), GNDCI Linea 1 (2001));
- a boundaryless approach based on the hierarchical application of geostatistical interpolation to obtain estimates of GEV distribution parameters in space (Deidda et al. (2021), Deidda (2022));
- an improved version of the patched kriging, previously described in Section 7.4.1.

The VAPI Sardegna method is based on the definition of homogeneous regions (and sub-regions) and adopts the Two Component Extreme Value (TCEV) distribution. It was developed considering the data of the maximum annual rainfall depths recorded over 30 and 45 minutes and 1, 3, 6, 12 and 24 consecutive hours of the period 1929-1982. Three different versions of this method were developed: in this work the version of Deidda and Piga (1998) is adopted as it is the most used version (Deidda (2021)). The mathematical formulation and the main results obtained from its application are reported in Appendix C.

The GEV boundaryless method suggested by Deidda et al. (2021) is based on the spatial interpolation of the rainfall depths measured from 1920 until 2008 through a kriging for uncertain data (KUD) which allows the appropriate treatment of data characterized by a modest variability and uncertainty mainly dictated by the limited length of the time series. Data of 256 stations with at least 30 years of data were used to estimate the daily index rainfall, while the information collected by 229 rain gauges with time series of at least 50 years were used to evaluate the moments of order greater than one. This method differs from the VAPI Sardinia being not based on the definition of homogeneous regions and allowing a better representation of the effects induced by topography and climatology on precipitation. With this approach, it is possible to make an assessment of the rarity of the event both for sub-hourly and sub-daily durations through mathematical expressions that depend on the daily index rainfall and on the dimensionless scale and shape parameters, interpolated throughout the area of interest. The mathematical formulation and the main results obtained from its application are reported in Appendix D.

The patched kriging consists in the sequential application, year by year, of an ordinary kriging to all the available annual maxima, regardless of the length of their time series. The patched kriging method, originally developed for an application in Piedmont, was here applied using the sub-daily (1 to 24 hours) annual maxima of the period 1929-2019 contained in the Improved Italian - Rainfall Extreme Dataset (I^2-RED) (Mazzoglio et al. (2020)). For this specific application, the modified version described in Section 7.4.1 was used.

The patched kriging method was not applied to sub-hourly durations due to the extreme fragmentation of the records and the low data density. However, specific analyses were carried out on the sub-hourly rainfall extremes using the data of the stations located near Bitti with a double purpose, that is to extend the estimates obtained with patched kriging to the sub-hourly durations and re-evaluate both the VAPI method and the boundaryless approach suggested by Deidda et al. (2021) using even more recent data.

Sub-hourly annual maxima were retried from the Hydrological Yearbooks of the SIMN and of the Regional Hydrological Service (for the 1951-2011 period), from the Hydrological Yearbooks of ARPA Sardegna (2012-2019 period) and from unpublished data of the Regional Hydrological Service, processed by Deidda et al. (2002) (1986-1996 period).

First of all, for each rain gauge located nearby Bitti with both sub-hourly and sub-daily measurements, the estimation of the scaling exponent *n'* of the average depth-duration curve was performed again only for the sub-hourly durations by using the equation

$$h_d = a \cdot d^{n'} \tag{7.13}$$

where h_d is the rainfall depth related to the interval d and a is the scale factor, also representing the best unbiased estimator oh the mean 1 h rainfall, kept constant for all durations, as it represents the junction point between the durations lower and higher of 1 hour. Equation 7.13 allowed to re-estimate the coefficient *n'* (i.e. the new scaling exponent evaluated for sub-hourly durations). To verify the reliability of this parameter, the ratio between the scaling exponents of the two sides of the average depth-duration curve, *n'* and n, was examined for each rain gauge through the equation:

$$\alpha = \frac{n'}{n} \tag{7.14}$$

Finally, the average value of this coefficient was used for the correction of the lower branch of the average depth-duration curves. The mean α value obtained with Equation 7.14 is equal to 1.51.

The so-computed relationship that links the lower and upper branches of the IDF curves was used both for the complete application of the patched kriging (the mathematical formulation and the main results obtained from its application are reported in Appendix E) and for the re-evaluation of the estimates concerning the sub-hourly durations made with the other methods (VAPI Sardinia and GEV boundaryless approach; see Appendix F for the formulation and the main results achieved). The application of this coefficient made it possible to obtain 5 different estimates: two with the VAPI Sardegna, two with the GEV boundaryless approach suggested by Deidda et al. (2021) and one with patched kriging. Finally, a sixth estimate was produced, obtained as the average of the return periods weighted on the number of observations used in each method. The severity diagram built on the basis of these six methods is shown in Figure 7.9.

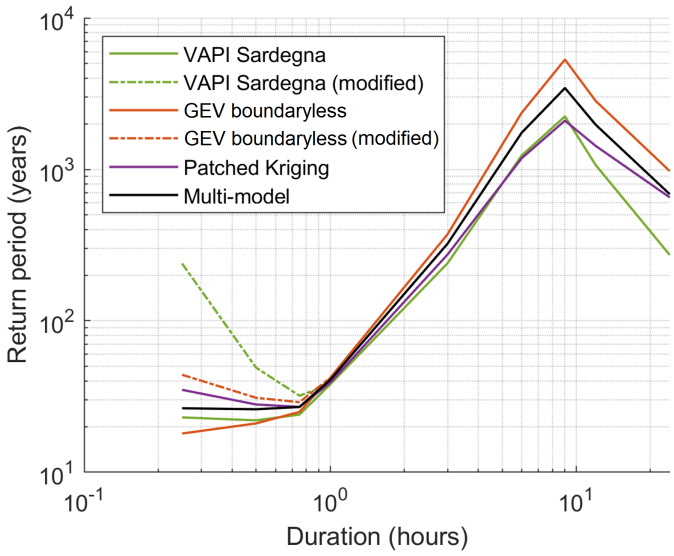

Fig. 7.9 Severity diagram containing the evaluation of the return periods performed with the different methods. The dashed curves were obtained with a modified model for sub-hourly durations evaluated introducing the coefficiente α. Source: Mazzoglio et al. (2022d).

The results obtained in this section show that the estimates obtained with the VAPI Sardegna, GEV boundaryless and patched kriging methods follow a similar path. The greatest difference is observed for the 15-minute duration, in the case of correction made to the VAPI Sardegna method. Given the large difference, it was considered appropriate to discard this estimate in the evaluation of the multi-model return period of the 15-minute duration. For durations smaller than 3 hours, the results obtained with the different methods converge to the same estimate while for longer durations the differences became larger. For durations greater than 9 hours, the patched kriging provides an intermediate evaluation between that of the Sardinia VAPI and that of the GEV boundaryless method. The differences among the approaches could be partially attributable to the different databases used in each study. An estimate based on a combined approach provides a robust assessment of the severity of the event, as well as helping to reduce the uncertainty in estimating quantiles for high return periods.

Further work could be conducted to repeat the study by including also the 2020 records, as performed for the Liguria case study. At this stage, these record were not included to be able to perform a "fair" comparison with the VAPI Sardegna method and the GEV boundaryless approach.

7.5 Development of a Regional Ombrian Model

7.5.1 Introduction of the Ombrian Model

As mentioned in Chapter 2, the intensity - duration - frequency (IDF) curves are a standard tool for estimation of the design rainfall. However, Koutsoyiannis and Iliopoulou (2022) pointed out that this name can be a misnomer because the term "duration" does not refer to the duration of the rainfall event but rather to a predetermined fixed time interval used to average the rainfall intensity, while "frequency" is here used not to define the actual frequency but its reciprocal, that is the return period. While introducing the new term "ombrian model", Koutsoyiannis and Iliopoulou (2022) and Iliopoulou et al. (2022) also revisited the entire formulation by including recent advances to stochastic modeling of rainfall intensity at any point in a given area, developing a framework that can be valid over any scale supported by the rainfall data. As a consequence, in the following part of this section, the term "ombrian model" will be used in place of IDF curves.

As pointed out by Iliopoulou et al. (2022), the construction of a regional ombrian curves can be performed using two different approaches. The first one consists of an at-site independent fitting approach combined with a spatial interpolation method for mapping the parameters over the entire region. Despite its simplicity, it presents the drawback of being very sensitive to the data of single stations, which are often plagued by missing data. The second one is a regional simultaneous fitting method applied after having appropriately pooled the data, with the aim of obtaining a single model that is valid for the entire area. The latter approach can thus be considered as the inverse of the first one and is, in theory, more powerful since it takes advantage of all the observations to limit uncertainty. However, a rigorous framework must be considered to deal with the different record lengths of the series and the possible presence of spatial dependence.

This new approach is based on an ombrian model structure common for each grid cell of the domain, except for a spatially-varying scale parameter modeled by applying a spatial smoothing model. The difficulties that could be encountered in the delineation of sub-regions on the basis of the similarity are bypassed here.

As mentioned before, the spatial dependence can play a not negligible role. The widely used regional frequency analysis based on L-moments (Hosking (1990), Hosk-

ing and Wallis (1997)) can decrease in accuracy as the spatial dependence increases (Hosking and Wallis (1988)). According to Koutsoyiannis (2019), L-moments can be better estimated and are effective in inferring the marginal distribution of stochastic processes, but cannot characterize second-order dependence of processes. A new rainfall frequency analysis framework was thus proposed to explicitly address the spatial dependence in the data while estimating higher-order properties. The fitting procedure is applied to the pooled sample using the knowable moments or K-moments recently introduced by Koutsoyiannis (2019) and Koutsoyiannis (2020).

More details about this methodology will be provided in the following sections. The reader is referred to Koutsoyiannis (2019), Koutsoyiannis (2020), Koutsoyiannis and Iliopoulou (2022) and Iliopoulou et al. (2022) for a complete description of the method.

7.5.2 Mathematical Formulation of the Ombrian Model

An ombrian model can be derived from the dependence structure and the marginal distribution of rainfall intensity. A non-simple scaling behavior is considered to link the rainfall intensity x to any timescale k and return period T. The quantity x is thus the quotient of two separate functions of the return period and the timescale, *b(T)* and *a(k)* (Iliopoulou et al. (2022)). The advantage of this approach is the separability of these two terms, which allows a two-step procedure for the parameter estimation.

In this application only small time scales are considered, for which a Pareto distribution can be used. More in detail, the rainfall intensity can be computed as

$$x = \frac{b(T)}{a(k)} = \lambda \frac{(T/\beta)^{\xi} - 1}{(1 + k/\alpha)^{\eta}} \tag{7.15}$$

where λ is an intensity scale parameter in the same units of x (e.g., mm/h), T is the return period, β is a timescale parameter in units of the return period (typically years), $\alpha \geq 0$ is a timescale parameter (typically expressed in hours), η is a dimensionless parameter ($0 < \eta < 1$) and $\xi > 0$ is the tail index of the process (Iliopoulou et al. (2022)).

If the rainfall frequency analysis is performed using Peak over Threshold (POT) series, a Pareto distribution (and thus Equation 7.15) can be assumed. When dealing with annual maxima, the Extreme Value Type 2 (EV2) distribution from the

Generalized Extreme Value (GEV) distribution family

$$F(y) = exp(-(1+\xi(\frac{y}{\nu}-\psi))^{-\frac{1}{\xi}}) \tag{7.16}$$

has to be preferred. In Equation 7.16, $y \geq \nu(\psi - \frac{1}{\xi})$, ψ (dimensionless), $\nu > 0$ (same units as y) and $\xi > 0$ are the location, scale and shape parameters of the GEV distribution. Equation 7.16 can be re-parameterized consistently to Equation 7.15 as

$$F(y) = exp(-\frac{\Delta}{\beta}(\frac{y}{\lambda}+1)^{-\frac{1}{\xi}}) \tag{7.17}$$

where $\beta = (1-\xi\psi)^{1/\xi}$, $\lambda = (1-\xi\psi)\nu/\xi$ and $\xi > 0$. In the end, the ombrian model follows the equation

$$x = \lambda \frac{(-(\beta/\Delta)ln(1-\Delta/T))^{-\xi}-1}{(1+k/\alpha)^{\eta}} \tag{7.18}$$

For small return periods, Equation 7.15 (derived from a Pareto distribution) provides higher intensity than Equation 7.18 (derived from a GEV distribution), while for larger return periods ($T > 10$ years) the two are almost indistinguishable.

7.5.3 Regionalization Method

The regional model aims at generalizing Equations 7.15 and 7.17 in space after having identified those parameters that can be considered as regionally varying, keeping in mind that they should be reliably estimated from at-site data.

On the basis of the available data, Iliopoulou et al. (2022) decided to spatially model the parameter λ of Equation 7.18 (i.e., one of the parameters of the numerator of Equation 7.18), which corresponds to the scale parameter of the EV2 distribution and is proportional to the mean annual maxima at each location for any timescale. Considering that the transformation between timescales is controlled by the $a(k)$ function, it is enough to model the average maxima at a single, convenient timescale. The 24 h maxima were selected here because they are usually available in a larger number (daily data could also be adopted). This choice is not new: the index flood method (Dalrymple (1960)) is a widely-known approach based on the same assumption.

Fine-scale records are needed to obtain a reliable estimate of α and η, which control the timescale transformations of the ombrian curves. Among the two, the parameter α proved to be very sensitive to small-scale intensities and theoretically requires sub-hourly data to be reliably estimated. Because sub-hourly and sub-daily data are generally scarce and with short time series in the region, they usually do not constitute a good choice for the spatial modeling. It was then decided to consider common values for these parameters, by selecting the values that minimize the sum of all stations' variance, as performed in Iliopoulou et al. (2022). In general terms, $\alpha > 0$ and $0 < \eta < 1$. Another possible option could be keeping α costant and considering a spatially-varying η.

After having selected the variable that needs to be regionalized, a proper spatial model needs to be identified. The bilinear surface smoothing (BSS) model (Malamos and Koutsoyiannis (2016a), Malamos and Koutsoyiannis (2016b)) was here selected. The interpolation is performed by approximating a surface with consecutive bilinear surfaces, which can be estimated by means of a least squares fitting procedure into a regression model with known breakpoints and adjustable smoothing terms (Malamos and Koutsoyiannis (2016a)). This approach is based on a trade-off between the objectives of minimizing the fitting error and the roughness of the fitted bilinear surface. The application of a larger weight of the first objective implies a rougher surface, while the opposite is true when using a larger weight of the second objective.

In the BSS framework, the fitting procedure is based on the minimization of the generalized cross-validation error (GCV) between measured and estimated values in gauged locations. This approach can be considered both local and global: it is local because it uses the four surrounding data points of the bilinear surface to estimate the target point, and it is global because the GCV procedure globally fits the bilinear surfaces to the data points. The general estimation function of BSS $\hat{z_u}$ in point u is

$$\hat{z_u} = d_u \tag{7.19}$$

where d_u is the value of the bilinear surface d at that point. The surface d is modeled and defined by using four adjustable parameters: the numbers of intervals along the horizontal and vertical direction (m_x and m_y) and the corresponding smoothing parameters ($\tau_{\lambda x}$ and $\tau_{\lambda y}$).

The BSS method can be further extended by introducing an additional explanatory variable that comes from a denser dataset compared to the one on the main variable (in

this case, we will refer to a bilinear surface smoothing with an explanatory variable, BSSE). Here, the methodology is focused on combining two bilinear surfaces into the same regression model to improve the interpolation accuracy: the first surface is fitted to the available data and the second one incorporates the influence of an explanatory variable available at a spatially denser dataset. If, in correspondence of the gauged sites, we also know the value of an explanatory variable t, the general estimation function for point u becomes

$$\hat{z_u} = d_u + t_u e_u \tag{7.20}$$

where d_u and e_u are the values of two fitted bilinear surfaces in point u, namely d and e, while t_u is the value of the explanatory variable at that point. In Equation 7.20 the quantities d_u and e_u change in space. In this case, six different parameters model the surface: the four parameters used in the BSS case (m_x, m_y, $\tau_{\lambda x}$ and $\tau_{\lambda y}$) and two smoothing parameters of the surface e, $\tau_{\mu x}$ and $\tau_{\mu y}$.

Both in the BSS and in the BSSE models the smoothing parameters are restricted in the interval [0, 1) for both directions (Malamos and Koutsoyiannis (2016a)): smoothing parameters close to 1 mean that the bilinear surface exhibit greater smoothness. For each m_x and m_y combination, the minimization of the GCV error provides the optimal values of $\tau_{\lambda x}$, $\tau_{\lambda y}$, $\tau_{\mu x}$ and $\tau_{\mu y}$.

In areas with complex terrain, it is probable that the elevation could influence the extremes. Thus, Iliopoulou et al. (2022) suggested to apply both BSS and BSSE approaches using the elevation as an explanatory variable.

The evaluation of the most accurate model (BSS or BSSE) can be performed using two statistical indexes, the root mean square error (RMSE) and the mean absolute error (MAE), both using all the data and using a leave-one-out cross-validation approach.

7.5.4 Moment Estimation

Let's consider a sample ($\underline{x}_1$, $\underline{x}_2$, ..., $\underline{x}_n$) of size n of a stochastic variable $\underline{x}$ with probability density function $f(x)$. The "underline" sign used in this chapter defines random variables and serves to distinguish them from regular variables, according to

the Dutch convention (Hemelrijk (1966). A continuous time series will be denoted by $\underline{x}(t)$ while a discrete one will be defined by $\underline{x}_\tau$.

The estimator of the non-central moment (that is the moment about the origin) of order p, $\underline{\hat{\mu}}'_p$, is

$$\underline{\hat{\mu}}'_p = \frac{1}{n}\sum_{i=1}^{n} \underline{x}_i^p \tag{7.21}$$

while the estimator of the central moment $\underline{\hat{\mu}}_p$ is

$$\underline{\hat{\mu}}_p = \frac{1}{n}\sum_{\tau=1}^{n} (\underline{x}_\tau - \underline{\hat{\mu}})^p \tag{7.22}$$

where $\hat{\mu} \equiv \underline{\hat{\mu}}'_1$ is the estimator of the mean (Koutsoyiannis (2020)).

According to Lombardo et al. (2014) and Koutsoyiannis (2020), the estimators of the central moments $\underline{\hat{\mu}}'_p$ are in theory unbiased but their use with $p > 2$ is unpractical.

The estimation of the second one is instead more complex. For large p and positive x_i we can consider the approximation

$$\Big(\sum_{i=1}^{n} x_i^p\Big)^{1/p} \approx \max_{1\le i\le n}(x_i) \tag{7.23}$$

This equation is related to the fact that the maximum norm is the limit of the p-norm as $p \to \infty$ (Koutsoyiannis (2019)). Therefore, for relatively large p, the estimate of μ'_p will be

$$\hat{\mu}'_p = \frac{1}{n}\sum_{i=1}^{n} x_i^p \approx \frac{1}{n}(\max_{1\le i\le n}(x_i))^p \tag{7.24}$$

In Equation 7.24 the term (1/n) can be omitted with a negligible error for large p. This equation suggests that $\hat{\mu}'_p$, while theoretically is an unbiased estimator of μ'_p, in practice is more an estimator of an extreme quantity than the actual estimator of μ'_p (i.e., the convergence to the maximum value is faster than the convergence of $\hat{\mu}'_p$ to μ'_p). Thus, Koutsoyiannis (2019) pointed out that the latter is a biased estimator for any $p > 1$ and that, even for relatively low p (as in the 2-4 range) the bias can be large. In the case of an *iid* sample and low p, the bias can be quantified and its entity is small, while for higher p the estimation of the moments becomes almost impossible due to the high variance and skewness of the estimators, which lead to

have an expected value different by orders of magnitude from the mode (i.e., the most probable value).

Due to this drawback, Koutsoyiannis (2019) re-named the classical moments as "unknowable moments" and discouraged their estimation from the data, introducing the "knowable moments" (or K-moments), which can reliably be estimated even for high orders and are particularly useful when dealing with extremes.

Let's introduce a stochastic variable $\underline{x}$ with $\underline{x}_1$, $\underline{x}_2$, ..., $\underline{x}_n$ the *iid* copies of it rearranged in increasing order of magnitude such that $\underline{x}_{(i:n)}$ is the ith smallest among the n, i.e.

$$\underline{x}_{(1:n)} \leq \underline{x}_{(2:n)} \leq \ldots \leq \underline{x}_{(i:n)} \tag{7.25}$$

The variable $\underline{x}_{(i:n)}$ is termed the ith order statistic. The maximum value of the sample corresponds to the highest order statistics, that is

$$\underline{x}_{(n)} = \underline{x}_{(n:n)} = max(\underline{x}_1, \underline{x}_2, \ldots, \underline{x}_n) \tag{7.26}$$

According to Koutsoyiannis (2020), the distribution function $F_{(n:n)}(x)$ and the probability density function $f_{(n:n)}(x)$ can be computed as

$$F_{(n:n)}(x) = (F(x))^n \tag{7.27}$$

and

$$f_{(n:n)}(x) = nf(x)(F(x))^{n-1} \tag{7.28}$$

where the former is n times $F(x)$ (equation justified by the *iid* assumption) while the latter is the derivative of $F_{(n:n)}(x)$ with respect to x.

The expected value of the maximum of order p of $\underline{x}$ is therefore

$$E[\underline{x}_p)] = E[max(\underline{x}_1, \underline{x}_2, \ldots, \underline{x}_p)] = pE[(F(\underline{x}))^{p-1}\underline{x}] \tag{7.29}$$

The expected value of Equation 7.29 is a statistical moment, i.e., the non-central knowable moment of order p, which can be defined as

$$K'_p = pE[(F(\underline{x}))^{p-1}\underline{x}] \tag{7.30}$$

for the moment order $p \geq 1$.

The estimators of the non-central K-moments are obtained using

$$K'_p = \sum_{i=1}^{n} b_{inp} \underline{x}_{(i:n)} \tag{7.31}$$

and

$$b_{inp} = \begin{cases} 0, & i < p \\ \frac{p}{n} \frac{\Gamma(n-p+1)}{\Gamma(n)} \frac{\Gamma(i)}{\Gamma(i-p+1)}, & i \geq p \geq 0 \end{cases} \tag{7.32}$$

where $\underline{x}_{(i:n)}$ is the ith smallest variable in a sample $\underline{x}$ of size n placed in ascending order, p is the order of the moment (which can be any positive number that satisfy $p \leq n$ and $\sum_{i=1}^{n} b_{inp} = 1$.

In Equation 7.32 the fact that $b_{inp} = 0$ means that fewer data are used in the estimation as the moment order increases. When only one is left, i.e. when dealing with the maximum, $p = n$ and $b_{nnn} = 1$. When $p > n$, $b_{inp} = 0$ for every i (with $1 \leq i \leq n$), and the estimation is impossible.

A return period can be assigned to each K-moment, using

$$\frac{T(K'_p)}{\Delta} = p\Lambda_p \approx \Lambda_\infty p + (\Lambda_1 - \Lambda_\infty) \tag{7.33}$$

where Λ_1 and Λ_∞ are coefficients that depend on the distribution function. Koutsoyiannis (2020) showed that, when dealing with the EV2 distribution, these coefficients depend on the shape parameter ξ, with

$$\Lambda_1 = \frac{1}{1 - exp(-(\Gamma(1-\xi))^{-\frac{1}{\xi}})} \tag{7.34}$$

and

$$\Lambda_\infty = \Gamma(1-\xi)^{\frac{1}{\xi}} \tag{7.35}$$

This procedure can be applied at an at-station level for assigning return periods to the K-moments of each individual station. Similarly, the parameters of the EV2 distribution can be obtained by minimizing an error statistic (MAE or RMSE) between the empirical and the theoretical K-moments (or between the corresponding return periods. However, the maximum return period that can be directly estimated from the pooled data is a function of the dependence structure of the sample itself.

When dealing with cross-correlated data, the amount of information decreases, but it is still more significant than that of an individual station.

To explicitly account for the dependence effect in the estimation of the return period, proper modification of the moment orders of the unified sample is performed by considering p'. When dealing with m stations with sample length equal to n_1, the quantity $n = mn_1$ represents the size of the merged sample. In this case:

- for $p \leq n_1$, $p' = p$ is set;
- for $p > n_1$ an approximation is used. More specifically, the equivalent Hurst parameter H is estimated on the basis of the spatial correlation of the station ρ, with

$$H = \frac{1}{2} + \frac{ln(1+\rho)}{2ln2} \tag{7.36}$$

that is used to compute a coefficient for the bias-correction

$$\Theta^{HK}(n,H) \approx \frac{2H(1-H)}{n-1} - \frac{1}{2(n-1)^{2-2H}} \tag{7.37}$$

Finally, the modified orders of the moments are obtained as

$$p' \approx 2\Theta + (1-2\Theta)(p-n_1+1)^{((1+\Theta)^2} + n_1 - 1 \tag{7.38}$$

and the corresponding return period are then adjusted using Equation 7.32.

The parameter n_1 controls the maximum moment order that is unaffected by spatial dependence: a higher n_1 value suggests an increase in the information gain because fewer return periods are modified downwards. If the stations have different time series lengths, n_1 can be estimated as the average record length of all stations. To reduce the uncertainty linked to the modification of the return periods, a good strategy can involve using moment orders up to n_1 for model calibration, while higher moments are used only for validation. Despite this subdivision, the moments used for the calibration are much more than those used in regular moment fitting procedures (typically 3 or 4 orders).

Coming back to the operation procedure, after having defined the α and η parameters of $a(k)$ as described in the previous section, it is necessary to specify the parameters of the $b(T)$ function. From a practical point of view, the sample can be

made by pooling all 24 h annual maxima after dividing them by their theoretical mean value given by the spatial smoothing model. The pooled standardized sample is used to fit the EV2 distribution using the method of the non-central K-moments described above. For each K-moment estimate a return period can be assigned with Equation 7.33, with a procedure that can also manage possible bias due to spatial dependence (see Equations 7.36 to 7.38).

The two-step fitting procedure (α and η in the first step, and then $b(T)$) represents an interesting methodology feature since it allows greater flexibility in using different data sources. As mentioned in Section 7.4.3, α and η are better estimated using sub-hourly and sub-daily data, while the $b(T)$ is better inferred using daily data.

After the calibration, the parameters of the EV2 distribution (as expressed in Equation 7.17) of the standardized mean 24 h annual maxima need to be transformed to the final ombrian parameters of *b(T)*. The rainfall intensity for any station at the 24 h timescale can be computed as

$$x_T^{(24h)} = \mu u_T / 24 \tag{7.39}$$

where u_T is the 24 h annual maximum rainfall value for return period T standardized by its mean value μ and μ is the mean value used in the standardization step (i.e, the one derived from the BSS/BSSE spatial models). Similarly, the quantity

$$y_T = x_T^{(24h)}(1+24/\alpha)^{\eta} \tag{7.40}$$

whose distribution defines the *b(T)* function become

$$y_T = \mu u_T (1+24/\alpha)^{\eta}/24 \tag{7.41}$$

As a consequence, the variable *y* has the same distribution function of the variable *u*, which keeps the same shape and location parameters and has a scale parameter that is proportional to the one of *u*, i.e.

$$\xi = \xi_u \tag{7.42}$$

$$\beta = \beta_u \tag{7.43}$$

$$\lambda = \lambda_u \mu (1+24/\alpha)^{\eta}/24 \tag{7.44}$$

where the subscript u denotes the standardized 24 h rainfall and α is expressed in hours.

Summarizing, the α and η parameters (estimated simultaneously by pooling the data of all the stations), the distribution parameters of the standardized 24 h maxima and the 24 h maxima spatially modeled with the BSS/BSSE models can fully determine the ombrian curves.

7.6 Approaches to Intercomparison: the Thessaly case study

Iliopoulou et al. (2022) applied for the first time the workflow needed to develop an ombrian model according to the theory described in Section 7.4. The first application of the regional ombrian curves was performed over the Water District of Thessaly, a 13,700 km^2 region of Greece delimited by mountains (Figure 7.10). Data of 55 rain gauges with at least 12 years of data are here used, with rainfall intensity data typically starting from fine scales (5 to 60 minutes) and extending to the 24 or 48 h scale. The data management operation is described in Iliopoulou et al. (2022).

Fig. 7.10 Area of interest with the position of the rain gauges (red dots).

The patched kriging was then applied over the same area to obtain a spatial interpolation of 24 h annual maxima, as performed using the BSSE method. Both methodologies differ from the classical rainfall RFA being developed to take advantage of all the information, even those included in short and fragmented time series. The main purpose of this step is the investigation of the rainfall pattern obtained using two completely different spatial models, that has in common only the inclusion of an external information in the spatialization approach. Then, the two interpolated maps will be used as input for the K-moment fitting. This step serves to investigate how the spatial model used to compute the rainfall quantiles influence the final results. Some preliminary results are reported in Mazzoglio et al. (2022b) and will be detailed here, especially for what concern the patched kriging.

The patched kriging was applied in the model configuration described by Libertino et al. (2018a), after having properly calibrated the main parameters. More specifically, the following steps where performed:

- detrending with the elevation of the 24 h annual maxima. More specifically, a positive variation of rainfall depth with elevation emerged over the region, as already pointed out by Iliopoulou et al. (2022);
- computation of the sample and theoretical variograms for each duration;
- application of the ordinary kriging using as input the detrended values to obtain a rainfall data cube made of measured and estimated values, with the corresponding kriging variance;
- bias-correction;
- computation of the 24 h mean rainfall depth.

A comparison between the interpolated mean 24 h rainfall depth at a 2 km resolution is shown in Figure 7.11a and b. Here, only BSSE and patched kriging are considered while the results obtained with BSS are not discussed here because this model provided a less accurate estimation in this case study compared to BSSE. The models efficiently capture the spatial variability of extreme rainfall, and their estimates are robust even under increased spatial uncertainty due to inconsistencies among the point data. It is worth highlighting that the spatial distribution of the λ values is similar to the one of the 24 h maxima because they are directly estimated from them using Equation 7.44.

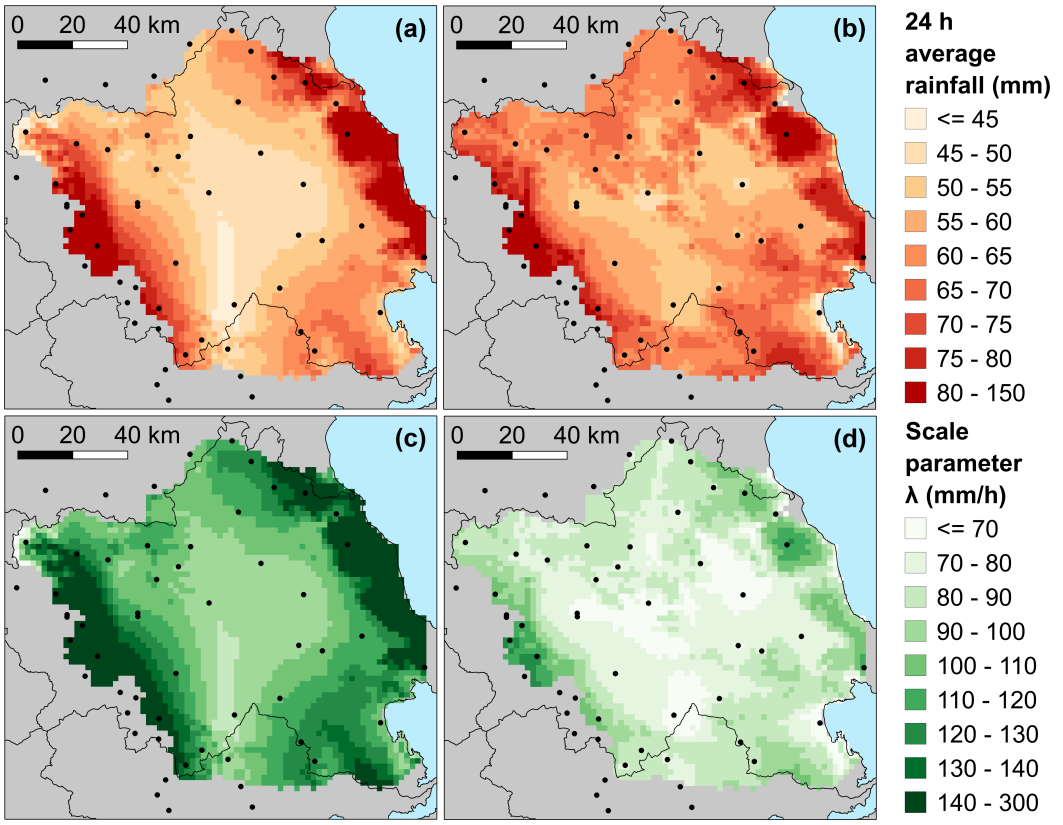

Fig. 7.11 Area of interest with the position of the rain gauges (black dots). Mean 24 h rainfall depth spatially modeled with the BSSE (a) and with the patched kriging (b). Scale parameter spatially modeled with the BSSE (c) and with the patched kriging (d).

The timescale parameters α and η are obtained through optimization by using the procedure detailed in Koutsoyiannis et al. (1998). The final results are reported in Table 7.4.

The distribution parameters are obtained by minimizing an error metric (MAE in this case) between the theoretical quantiles and the empirical K-moments, using the methodology described in Section 7.4.4. The moment calibration (Figure 7.12) is performed using the moment orders up to n_1 (here 42, corresponding to the average record length of all stations). Higher moments (in total 2305) are used for validation. As also highlighted before, with this approach the moments used in calibration are many more (42) than those used in regular moment fitting procedures (typically up to 3 or 4 orders). Also the main parameters of the two ombrian models are listed in Table 7.4.

Table 7.5 Model parameter of both BSSE and patched kriging.

Parameter	BSSE	Kriging
α (h)	0.03	0.03
η (-)	0.64	0.64
ξ (-)	0.18	0.2
beta (years)	0.013	0.006
λ (mm/h)	Spatially varying	Spatially varying

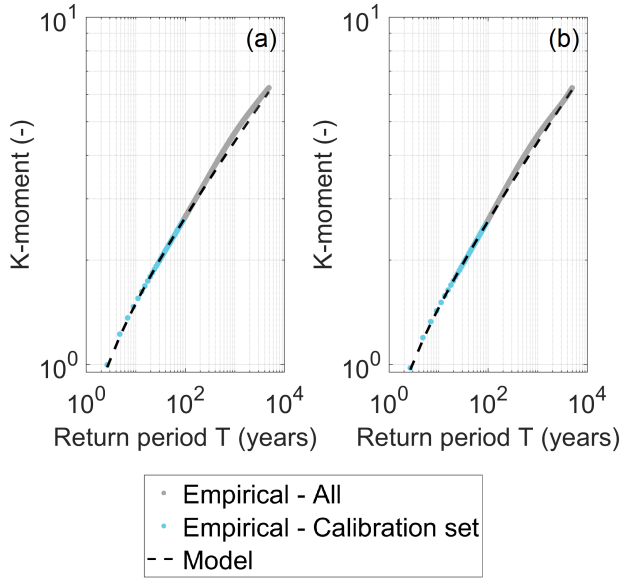

Fig. 7.12 Empirical K-moments obtained on the basis of the pooled standardized 24 h mean rainfall depths modeled with an EV2 distribution and the corresponding return periods, computed with 24 h maxima modeled with BSSE (a) and with the patched kriging (b).

From a comparison of the results it is possible to affirm that no out-performing spatial model emerges, both in terms of 24 hour mean rainfall depth interpolation (MAE_{BSSE} = 5.3 mm while $MAE_{KRIGING}$ = 3.9 mm) and K-moment estimation (MAE_{BSSE} = 0.00489 while $MAE_{KRIGING}$ = 0.00610). The patched kriging resulted in lower λ estimates compared to BSSE but, conversely, it provided a higher shape parameter ξ.

Ombrian curves were calculated for each gauged station on the basis of BSSE and patched kriging models. Results related to the Trikala station are reported in Figure 7.13, where it is possible to see the theoretical and empirical distributions of annual maximum intensities at 10 minutes to 48 hours scales. Figure 7.13 also

shows the estimates from the order statistics computed with the relationship

$$\frac{T_{(i:n)}}{\Delta} = \frac{n + e^{1-\gamma} - 1}{n - i + e^{-\gamma}} = \frac{n + 0.526}{n - i + 0.561} \tag{7.45}$$

It is possible to observe that the empirical values are in good agreement with the theoretical ones, with some (non-systematic) deviations at higher return periods for some durations in both cases. A clear optimal model can thus not be identified on the basis of these results. However, this is not a drawback of the methodology: these results confirm the robustness of the two approaches.

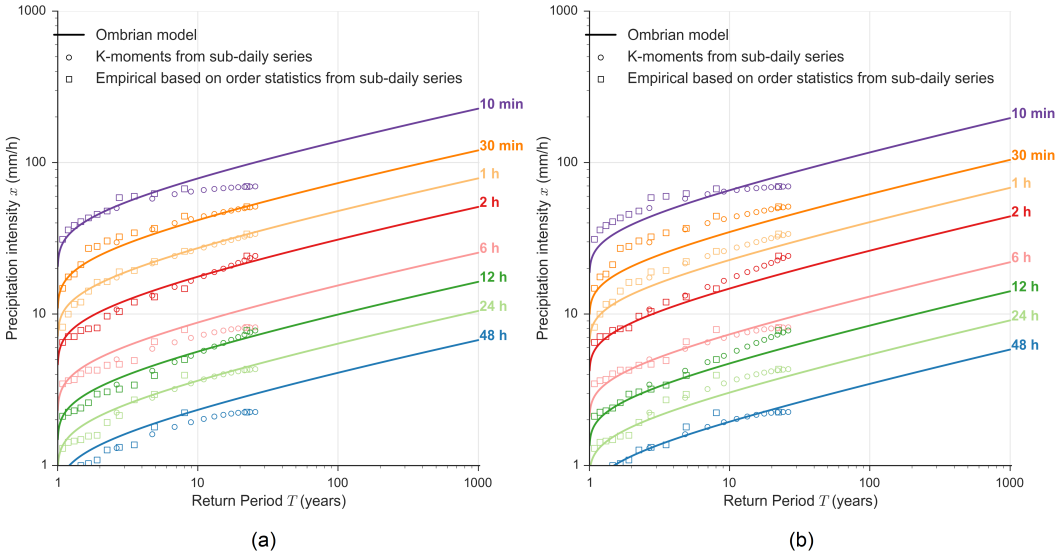

Fig. 7.13 Ombrian curves for Trikala weather station computed on the basis of BSSE (a) and patched kriging (b) models.

7.7 Conclusion

This chapter summarizes the research effort performed to improve currently-available methodologies for the estimation of the design rainfall in ungauged sites also in the presence of short and fragmented records.

This fragmentation is handled with a different approach in the two methods used here. The patched kriging treats each annual maxima as a point in the (x, y, t) space with the aim of reconstructing spatio-temporal information that are consistent with the time series used as an input, without discarding records included in short time

series. The ombrian model, instead, is based on a different concept: in this case, each measurement is used to compute parameters in the (x, y) space, while the time information is here not considered. In this case, a minimum threshold is applied.

The first results reported in Section 7.6 show similar performance in terms of recostruction of the 24 hour index rainfall and K-moment estimation. However, further analyses over bigger and more complex areas are mandatory to draw more reliable conclusions.

Regarding the patched kriging, the results reported in Section 7.3 show improvements when appropriately managing the possible influence of an external variable (elevation, in this case). The four different patched kriging configurations provide results that are coherent but that are different in terms of accuracy. Moreover, Section 7.3 represent a first application of the research work performed in Chapter 6.

The methodologies here discussed provide the basis for a reliable frequency analysis over large areas.

Chapter 8

Conclusions

The work described in this chapter has been partially derived from Mazzoglio et al. (2020), Mazzoglio et al. (2022a), Mazzoglio et al. (2022b), Mazzoglio et al. (2022c), Mazzoglio et al. (2022d) and Claps et al. (2022b).

8.1 Conclusions

Most of the achievements of this dissertation are related to the renovation and use of a national-scale database of short-duration annual maximum rainfall depths, measured since early 1900 from more than 5200 rain gauges. The work described here attempts to provide an updated view of the spatial variability of the rainfall extremes at the national scale, also considering how the local climatology and morphology can be shown to significantly affect this variability. The overall work was performed with the aim of improving currently available rainfall frequency analysis methodologies that are typically developed and applied over relatively small regions.

The state of the art of regionalization techniques applied to rainfall data is first presented in Chapter 2, starting from the identification of today's problems in data availability, and then highlighting the differences between traditional and more innovative approaches aimed to provide the computation of intensity – duration – frequency curves. Considering the significant changes observed over time in station density over large areas, the chapter deals with the advantages of interpolation methods over the homogeneous region paradigm, addressing the valorization of the local information deriving from short or intermittent records.

Chapter 3 describes the methodological approach adopted to build an improved and quality-controlled version of I-RED (in terms of both the rainfall depth values and the position of the rain gauges). The new database can be used as a more reliable research support for the frequency analysis of the rainfall extremes. The so-call Improved Italian - Rainfall Extreme Dataset (I^2-RED) contains rainfall annual maxima rainfall of 1, 3, 6, 12 and 24 h from 1916 to the present, counts more than 5200 rain gauges and has been corroborated by a re-positioning and elevation-checking of 15% of the stations. A descriptive analysis of the 24 h maximum values of the stations is also presented to exemplify additional quality checks and discussing intriguing spatial features of Super-Extreme rainfall events in relation to the local climatology.

As the majority of rainfall measurements in the world is at the daily scale, i.e. related to a specific calendar day and measured over fixed 24 h, a specific research effort is appropriate, considering that, on these data, daily annual maximum rainfall depths (F-maxima) series can be easily obtained. The research goal is to connect these maxima to 24 h annual maximum rainfall depths (S-maxima), which refer to a period starting at any instant, and that is a more useful indicator of the extreme rainfall features, being connected to the maxima of whatever (smaller) duration. The ratio between these extremes, called Hershfield factor (H), has been studied to move from F-maxima to S-maxima, allowing to take advantage of the relevant amount of information included in historical records of daily extremes. In Chapter 4, the possibility of using F-maxima to complement the S-maxima records was investigated over the Po river basin and the Liguria region (North of Italy). The annual H for all the stations and all the years where both the F- and S-maxima are available were computed and analyzed in their temporal and spatial variability. The values of H obtained were similar to those reported in the literature. Their spatial distribution was found related to the geographic position of the stations, allowing the possibility to identify some distinct areas with positive or negative anomalies. The obtained map of the H factor, with interpolated local anomalies, will allow reconstructing the missing S-maxima in stations where only F-maxima are available, and has the potential to improve the knowledge of the spatial variability of sub-daily rainfall extremes.

Before tackling the themes of the quantitative spatial variability of extreme rainfall parameters, in Chapter 5, the results of a national-scale investigation of the presence of trends in the time series has been presented. This work represents one

of the first attempts to deal with this topic using both historical and recent records throughout all Italy. The results confirmed earlier findings (Libertino et al. (2019)), i.e. that rainfall extremes of different durations are not increasing uniformly over Italy, and that separate tendencies emerge in different sectors, even at close distances. Compared to Libertino et al. (2019), the presence of reinforced trends appears to be more relevant.

Chapter 6 addresses the spatial variability of the average of rainfall extremes. This has been undertaken through a systematic study of the relationship between geomorphological forms and the average annual maxima (index rainfall) across the whole of Italy. The dependence of sub-daily rainfall depths on elevation and other landscape indices was first investigated through univariate and multivariate linear regressions. The results of the national-scale regression analysis did not confirm the assumption of elevation being the sole driver of the variability of the index rainfall. The inclusion of other variables, such as longitude, latitude, distance from the coastline, morphological obstructions and mean annual rainfall, contributes to the explanation of a larger percentage of the variance, even though this connection is different for different durations (1 to 24 h). After analyzing the spatial variability of the regression residuals, the analysis was repeated on geomorphological subdivisions of Italy. Comparing the results of the best multivariate regression models with univariate regressions applied to the small zones deriving from morphological subdivisions, we found that "zonal" rainfall–topography relationships outperform the country-wide multiple regressions, offering a more uniform error spatial distribution and allowing the effect of morphology on rainfall extremes to be better reproduced.

In a subsequent evolution of the work, the orographic effect was analyzed through a local regression approach, in which every station become the center of a "local region", using a grid covering the entire Italian territory at 1-km resolution. This approach aims to find general rules that can allow the estimation of the average extreme rainfall in every cell of the national grid, considering a "local sample" made of the few closer stations falling in the reference circle surrounding any cell. Before testing the procedures systematically, several constraints had to be considered to tackle problems such as those determined by the low data density in some parts of Italy (e.g., Sardinia or the lowlands in the Po river basin) or by the extrapolation at low/high elevations. Different criteria for selecting the local sample were examined, using cross-validation to compare the related performances, and always checking the spatial uniformity of the regression residuals. The results obtained allow to produce

detailed maps of the estimated rainfall average extreme throughout Italy and confirm previous findings, such as a generally positive gradient with elevation of the 24 h extremes, and the evidence of negative gradients in large mountainous areas of the 1 h average. With reference to the latter, the use of a local regression approach allows to identify with an increased detail the areas showing the inverse orographic effect, providing material for future investigations on the physical explanation of this empirical evidence. At the same time, the reconstructed maps allow to apply more accurate detrending approaches in the subsequent research steps related to spatial analysis of other statistics of the rainfall extremes, such as the quantiles required for hydrologic design.

In Chapter 7 this last issue is tackled, starting from some practical application that have the role of offering several problems to solve in addressing large-scale rainfall frequency analysis. The case studies have been addressed with the aim to stress currently available methodologies, gathering issues to solve at the national scale, and suggesting possible improvements. Some case studies stem from the necessity to deal, at the regional scale, with the additional knowledge resulting from the occurrence of very severe rainfall events, as those occurred in Sardinia in 2020 and in Liguria in 2021 (the latter broke some of the all-time Italian records). In other words, these analyses are relevant for investigating the need of updating the rainfall quantiles in a region after the occurrence of a major event. In the overall aim of checking the significance of individual methodologies on the final maps of quantiles, a comparison was undertaken between the patched kriging methodology (Libertino et al. (2018a)) and the regional ombrian curves suggested by Iliopoulou et al. (2022) over the Thessaly region. As no outperforming model emerged, it was concluded that although the development of IDF curves has been a widely investigated topic for about one hundred years, clear guidelines and standardized and universal approaches for the selection of a regional rainfall frequency model are still needed.

The Improved Italian - Rainfall Extreme Dataset was also used in other research studies, not discussed in this dissertation. It is worth mentioning:

- a project funded by the "Autorità di Bacino Distrettuale del Fiume Po" for the development of updated rainfall and flood frequency analyses in the Po River basin, also taking into account the influence of climate change scenarios;

- a project funded by the "Autorità di Bacino Distrettuale dell'Appennino Meridionale" for the development of an updated rainfall frequency analysis over Southern Italy;
- the development of the first Italian database of geomorphological, climatological and land use/cover attributes (Claps et al. (2022a));
- the ranking of the Italian dams based on their flood attenuation potential (Evangelista et al. (2022)).

A discussion of the possible developments emerging from this dissertation involves several "layers" that are expounded below.

In terms of the description of the empirical evidence of the spatial distribution of the "Super- Extremes", as described in Chapter 3, more work could be dedicated to the assessment of the nature and the behavior of quasi-maxima, using comparisons between n and n-1 ranked extremes. Also, extremes for durations shorter than 24 hours should be considered.

Regarding the computation of the Hershfield factor described in Chapter 4, further work could be addressed to apply the methodology described in Papalexiou et al. (2016), where an approach that simultaneously corrects both the mean and the standard deviation errors is proposed.

One of the main limitations of the work described in Chapter 5 is the non-uniform temporal coverage of dataset, due to extremely fragmented data acquisition policies and also a considerable variability in the delay in the publication of validated data from the regional hydrological agencies. Future work could be addressed to: i) the investigation of the influence of a threshold record length (20, 30 or 40 years, as an example) applied to select only the longer time series; ii) investigate if different results are obtained when reducing the period under investigation or when using also the values reconstructed with the patched kriging; iii) the research of new methods for delineating areas needed to pool data and apply the record-breaking analysis and the regional Kendall test in search of trends of rainfall extremes. In the latter case, the geomorphological classifications introduced in Chapter 6 could provide a research path.

The 24 h extremes reconstructed by applying the Hershfield factor could also be integrated in the dataset used in Chapter 6 and 7. Further work could be performed

with the aim of investigating: i) the influence of elevation on the index rainfall and ii) if the 24 h extremes reconstructed using the Hershfield factor can improve the estimates performed with the patched kriging. If some improvements, especially in orographically-complex areas are achieved, an extension of the computation of the Hershfield factor all over Italy would become advisable.

One of the main open points concerning the practical needs related to the themes of this dissertation is the investigation of the influence of a single, major event on the overall rainfall frequency map over an area. This is something that has been already pointed out for example in Germany (Shehu et al. (2022)) but that, up to now, still requires efforts to be understood. Providing a unique answer that can be relevant for regions with very different geographic and morphological features, as is the case of Italy, is a challenge worth to deal with. In this dissertation a preliminary investigation is performed for the Liguria case study taking into account the 2021 annual maxima and weather radar. The combined analysis of data from raingauges and radar, already available in some literature works, is another research direction that has a great potential to provide answers to this issue.

Future work could also be addressed to improve the terms of comparisons between rainfall frequency analysis models over large and complex areas. Reliable metrics related to the sensitivity and uncertainty of different rainfall quantiles are to be developed, to clarify the terms of transferability to research achievements to the end users, that await new and more reliable methods to update the available design rainfall in a perspective of climate change.

References

Accorsi, S. (2016). SOIUSA (Suddivisione Internazionale Unificata del Sistema Alpino) classification. ARPA Piemonte [dataset], https://webgis.arpa.piemonte.it/geoportalserver_arpa/catalog/search/resource/details.page?uuid=ARLPA_TO:12.03.01-D_2016-09-20-15:00&title=Arpa%20Piemonte%20-%20Suddivisione%20Orografica%20Internazionale%20Unificata%20del%20Sistema%20Alpino%20-%20SOIUSA, accessed on 13th November 2022.

Acreman, M. and Wiltshire, S. (1989). The regions are dead. Long live the regions. Methods of identifying and dispensing with regions for flood frequency analysis. In Roald, L., Nordseth, K., and Hassel, K., editors, *FRIENDS in Hydrology*. IAHS-AISH Publication 187.

Adler, A. (2015). Strong laws for ratios of order statistics from exponentials. *Bulletin of the Institute of Mathematics Academia Sinica (New Series)*, 10(1):101–111.

Agrillo, G. and Bonati, V. (2013). *Atlante climatico della Liguria*. ARPAL - Centro Funzionale Meteoidrologico di Protezione Civile.

Ahmed, S. and De Marsily, G. (1987). Comparison of geostatistical methods for estimating transmissivity using data on transmissivity and specific capacity. *Water Resources Research*, 23(9):1717–1737.

Alila, Y. (1999). A hierarchical approach for the regionalization of precipitation annual maxima in Canada. *Journal of Geophysical Research: Atmospheres*, 104(D24):31645–31655.

Allamano, P., Claps, P., Laio, F., and Thea, C. (2009). A data-based assessment of the dependence of short-duration precipitation on elevation. *Physics and Chemistry of the Earth, Parts A/B/C*, 34(10):635–641.

Alvioli, M., Guzzetti, F., and Marchesini, I. (2020). Parameter-free delineation of slope units and terrain subdivision of Italy. *Geomorphology*, 358:107124.

Alvioli, M., Marchesini, I., Reichenbach, P., Rossi, M., Ardizzone, F., Fiorucci, F., and Guzzetti, F. (2016). Automatic delineation of geomorphological slope units with `r.slopeunits v1.0` and their optimization for landslide susceptibility modeling. *Geoscientific Model Development*, 9(11):3975–3991.

Amadei, M., Bagnaia, R., Laureti, L., Lugeri, F., Lugeri, N., Feoli, E., Dragan, M., Fernetti, M., and Oriolo, G. (2003). *Il Progetto Carta della Natura alla scala 1:250,000*. APAT - Agenzia per la Protezione dell'Ambiente e per i Servizi Tecnici, Roma (Italy).

Arnone, E., Pumo, D., Viola, F., Noto, L. V., and La Loggia, G. (2013). Rainfall statistics changes in Sicily. *Hydrology and Earth System Sciences*, 17(7):2449–2458.

Avanzi, F., De Michele, C., Gabriele, S., Ghezzi, A., and Rosso, R. (2015). Orographic signature on extreme precipitation of short durations. *Journal of Hydrometeorology*, 16(1):278–294.

Basist, A., Bell, G. D., and Meentemeyer, V. (1994). Statistical relationships between topography and precipitation patterns. *Journal of Climate*, 7(9):1305–1315.

Beguería, S. and Vicente-Serrano, S. M. (2006). Mapping the hazard of extreme rainfall by peaks over threshold extreme value analysis and spatial regression techniques. *Journal of Applied Meteorology and Climatology*, 45(1):108 – 124.

Bernard, M. M. (1932). Formulas for rainfall intensities of long duration. *Transactions of the American Society of Civil Engineers*, 96(1):592–606.

Berndt, C., Rabiei, E., and Haberlandt, U. (2014). Geostatistical merging of rain gauge and radar data for high temporal resolutions and various station density scenarios. *Journal of Hydrology*, 508:88–101.

Blöschl, G. (2011). Scaling and regionalization in hydrology. In Wilderer, P., editor, *Treatise on Water Science*, pages 519–535. Elsevier, Oxford.

Bonaccorso, B., Cancelliere, A., and Rossi, G. (2005). Detecting trends of extreme rainfall series in Sicily. *Advances in Geosciences*, 2:7–11.

Bonanno, R., Lacavalla, M., and Sperati, S. (2019). A new high-resolution Meteorological Reanalysis Italian Dataset: MERIDA. *Quarterly Journal of the Royal Meteorological Society*, 145(721):1756–1779.

Borga, M., Vezzani, C., and Dalla Fontana, G. (2005). Regional rainfall depth-duration-frequency equations for an alpine region. *Natural Hazards*, 36(1):221–235.

Braca, G., Bussettini, M., Lastoria, B., Mariani, S., and Piva, F. (2021). Elaborazioni modello BIGBANG versione 4.0. Istituto Superiore per la Protezione e la Ricerca Ambientale – ISPRA [dataset], https://groupware.sinanet.isprambiente.it/bigbang-data/library/bigbang40, accessed on 13th November 2022.

Brunsdon, C., McClatchey, J., and Unwin, D. (2001). Spatial variations in the average rainfall–altitude relationship in Great Britain: an approach using geographically weighted regression. *International Journal of Climatology*, 21(4):455–466.

Burlando, P. and Rosso, R. (1996). Scaling and multiscaling models of depth-duration-frequency curves for storm precipitation. *Journal of Hydrology*, 187(1):45–64.

Burn, D. H. (1990). Evaluation of regional flood frequency analysis with a region of influence approach. *Water Resources Research*, 26(10):2257–2265.

Caracciolo, D., Lo Conti, F., Francipane, A., Cannarozzo, M., and La Loggia, G. (2012). L'influenza della morfologia sulla distribuzione delle piogge intense. In *Proceedings of the XXXIII Convegno Nazionale di Idraulica e Costruzioni Idrauliche, Brescia (Italy)*, pages 10–15.

Carey-Smith, T., Henderson, R., and Singh, S. (2018). High intensity rainfall design system version 4. Technical report, National Institute of Water and Atmospheric Research Ltd (NIWA).

Carreau, J., Neppel, L., Arnaud, P., and Cantet, P. (2013). Extreme rainfall analysis at ungauged sites in the South of France: Comparison of three approaches. *Journal de la société française de statistique*, 154(2):119–138.

Cavicchia, L., von Storch, H., and Gualdi, S. (2014). A long-term climatology of medicanes. *Climate dynamics*, 43(5):1183–1195.

Centro Funzionale Regione Autonoma Valle d'Aosta and Fondazione CIMA (2009). Rapporto tecnico-scientifico della regionalizzazione delle precipitazioni intense. Technical report, Fondazione CIMA.

Cesarini, L. and Martina, M. L. V. (2019). Are the short and intense precipitations in North of Italy affected by a significant trend? In *Climate Risk: Implications for Ecosystem Services and Society, Challenges, Solutions. SISC Seventh Annual Conference, Trento (Italy)*.

Cifrodelli, M., Corradini, C., Morbidelli, R., Saltalippi, C., and Flammini, A. (2015). The influence of climate change on heavy rainfalls in Central Italy. *Procedia Earth and Planetary Science*, 15:694–701. World Multidisciplinary Earth Sciences Symposium, WMESS 2015.

Claps, P., Barberis, C., Agostino, M. D., Gallo, E., Laguardia, G., Laio, F., Miotto, F., Plebani, F., Vezzù, G., Viglione, A., and Zanetta, M. (2008). Development of an Information System of the Italian basins for the CUBIST project. In *EGU General Assembly 2008*.

Claps, P., Brunetto, M., Evangelista, G., Mazzoglio, P., and Monforte, I. (2022a). FaBI: A new collection of flood data and attributes of basins in Italy. In *EGU General Assembly 2022*.

Claps, P., Ganora, D., and Mazzoglio, P. (2022b). Rainfall regionalization techniques. In Morbidelli, R., editor, *Rainfall*, pages 327–350. Elsevier.

Claps, P. and Laio, F. (2003). Can continuous streamflow data support flood frequency analysis? An alternative to the partial duration series approach. *Water Resources Research*, 39(8).

Claps, P., Laio, F., Allamano, P., Libertino, A., and Iavarone, M. (2015). Attività di ricerca nell'ambito del progetto Strada 2.0 Modulo CAPPIO (capitalizzazione azione di caratterizzazione delle piogge estreme). Technical report, Consorzio Interuniversitario per l'Idrologia (CINID), Potenza, Italy.

Claps, P. and Siccardi, F. (1999). *Mediterranean storms*. BIOS, Cosenza (Italy).

Cole, G. (1966). An application of the regional analysis of flood flows. In *River Flood Hydrology*, pages 39–57.

Crespi, A., Brunetti, M., Lentini, G., and Maugeri, M. (2018). 1961–1990 high-resolution monthly precipitation climatologies for Italy. *International Journal of Climatology*, 38(2):878–895.

Crespi, A., Brunetti, M., Ranzi, R., Tomirotti, M., and Maugeri, M. (2021). A multi-century meteo-hydrological analysis for the Adda river basin (Central Alps). Part I: Gridded monthly precipitation (1800–2016) records. *International Journal of Climatology*, 41(1):162–180.

Creutin, J. D. and Obled, C. (1982). Objective analyses and mapping techniques for rainfall fields: an objective comparison. *Water Resources Research*, 18(2):413–431.

Crisci, A., Gozzini, B., Meneguzzo, F., Pagliara, S., and Maracchi, G. (2002). Extreme rainfall in a changing climate: regional analysis and hydrological implications in Tuscany. *Hydrological Processes*, 16(6):1261–1274.

Cuomo, A., Guida, D., and Palmieri, V. (2011). Digital orographic map of peninsular and insular Italy. *Journal of Maps*, 7(1):447–463.

Dalrymple, T. (1960). Flood-frequency analyses. manual of hydrology: part 3. flood-flow techniques. Technical report, United States Government Printing Office, Washington (United States).

Daly, C. (2006). Guidelines for assessing the suitability of spatial climate data sets. *International Journal of Climatology*, 26(6):707–721.

Daly, C., Gibson, W. P., Taylor, G. H., Johnson, G. L., and Pasteris, P. (2002). A knowledge-based approach to the statistical mapping of climate. *Climate research*, 22(2):99–113.

Daly, C., Neilson, R. P., and Phillips, D. L. (1994). A statistical-topographic model for mapping climatological precipitation over mountainous terrain. *Journal of Applied Meteorology and Climatology*, 33(2):140–158.

Das, S. (2019). Extreme rainfall estimation at ungauged sites: Comparison between region-of-influence approach of regional analysis and spatial interpolation technique. *International Journal of Climatology*, 39(1):407–423.

Davolio, S., Fera, S. D., Laviola, S., Miglietta, M. M., and Levizzani, V. (2020). Heavy precipitation over Italy from the Mediterranean storm "Vaia" in October 2018: Assessing the role of an atmospheric river. *Monthly Weather Review*, 148(9):3571–3588.

Dayan, U., Nissen, K., and Ulbrich, U. (2015). Review article: Atmospheric conditions inducing extreme precipitation over the eastern and western Mediterranean. *Natural Hazards and Earth System Sciences*, 15(11):2525–2544.

De Marsily, G. (1986). *Quantitative Hydrogeology: Groundwater Hydrology for EngineerS*. Academic Press, Orlando.

Deidda, R. (2021). Personal communication.

Deidda, R. (2022). Sugli studi degli eventi estremi di precipitazione in Sardegna. *L'Acqua*, 1.

Deidda, R., Hellies, M., and Langousis, A. (2021). A critical analysis of the shortcomings in spatial frequency analysis of rainfall extremes based on homogeneous regions and a comparison with a hierarchical boundaryless approach. *Stochastic Environmental Research and Risk Assessment*, 35(12):2605–2628.

Deidda, R., Palomba, A., Piga, E., and Sechi, G. M. (2002). Utilizzazione delle registrazioni su supporto magnetico dell'informazione pluviometrica: creazione di un database e prime analisi comparative. *Quaderni di Ricerca, Dipartimento di Ingegneria del Territorio, Università di Cagliari*, pages 1–35.

Deidda, R. and Piga, E. (1998). Curve di possibilità pluviometrica basate sul modello TCEV. *Informazione*, 81:9–14.

Di Baldassarre, G., Laio, F., and Montanari, A. (2009). Design flood estimation using model selection criteria. *Physics and Chemistry of the Earth, Parts A/B/C*, 34(10):606–611.

Di Piazza, A., Conti, F. L., Noto, L., Viola, F., and La Loggia, G. (2011). Comparative analysis of different techniques for spatial interpolation of rainfall data to create a serially complete monthly time series of precipitation for Sicily, Italy. *International Journal of Applied Earth Observation and Geoinformation*, 13(3):396–408.

Diodato, N. and Ceccarelli, M. (2005). Interpolation processes using multivariate geostatistics for mapping of climatological precipitation mean in the Sannio Mountains (southern Italy). *Earth Surface Processes and Landforms*, 30(3):259–268.

Dwyer, I. J. and Reed, D. W. (1995). Correcting mean annual maxima for data discretization. *Proceeding of the 6th International Meeting on Statistical Climatology, Galway (Ireland)*, pages 447–450.

European Environment Agency (2016). European Digital Elevation Model (EU-DEM), version 1.1. Copernicus programme [dataset], https://land.copernicus.eu/imagery-in-situ/eu-dem/eu-dem-v1.1?tab=mapview, accessed on 13th November 2022.

Evangelista, G., Mazzoglio, P., Pianigiani, F., and Claps, P. (2022). Towards the assessment of the flood attenuation potential of Italian dams: first steps and sensitivity to basic model features. In *Proceedings of the 39th IAHR World Congress, Granada (Spain)*.

Farr, T. G., Rosen, P. A., Caro, E., Crippen, R., Duren, R., Hensley, S., Kobrick, M., Paller, M., Rodriguez, E., Roth, L., Seal, D., Shaffer, S., Shimada, J., Umland, J., Werner, M., Oskin, M., Burbank, D., and Alsdorf, D. (2007). The Shuttle Radar Topography Mission. *Reviews of Geophysics*, 45(2).

Faulkner, D. (1999). *Flood Estimation Handbook: Rainfall frequency estimation. Volume 2*. Institute of Hydrology.

Faulkner, D. S. and Prudhomme, C. (1998). Mapping an index of extreme rainfall across the UK. *Hydrology and Earth System Sciences*, 2(2/3):183–194.

Fick, S. E. and Hijmans, R. J. (2017). Worldclim 2: new 1-km spatial resolution climate surfaces for global land areas. *International Journal of Climatology*, 37(12):4302–4315.

Fiori, E., Comellas, A., Molini, L., Rebora, N., Siccardi, F., Gochis, D., Tanelli, S., and Parodi, A. (2014). Analysis and hindcast simulations of an extreme rainfall event in the Mediterranean area: The Genoa 2011 case. *Atmospheric Research*, 138:13–29.

Forestieri, A., Lo Conti, F., Blenkinsop, S., Cannarozzo, M., Fowler, H. J., and Noto, L. V. (2018). Regional frequency analysis of extreme rainfall in Sicily (Italy). *International Journal of Climatology*, 38(S1):e698–e716.

Formetta, G., Marra, F., Dallan, E., Zaramella, M., and Borga, M. (2022). Differential orographic impact on sub-hourly, hourly, and daily extreme precipitation. *Advances in Water Resources*, 159:104085.

Fotheringham, A. S., Brunsdon, C., and Charlton, M. (2003). *Geographically weighted regression: the analysis of spatially varying relationships*. John Wiley & Sons.

Fouedjio, F. (2017). Second-order non-stationary modeling approaches for univariate geostatistical data. *Stochastic Environmental Research and Risk Assessment*, 31:1887–1906.

Fowler, H. J., Lenderink, G., Prein, A. F., Westra, S., Allan, R. P., Ban, N., Barbero, R., Berg, P., Blenkinsop, S., Do, H. X., et al. (2021a). Anthropogenic intensification of short-duration rainfall extremes. *Nature Reviews Earth & Environment*, 2(2):107–122.

Fowler, H. J., Wasko, C., and Prein, A. F. (2021b). Intensification of short-duration rainfall extremes and implications for flood risk: current state of the art and future directions. *Philosophical Transactions of the Royal Society A: Mathematical, Physical and Engineering Sciences*, 379(2195):20190541.

Frei, C. and Schär, C. (1998). A precipitation climatology of the Alps from high-resolution rain-gauge observations. *International Journal of Climatology*, 18(8):873–900.

Furcolo, P. and Pelosi, A. (2018). Orographic effects on extreme rainfall at different durations: a case study in Campania region (Southern Italy). *Journal of Geoscience and Environment Protection*, 6(11):77–88.

Furcolo, P., Pelosi, A., and Rossi, F. (2016). Statistical identification of orographic effects in the regional analysis of extreme rainfall. *Hydrological Processes*, 30(9):1342–1353.

Furcolo, P., Villani, P., and Rossi, F. (1995). Statistical analysis of the spatial variability of very extreme rainfall in the Mediterranean area. In *Proceedings of the US-Italy Research Workshop on the Hydrometeorology, Impacts and Management of extreme floods, Perugia (Italy)*.

Gaál, L., Kyselý, J., and Szolgay, J. (2008). Region-of-influence approach to a frequency analysis of heavy precipitation in Slovakia. *Hydrology and Earth System Sciences*, 12(3):825–839.

Ganora, D. and Laio, F. (2016). A comparison of regional flood frequency analysis approaches in a simulation framework. *Water Resources Research*, 52(7):5644–5661.

Glick, N. (1978). Breaking records and breaking boards. *The American Mathematical Monthly*, 85(1):2–26.

GNDCI Linea 1 (2001). Rapporto di sintesi sulla valutazione delle piene in Italia. Technical report, Consiglio Nazionale delle Ricerche (CNR).

Golzio, A., Crespi, A., Bollati, I. M., Senese, A., Diolaiuti, G. A., Pelfini, M., and Maugeri, M. (2018). High-resolution monthly precipitation fields (1913–2015) over a complex mountain area centred on the Forni Valley (Central Italian Alps). *Advances in Meteorology*, 2018.

Goovaerts, P. (1999). Using elevation to aid the geostatistical mapping of rainfall erosivity. *CATENA*, 34(3):227–242.

Goovaerts, P. (2000). Geostatistical approaches for incorporating elevation into the spatial interpolation of rainfall. *Journal of Hydrology*, 228(1):113–129.

Goudenhoofdt, E., Delobbe, L., and Willems, P. (2017). Regional frequency analysis of extreme rainfall in Belgium based on radar estimates. *Hydrology and Earth System Sciences*, 21(10):5385–5399.

Grasso, S., Libertino, A., and Claps, P. (2020). MultiRain: a GIS-based tool for multi-model estimation of regional design rainfall for scientists and practitioners. *Journal of Hydroinformatics*, 22(1):148–159.

Greco, A., De Luca, D. L., and Avolio, E. (2020). Heavy precipitation systems in Calabria region (Southern Italy): High-resolution observed rainfall and large-scale atmospheric pattern analysis. *Water*, 12(5).

Grimaldi, S., Kao, S. C., Castellarin, A., Papalexiou, S. M., Viglione, A., Laio, F., Aksoy, H., and Gedikli, A. (2011). Statistical hydrology. In Wilderer, P., editor, *Treatise on Water Science*, pages 479–517. Elsevier, Oxford.

Grimes, D. I. F. and Pardo-Igúzquiza, E. (2010). Geostatistical analysis of rainfall. *Geographical Analysis*, 42(2):136–160.

Gumbel, E. J. (1954). Statistical theory of extreme values and some practical applications. Technical report, United States Government Printing Office.

Guzzetti, F. and Reichenbach, P. (1994). Towards a definition of topographic divisions for Italy. *Geomorphology*, 11(1):57–74.

Harihara Ayyar, P. and Tripathi, N. (1973). Relationship of the clock-hour to 60-min and the observational day to 1440-min rainfall. *Indian Journal of Meteorology, Hydrology and Geophysics*, 24(3):279–282.

Helsel, D. R. and Frans, L. M. (2006). Regional Kendall test for trend. *Environmental Science & Technology*, 40(13):4066–4073.

Hemelrijk, J. (1966). Underlining random variables. *Statistica Neerlandica*, 20(1):1–7.

Hengl, T. (2007). A practical guide to geostatistical mapping of environmental variables. Technical report, Office for Official Publications of the European Communities, Luxembourg, Luxembourg.

Hengl, T., Heuvelink, G., and Stein, A. (2003). Comparison of kriging with external drift and regression-kriging. Technical report, International Institute for Geoinformation Science and Earth Observation (ITC), Netherlands.

Hershfield, D. M. (1961). Technical paper no. 40: Rainfall frequency atlas of the United States. Technical report, United States Department of Agriculture, Soil Conservation Service Engineering Division.

Hosking, J. R. M. (1990). L-moments: Analysis and estimation of distributions using linear combinations of order statistics. *Journal of the Royal Statistical Society: Series B (Methodological)*, 52(1):105–124.

Hosking, J. R. M. and Wallis, J. R. (1988). The effect of intersite dependence on regional flood frequency analysis. *Water Resources Research*, 24(4):588–600.

Hosking, J. R. M. and Wallis, J. R. (1997). *Regional frequency analysis: an approach based on L-Moments*. Cambridge University Press, Cambridge.

Hudson, G. and Wackernagel, H. (1994). Mapping temperature using kriging with external drift: Theory and an example from Scotland. *International Journal of Climatology*, 14(1):77–91.

Iliopoulou, T., Malamos, N., and Koutsoyiannis, D. (2022). Regional ombrian curves: Design rainfall estimation for a spatially diverse rainfall regime. *Hydrology*, 9(5).

IPCC (2021). Summary for policymakers. In *Climate Change 2021: The Physical Science Basis. Contribution of Working Group I to the Sixth Assessment Report of the Intergovernmental Panel on Climate Change*. Cambridge University Press, Cambridge, United Kingdom and New York, NY, USA.

Isotta, F. A., Frei, C., Weilguni, V., Perčec Tadić, M., Lassègues, P., Rudolf, B., Pavan, V., Cacciamani, C., Antolini, G., Ratto, S. M., Munari, M., Micheletti, S., Bonati, V., Lussana, C., Ronchi, C., Panettieri, E., Marigo, G., and Vertačnik, G. (2014). The climate of daily precipitation in the Alps: development and analysis of a high-resolution grid dataset from pan-alpine rain-gauge data. *International Journal of Climatology*, 34(5):1657–1675.

Iwahashi, J. and Pike, R. J. (2007). Automated classifications of topography from DEMs by an unsupervised nested-means algorithm and a three-part geometric signature. *Geomorphology*, 86(3):409–440.

Kašpar, M., Bližňák, V., Hulec, F., and Müller, M. (2021). High-resolution spatial analysis of the variability in the subdaily rainfall time structure. *Atmospheric Research*, 248:105202.

Kidd, C., Becker, A., Huffman, G. J., Muller, C. L., Joe, P., Skofronick-Jackson, G., and Kirschbaum, D. B. (2017). So, how much of the Earth's surface is covered by rain gauges? *Bulletin of the American Meteorological Society*, 98(1):69–78.

Kitanidis, P. (1997). *Introduction to Geostatistics: Applications in Hydrogeology*. Cambridge University Press.

Konrad II, C. E. (1996). Relationships between precipitation event types and topography in the southern Blue Ridge mountains of the southeastern USA. *International Journal of Climatology*, 16(1):49–62.

Kottegoda, N. T. and Rosso, R. (2008). *Applied statistics for civil and environmental engineers*. Blackwell Publishing.

Koutsoyiannis, D. (2019). Knowable moments for high-order stochastic characterization and modelling of hydrological processes. *Hydrological Sciences Journal*, 64(1):19–33.

Koutsoyiannis, D. (2020). *Stochastics of Hydroclimatic Extremes*. National Technical University of Athens, Athens (Greece).

Koutsoyiannis, D. and Iliopoulou, T. (2022). Ombrian curves advanced to stochastic modeling of rainfall intensity. In Morbidelli, R., editor, *Rainfall*, pages 261–284. Elsevier.

Koutsoyiannis, D., Kozonis, D., and Manetas, A. (1998). A mathematical framework for studying rainfall intensity-duration-frequency relationships. *Journal of Hydrology*, 206(1):118–135.

Laio, F., Allamano, P., and Claps, P. (2010). Exploiting the information content of hydrological "outliers" for goodness-of-fit testing. *Hydrology and Earth System Sciences*, 14(10):1909–1917.

Laio, F., Ganora, D., Claps, P., and Galeati, G. (2011). Spatially smooth regional estimation of the flood frequency curve (with uncertainty). *Journal of Hydrology*, 408(1):67–77.

Le Gall, P., Favre, A.-C., Naveau, P., and Prieur, C. (2022). Improved regional frequency analysis of rainfall data. *Weather and Climate Extremes*, 36:100456.

Lehmann, J., Coumou, D., and Frieler, K. (2015). Increased record-breaking precipitation events under global warming. *Climatic Change*, 132(4):501–515.

Li, H., Sun, J., Zhang, H., Zhang, J., Jung, K., Kim, J., Xuan, Y., Wang, X., and Li, F. (2018). What large sample size is sufficient for hydrologic frequency analysis?—a rational argument for a 30-year hydrologic sample size in water resources management. *Water*, 10(4).

Libertino, A. (2017). *Advances in the space-time analysis of rainfall extremes*. PhD thesis, Politecnico di Torino (Italy).

Libertino, A., Allamano, P., Laio, F., and Claps, P. (2018a). Regional-scale analysis of extreme precipitation from short and fragmented records. *Advances in Water Resources*, 112:147–159.

Libertino, A., Ganora, D., and Claps, P. (2018b). Technical note: Space-time analysis of rainfall extremes in Italy: clues from a reconciled dataset. *Hydrology and Earth System Sciences*, 22(5):2705–2715.

Libertino, A., Ganora, D., and Claps, P. (2019). Evidence for increasing rainfall extremes remains elusive at large spatial scales: The case of Italy. *Geophysical Research Letters*, 46(13):7437–7446.

Libertino, A., Macchia, S., and Claps, P. (2016). Nubifragi eccezionali in Italia: Analisi preliminare di rilevanza sugli eventi 1920-2000. In *Proceedings of the XXXV Convegno Nazionale di Idraulica e Costruzioni Idrauliche, Bologna (Italy)*, pages 14–16.

Llabrés-Brustenga, A., Rius, A., Rodríguez-Solà, R., and Casas-Castillo, M. C. (2020). Influence of regional and seasonal rainfall patterns on the ratio between fixed and unrestricted measured intervals of rainfall amounts. *Theoretical and Applied Climatology*, 140:389–399.

Lombardo, F., Volpi, E., Koutsoyiannis, D., and Papalexiou, S. M. (2014). Just two moments! A cautionary note against use of high-order moments in multifractal models in hydrology. *Hydrology and Earth System Sciences*, 18(1):243–255.

Madsen, H., Rasmussen, P. F., and Rosbjerg, D. (1997). Comparison of annual maximum series and partial duration series methods for modeling extreme hydrologic events: 1. at-site modeling. *Water Resources Research*, 33(4):747–757.

Malamos, N. and Koutsoyiannis, D. (2016a). Bilinear surface smoothing for spatial interpolation with optional incorporation of an explanatory variable. Part 1: Theory. *Hydrological Sciences Journal*, 61(3):519–526.

Malamos, N. and Koutsoyiannis, D. (2016b). Bilinear surface smoothing for spatial interpolation with optional incorporation of an explanatory variable. Part 2: Application to synthesized and rainfall data. *Hydrological Sciences Journal*, 61(3):527–540.

Mann, H. B. (1945). Nonparametric tests against trend. *Econometrica: Journal of the econometric society*, pages 245–259.

Marani, M. (2003). On the correlation structure of continuous and discrete point rainfall. *Water Resources Research*, 39(5).

Marani, M. and Zanetti, S. (2015). Long-term oscillations in rainfall extremes in a 268 year daily time series. *Water Resources Research*, 51(1):639–647.

Marra, F., Armon, M., Borga, M., and Morin, E. (2021). Orographic effect on extreme precipitation statistics peaks at hourly time scales. *Geophysical Research Letters*, 48(5):e2020GL091498.

Matheron, G. (1963). Principles of geostatistics. *Economic Geology*, 58:1246–1266.

Mazzoglio, P., Butera, I., Alvioli, M., and Claps, P. (2022a). The role of morphology in the spatial distribution of short-duration rainfall extremes in Italy. *Hydrology and Earth System Sciences*, 26(6):1659–1672.

Mazzoglio, P., Butera, I., and Claps, P. (2020). I^2-RED: A massive update and quality control of the Italian annual extreme rainfall dataset. *Water*, 12(12).

Mazzoglio, P., Claps, P., Iliopoulou, T., Dimitriadis, P., Malamos, N., Butera, I., and Koutsoyiannis, D. (2022b). Estimation of the design rainfall in ungauged sites using novel regionalization approaches: an application over Thessaly region, Greece. In *STAHY2022 – 12th International Workshop on Statistical Hydrology, Chia (Italy), 17-20 September 2022*.

Mazzoglio, P., Ganora, D., and Claps, P. (2022c). Long-term spatial and temporal rainfall trends over Italy. *Environmental Sciences Proceedings*, 21(1).

Mazzoglio, P., Volpini, G., Deidda, R., and Claps, P. (2022d). Stima multi-modello della severità di un evento alluvionale: il caso di Bitti, novembre 2020. In *Proceedings of the XXXVIII Convegno Nazionale di Idraulica e Costruzioni Idrauliche, Reggio Calabria (Italy), 4-7 September 2022*.

Meybeck, M., Green, P., and Vörösmarty, C. (2001). A new typology for mountains and other relief classes: An application to global continental water resources and population distribution. *Mountain Research and Development*, 21:34–45.

Modarres, R. and Sarhadi, A. (2011). Statistically-based regionalization of rainfall climates of Iran. *Global and Planetary Change*, 75(1):67–75.

Montgomery, D. C., Peck, E. A., and Vining, G. G. (2012). *Introduction to linear regression analysis*. John Wiley & Sons.

Morbidelli, R., Saltalippi, C., Dari, J., and Flammini, A. (2021). A review on rainfall data resolution and its role in the hydrological practice. *Water*, 13(8).

Muñoz Sabater, J. (2019). ERA5-Land hourly data from 1950 to present. Copernicus Climate Change Service (C3S) Climate Data Store (CDS) [dataset], https://doi.org/10.24381/cds.e2161bac, accessed on 13th November 2022.

Naghettini, M. and Pinto, E. J. d. A. (2017). *Regional Frequency Analysis of Hydrologic Variables*, pages 441–495. Springer International Publishing, Cham.

Napoli, A., Crespi, A., Ragone, F., Maugeri, M., and Pasquero, C. (2019). Variability of orographic enhancement of precipitation in the Alpine region. *Scientific reports*, 9(1):1–8.

Nash, J. and Sutcliffe, J. (1970). River flow forecasting through conceptual models part I — A discussion of principles. *Journal of Hydrology*, 10(3):282–290.

Ngongondo, C. S., Xu, C.-Y., Tallaksen, L. M., Alemaw, B., and Chirwa, T. (2011). Regional frequency analysis of rainfall extremes in Southern Malawi using the index rainfall and L-moments approaches. *Stochastic Environmental Research and Risk Assessment*, 25:939–955.

Ochoa-Rodriguez, S., Wang, L.-P., Willems, P., and Onof, C. (2019). A review of radar-rain gauge data merging methods and their potential for urban hydrological applications. *Water Resources Research*, 55(8):6356–6391.

Ouali, D., Chebana, F., and Ouarda, T. B. M. J. (2016). Quantile regression in regional frequency analysis: A better exploitation of the available information. *Journal of Hydrometeorology*, 17(6):1869–1883.

Papalexiou, S. M., Dialynas, Y. G., and Grimaldi, S. (2016). Hershfield factor revisited: Correcting annual maximum precipitation. *Journal of Hydrology*, 542:884–895.

Pappas, C., Papalexiou, S. M., and Koutsoyiannis, D. (2014). A quick gap filling of missing hydrometeorological data. *Journal of Geophysical Research: Atmospheres*, 119(15):9290–9300.

Pavan, V., Antolini, G., Barbiero, R., Berni, N., Brunier, F., Cacciamani, C., Cagnati, A., Cazzuli, O., Cicogna, A., De Luigi, C., et al. (2019). High resolution climate precipitation analysis for north-central Italy, 1961-2015. *Climate Dynamics*, 52(5):3435–3453.

Pellicone, G., Caloiero, T., Modica, G., and Guagliardi, I. (2018). Application of several spatial interpolation techniques to monthly rainfall data in the Calabria region (southern Italy). *International Journal of Climatology*, 38(9):3651–3666.

Pelosi, A. and Furcolo, P. (2015). An amplification model for the regional estimation of extreme rainfall within orographic areas in Campania region (Italy). *Water*, 7(12):6877–6891.

Pelosi, A., Furcolo, P., Rossi, F., and Villani, P. (2020). The characterization of extraordinary extreme events (EEEs) for the assessment of design rainfall depths with high return periods. *Hydrological Processes*, 34(11):2543–2559.

Persiano, S., Ferri, E., Antolini, G., Domeneghetti, A., Pavan, V., and Castellarin, A. (2020). Changes in seasonality and magnitude of sub-daily rainfall extremes in Emilia-Romagna (Italy) and potential influence on regional rainfall frequency estimation. *Journal of Hydrology: Regional Studies*, 32:100751.

Prudhomme, C. and Reed, D. W. (1998). Relationships between extreme daily precipitation and topography in a mountainous region: a case study in Scotland. *International Journal of Climatology*, 18(13):1439–1453.

Prudhomme, C. and Reed, D. W. (1999). Mapping extreme rainfall in a mountainous region using geostatistical techniques: a case study in Scotland. *International Journal of Climatology*, 19(12):1337–1356.

Qamar, M. U., Azmat, M., Shahid, M. A., Ganora, D., Ahmad, S., Cheema, M. J. M., Faiz, M. A., Sarwar, A., Shafeeque, M., and Khan, M. I. (2017). Rainfall extremes: a novel modeling approach for regionalization. *Water Resources Management*, 31:1975–1994.

Reed, D. W., Jakob, D., Robson, A. J., Faulkner, D. S., and Stewart, E. J. (1999). Regional frequency analysis: a new vocabulary. In Gottschalk, L., Olivry, J. C., Reed, D., and Rosbjerg, D., editors, *Hydrological Extremes: Understanding, Predicting, Mitigating*, pages 237–243. IAHS-AISH Publication 255.

Rossi, F. and Villani, P. (1994a). *Regional flood estimation methods*, pages 135–169. Springer Netherlands, Dordrecht.

Rossi, F. and Villani, P. (1994b). Valutazione delle piene in Campania. Technical report, Consiglio Nazionale delle Ricerche (CNR).

Satyanarayana, P. and Srinivas, V. V. (2008). Regional frequency analysis of precipitation using large-scale atmospheric variables. *Journal of Geophysical Research: Atmospheres*, 113(D24).

Schaefer, M. G. (1990). Regional analyses of precipitation annual maxima in Washington State. *Water Resources Research*, 26(1):119–131.

Schneider, U., Becker, A., Finger, P., Meyer-Christoffer, A., Rudolf, B., and Ziese, M. (2011). GPCC Monitoring Product: near real-time monthly land-surface precipitation from rain-gauges based on SYNOP and CLIMAT Data. Global Precipitation Climatology Centre (GPCC) at Deutscher Wetterdienst [dataset], https://doi.org/10.5676/DWD_GPCC/MP_M_V4_100, accessed on 13th November 2022.

Shehu, B., Willems, W., Stockel, H., Thiele, L., and Haberlandt, U. (2022). Regionalisation of rainfall depth-duration-frequency curves in Germany. *Hydrology and Earth System Sciences Discussions*, 2022:1–29.

Sherman, C. W. (1931). Frequency and intensity of excessive rainfalls at Boston, Massachusetts. *Transactions of the American Society of Civil Engineers*, 95(1):951–960.

Slivinski, L. C., Compo, G. P., Whitaker, J. S., Sardeshmukh, P. D., Giese, B. S., McColl, C., Allan, R., Yin, X., Vose, R., Titchner, H., Kennedy, J., Spencer, L. J., Ashcroft, L., Brönnimann, S., Brunet, M., Camuffo, D., Cornes, R., Cram, T. A., Crouthamel, R., Domínguez-Castro, F., Freeman, J. E., Gergis, J., Hawkins, E., Jones, P. D., Jourdain, S., Kaplan, A., Kubota, H., Blancq, F. L., Lee, T.-C., Lorrey, A., Luterbacher, J., Maugeri, M., Mock, C. J., Moore, G. K., Przybylak, R., Pudmenzky, C., Reason, C., Slonosky, V. C., Smith, C. A., Tinz, B., Trewin, B., Valente, M. A., Wang, X. L., Wilkinson, C., Wood, K., and Wyszyński, P. (2019). Towards a more reliable historical reanalysis: Improvements for version 3 of the Twentieth Century Reanalysis system. *Quarterly Journal of the Royal Meteorological Society*, 145(724):2876–2908.

Smith, R. B. (1979). The influence of mountains on the atmosphere. volume 21 of *Advances in Geophysics*, pages 87–230. Elsevier.

Smithers, J. and Schulze, R. (2001). A methodology for the estimation of short duration design storms in South Africa using a regional approach based on L-moments. *Journal of Hydrology*, 241(1):42–52.

Soltani, S., Helfi, R., Almasi, P., and Modarres, R. (2017). Regionalization of rainfall intensity-duration-frequency using a simple scaling model. *Water Resources Management*, 31:4253–4273.

Svensson, C. and Jones, D. (2010). Review of rainfall frequency estimation methods. *Journal of Flood Risk Management*, 3(4):296–313.

Tabios III, G. Q. and Salas, J. D. (1985). A comparative analysis of techniques for spatial interpolation of precipitation. *JAWRA Journal of the American Water Resources Association*, 21(3):365–380.

Taleb, N. N. (2007). *The black swan: The impact of the highly improbable*, volume 2. Random house.

Teegavarapu, R. S. and Nayak, A. (2017). Evaluation of long-term trends in extreme precipitation: Implications of in-filled historical data use for analysis. *Journal of Hydrology*, 550:616–634.

Thornton, P. E., Running, S. W., and White, M. A. (1997). Generating surfaces of daily meteorological variables over large regions of complex terrain. *Journal of Hydrology*, 190(3):214–251.

Thornton, P. E., Shrestha, R., Thornton, M., Kao, S.-C., Wei, Y., and Wilson, B. E. (2021). Gridded daily weather data for North America with comprehensive uncertainty quantification. *Scientific Data*, 8(1):1–17.

Trefry, C. M., Watkins, D. W., and Johnson, D. (2005). Regional rainfall frequency analysis for the state of Michigan. *Journal of Hydrologic Engineering*, 10(6):437–449.

Treppiedi, D., Cipolla, G., Francipane, A., and Noto, L. (2021). Detecting precipitation trend using a multiscale approach based on quantile regression over a mediterranean area. *International Journal of Climatology*, 41(13):5938–5955.

Trigila, A., Iadanza, C., Bussettini, M., and Lastoria, B. (2018). Dissesto idrogeologico in italia: Pericolosità e indicatori di rischio — edizione 2018. Technical report, Istituto Superiore per la Protezione e la Ricerca Ambientale (ISPRA).

Uboldi, F. and Lussana, C. (2018). Evidence of non-stationarity in a local climatology of rainfall extremes in northern Italy. *International Journal of Climatology*, 38(1):506–516.

Uboldi, F., Sulis, A. N., Lussana, C., Cislaghi, M., and Russo, M. (2014). A spatial bootstrap technique for parameter estimation of rainfall annual maxima distribution. *Hydrology and Earth System Sciences*, 18(3):981–995.

van Belle, G. and Hughes, J. P. (1984). Nonparametric tests for trend in water quality. *Water Resources Research*, 20(1):127–136.

Van de Vyver, H. (2012). Spatial regression models for extreme precipitation in Belgium. *Water Resources Research*, 48(9).

van Montfort, M. A. (1990). Sliding maxima. *Journal of Hydrology*, 118(1):77–85.

van Montfort, M. A. (1997). Concomitants of the Hershfield factor. *Journal of Hydrology*, 194(1):357–365.

Varentsov, M., Esau, I., and Wolf, T. (2020). High-resolution temperature mapping by geostatistical kriging with external drift from large-eddy simulations. *Monthly Weather Review*, 148(3):1029–1048.

Velázquez, J. A., Anctil, F., Ramos, M. H., and Perrin, C. (2011). Can a multi-model approach improve hydrological ensemble forecasting? A study on 29 French catchments using 16 hydrological model structures. *Advances in Geosciences*, 29:33–42.

Viglione, A., Merz, R., Salinas, J. L., and Blöschl, G. (2013). Flood frequency hydrology: 3. a bayesian analysis. *Water Resources Research*, 49(2):675–692.

Villani, P. (2003). Rapporto sulla valutazione delle piene in Piemonte. In: Relazione delle attività del CUGRI fino al 2001. Technical report.

Wackernagel, H. (1998). *Multivariate Geostatistics*. Springer Berlin, Heidelberg.

Wasserman, L. (2004). Models, statistical inference and learning. In *All of Statistics*, pages 87–96. Springer.

Yokoyama, R., Shirasawa, M., and Pike, R. J. (2002). Visualizing topography by openness: a new application of image processing to digital elevation models. *Photogrammetric engineering and remote sensing*, 68(3):257–266.

Zhang, W., Villarini, G., Scoccimarro, E., and Napolitano, F. (2021). Examining the precipitation associated with medicanes in the high-resolution ERA-5 reanalysis data. *International Journal of Climatology*, 41(S1):E126–E132.

Zorzetto, E. and Marani, M. (2020). Extreme value metastatistical analysis of remotely sensed rainfall in ungauged areas: Spatial downscaling and error modelling. *Advances in Water Resources*, 135:103483.

Appendix A

I^2-RED Data Policy

This appendix summarizes the information about the regional agencies involved in the data collection and management after the dismantling of SIMN. This list represents an updated version of the one reported in Mazzoglio et al. (2020). The number assigned to each "region" mentioned in this list is equal to the station ID reported in I^2-RED.

1. Abruzzo, Ufficio Idrografico e Mareografico Regione Abruzzo: data acquired until 2011 are available free of charge on https://www.regione.abruzzo.it/content/annali-idrologici, while data acquired from 2012 onward are available free of charge for research and no-profit purposes, upon request.

2. Basilicata, Dipartimento Protezione Civile Regione Basilicata: data are available free of charge on http://www.centrofunzionalebasilicata.it/it/annali1.php.

3. Calabria, ARPACAL–Centro Funzionale Mulirischi: data are available on http://www.cfd.calabria.it (password-protected website, access granted upon request).

4. Campania, Centro Funzionale Regione Campania: data are available free of charge for research and no-profit purposes, upon request.

5. Emilia-Romagna, ARPA Emilia-Romagna: data are available free of charge on https://www.arpae.it/it/temi-ambientali/meteo/report-meteo/annali-idrologici.

6. Friuli Venezia Giulia, ARPA Friuli Venezia Giulia: data are available free of charge for research and no-profit purposes, upon request.

7. Lazio, Centro Funzionale Regione Lazio: data acquired until 2004 are available free of charge on http://www.regione.lazio.it/rl_protezione_civile/?vw=contenutidettaglio&id=153, while data acquired from 2005 onward are available free of charge for research and no-profit purposes, upon request.

8. Liguria, ARPA Liguria: data are available free of charge on https://www.regione.liguria.it/articoli/26-servizi-online/14279-banca-dati-meteoclimatica.html.

9. Lombardy, ARPA Lombardia: data are available free of charge on http://idro.arpalombardia.it/pmapper-4.0/map.phtml.

10. Marche, Dipartimento di Protezione Civile Regione Marche: data are available on http://console.protezionecivile.marche.it (password-protected website; access granted upon request).

11. Molise, Centro Funzionale Regione Molise: data are available free of charge for research and no-profit purposes, upon request.

12. Piedmont, ARPA Piemonte: data can be accessed free of charge through the "Banca dati meteorologica" after having downloaded a Java application from https://www.arpa.piemonte.it/rischinaturali/accesso-ai-dati/annali_meteoidrologici/annali-meteo-idro/banca-dati-meteorologica.html.

13. Apulia, Dipartimento di Protezione Civile Regione Puglia: data are available free of charge on https://protezionecivile.puglia.it/annali-idrologici-parte-i.

14. Sardinia, ARPA Sardegna: data acquired until 2011 are available free of charge on https://www.regione.sardegna.it/j/v/25?s=205270&v=2&c=5650&t=1, while data acquired from 2012 onward are available free of charge on http://www.sardegnaambiente.it/index.php?xsl=611&s=21&v=9&c=93749&na=1&n=10. Other data acquired from ARPAS are available upon payment.

15. Sicily, Autorità di Bacino del Distretto Idrografico della Sicilia: data of the 1916-2018 period can be downloaded free of charge in pdf format from https://www.regione.sicilia.it/istituzioni/regione/strutture-regionali/presidenza-regione/autorita-bacino-distretto-idrografico-sicilia/annali-idrologici.

16. Tuscany, Servizio Idrografico Regione Toscana: data are available free of charge on http://www.sir.toscana.it/consistenza-rete.

17. Autonomous Province of Trento, Centro Funzionale Provincia Autonoma di Trento: data are available free of charge on https://www.meteotrentino.it/#!/content?menuItemDesktop=143.

18. Autonomous Province of Bolzano – Alto Adige, Ufficio Idrografico Provincia Autonoma di Bolzano–Alto Adige: data are available free of charge for research and no-profit purposes, upon request.

19. Umbria, Regione Umbria–Servizio Idrografico Regionale: data are available free of charge on https://annali.regione.umbria.it/#.

20. Aosta Valley, Centro Funzionale Regione Autonoma Valle d'Aosta: data are available free of charge on http://presidi2.regione.vda.it/str_dataview.

21. Veneto, ARPA Veneto: data freely available on https://www.arpa.veneto.it/bollettini/storico/precmax/.

Although the Italian law requires an Open Source policy for all public data, this right has not yet been implemented by all the Italian agencies. The agreements we signed with some of the agencies involved in the data collection, aimed at monitoring the correct use of the data, restricted their use to the aims of the authors' project. As a result of these legal restrictions, a complete version of I^2-RED can only be provided to two groups of people:

- people in the authors' research group (who are already fully authorized to use the data);
- people who can prove they have received clearance from the regional authorities.

Currently, the entire quality-controlled database is available on Zenodo, albeit with restricted access. The data can be used by third parties, for an indefinite timeframe, upon having completed an agreement either with the authors or the regional agencies involved in the data collection.

Appendix B

Four-regions Multiple Linear Regression Models

The best regression models built for the four-regions using up to four covariates are reported hereafter, together with the corresponding R^2_{adj}.

Alps

$$\overline{h}_1 = 12.5631 - 0.0053 \cdot z + 0.0145 \cdot MAR \tag{B.1}$$

$$\overline{h}_1 = -28.0382 - 0.0051 \cdot z + 0.0139 \cdot MAR + 29.5758 \cdot OP \tag{B.2}$$

$$\overline{h}_1 = 60.9365 - 1.6664 \cdot 10^{-5} \cdot LAT - 0.0046 \cdot z + 0.0148 \cdot MAR + \\ + 25.1825 \cdot OP \tag{B.3}$$

$$\overline{h}_{24} = 751.4719 - 1.4892 \cdot 10^{-4} \cdot LAT + 0.0839 \cdot MAR \tag{B.4}$$

$$\overline{h}_{24} = 63.0269 - 7.2339 \cdot 10^{-5} \cdot LONG - 0.2079 \cdot C + 0.0828 \cdot MAR \tag{B.5}$$

$$\overline{h}_{24} = 59.0632 - 7.2955 \cdot 10^{-5} \cdot LONG - 0.2223 \cdot C + 0.4306 \cdot OBS + \\ + 0.0822 \cdot MAR \quad \text{(B.6)}$$

The R^2_{adj} values in Equations B.1 to B.3 are 0.65, 0.73 and 0.75, respectively. The R^2_{adj} values in Equations B.4 to B.6 are instead 0.74, 0.76 and 0.76.

Apennines

$$\overline{h}_1 = 19.5774 - 0.0083 \cdot z + 0.0128 \cdot MAR \quad \text{(B.7)}$$

$$\overline{h}_1 = 21.5180 - 0.0075 \cdot z - 0.0387 \cdot C + 0.0122 \cdot MAR \quad \text{(B.8)}$$

$$\overline{h}_1 = -12.0037 - 0.0072 \cdot z - 0.0399 \cdot C + 0.0139 \cdot MAR + 20.8086 \cdot OP \quad \text{(B.9)}$$

$$\overline{h}_{24} = 22.8286 - 0.1775 \cdot C + 0.0645 \cdot MAR \quad \text{(B.10)}$$

$$\overline{h}_{24} = 35.6610 - 1.2603 \cdot 10^{-5} \cdot LONG - 0.2097 \cdot C + 0.0629 \cdot MAR \quad \text{(B.11)}$$

$$\overline{h}_{24} = 179.2636 - 3.3612 \cdot 10^{-5} \cdot LONG - 2.6594 \cdot 10^{-5} \cdot LAT + \\ - 0.1979 \cdot C + 0.0623 \cdot MAR \quad \text{(B.12)}$$

The R^2_{adj} values in Equations B.7 to B.9 are 0.36, 0.40 and 0.41, respectively. The R^2_{adj} values in Equations B.10 to B.12 are instead 0.66, 0.67 and 0.68.

Sicily

$$\overline{h}_1 = 11.2186 - 1.9845 \cdot 10^{-5} \cdot LONG - 0.0036 \cdot z \quad \text{(B.13)}$$

$$\overline{h}_1 = 252.6852 - 5.5699 \cdot 10^{-5} \cdot LAT - 0.0061 \cdot z + 0.0163 \cdot MAR \quad \text{(B.14)}$$

$$\overline{h}_1 = 187.8533 - 5.4790 \cdot 10^{-5} \cdot LAT - 0.0069 \cdot z + 0.0220 \cdot MAR + \\ + 37.6608 \cdot OP \quad \text{(B.15)}$$

$$\overline{h}_{24} = 975.8822 - 0.0002 \cdot LAT + 0.1077 \cdot MAR \quad \text{(B.16)}$$

$$\overline{h}_{24} = 704.6903 + 8.9786 \cdot 10^{-5} \cdot LONG - 0.0002 \cdot LAT + 0.0916 \cdot MAR \quad \text{(B.17)}$$

$$\overline{h}_{24} = 816.4861 + 8.5718 \cdot 10^{-5} \cdot LONG - 0.0002 \cdot LAT - 0.0140 \cdot z + \\ + 0.1064 \cdot MAR \quad \text{(B.18)}$$

The R^2_{adj} values in Equations B.13 to B.15 are 0.12, 0.25 and 0.34, respectively. The R^2_{adj} values in Equations B.16 to B.18 are instead 0.53, 0.61 and 0.65.

Sardinia

$$\overline{h}_1 = 42.1910 + 3.8767 \cdot 10^{-5} \cdot LONG - 25.3164 \cdot OP \quad \text{(B.19)}$$

$$\overline{h}_1 = 42.3615 + 4.3842 \cdot 10^{-5} \cdot LONG - 0.0693 \cdot C - 26.2139 \cdot OP \quad \text{(B.20)}$$

$$\overline{h}_1 = 54.8897 + 4.1827 \cdot 10^{-5} \cdot LONG - 1.3045 \cdot 10^{-5} \cdot LAT + \\ - 0.0890 \cdot C + 0.0091 \cdot MAR \quad \text{(B.21)}$$

$$\overline{h}_{24} = -171.0751 + 0.0003 \cdot LONG + 0.0964 \cdot MAR \quad \text{(B.22)}$$

$$\overline{h}_{24} = -186.5050 + 0.0004 \cdot LONG - 0.7802 \cdot C + 0.1167 \cdot MAR \quad \text{(B.23)}$$

$$\overline{h}_{24} = -169.9531 + 0.0004 \cdot LONG - 0.7002 \cdot C + 0.8954 \cdot MSA + \\ + 0.0965 \cdot MAR \quad \text{(B.24)}$$

The R^2_{adj} values in Equations B.19 to B.21 are 0.18, 0.23 and 0.29, respectively. The R^2_{adj} values in Equations B.22 to B.24 are instead 0.54, 0.68 and 0.71.

Appendix C

Application of the VAPI Sardegna Method in the Bitti Case Study

This appendix contains the step-by-step procedure used to evaluate the rainfall quantiles $h_{d,T}$ with the VAPI Sardegna approach for the point where the San Giovanni - Bitti rain gauge is installed. The procedure requires two steps: the computation of the index rainfall and the assessment of the growth factor.

The evaluation of the index rainfall is performed using the equation

$$\mu(d) = a_1 \cdot d^{n_1} \tag{C.1}$$

with d the duration and a_1 and n_1 defined on the basis of equations

$$a_1 = \frac{\mu_g}{0.886 \cdot 24^{n_1}} \tag{C.2}$$

$$n_1 = -0.493 + 0.476 \cdot log_{10}\mu_g \tag{C.3}$$

where the daily index rainfall μ_g is obtained from a raster map proposed by Deidda and Piga (1998).

The point under investigation presents μ_g equal to 81.7 mm, a_1 equal to 24.49 and n_1 equal to 0.42.

The growth factor $K_{d,T}$ related to return period T and duration d can be computed with equation

$$K_{d,T} = a_2 \cdot d^{n_2} \tag{C.4}$$

with a_2 and n_2 depending on the return period. Two different cases could be encountered: $T \leq 10$ years or $T > 10$ years.

For return period $T \leq 10$ years the parameters a_2 and n_2 can be computed as

$$a_2 = 0.62408 + 0.95234 \cdot log_{10}T \tag{C.5}$$

$$n_2 = -2.5392 \cdot 10^{-2} + 4.7188 \cdot 10^{-2} \cdot log_{10}T \tag{C.6}$$

Conversely, for return period $T > 10$ years the parameter a_2 can be computed as

$$a_2 = 0.41273 + 1.1370 \cdot log_{10}T \tag{C.7}$$

while the parameter n_2 is evaluable with

$$n_2 = -0.19055 + 0.25937 \cdot log_{10}T - 3.8160 \cdot 10^{-2} \cdot (log_{10}T)^2 \tag{C.8}$$

for durations $d \leq 1$ hour and with

$$n_2 = 1.5878 \cdot 10^{-2} + 7.6250 \cdot 10^{-3} \cdot log_{10}T \tag{C.9}$$

for durations $d \geq 1$ hour.

The growth factor for each combination of return period and duration is reported in Table C.1, where each row represent a return period T (expressed in years) and each column is a different duration d (expressed in hours).

Table C.1 Growth factors $K_{T,d}$ for different return period T (rows) and durations d (columns).

-	0.25	0.5	0.75	1	3	6	9	12	24
2	0.925	0.918	0.914	0.911	0.900	0.893	0.889	0.886	0.879
5	1.276	1.283	1.287	1.290	1.301	1.307	1.311	1.314	1.321
10	1.530	1.553	1.567	1.576	1.615	1.639	1.654	1.664	1.689
20	1.688	1.787	1.848	1.892	1.946	1.982	2.002	2.017	2.054
50	1.931	2.128	2.252	2.344	2.420	2.469	2.498	2.519	2.569
100	2.106	2.379	2.554	2.687	2.780	2.841	2.877	2.903	2.966
200	2.282	2.629	2.856	3.029	3.142	3.216	3.260	3.291	3.368
500	2.526	2.965	3.257	3.481	3.624	3.716	3.772	3.812	3.909
1000	2.726	3.228	3.564	3.824	3.990	4.099	4.164	4.210	4.325

The results reported in Table C.1 were then used to compute both the IDF curves (Figure C.1) and the return period (Table C.2) of the heavy rainfall event that affected Bitti during 28th November 2020.

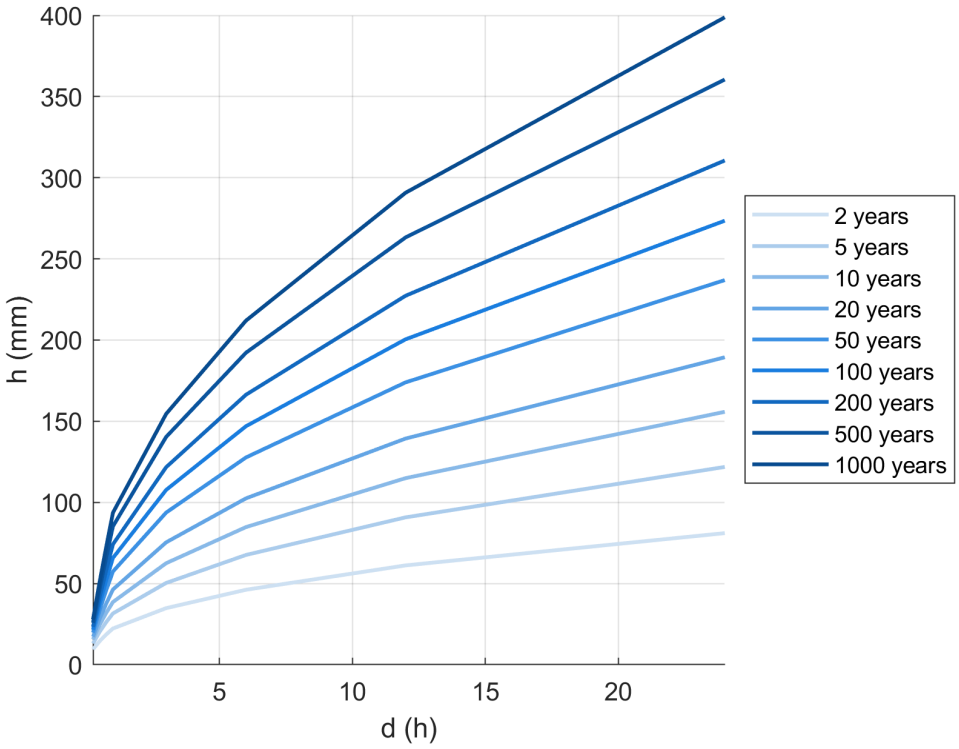

Fig. C.1 IDF curves computed using the VAPI Sardegna method.

Table C.2 Return period of the 28th November 2020 event maxima of different durations. The $\mu(h_d)$ values are computed as $a_1 \cdot d^{n_1}$ while $K_{d,T}^{obs}$ is computed as $h/\mu(h_d)$.

d (h)	h (mm)	$\mu(h_d)$ (mm)	$K_{d,T}^{obs}$ (-)	T (years)
0.25	23.8	13.7	1.733	23
0.5	33.6	18.3	1.832	22
0.75	42	21.7	1.934	24
1	54	24.5	2.205	38
3	125.4	38.7	3.238	240
6	218	51.7	4.216	1235
9	283.2	61.2	4.624	2239
12	293.4	69.1	4.249	1068
24	327.2	92.2	3.548	272

Appendix D

Application of the GEV Boundaryless Method in the Bitti Case Study

This appendix contains the step-by-step procedure used to evaluate the rainfall quantiles $h_{d,T}$ with the GEV boundaryless approach for the point where the San Giovanni - Bitti rain gauge is installed.

The short-duration rainfall quantile $h_T(\tau)$ can be computed as

$$h_T(\tau) = m(\tau) \cdot y_T(\tau) = \begin{cases} a_1 \cdot \tau^{n_1} & \tau \leq 1hour \\ a_2 \cdot \tau^{n_2} & \tau \geq 1hour \end{cases} \tag{D.1}$$

where $m(\tau)$ is the index rainfall and $y_T(\tau)$ is the adimentional reduced variable, that can be computed as

$$m(\tau) = \begin{cases} a_{1m} \cdot \tau^{n_{1m}} & \tau \leq 1hour \\ a_{2m} \cdot \tau^{n_{2m}} & \tau \geq 1hour \end{cases} \tag{D.2}$$

$$y_T(\tau) = \begin{cases} a_{1y} \cdot \tau^{n_{1y}} & \tau \leq 1hour \\ a_{2y} \cdot \tau^{n_{2y}} & \tau \geq 1hour \end{cases} \tag{D.3}$$

The parameters of the index rainfall $m(\tau)$ depend on the daily index rainfall m_D trough the equations

$$n_{1m} = -0.20 + 0.33 \cdot log_{10} m_D \tag{D.4}$$

$$n_{2m} = -0.60 + 0.52 \cdot log_{10} m_D \tag{D.5}$$

$$a_{1m} = a_{2m} = \frac{-10 + 1.25 \cdot m_D}{24^{n_{2m}}} \tag{D.6}$$

In this case study, m_D is equal to 64.5 mm (value obtained from the daily index rainfall map obtained by Deidda et al. (2021), also reported in Figure 7.7).

The parameters related to the adimentional reduced variable $y_T(\tau)$ depend on the return period T and on the shape κ_D and adimensional scale σ_D^* parameters trough the equations

$$n_{1y} = n_{1y_p} + n_{1y_q} \cdot log_{10} T \tag{D.7}$$

$$n_{2y} = n_{2y_p} + n_{2y_q} \cdot log_{10} T \tag{D.8}$$

$$a_{1y} = a_{2y} = 10^{a_{1y_p} + a_{1y_q} \cdot log_{10} T + a_{1y_r} \cdot (log_{10} T)^2} \tag{D.9}$$

where

$$n_{1y_p} = -0.08441 - 0.09092\kappa_D + 0.07846\sigma_D^* + 0.32383\kappa_D^2 + 0.00793\kappa_D\sigma_D^* + 0.01891\sigma_D^{*2} \tag{D.10}$$

$$n_{1y_q} = +0.02720 + 0.13097\kappa_D + 0.18360\sigma_D^* - 0.37370\kappa_D^2 - 0.07701\kappa_D\sigma_D^* - 0.07303\sigma_D^{*2} \tag{D.11}$$

$$n_{2y_p} = +0.01206 - 0.17695\kappa_D + 0.01612\sigma_D^* - 0.67415\kappa_D^2 - 0.05609\kappa_D\sigma_D^* + 0.13555\sigma_D^{*2} \tag{D.12}$$

$$n_{2y_q} = -0.10358 + 0.17971\kappa_D + 0.29584\sigma_D^* + 0.74819\kappa_D^2 + 0.36062\kappa_D\sigma_D^* - 0.34968\sigma_D^{*2} \tag{D.13}$$

$$a_{1y_p} = -0.06465 - 0.04403\kappa_D - 0.08110\sigma_D^* + 0.08870\kappa_D^2 + 0.06253\kappa_D\sigma_D^* + 0.05123\sigma_D^{*2} \tag{D.14}$$

$$a_{1y_q} = +0.20019 + 0.06131\kappa_D + 0.38674\sigma_D^* - 0.09988\kappa_D^2 - 0.10208\kappa_D\sigma_D^* - 0.10724\sigma_D^{*2} \tag{D.15}$$

$$a_{1y_r} = -0.01193 - 0.00329\kappa_D - 0.05745\sigma_D^* - 0.01044\kappa_D^2 + 0.01938\kappa_D\sigma_D^* + 0.01084\sigma_D^{*2} \tag{D.16}$$

Table D.1 Adimentional reduced variable $y_T(\tau)$ for different return period T (rows) and durations d (columns).

-	0.25	0.5	0.75	1	3	6	9	12	24
2	1.065	1.039	1.025	1.014	1.008	1.004	1.002	1.000	0.996
5	1.324	1.324	1.324	1.324	1.327	1.329	1.330	1.330	1.332
10	1.539	1.568	1.585	1.597	1.610	1.619	1.623	1,627	1.635
20	1.766	1.833	1.873	1.902	1.930	1.947	1.958	1.965	1.983
50	2.079	2.211	2.292	2.351	2.405	2.439	2.459	2.474	2.509
100	2.317	2.511	2.631	2.720	2.799	2.850	2.881	2.903	2.956
200	2.552	2.816	2.983	3.107	3.218	3.290	3.332	3.363	3.438
500	2.843	3.215	3.455	3.635	3.796	3.901	3.963	4.008	4.119
1000	3.041	3.503	3.805	4.035	4.239	4.373	4.453	4.511	4.654

The parameters κ_D and σ_D^* are obtained from Deidda et al. (2021) by sampling the raster map of these two variables at the Sain Giovanni - Bitti rain gauge point: in this case, κ_D is equal to 0.15 and σ_D^* is equal to 0.34.

The adimentional reduced variable $y_T(\tau)$ for each combination of return period and duration is reported in Table D.1, where each row represent a return period T (expressed in years) and each column is a different duration d (expressed in hours).

The results reported in Table D.1 were then used to compute both the IDF curves (Figure D.1) and the return period (Table D.2) of the heavy rainfall event that affected Bitti during 28th November 2020.

Table D.2 Return period of the 28th November 2020 event maxima of different durations. The $\mu(h_d)$ values are computed as $a_1 \cdot d^{n_{1j}}$ with j equal to m or n depending on the duration (smaller or greather than 1 hour) while $K_{d,T}^{obs}$ is computed as $h/\mu(h_d)$.

d (h)	h (mm)	$\mu(h_d)$ (mm)	$K_{d,T}^{obs}$ (-)	T (years)
0.25	23.8	13.8	1.727	18
0.5	33.6	18.1	1.852	21
0.75	42	21.3	1.970	25
1	54	23.9	2.260	42
3	125.4	34.8	3.608	373
6	218	44	4.953	2363
9	283.2	50.5	5.603	5314
12	293.4	55.8	5.263	2831
24	327.2	70.6	4.634	974

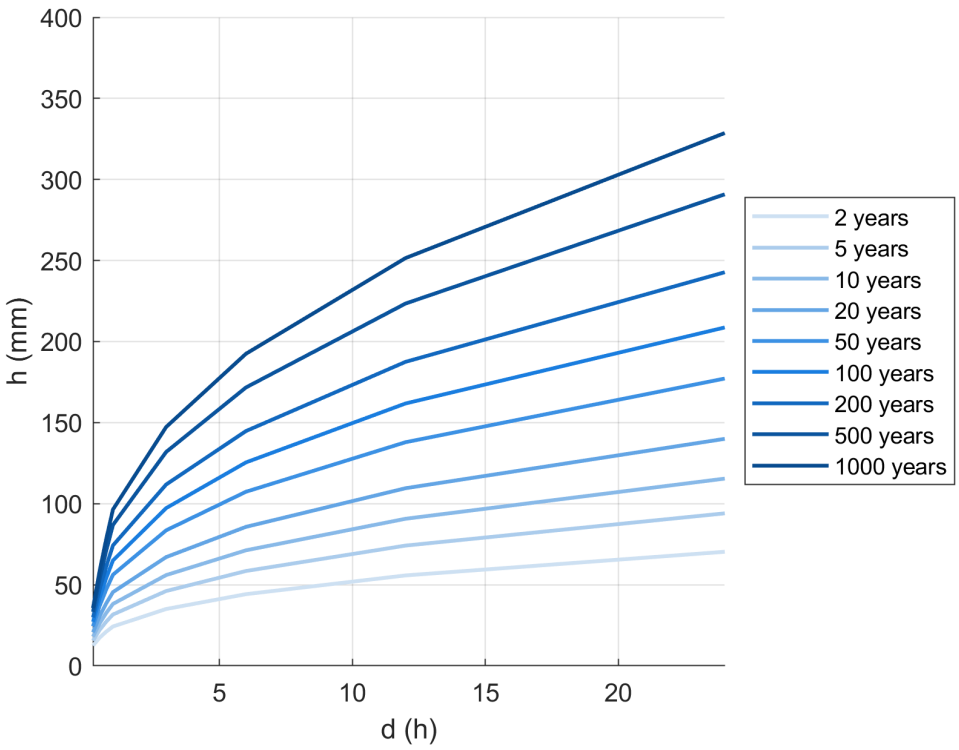

Fig. D.1 IDF curves computed using the GEV boundaryless method.

Appendix E

Application of the Patched Kriging Method in the Bitti Case Study

This appendix contains the step-by-step procedure used to evaluate the rainfall quantiles $h_{d,T}$ with the patched kriging approach for the point where the San Giovanni - Bitti rain gauge is installed.

The average depth-duration curve can be expressed, for durations equal to or greater than 1 hour, with equation

$$\overline{h} = a \cdot d^n \tag{E.1}$$

where a is the scale factor and n is the scaling exponent. By sampling with the coordinates of the San Giovanni - Bitti rain gauge the maps obtained with the patched kriging, it is possible to obtain an a parameter equal to 23.77 mm and an n parameter equal to 0.38. The index rainfall obtained on the basis of these parameters is reported in Table E.1.

Table E.1 Event maxima of the 28th November 2020 and index rainfall $\mu(h_d)$ values, computed as $a \cdot d^n$.

d (h)	h (mm)	$\mu(h_d)$ (mm)
0.25	23.8	10.8
0.5	33.6	16
0.75	42	20.2
1	54	23.8
3	125.4	36
6	218	46.7
9	283.2	54.4
12	293.4	60.6
24	327.2	78.7

As highlighted in Chapter 7, for the sub-hourly durations it is possible to consider the equation

$$\overline{h} = a \cdot d^{n'} \tag{E.2}$$

where *n'* is the scaling exponent of the sub-hourly durations, linked to the *n* parameter trough the equation

$$\alpha = \frac{n'}{n'} \tag{E.3}$$

with α = 1.51 (mean value computed on the basis of the rain gauges located near Bitti; more details are reported in Chapter 7). In this case, *n'* is equal to 0.57. The index rainfall for sub-hourly durations complements Table E.1.

Once defined the most appropriate distribution (GEV in this case), it is possible to compute the growth factor

$$K_T = \theta_1 + \frac{\theta_2}{\theta_3}[1 - (-ln(1 - \frac{1}{T}))^{\theta_3}] \tag{E.4}$$

with θ_1 the location parameter, θ_2 the scale parameter and θ_3 the shape parameter evaluated at the San Giovanni - Bitti station. In this case, θ_1 = 0.768779, θ_2 = 0.307428 and θ_3 = -0.15165, while the main results related to the computation of the growth factor are reported in Table E.2. The results reported in Tables E.1 and E.2 were then used to compute the IDF curves (Figure E.1).

Table E.2 Growth factors for different return periods. A simple scaling approach is here used and , thus, the growth factor depends only on the return period and is kept constant for all the durations.

d (h)	K_T (-)
2	0.885
5	1.287
10	1.593
20	1.922
50	2.405
100	2.814
200	3.267
500	3.943
1000	4.520

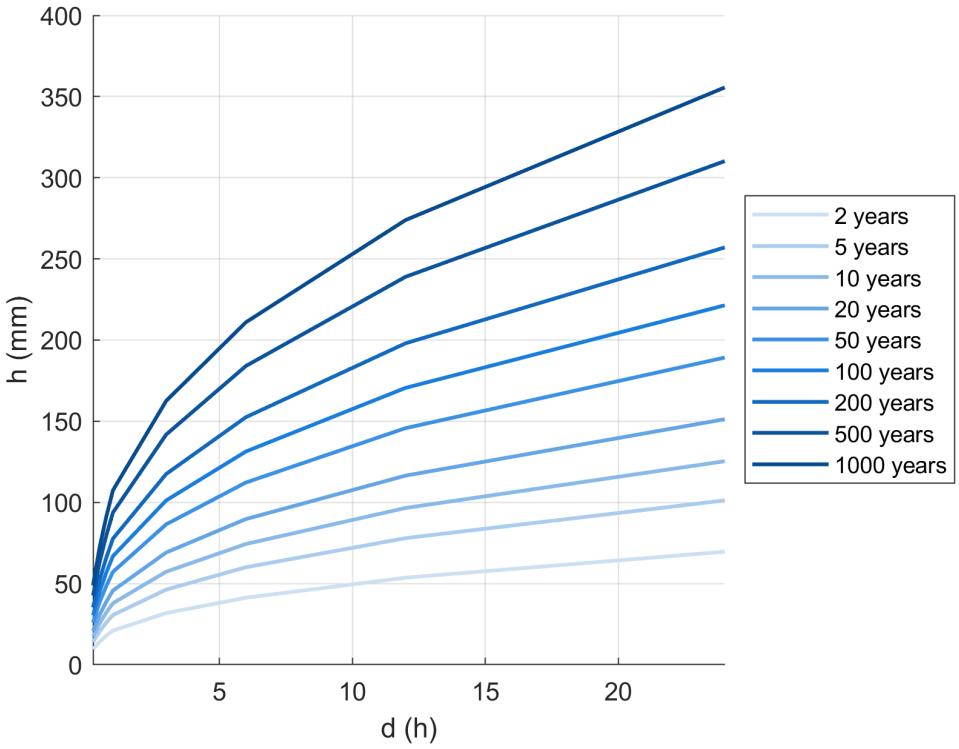

Fig. E.1 IDF curves computed using the patched kriging method.

Table E.3 Return period of the 28th November 2020 event maxima of different durations.

d (h)	h (mm)	$\mu(h_d)$ (mm)	K_T^{obs} (-)	y (-)	F (-)	T (years)
0.25	23.8	10.8	2.202	3.527	0.9710	35
0.5	33.6	16.0	2.096	3.322	0.9646	28
0.75	42	20.2	2.081	3.291	0.9635	27
1	54	23.8	2.272	3.657	0.9745	39
3	125.4	36.0	3.488	5.610	0.9963	274
6	218	46.7	4.670	7.076	0.9992	1184
9	283.2	54.4	5.208	7.649	0.9995	2099
12	293.4	60.6	4.842	7.264	0.9993	1429
24	327.2	78.7	4.159	6.481	0.9985	653

The return periods of the event maxima can be computed as

$$T = \frac{1}{1 - F(x)} \tag{E.5}$$

where $F(x)$ is the cumulative probability function of the GEV distribution evaluable as

$$F(x) = e^{-e^{-y}} \tag{E.6}$$

and

$$y = \frac{-ln(1 - \theta_3 \frac{K_T^{obs} - \theta_1}{\theta_2})}{\theta_3} \tag{E.7}$$

The main results in terms of return period assessment are reported in Table E.3.

Appendix F

Application of the Modified Versions of both VAPI Sardegna and GEV Boundaryless Methods in the Bitti Case Study

This appendix contains the step-by-step procedure used to evaluate the rainfall quantiles $h_{d,T}$ with the modified versions of both VAPI Sardegna and GEV boundaryless methods for the point where the San Giovanni - Bitti rain gauge is installed.

Regarding the VAPI Sardegna method, the application follows what described in Appendix C. The only difference is the computation of the index rainfall for durations smaller than 1 hour. In this case, Equation C.1 become

$$\mu(d) = a_1 \cdot d^{n'_1} \tag{F.1}$$

where

$$n'_1 = 1.51 \cdot n_1 \tag{F.2}$$

Table F.1 Return period of the 28th November 2020 event maxima of different durations. The $\mu(h_d)$ values are computed as $a_1 \cdot d^{n'_1}$ for duration shorter than 1 hour and as $a_1 \cdot d^{n_1}$ for duration greater than 1 hour, while $K^{obs}_{d,T}$ is computed as $h/\mu(h_d)$.

d (h)	h (mm)	$\mu(h_d)$ (mm)	$K^{obs}_{d,T}$ (-)	T (years)
0.25	23.8	10.2	1.733	239
0.5	33.6	15.8	1.832	49
0.75	42	20.4	1.934	32
1	54	24.5	2.205	38
3	125.4	38.7	3.238	240
6	218	51.7	4.216	1235
9	283.2	61.2	4.624	2239
12	293.4	69.1	4.249	1068
24	327.2	92.2	3.548	272

on the basis of the correction factor α described in Section 7.4.2. The results obtained during the computation of the return period of the heavy rainfall event that affected Bitti during 28th November 2020 are reported in Table F.1.

Similarly, the application of the modified GEV boundaryless method follows what described in Appendix D. The only difference is the computation of the index rainfall for durations smaller than 1 hour. In this case, in Equation D.2 become necessary to use

$$n_{1m} = 1.51 \cdot n_{2m} \tag{F.3}$$

The results obtained during the computation of the return period of the heavy rainfall event that affected Bitti during 28th November 2020 are reported in Table F.2.

Table F.2 Return period of the 28th November 2020 event maxima of different durations. The $\mu(h_d)$ values are computed as detailed in this section while $K_{d,T}^{obs}$ is computed as $h/\mu(h_d)$.

d (h)	h (mm)	$\mu(h_d)$ (mm)	$K_{d,T}^{obs}$ (-)	T (years)
0.25	23.8	11.7	1.727	44
0.5	33.6	16.7	1.852	31
0.75	42	20.6	1.970	29
1	54	23.9	2.260	42
3	125.4	34.8	3.608	373
6	218	44	4.953	2363
9	283.2	50.5	5.603	5314
12	293.4	55.8	5.263	2831
24	327.2	70.6	4.634	974